A FINITE ELEMENT APPROACH IN METALWORKING AND ITS APPLICATION TO THE RADIAL UPSETTING OF ~~PROCESS~~ FLANGES

A dissertation submitted for the award of the
Diploma of Membership of Imperial College
and of the degree of
Doctor of Philosophy
in the Faculty of Engineering
University of London

by

ARNO BLASS
B. Sc. (Mech.), M. Sc. (Mech.) (COPPE/Brazil)

Applied Mechanics Section
Mechanical Engineering Department
Imperial College of Science and Technology
London SW7

February 1976

ABSTRACT

A finite element formulation, considering both material and geometrical nonlinearities, is presented, for the elastic-plastic analysis of metalworking processes. The restrictions imposed are those of isotropic material behaviour, isothermal deformation, absence of Bauschinger effect and infinitesimal elastic deformation. The analysis is performed in a Lagrangean frame of reference.

A computer program is implemented and applied to the analysis of a novel deformation process, here referred to as radial upsetting. A related indentation problem is also considered.

For the purposes of comparison, experimental work has been conducted on the same process, the discussion and results being presented. Also for comparison purposes, an upper bound solution to the radial upsetting process has been found, being presented as an appendix. Finite element results are shown to represent a slight improvement over the upper bound solution. It is also shown, however, that the complexity of the three-dimensional process considered leads to difficulties, and that the finite element solution is expensive and not fully satisfactory. This is mainly due to the difficulty in prescribing the adequate boundary conditions to the problem. The results presented are satisfactory at the early stages of deformation, but a progressive degradation of the solution algorithm eventually leads to failure of the program.

Contrary to initial observations, the latest literature on the subject tends to suggest that an Eulerian approach might be more advantageous than the Lagrangean one. But it is quite possible, though not undertaken in this work, that the analysis of a simpler - preferably two-dimensional - process might produce more encouraging results.

Colateral material (a study of temperature distribution in the forming zone, the upper bound solution, a study on the optimization of the numerical solution of the stiffness equation and computer program listings) is presented in the form of appendices.

ACKNOWLEDGEMENTS

I would like to express my gratitude to the Brazilian People for the financial support to this project, expressed through a scholarship from the Coordenação do Aperfeiçoamento do Pessoal de Nível Superior (CAPES), during the early stages, and through a grant of study leave from the Universidade Federal de Santa Catarina (UFSC) during the whole period of my work leading to this thesis.

I would also like to express my sincere appreciation and profound gratitude to my supervisor, Dr. Bela Lengyel, for his constant guidance, interest and encouragement at all stages of my work.

Thanks are also due to

Prof. J. M. Alexander, for the permission to use the experimental facilities in the Metalworking Laboratory of the Department of Mechanical Engineering, Imperial College;

Mr. P. Ashford, for helpful suggestions in the design of the experimental rig;

Mr. W. Plumb, for his continuous and efficient assistance during the experimental stage of the investigation;

All members of the Laboratory staff;

and to

my colleague, Mr. R. M. Guha,

Dr. E. H. Lee (Stanford University) and

Dr. R. T. Fenner (Imperial College),

for their invaluable help in extensive discussions which have served to broaden my view of the subject and to clarify the problems it poses.

Last, but not least, I wish to thank my wife Grescy for her continuous encouragement and understanding.

CONTENTS

ABSTRACT 2

ACKNOWLEDGEMENTS 4

CONTENTS 5

LIST OF ILLUSTRATIONS 10

CHAPTER 1 - INTRODUCTION 14

1.1 - Critical Review of the Analysis of Metalworking Processes 14

1.2 - Critical Review of Radial Upsetting 17

1.3 - The Finite Element Method 22

1.4 - Aims of the Present Work 23

CHAPTER 2 - BASIC CONCEPTS OF CONTINUUM MECHANICS 25

2.1 - Introduction and Notation 25

2.2 - Measure of Strain 26

2.3 - Rate of Deformation 31

2.4 - The Concept of Stress 32

2.5 - Stress-Strain Relation (Eulerian) 35

2.5.a - Introduction 35

2.5.b - Flow Rule and Constitutive Tensor 36

2.5.c - Particularization to von Mises's Criterion 40

2.5.d - Finite Strain 44

2.6 - Stress-Strain Relation (Lagrangean) 46

2.7 - Additional Remarks 48

2.8 - Virtual Velocity Equation 50

CHAPTER 3 - A FINITE ELEMENT FORMULATION FOR THE ELASTIC-PLASTIC ANALYSIS OF PROBLEMS OF LARGE STRAINS AND LARGE DISPLACEMENTS 52

3.1 - Review of Literature 52

3.1.a - Introduction: Two Conceptual Approaches 52

3.1.b - Three Algorithms 57
3.1.c - Recent Trends 62
3.2 - Formulation 69
3.2.a - Incremental Stiffness Equation (Elemental) 69
3.2.b - Initial Load Stiffness Matrix 74
3.2.c - Incremental Stiffness Equation (Overall) 77
3.2.d - Iterative Correction of Incremental Stresses 77
3.2.e - Friction Considerations 78
3.3 - Modified Initial Stress Method 80
3.3.a - Introduction 80
3.3.b - Description of the Method 80
3.3.c - Additional Remarks 83
3.3.c.1 - Rating Factor 84
3.3.c.2 - Limiting the Number of Corrective Cycles 86
3.3.c.3 - Plastic Strain Increment 86
3.3.c.4 - Drift from Stress-Strain Curve 86
3.4 - Conclusion 87
CHAPTER 4 - APPLICATION AND COMPUTER PROGRAM IMPLEMENTATION 88
4.1 - Introduction 88
4.2 - Material Considerations 89
4.3 - Application to the Radial Upsetting Process 94
4.3.a - Reference System 94
4.3.b - Effective Nodal Forces 95
4.3.c - Boundary Conditions 97
4.3.c.1 - Over the mid-plane 97
4.3.c.2 - Elsewhere in the sector/specimen interface 98
4.3.c.3 - Contact area 100
4.3.d - Delimitation of the Contact Arc 102
4.3.e - Contact Angles in Roller and Specimen 103
4.4 - Implementation of the Boundary Conditions 104
4.4.a - Iterative Solution of Incremental Displacements 104
4.4.b - Optimization of the Over-relaxation Factor 107
4.4.c - Implementation of the Boundary Conditions 108
4.4.c.1 - Case when one component of displacement vanishes 108
4.4.c.2 - Case when two components of displacement vanish 109
4.4.c.3 - Rigid nodes 109

4.4.d - Externally loaded Nodes 109
4.5 - Further Application: the Indentation Problem 112
4.6 - The Finite Element Mesh 113
4.7 - The Computer Program 118
4.7.a - Introduction 118
4.7.b - Analysis of the Program 118
4.7.b.1 - Module 1 (Data) 121
4.7.b.2 - Module 2 (Initializations) 121
4.7.b.3 - Module 3 (Assemble overall stiffness matrix) 122
4.7.b.4 - Module 4 (Incremental force-displacement relation) 122
4.7.b.5 - Module 5 (Strain and stress increments) 123
4.7.b.6 - Module 6 (Nodal updating) 123
4.7.b.7 - Module 7 (Updating elemental variables and computing residual stresses) 123
4.7.b.8 - Module 8 (Corrective force increments) 124
4.7.b.9 - Module 9 (Outputs, checks and reinitializations) 124
4.7.c - Subroutines 125
4.7.c.1 - CØEFF 125
4.7.c.2 - DERIV 125
4.7.c.3 - DERI2 125
4.7.c.4 - EPMM 126
4.7.c.5 - GAUSS 126
4.7.c.6 - STIFT 131
4.7.c.7 - FIRST 133
4.7.c.8 - TSTIFT 134
4.7.c.9 - Function Subroutines 135
4.7.d - Concluding Remarks 136
CHAPTER 5 - EXPERIMENTAL WORK 137
5.1 - The Experimental Equipment 137
5.1.a - Introduction 137
5.1.b - Basic Equipment 139
5.1.c - Heating Equipment 144
5.1.d - Measuring Equipment 148
5.1.d.1 - Temperature measurement 148

5.1.d.2 - Strain measurement 151
5.1.d.3 - Displacement transducer 152
5.1.d.4 - Outputs 153
5.1.e - Calibrations 154
5.1.e.1 - Infra-red radiometer 154
5.1.e.2 - Strain-gauges 160
5.2 - Experimental Work 162
5.2.a - Introduction 162
5.2.b - Deformation Mode 171
5.2.c - Forces in Terms of Penetration 175
5.2.d - The Indentation Problem 179
CHAPTER 6 - THE FINITE ELEMENT SOLUTION 184
6.1 - Introduction 184
6.2 - The Radial Upsetting Problem 185
6.2.a - Introduction 185
6.2.b - Force/Penetration Relationship 187
6.2.c - Deformation Mode 189
6.2.d - Stress-Strain Curve 195
6.3 - The Indentation Problem 195
6.3.a - Introduction 195
6.3.b - Force/Penetration Relationship 198
6.3.c - Deformation Mode 201
6.3.d - Stress-Strain Curve 210
CHAPTER 7 - DISCUSSION AND CONCLUSION 214
7.1 - Discussion 214
7.2 - Conclusion 219
REFERENCES 221
NOMENCLATURE 234
N.1 - Review of Conventions 234
N.2 - List of variables 235
APPENDIX 1 - OPTIMIZATION OF THE OVER-RELAXATION FACTOR 240
A-1 - Introductory Note 240
A-2 - Successive Over-relaxation Method 240
A-3 - Estimation of ω_o 244
A-4 - Block Relaxation (SBOR) 247
A-5 - The Specific Problem 248
A-6 - The Specific Algorithm 251
A-7 - Nomenclature 254

APPENDIX 2 - EPFELDA - LISTING OF PROGRAM, FUNCTIONS AND SUBROUTINES 255
Main Program 255
Functions EQST, KNV and KVN 267
Function RATST, subroutine COEFF 268
Subroutine DERIV 269
Subroutines DERI2 and EPMM 270
Subroutine FIRST 271
Subroutine GAUSS 272
Subroutine STIFF 276
Subroutine TSTIFF 277
APPENDIX 3 - EPFELDA - LISTING OF VARIABLES 280
Convention, Main Program 280
Functions EQST, KNV, KVN and RATST 286
Subroutine COEFF
Subroutines DERIV, DERI2 and EPMM 287
Subroutine FIRST 288
Subroutine GAUSS 289
Subroutines STIFF and TSTIFF 291
APPENDIX 4 - TEMPERATURE DISTRIBUTION IN THE RADIAL UPSETTING OF A FLAT DISC - Procs. of the 2nd. North American Metalworking Research Conference, 60-72 (1974) 293
APPENDIX 5 - RADIAL UPSETTING OF FLANGES - Paper to be presented to the 4th. North American Metalworking Research Conference, to be held in Columbus, Ohio, in May 1976 and to be published in the Proceedings of that Conference 307

LIST OF ILLUSTRATIONS

1-1 - Deformation Modes in Edge Upsetting (Paramour[20]) 21

2-1 - Concept of Strain 27

2-2 - The Concept of Lagrangean and Eulerian Stress 33

2-3 - Loading Situations for $\frac{\partial f}{\partial s_{ij}} ds_{ij} > 0$ and Consistency Condition 38

3-1 - Yamada's[37] Method for Rating Load Increments 58

3-2 - The Concept of Partial Stiffness (Marçal et al[59]) 59

3-3 - Initial Stress Method (Zienkiewicz et al[39]) 61

3-4 - Internal and External Numbering of Elemental Nodes 71

3-5 - Modified Initial Stress Method 81

3-6 - Convergence of Initial Stress Methods 84

3-7 - Stress Space Representation for Estimation of Rating Coefficient ζ 85

4-1 - Flow Stress in Terms of Plastic Strain for Commercially Pure Aluminium[119] 92

4-2 - Flow Stress versus Equivalent Plastic Strain for Commercially Pure Aluminium[119] 93

4-3 - Reference Systems and Equivalent Nodal Forces 95

4-4 - Detail of Forming Zone with Sector of Specimen removed for Finite Element Analysis 98

4-5 - Boundary Condition for the Contact Area 101

4-6 - Check if a Node is in Contact Area 101

4-7 - Contact Angles in Roller and Specimen 103

4-8 - The Indentation Problem 113

4-9 - Basic Blocks and its Constitutive Super-elements 114

4-10 - Decomposition of the Super-elements into Tetrahedral Units 116

4-11 - Program EPFELDA (Condensed Flow Block Diagram) 119
4-12 - Subroutine GAUSS (Condensed Flow Block Diagram) 127
4-13 - Subroutine GAUSS (Module 2) - Flow Block Diagram - SOR and Boundary Conditions) 129
4-14 - Subroutine GAUSS (Module 3) - Flow Block Diagram - Multiplying Factor and Load Redistribution 130
4-15 - Subroutine GAUSS (Module 4) - Flow Block Diagram - Optimization of Over-relaxation Factor 132
5- 1 - Radial Upsetting - Basic Equipment 138
5- 2 - Exploded View of Sliding Turret 140
5- 3 - The Concept of the Radial Upsetting Process 140
5- 4 - Basic Radial Upsetting Equipment 143
5- 5 - General View of Radial Upsetting Rig 143
5- 6 - Experimental Rig and Instrumentation 145
5- 7 - Overall Assembly for the Radial Upsetting Process 145
5- 8 - Execution of Heating Coil 147
5- 9 - Depth of Penetration as a Function of Frequency in Induction Heating (Lozinskii[137]) 148
5-10 - Schematic Representation of the Infra-red Radiometer[139] 150
5-11 - Optical Tube used with the Infra-red Radiometer[139] 150
5-12 - Strain-gauge Bridge 152
5-13 - Calibration Curve of Displacement Transducer 153
5-14 - Spectral Emissivity for roughened and polished Aluminium plotted against Wavelength, for several Values of Temperature[142-143] 156
5-15 - Calibration Curves for the IR Radiometer 31 158
5-16 - UV Recorder Output versus Surface Temperature of Specimen in Forming Zone 159
5-17 - Radiometer Rectifying Circuit 160
5-18 - Strain-gauge Calibrations 161
5-19 - Irregular Deformation of Lead Specimens 164
5-20 - Regular Deformation in the Radial Upsetting of Aluminium 164
5-21 - Deformed Specimens and Deformation Front 164

5-22 - Sound (symmetric) and unsound (buckled) Deformation in Radial Upsetting 166
5-23 - A Sample of Specimens at various Stages of Deformation 166
5-24 - An indented Specimen 166
5-25 - Possible non-symmetrical Deformation Modes 167
5-26 - Deformation Modes in Radial Upsetting 168
5-27 - Increase in Semithickness in Terms of Penetration 169
5-28 - A Measure of the Degree of Symmetry in sound Radial Upsetting 170
5-29 - Deformation in hot and cold Radial Upsetting 173
5-30 - Parameters of out-of-plane Deformation in Radial Upsetting 174
5-31 - Output Report from UV Recorder (Typical Sample) 175
5-32 - Relationship between applied Force and Deformation (Penetration) achieved in the Radial Upsetting of commercially pure Aluminium 177
5-33 - Indentation of cylindrical Specimens by a cylindrical Roller - Deformation Mode for $\Delta = 3.95$ mm 180
5-34 - Idem, idem - Deformation Mode for $\Delta = 2.90$ mm 181
5-35 - Idem, idem - Force/Penetration Relationship 182
6- 1 - Force in Terms of Penetration in Radial Upsetting: a Comparison of Finite Element, Upper Bound and experimental Data 186
6- 2 - Effect of a Nonzero Friction Coefficient on the Finite Element Solution to the Radial Upsetting Problem 187
6- 3 - Finite Element Solutions to Radial Upsetting using a large deep and a small shallow mesh 188
6- 4 - Comparison of theoretical (Finite Element) and experimental Deformation Modes 190
6- 5 - Effect of a Nonzero Friction Coefficient on the Deformation Mode in Radial Upsetting 191
6- 6 - Deformation Mode in Radial Upsetting using the reduced Mesh 192
6- 7 - Equivalent Stress / Plastic Strain for a Sample of Elements using the larger Finite Element Mesh 193
6- 8 - Equivalent Stress / Plastic Strain for a Sample of Elements using the reduced Finite Element Mesh 194

6- 9 - Predicted Force in the Finite Element Solution of the frictionless Indentation Problem and Comparison with experimental Results 197
6-10 - Effect of Friction on the predicted Force in the Finite Element Solution to the Indentation Problem 198
6-11 - Predicted Force in the Finite Element Solution to the Indentation Problem using the rigid Boundary Condition 199
6-12 - Predicted Deformation Mode in Indentation (by Finite Elements and using the relaxed Boundary Condition) 203
6-13 - Idem - Alternative Cases 204
6-14 - Predicted Deformation Mode in Indentation (by Finite Elements, using the relaxed Boundary Condition and considering Friction) 205
6-15 - Deformation Mode in Indentation, predicted by the Finite Element Method, using the rigid Boundary Condition 206
6-16 - Idem (Contd.) 207
6-17 - Idem (Contd.) 208
6-18 - Equivalent Stress / Plastic Strain in the Finite Element Solution to the Indentation Problem (Relaxed Boundary Condition) 211
6-19 - Idem (Rigid Boundary Condition) 212
6-20 - Idem (Rigid Boundary Condition) - Contd. 213
A- 1 - Dependence of the Eigenvalue Moduli $|\lambda_i|$ on the Over-relaxation Factor ω 246
A- 2 - A Sample of Results of the Application of Carré's Method for the Optimization of the Over-relaxation Factor 252

CHAPTER 1

INTRODUCTION

1.1 - CRITICAL REVIEW OF THE ANALYSIS OF METALWORKING PROCESSES

Metalworking processes have been in use for several thousand years[1]. Since Man learned how to win iron from its ore, in open fires, he has used this material to forge the arms and instruments he required, and the ornaments for his personal use. Forging was considered a highly skilled activity, which brought regard to those who could master it. Coining of noble metals, such as gold and silver, produced between stone dies, is known to have been used in Mycenae and Crete since 1600 BC. Wire drawing was extensively used in the Middle Ages, to supply the material needed in the manufacture of the coats of mail of knights and warriors; Cluny Museum, in Paris, exhibits a drawing bench of this period. Primitive metalworking machines were known and used in the 15th century, and it is not surprising to learn that Leonardo da Vinci produced sketches for a drop-forge hammer.

However, only when Man learned to use steam - and electricity some time later - as a substitute for muscular force, did the progress of the art become considerable, requiring a deeper insight into the mechanics of metal deformation and a more profound knowledge on material properties and material behaviour, when subjected to pressure, either at room or at higher temperature. From then on the research into the analysis of metalworking processes gained momentum

and was conducted along two different but inter-related lines. On the one side, experiments were carried out, in conventional or special equipment, and the results were thoroughly analysed and interpreted. On the other, theoretical analysis was used to explain metal behaviour and deformation processes by applying the knowledge and analogies from well established sectors such as Stress Analysis and Metalurgy. Eventually the validity of the theoretical analysis was tested experimentally, and experimental results induced corrections or defined limitations to the theories under scrutiny. This is, in rough terms, the dual approach system still employed nowadays.

The second half of the 19th century is the starting point in the extensive research into metalworking processes. Earlier works, like, for instance, Blass's theory of the rolling process[2], in which spread, acceleration, rolling pressure and force are obtained by means of simple geometrical considerations, clearly reflect the poorness of the scientific background and the lack of appropriate measuring instruments at the time. One should not forget, however, that decisive results were achieved which, even if representing only approximations, are still considered nowadays. Tresca's yield criterion is perhaps the most remarkable work in this category. It was postulated in accordance with observations made by Tresca[3], when conducting experiments on the flow of metals through orifices, under the action of pressure. The preliminary report on these experiments, published in 1864, may be regarded as representing the beginning of the Theory of Plasticity, in despite of previous work by Coulomb, Rankine and others which, although dealing with yielding criteria, envisaged collapse criteria for non-metalic civil engineering materials.

Since then the progress in the analysis of metalworking processes has been closely related to the developments in the Theory of Plasticity. Extensive and up-to-date surveys are presented in several textbooks and need not be repeated here. However, reference must be made to two powerful tools derived in this century for the analysis of two dimensional (plane strain and axisymmetric) problems.

The first is the Slip-Line Field Method, based on two Hencky theorems, developed in the thirties, mainly by Geiringer[4]; important slip-line solutions were obtained after the War, and are referred in most good textbooks[5-7]. The other one is the Visioplasticity Method, combining analysis and experiment, developed by Thomsen and Lapsley[8] and others, and well explained in Thomsen, Yang and Kobayashi's book[9].

The continuous development of Technology imposes the research into sophisticated variants of conventional metalworking processes. This is the case of hydrostatic extrusion, which has now been studied for nearly a decade, and whose present state of knowledge is thoroughly presented by Pugh[10] or by Alexander and Lengyel[11].

The extension of the preliminary concepts of the Theory of Plasticity to work-hardening materials was achieved by Prager[12], and a postulate due to Drucker[13] went a step further, by allowing a unified treatment of the constitutive equations and of several and fundamental aspects related to them. Since then, the Theory of Plasticity has evolved mainly via a Continuum Mechanics approach, which therefore also pervaded the literature concerning metalworking processes. A good review of the basic concepts and modern trends in theoretical and experimental research on the plastic behaviour of materials can be found in Creus and Helman[14].

All the methods and techniques developed for the analysis of forming processes allowed the attainment of exact or approximate solutions, in closed, numerical or graphical form, to a number of problems but, at the same time, proved to be either inapplicable or too cumbersome to be used in certain cases. Three-dimensional problems in particular, especially when associated to complicated geometries, remain either unsolved, or have been solved in a very crude way. New techniques are required for this family of problems. Two alternatives are currently envisaged for this purpose. The Finite Element Method, when conveniently extended, will be a possible solution; this work will deal with this alternative. Another one lies in the use of the Method of Weighted Residuals[15]; pioneering applications of this method to metalworking problems have been presented

by Steck[16, 7]. Lately, a weighted residuals analysis of hydrostatic extrusion has been obtained by Helman[17].

Both the Finite Element and the Weighted Residuals Method are particular cases of Ritz's method and therefore constitute upper bound solutions to the problem considered.

1.2 - CRITICAL REVIEW OF RADIAL UPSETTING

The theoretical formulation to be presented further on will be used to describe the flow of material in radial upsetting. It is worthwile, therefore, to start by explaining the meaning of this process, as well as the review of experimental work already done in this or correlated fields.

Radial upsetting is one of a family bulk metal gathering processes, in which local thickening of a specimen is achieved by means of compressive forces producing lateral spread, which may or may not be contained (controlled) by the use of lateral dies. Deformation bears similarity with spreading in rolling, and conclusions may be derived from the analysis of this process.

In radial upsetting the specimen is a sheet metal disc, and deformation is achieved by means of a compression roller, as shown schematically in Figs. 5-1 and 5-3. The disc is driven whilst the roller may be driven or may rotate purely due to friction. It is, however, gradually fed into the specimen, as deformation progresses, this penetration being continuous or intermitent. The specimen must be firmly held by two clamps, whose radius must be of adequate size, in order to avoid buckling of the free portion of the specimen. Depending on the material used, heating may be required, this being achieved locally by some means. In the experiments to be described later, induction heating was used, the heating coil being placed just above the forming roller. Local heating provides a strong supporting surrounding, thus reducing the risk of buckling during deformation.

The interest in such a deformation process is justified

from the economic point of view. In metalworking, usually, large lumps of material are deformed, requiring the application of vast forces, enormous equipment and large initial capital outlay. If smaller volumes of material could be progressively deformed, the instantaneous forming load could be decreased, thus leading to reduced equipment size and smaller initial outlay. When production is not the decisive factor, these considerations will prevail. From the product point of view, one obtains local accumulation of material, and this could be used for at least two purposes: first, if the part should be subjected to subsequent welding operations, additional material could be supplied to the welding zone, to overcome the deterioration in material characteristics due to this process; secondly, if a certain thickness is required only locally, a substantial economy could be achieved by bringing material to where it is effectively required, instead of removing excess material in a subsequent machining operation. This is particularly true when expensive and sophisticated materials are used.

There are three characteristic features which must be taken into account when analysing this process: its three-dimensional nature, the risk of buckling and the presence of free boundaries. No reference specifically related to radial upsetting has been found in the literature. Some references related to specific aspects of bulk metal gathering have been found, but proved of little help for the study of radial upsetting.

Helmi and Alexander[18] examined lateral spread in hot rolling of steel for several geometrical configurations, and compared their results with the ones predicted by the empirical formulae of Wusatowski and Sparling, and by the theoretically-based formula of Hill, which contains one empirical exponent. Helmi and Alexander found that the mode of deformation depends on the width/height ratio, and that a modified form of Sparling's formula best predicts the lateral spread. In radial upsetting, however, the concepts of width and height are reciprocal to those in conventional rolling, and additional work would be required to adequately modify the empirical formulae, in order to render them of some use.

Slater et al[19] have been using the experimental rotary

forging machine in which, similarly as in radial upsetting, deformation of the workpiece is achieved progressively, beneath a rolling tool. They point out that a reduction in the axial force required for deformation can be achieved by confining the deformation zone to a small region beneath the compressing tool, just as occurs in radial upsetting. They used rotary forging to deform cylindrical specimens of lead, to simulate the hot working of steel, and found that the mode of deformation depended on the amount of reduction imposed at each pass. Again, however, the reduction in height in a thick cylinder is not strictly comparable to the reduction in radius in a thin cylinder, by radial upsetting. Their results can only be appreciated from a qualitative point of view.

The reference which might prove most valuable concerns a research work recently concluded by Paramour[20] at the Imperial College, under the supervision of Dr. A. H. Meleka. He used linear specimens of copper and lead travelling underneath a compression roller, in a deformation process termed as "edge-upsetting". This process is a limiting case of radial upsetting, when the diameter of the specimen becomes considerably large.

Paramour used test strips with 2.5 mm in thickness and 305 mm in length. The width is immaterial, provided it supplies enough material to be held between the clamping jaws. Tests were carried out on a horizontal milling machine, in which a forming roller substituted the cutting tool. A strain gauge milling dynamometer was mounted on the table of the machine, and the specimens were clamped on top of the dynamometer, supported by packing pieces of different heights, in order to provide for different thickness / free height ratios. Several experiments were then carried out, varying this ratio, the depth of impression and the table speed, and also using driven and undriven roller. Forces were measured by the dynamometer.

The experiments with copper did not prove successful, as the forces required exceeded the capacity of the dynamometer; thinner specimens were tried in order to reduce the force, but they also proved unsuccessful, presenting uneven deformation due to the shape effect of the serrated top edges of the clamping jaws.

The results to be described refer, therefore, to the experiments with the lead specimens. Five modes of deformation were observed, designated by the author as straight, rippled, bent, folded and unsteady (Fig. 1-1). The straight mode corresponds to uniform deformation, as should be expected under normal conditions, constituting the sought mode of deformation. The rippled mode corresponds to the presence of instability conditions leading to transversal buckling; in extreme cases, the smooth ripples tend to be replaced by jagged zig-zags. In the bent mode, all the deformed material moves to one side of the specimen. The folded mode corresponds to vertical buckling and the unsteady mode to a combination of the previous ones, especially the rippled and the folded modes; both the folded and the unsteady mode occurred only sporadically, the causes being beyond the control of the author. The observed results led to the following conclusions:

a) Under similar conditions, the deformation force increased when using rollers of larger diameter, and, for a given roller, when increasing the depth of the impression. The first conclusion is explained by the increase in contact area, and the second one is self-evident. Deformation was usually of the straight mode, except for extreme depths of impression, when a rippled mode was observed; the critical depth of impression, when change of mode occurred, was smaller for smaller roller radii.

b) The same behaviour was also observed with respect to the final width of the deformed zone.

c) When operating with undriven roller, the table speed had little effect on the horizontal force, but affected substantially the vertical component; when it was increased from 50 to 2000 mm/min, an increase of about 20% was observed in the horizontal component, against about 50% in the vertical one. Besides, wavelength and width of ripples, which were always present, were also increased by increasing table speeds. When operating with driven roller, a bent mode of deformation was produced at low, and a rippled one at high table speeds. In

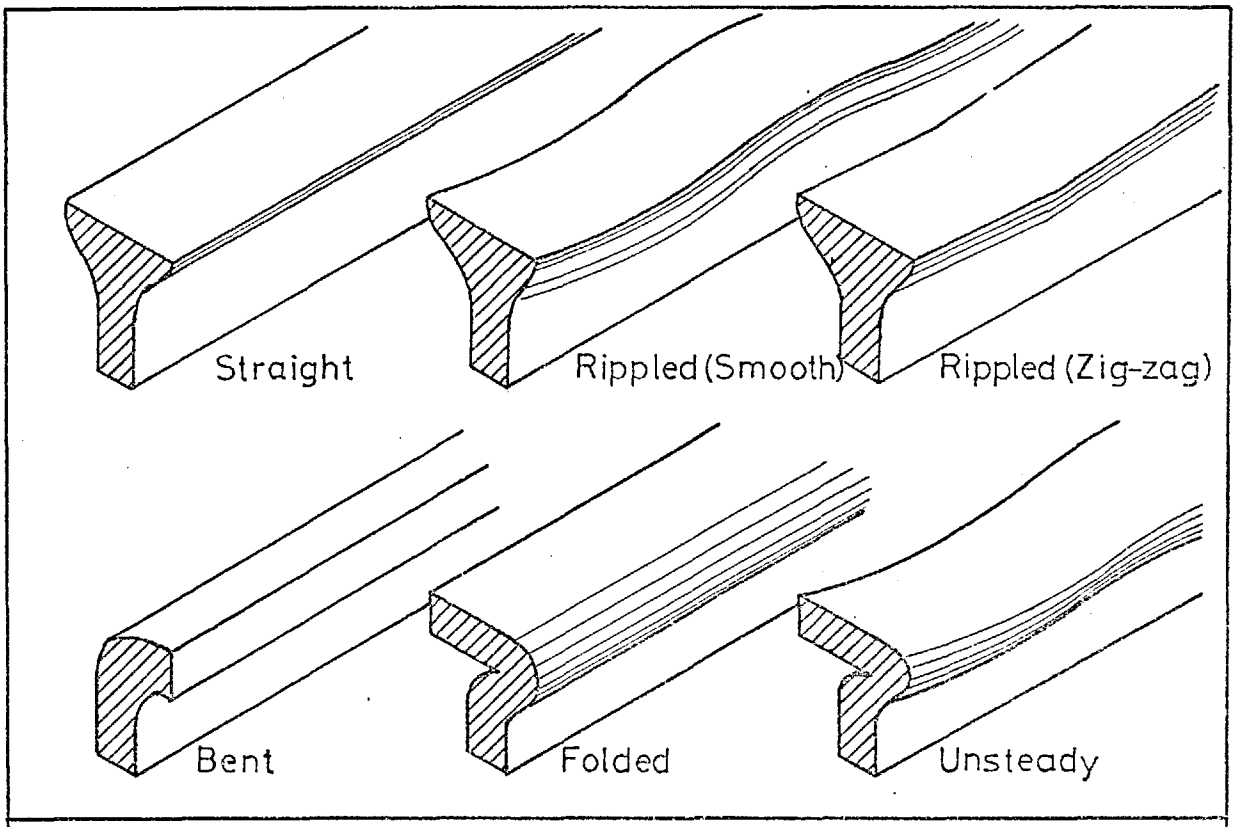


FIG. 1-1 - DEFORMATION MODES IN EDGE UPSETTING (Paramour[20])

an intermediate range, from 1000 to 1600 mm/min, steady deformation could be achieved.

d) The horizontal component of force varied nearly linearly with increasing width/free depth ratio, and the mode of deformation varied from straight to rippled; the vertical component presented a maximum for a critical value of this ratio, dropping afterwards. The ocurrence of the rippled mode could be prevented, to a certain extent, by lubricating the specimen with graphite grease.

One should expect to find similar behaviour in radial upsetting, since edge-upsetting, as mentioned before, is a limiting is a limiting case of that deformation process.

1.3 - THE FINITE ELEMENT METHOD

The Finite Element Method is a technique introduced by Argyris[21] and by Turner[22] and his associates, in the fifties, to solve problems in the stress analysis of structures. The method is strongly related to the matrix formulation of structural analysis, and has been developed as a direct consequence of the concurrent availability of the large electronic computers it requires.

The basic idea of the Finite Element Method consists in discretizing a continuum (not necessarily a truss structure) into a finite number of pieces (or elements), each one isolated by some imaginary boundaries, which will be lines or surfaces, depending on whether the continuum is two- or three-dimensional. Those elements are assumed to be interconnected at a discrete number of nodes, situated at those boundaries; the displacements of these nodes - in the so-called displacement method - will be the basic unknown parameters of the problem, as occurs in truss analysis. A function, or sets of functions, are chosen to uniquely define the displacements of points within an element, in terms of its nodal displacements. The state of strain thus becomes equally and uniquely defined and, together with initial and boundary conditions and the material properties within the element, will define the state of stress throughout this element. A system of nodal forces, equilibrating the boundary stresses and distributed loads, is thus determined, resulting in an elemental stiffness relationship. The elements are then assembled and equilibrium conditions are established at the nodal points. Equations containing nodal displacements as unknowns are obtained, and once they are solved, strains and stresses can be obtained, for any material point, and the problem is solved. This technique is well explained in the available handbooks on the subject as, for instance, Zienkiewicz[23] or Desai and Abel[24].

From the mathematical point of view the method can be thought of as a piecewise polynomial approximation of the displacement field in the continuum, the stiffness terms being obtained

by an appropriate energy or variational principle[23-25]. Arantes e Oliveira[26] has shown that, when conforming elements are used, the equilibrium conditions at the nodes give a displacement field which corresponds to a minimum potential energy for the selected displacement pattern, and the Finite Element Method is a particular case of Ritz's method, so that convergence can be assured as long as completeness is assured. Conforming elements are the ones for which imposed continuity at the nodes yields continuity along the common boundaries. Completeness in energy, in rough terms, means that displacements in two adjacent elements tend to become reasonably identical if the mesh is suitably refined.

Although the Finite Element Method was derived to solve problems in structural analysis, its application as a mathematical algoritm has been extended to cover other fields[23-24], such as steady state problems in heat transfer, electric potential and fluid flow, and dynamic problems, in vibrations. In stress analysis, the initial requirements of infinitesimal displacements and linear behaviour of the material have been discarded, for specific applications, by introducing suitable modifications in the method. This, however, will be analysed and reviewed in Chapter 3.

1.4 - AIMS OF THE PRESENT WORK

The basic aim of the work described in this thesis is to present a finite element formulation to be used in the analysis of metalworking processes, with particular reference to radial upsetting.

Coulomb friction is assumed. A computer program is developed, based in the formulation, and is discussed in Chapter 4.

In order to compare the results obtained from the program, a special rig has been built, and radial upsetting experiments have been conducted on it, using commercially pure aluminium specimens. A few qualitative experiments have also been performed on lead specimens, and one on a mild steel specimen. In these experiments,

strain-gauge measurements were made to estimate the applied load, and the mean temperature in the forming region was controlled (except for the tests with lead specimens, which were performed at room temperature).

The experimental apparatus could be used for more complex experiments, but for the purposes of this work, only simple compression by the forming roller was considered. Lateral spread was accepted as it resulted, and no facility was used to control its shape. Several penetration values were used.

A few experiments were conducted with a non-rotating specimen, constituting, therefore, a simple indentation test. The computer program was also used to analyse such alternative, and experimental and computed results are presented and compared.

The formulation presented is restricted by the following assumptions:

a) Elastic deformations remain infinitesimal throughout the deformation process;

b) Absence of Bauschinger effect;

c) Isothermal deformation;

d) Isotropic material behaviour.

CHAPTER 2
BASIC CONCEPTS OF CONTINUUM MECHANICS

2.1 - INTRODUCTION AND NOTATION

It is advisable to start this work by reviewing some of the basic concepts and definitions of Continuum Mechanics and Theory of Plasticity which will be required later, in order to present them in a unified way, consistent with the applications to be given to them in the next chapter. It is also worthwile to present now some considerations regarding the notation to be used.

Rectangular Cartesian coordinates will be used throughout. Subscripts will be used to denote coordinate directions, and superscripts to denote nodal points. The summation convention is used in its generalised form, as proposed by Wissmann[27], but it does not apply when the indices are underlined. Wissmann's convention states that

> an operation contains the summation over all possible values of the index, if this index does not appear on both sides of an equation.

Thus, summations need not be extended exclusively over the

dimension of the geometrical space considered, and different indices may be summed to different limits. Subscripts will cover the range 1, 2, 3 (in three-dimensional applications) but superscripts will cover the number of nodes in the element under consideration (1 to 4 when tetrahedral elements are considered).

Quantities associated with nodal points are barred. Initial (Lagrangean) coordinates will be given in capitals, while current (instantaneous) coordinates will be given in lower case. Derivatives with respect to initial coordinates will be identified by commas, and with respect to instantaneous coordinates by strokes. Thus, $u_{i,j}$ denotes the derivative of the i^{th} component of displacement with respect to the j^{th} Lagrangean coordinate component, and $u_{i/k}$ the derivative of the same component of displacement with respect to the k^{th} component of the instantaneous coordinates.

Incremental variables are characterised by the prefix Δ. Variables affected by the superindex "o" refer to the original (undeformed) state of the continuum. Superindices "e" and "p" will be used to identify variables referred to the elastic and plastic states, respectively. Of course, no summation is ever intended over these indices.

2.2 - MEASURE OF STRAIN[28-32]

In a Continuum Mechanics formulation the configuration of a body is described by a continuous mathematical model whose geometrical points are identified with the position of the material particles of this body. When the configuration is changed, due to some form of physical action, assumption is made that this change is continuous, that is, that particles lying near to each other before the change remain near to each other after the deformation.

Let an orthogonal Cartesian coordinate system X be chosen to describe the initial (undeformed) configuration C^o of the continuum, and a coincident orthogonal Cartesian coordinate

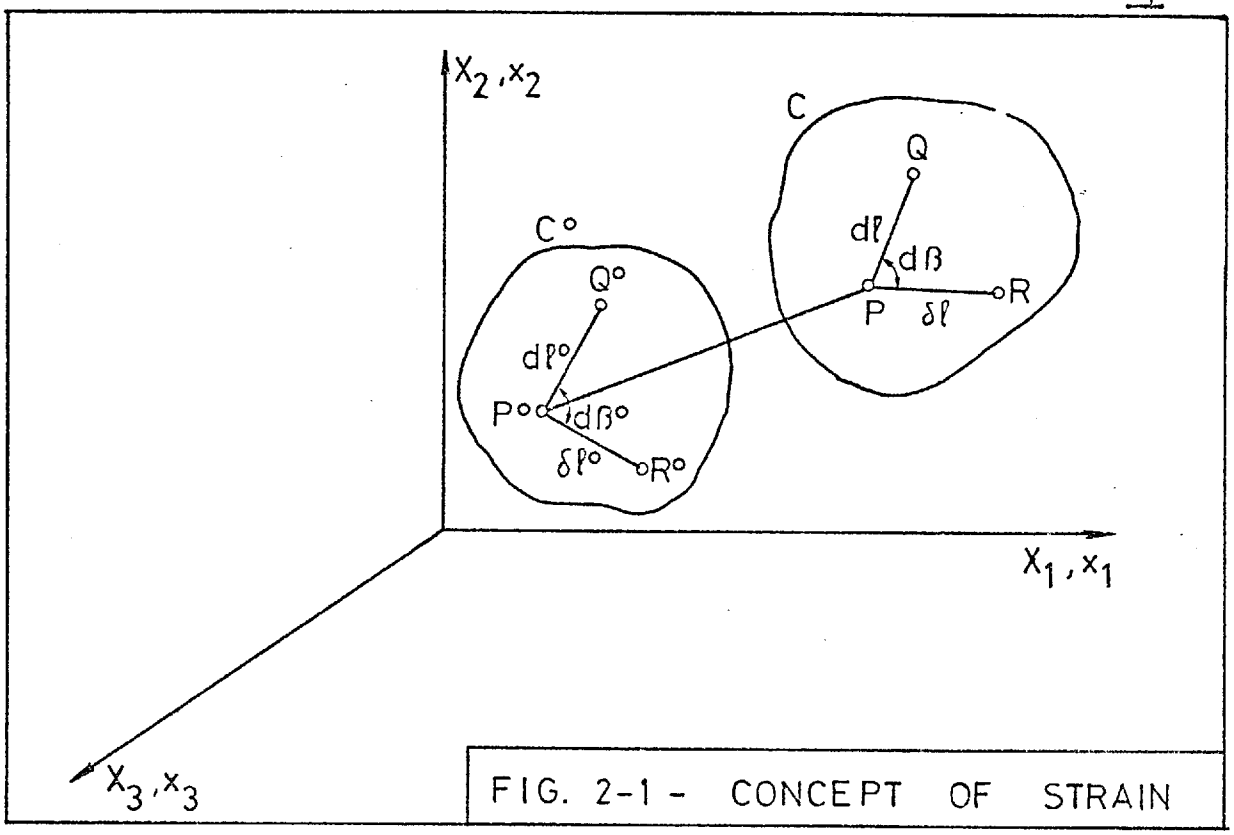


FIG. 2-1 - CONCEPT OF STRAIN

system x be chosen to describe any new (deformed) configuration C (Fig. 2-1). Let $P^{o}(X_i)$ be the position of a certain particle in C^{o}, and $P(x_i)$ be its image in C. The transformation

$$x_i = X_i + u_i \qquad (2\text{-}1)$$

maps the position of this image in the deformed configuration, u_i being one of the components of the displacement vector. Considering now a second particle in the neighbourhood of P^{o}, say $Q^{o}(X_i+dX_i)$, its image, by the assumption of continuity, will be mapped into a neighbourhood of P, say into $Q(x_i+dx_i)$. The distance from P^{o} to Q^{o} is expressed by

$$d\ell^{o} = \sqrt{dX_i\ dX_i}$$

whilst the corresponding distance of their images is given by

$$d\ell = \sqrt{dx_i\ dx_i}\ .$$

The assumed continuity of the functions interrelating

both coordinate systems allows us to rewrite these distances in the form

$$(d\ell^o)^2 = X_{i/m}\, X_{i/n}\, dx_m\, dx_n$$

and

$$(d\ell)^2 = x_{i,m}\, x_{i,n}\, dX_m\, dX_n .$$

The difference between these expressions, after suitable manipulation of the indices, can be written either as

$$(d\ell)^2 - (d\ell^o)^2 = (x_{k,i}\, x_{k,j} - \delta_{ij})\, dX_i\, dX_j$$

or as

$$(d\ell)^2 - (d\ell^o)^2 = (\delta_{ij} - X_{k/i}\, X_{k/j})\, dx_i\, dx_j ,$$

δ_{ij} being the Kronecker delta, equal to unity if $i = j$, and zero otherwise. By similar reasoning, and considering a third particle in the same neighbourhood, one could express the angular variation

$$d\beta - \frac{d\ell^o\, \delta\ell^o}{d\ell\, \delta\ell}\, d\beta^o = (x_{k,i}\, x_{k,j} - \delta_{ij})\, dX_i\, \delta X_j$$

$$= (\delta_{ij} - X_{k/i}\, X_{k/j})\, dx_i\, \delta x_j .$$

The expressions inside the brackets of these last four equations are used to define the Lagrangean and Eulerian strain tensors. In effect, by definition,

$$E_{ij} = \frac{1}{2}\,(x_{k,i}\, x_{k,j} - \delta_{ij})$$

is Green's strain tensor, introduced by Green and St. Venant, often simply referred to as the Lagrangean strain tensor, whilst

$$e_{ij} = \frac{1}{2}\,(\delta_{ij} - X_{k/i}\, X_{k/j})$$

is Almansi's strain tensor, introduced by Almansi and Hamel, and sometimes referred to as the Eulerian strain tensor. Obviously, both these expressions represent symmetric tensors.

Now, from Eqn. (2-1),

$$x_{i,j} = \delta_{ij} + u_{i,j} \qquad (2\text{-}2a)$$

and

$$X_{i/j} = \delta_{ij} - u_{i/j} . \qquad (2\text{-}2b)$$

Use of these expressions in the strain tensor definitions converts them to

$$E_{ij} = \frac{1}{2} (u_{i,j} + u_{j,i} + u_{k,i}\, u_{k,j}) \qquad (2\text{-}3a)$$

and

$$e_{ij} = \frac{1}{2} (u_{i/j} + u_{j/i} - u_{k/i}\, u_{k/j}) \qquad (2\text{-}3b)$$

If the displacement components are such that their first derivatives are very small, the quadratic terms in the above expressions become negligible, and Cauchy's infinitesimal strain tensors

$$E_{ij} = \frac{1}{2} (u_{i,j} + u_{j,i})$$

and

$$e_{ij} = \frac{1}{2} (u_{i/j} + u_{j/i})$$

are obtained. In that case, the distinction between Lagrangean and Eulerian strains disappears, and it becomes immaterial whether the displacement derivatives are computed with respect to initial or current coordinates. Those expressions coincide with the measure of strain usually found in infinitesimal strain analysis.

Multiplying the definition for Green's strains by $X_{i/r}\, X_{j/s}$ and taking into account that

$$X_{i/r}\, x_{k,i} = \delta_{kr} ,$$

a simple relation is obtained, connecting Green's and Almansi's strains[28]:

$$e_{rs} = X_{i/r}\, X_{j/s}\, E_{ij} \qquad (2\text{-}4)$$

and, conversely,

$$E_{ij} = x_{i,r}\, x_{j,s}\, e_{rs}\,.$$

Other definitions of strain exist, but will not be considered here, nor will they be considered in the subsequent chapters.

The derivatives appearing in Eqns. (2-3a,b) are in general not symmetric. For instance, one should expect

$$u_{i/j} \neq u_{j/i}\,;$$

it is possible, however, to express those derivatives as the sum

$$u_{i/j} = \epsilon_{ij} + \omega_{ij}$$

of a symmetric tensor

$$\epsilon_{ij} = \frac{1}{2}\,(u_{i/j} + u_{j/i}) = \epsilon_{ji} \qquad (2\text{-}5a)$$

and an antisymmetric tensor

$$\omega_{ij} = \frac{1}{2}\,(u_{i/j} - u_{j/i}) = -\omega_{ji}\,, \qquad (2\text{-}5b)$$

known, respectively, as the <u>deformation tensor</u> and the <u>rotation tensor</u>. It is evident that the deformation tensor has an expression which is identical to Cauchy's infinitesimal strain tensor, therefore the rotation term must vanish when infinitesimal strains are concerned. We can express Almansi's strain tensor as a function of the deformation and rotation tensors by replacing the derivatives in Eqn. (2-3b) by their new expression, obtaining

$$e_{ij} = \epsilon_{ij} - \frac{1}{2}\,(\epsilon_{ki} - \omega_{ki})(\epsilon_{kj} - \omega_{kj})\,.$$

Clearly, in the case of rigid body motion,

$$\epsilon_{ij} = 0\,,$$

$$u_{i/j} = \omega_{ij}$$

and

$$e_{ij} = \frac{1}{2}\omega_{ki}\omega_{kj} .$$

Similar concepts of deformation and rotation can also be developed with respect to the Lagrangean description, and Green's strain tensor will also be expressed as a function of the Lagrangean definitions of deformation and rotation.

2.3 - RATE OF DEFORMATION[28-32]

When motion is considered, an instantaneous (Eulerian) description is preferred, and we will assume that the velocity of a particle is a function of the coordinates of its instantaneous position: $v_i = v_i(x_1,x_2,x_3)$. By similarity with Eqns. (2-5a,b), we express the spatial derivatives of velocities as the sum

$$v_{i/j} = V_{ij} + \Omega_{ij}$$

of a symmetric tensor

$$V_{ij} = \frac{1}{2}(v_{i/j} + v_{j/i}) = V_{ji}$$

and an antisymmetric tensor

$$\Omega_{ij} = \frac{1}{2}(v_{i/j} - v_{j/i}) = -\Omega_{ji} ,$$

defined, respectively, as the rate of deformation tensor and the spin tensor. The reason for these names becomes apparent if we consider that, for an infinitesimal time increment, a proportionality exists between velocities and displacements, that is,

$$u_i = v_i \, dt ,$$

which allows those defining equations to be rewritten to

$$V_{ij} \, dt = \frac{1}{2}(u_{i/j} + u_{j/i}) = \epsilon_{ij} \qquad (2\text{-}6a)$$

and

$$\Omega_{ij}\, dt = \frac{1}{2}\,(u_{i/j} - u_{j/i}) = \omega_{ij}\,. \qquad (2\text{-}6b)$$

2.4 - THE CONCEPT OF STRESS(28-32)

The natural definition of stress has a physical meaning, and is referred to the strained state of the continuum. However, when stresses have to be related to strains, it is adequate to use a definition of stress similar to the corresponding definition of strain. That is, in a Lagrangean description stresses should be defined in terms of the undeformed geometry of the continuum.

Consider a strained solid volume element of configuration C surrounding particle P, at the right side of Fig. 2-2. A force vector dT acts on one of its faces, whose area is dA. The original position of the particle, in configuration C^o, is P^o, and surrounding it is the unstrained configuration of the same volume element. On the corresponding face, a force vector dT^o acts over an area dA^o. Stresses, in each case, will be expressed as the limiting ratios

$$\frac{dT}{dA} \quad \text{and} \quad \frac{dT^o}{dA^o},$$

when the volume elements are reduced in size, tending to zero volume. There is no unique correspondence rule to connect dT and dT^o, but mathematical consistency is a requirement for the adopted relation. We could either assume simply

$$dT_i^o = dT_i$$

or select a more sophisticated relation like, for instance,

$$dT_i^o = X_{i/j}\, dT_j\,,$$

meaning that the forces are transformed by the same rule as the coordinate variations,

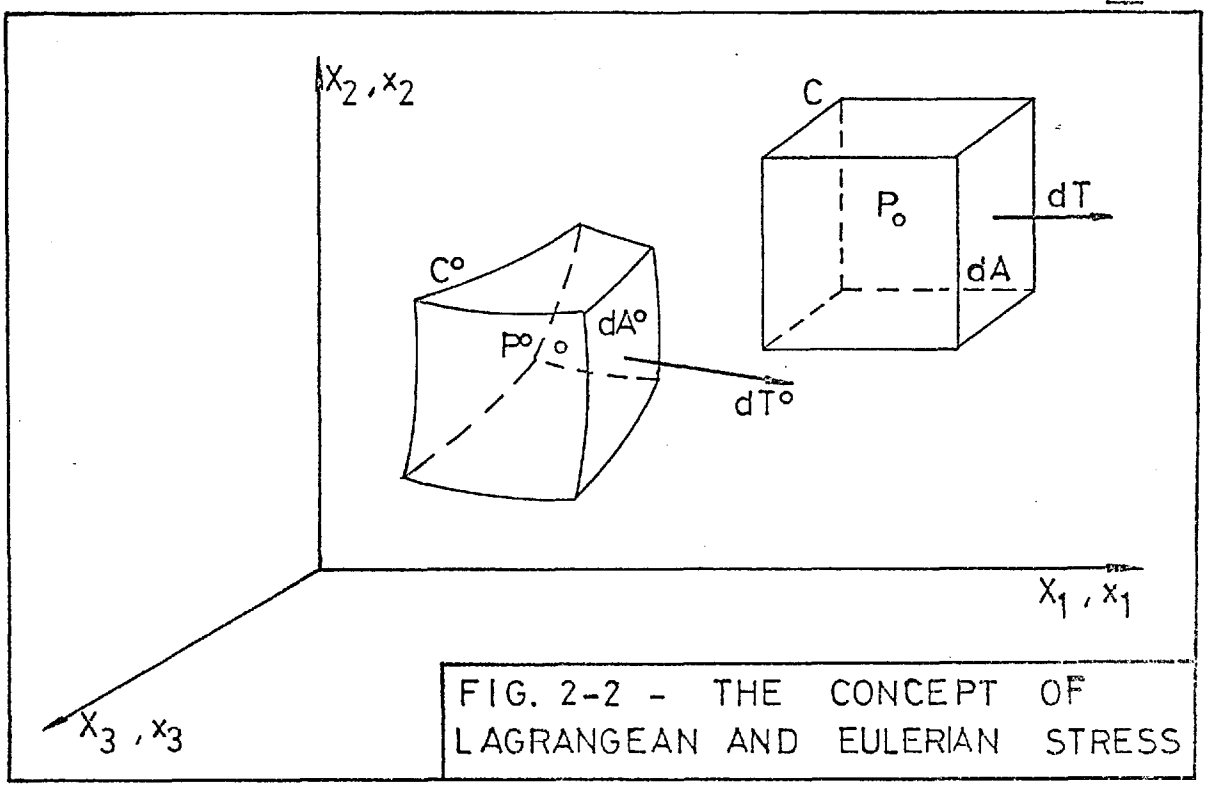


FIG. 2-2 - THE CONCEPT OF LAGRANGEAN AND EULERIAN STRESS

$$dX_i = X_{i/j}\, dx_j .$$

If n is the unit outward normal vector acting on dA, and if n^o is its corresponding unit vector acting on dA^o, we have, for the strained state,

$$dT_i = s_{ij}\, n_j\, dA , \qquad (2\text{-}7a)$$

where s_{ij} is a component of the Eulerian (or Cauchy) stress tensor. In the Lagrangean description we would have either

$$dT_i^o = T_{ij}\, n_j^o\, dA^o = dT_i \qquad (2\text{-}7b)$$

or

$$dT_i^o = S_{ij}\, n_j^o\, dA^o = X_{i/j}\, dT_j , \qquad (2\text{-}7c)$$

or other relation, according to the force correspondence utilised. In these expressions, T_{ij} is Lagrange's stress tensor, whilst S_{ij} is Kirchhoff's stress tensor. We now have to interrelate these tensors with Cauchy's. The components of the area vectors are ex-

pressed by

$$n_i \, dA = \epsilon_{ijk} \, dx_j \, dx_k$$

and

$$n_i^o \, dA^o = \epsilon_{ijk} \, dX_j \, dX_k ,$$

ϵ_{ijk} being the permutation symbols of Tensor Calculus, equal to

$$\begin{cases} +1 & \text{if } i, j, k \text{ form a cyclic permutation} \\ -1 & \text{if } i, j, k \text{ form an anticyclic permutation, and} \\ 0 & \text{if there is a repetition of any index.} \end{cases}$$

The Jacobean of the $X - x$ coordinate transformation is given by

$$J = \left| x_{p,q} \right| = \epsilon_{ijk} \, x_{i,1} \, x_{j,2} \, x_{k,3} , \qquad (2\text{-}8a)$$

from which also

$$X_{p/q} = \frac{1}{J} \epsilon_{mnp} \, x_{r,m} \, x_{s,n} , \qquad (2\text{-}8b)$$

can be obtained, with (q, r, s) forming a positive cyclic permutation of the set $(1, 2, 3)$.

It is thus possible to write, after suitable manipulation of the indices,

$$J \, X_{i/j} \, n_i^o \, dA^o = n_j \, dA ,$$

hence, from Eqns. (2-7a,b,c),

$$T_{ji} = J \, X_{j/k} \, s_{ik}$$

and

$$S_{ij} = J \, X_{i/r} \, X_{j/s} \, s_{rs} . \qquad (2\text{-}9a)$$

The Eulerian stress tensor is symmetric, thus we can con-

clude that Lagrange's is not, but Kirchhoff's is also symmetric. Lagrange's stress tensor, therefore, is not a convenient definition of stress to be used with an always symmetric strain tensor. Kirchhoff's definition is more suitable for that purpose.

Eqn. (2-9a) can also be written in the inverted form

$$s_{rs} = \frac{1}{J} x_{r,i} x_{s,j} S_{ij} . \qquad (2\text{-}9b)$$

As with strains, other definitions of stress can be presented, but will not be used in this work.

2.5 - STRESS-STRAIN RELATION (EULERIAN)

2.5.a - INTRODUCTION

The general case of elastic-plastic deformation, in which both components - elastic and plastic - of strain are finite, has been considered by Lee[33], who has shown that, in those circumstances, the usual assumption of small strain Plasticity, namely that the total strain components can be decomposed into a purely elastic and a purely plastic component,

$$e_{ij} = e^{e}_{ij} + e^{p}_{ij} , \qquad (2\text{-}10)$$

is not true, being replaced by a much more complicated matrix relation. However, if the elastic strains can be considered infinitesimal, the elastic matrix in Lee's formulation reduces to a unit matrix, and Eqn. (2-10) can be accepted. This assumption will be made in the rest of this work.

We will also assume isotropic material behaviour, the absence of Bauschinger effect and isothermal deformation.

In infinitesimal Hookean Elasticity, stresses and strains, as well as their increments, are related by the generalized form of Hooke's Law, which can be written incrementally as

$$\Delta s_{ij} = D^{e}_{ijrs}\,\Delta e^{e}_{rs}\,, \qquad (2\text{-}11)$$

where D^{e}_{ijrs} are the components of the elastic constitutive tensor, given by

$$D^{e}_{ijrs} = \lambda\,\delta_{ij}\,\delta_{rs} + \mu(\delta_{ir}\,\delta_{js} + \delta_{jr}\,\delta_{is})\,,$$

λ and μ being Lamé's constants,

$$\lambda = \frac{2G\nu}{1 - 2\nu} \qquad \text{and} \qquad \mu = G\,,$$

with

$$G = \frac{E}{2(1 + \nu)}\,.$$

Thus

$$D^{e}_{ijrs} = 2G\left[\frac{\nu}{1 - 2\nu}\,\delta_{ij}\,\delta_{rs} + \frac{1}{2}\,(\delta_{ir}\,\delta_{js} + \delta_{is}\,\delta_{jr})\right]\,. \qquad (2\text{-}11a)$$

This is a hemitropic tensor, meaning that it possesses the following symmetry properties:

$$D^{e}_{ijrs} = D^{e}_{jirs} = D^{e}_{ijsr} = D^{e}_{rsij}\,. \qquad (2\text{-}11b)$$

Under infinitesimal Plasticity, a relation similar to Eqn. (2-10) holds, and we write simply

$$\Delta s_{ij} = D'_{ijrs}\,\Delta e_{rs}\,, \qquad (2\text{-}12)$$

in which the constitutive tensor D'_{ijrs} is also hemitropic and obtained from D^{e}_{ijrs}, as will be shown later.

2.5.b - FLOW RULE AND CONSTITUTIVE TENSOR

A general theory of Plasticity developed by Green and Naghdi[34] will be considered here, under the assumptions mentioned in the preceding sub-section. In this theory, the existence of a scalar yield (or loading) function $f(s_{ij}, e^{p}_{ij}, k)$, depending on the states of stress and plastic strain and, via the work-hardening parameter k, on the loading history, is assumed, this function characterizing the yielding of the material. Equation

$$f(s_{ij},\ e^{p}_{ij},\ k) = 0 \qquad (2\text{-}13a)$$

represents a closed surface in the stress space. If $f < 0$, no change can take place in plastic deformation; when $f = 0$, changes in plastic deformation are possible; $f > 0$ has no meaning in this theory. This characterization brings an immediate and important consequence: if at a certain moment $f = 0$, the sign of

$$df = \frac{\partial f}{\partial s_{ij}}\, ds_{ij} + \frac{\partial f}{\partial e^{p}_{ij}}\, de^{p}_{ij} + \frac{\partial f}{\partial k}\, dk \qquad (2\text{-}13b)$$

governs the character of the changes taking place in deformation. In effect, $df < 0$ would imply $f < 0$ in the next instant of time, leading thus to an elastic state (unloading); but in that case, no changes can occur in the plastic strain nor in the plastic strain-hardening parameter. The unloading situation is thus characterized by

$$f = 0\,, \qquad \frac{\partial f}{\partial s_{ij}}\, ds_{ij} < 0\,.$$

The other alternatives are

$$f = 0\,, \qquad \frac{\partial f}{\partial s_{ij}}\, ds_{ij} = 0\,,$$

occurring during neutral loading, and

$$f = 0\,, \qquad \frac{\partial f}{\partial s_{ij}}\, ds_{ij} > 0$$

during general loading situations (Fig. 2-3).

Since the yield surface is assumed to be a closed one, the above mentioned states can be related to the stress increment vector: it is oriented either towards the inside (unloading), tangent to (neutral loading) or oriented towards the outside (general loading) of the yield surface.

Drucker[13,35], considering the work done by an external agency (that is, different from the one causing the existing state of stress), slowly applying and then slowly removing a set of self-

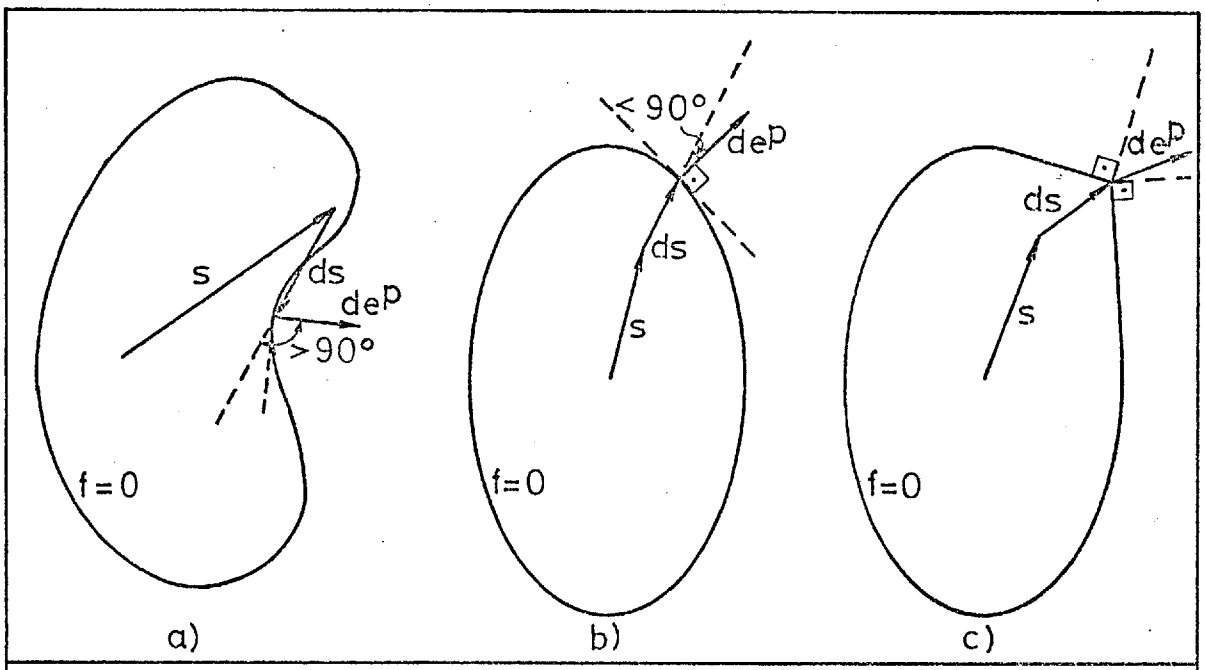


FIG. 2-3 - LOADING SITUATIONS FOR $\frac{\partial f}{\partial s_{ij}} ds_{ij} > 0$ AND CONSISTENCY CONDITION

equilibrating forces, redefines hardening by stating that the work performed by this external agent is positive during loading, and non-negative over the whole cycle. As only the elastic part of the strain components is recovered, upon unloading, this means that no useful net energy above the elastic energy can be extracted from the material and the system of forces acting over it. Thus, work-hardening occurs if

$$ds_{ij}\, de_{ij} > 0 \qquad \text{during loading}$$

and

$$ds_{ij}\, de^{p}_{ij} \geq 0 \qquad \text{on completing the cycle .}$$

This last inequality represents the dot product between the vectors ds and de^p, therefore the positive directions of these vectors must make a non-obtuse angle with each other. In other words, given de^p, the range of possible choices for ds cannot cover more than an angle of 180^o. A corollary to this conclusion states that the yield surface must always be convex; another corollary states that the vector de^p must be normal to the yield surface at any smooth point (Fig. 2-3b), or lie between normals at a singu-

larity (corner) point (Fig. 2-3c), to assure that $d\bar{\varepsilon}^p$ lies at no more than 90° with any possible ds ; Fig. 2-3a, therefore, clearly represents an impossible situation. This last corollary, when restricted to a smooth point of the yield surface requires[35]

$$de^p_{ij} = d\lambda \frac{\partial f}{\partial s_{ij}} , \qquad (2\text{-}14)$$

$d\lambda$ being a constant which is dependent upon stress, stress-rate, strain and strain history, which, by Drucker's definition of work-hardening, must be non-negative.

Loading occurs at points successively satisfying Eqn. (2-13a), which has been called the consistency condition by Prager, meaning that loading from a plastic state must lead to another plastic state. For consistency, therefore, also Eqn. (2-13b) must be identically zero during loading. Assuming k to be a function of plastic strain we have, thus

$$\frac{\partial f}{\partial s_{ij}} ds_{ij} + \frac{\partial f}{\partial e^p_{ij}} de^p_{ij} + \frac{\partial f}{\partial k} \frac{\partial k}{\partial e^p_{ij}} de^p_{ij} = 0 . \qquad (2\text{-}13c)$$

Introducing now Eqns. (2-14) into (2-13c), and using also (2-10), taken in incremental form, and (2-11) we get

$$d\lambda = \frac{\frac{\partial f}{\partial s_{ij}} D^e_{ijrs} de_{rs}}{\frac{\partial f}{\partial s_{mn}} \left[D^e_{mnpq} \frac{\partial f}{\partial s_{pq}} - \frac{\partial f}{\partial e^p_{mn}} - \frac{\partial f}{\partial k} \frac{\partial k}{\partial e^p_{mn}} \right]} \qquad (2\text{-}14a)$$

and reintroducing this expression into Eqn. (2-14), again using Eqns. (2-10) and (2-11),

$$de^p_{ij} = \frac{\frac{\partial f}{\partial s_{ij}} \frac{\partial f}{\partial s_{k\ell}} D^e_{k\ell rs}}{\frac{\partial f}{\partial s_{mn}} \left[D^e_{mnpq} \frac{\partial f}{\partial s_{pq}} - \frac{\partial f}{\partial e^p_{mn}} - \frac{\partial f}{\partial k} \frac{\partial k}{\partial e^p_{mn}} \right]} de_{rs} , \qquad (2\text{-}14b)$$

showing that a linear relationship exists between plastic strain and total strain increments.

A generalization of this expression to singularity (corner) points has been obtained by Koiter[36], but is outside the sco-

pe of the present work.

Using now Eqn. (2-14b) in the incremental form of Eqn. (2-10), and the resulting expression in (2-11), we finally get an expression for the constitutive tensor of Eqn. (2-12), valid at least for elastic-plastic infinitesimal strains, in the elastic-plastic range:

$$D'_{ijrs} = D^e_{ijrs} - \frac{D^e_{ijk\ell} \frac{\partial f}{\partial s_{k\ell}} \frac{\partial f}{\partial s_{tu}} D^e_{turs}}{\frac{\partial f}{\partial s_{mn}} \left[D^e_{mnpq} \frac{\partial f}{\partial s_{pq}} - \frac{\partial f}{\partial e^p_{mn}} - \frac{\partial f}{\partial k} \frac{\partial k}{\partial e^p_{mn}} \right]} . \quad (2\text{-}15)$$

As can be easily verified, this tensor is also hemitropic, enjoying the same symmetry properties listed in Eqn. (2-11b).

2.5.c - PARTICULARIZATION TO VON MISES'S CRITERION[14,31]

Additional information with respect to the yield function f can be given in specific situations. For instance, when von Mises's criterion is considered, which is in accordance with the assumptions previously made,

$$f = J_2 - k^2, \quad (2\text{-}16)$$

J_2 being the second invariant of stress deviation, expressed by

$$J_2 = \frac{1}{2} s'_{ij} s'_{ij}$$

$$= \frac{1}{2} s_{ij} s_{ij} - \frac{1}{6} (s_{kk})^2 , \quad (2\text{-}16a)$$

for which

$$\frac{\partial J_2}{\partial s_{ij}} = s'_{ij} = s_{ij} - \frac{1}{3} s_{kk} \delta_{ij} . \quad (2\text{-}16b)$$

The work-hardening parameter k is obtained under consideration of the flow rule associated with von Mises's criterion. Using Eqn. (2-16b), we can rewrite Eqn. (2-14) as

$$de^p_{ij} = d\lambda \, s'_{ij} .$$

This expression represents the well-known Prandtl-Reuss equations, which constitute the associated flow rule required. In order to give them a practical meaning we have to relate them to some easily performable test, as, for instance, the uniaxial tension or compression test. Functions must be found which correlate stresses and which correlate strains; such functions will be referred to, from now on, as the "effective stress" and the "effective strain". They relate any arbitrary loading/deformation situation with the uniaxial stress-strain curve. As a consequence, the effective stress $\bar{\bar{s}}$ must coincide with the uniaxial tension (or compression) stress. This means that for a certain value of $\bar{\bar{s}}$, plastic yielding must occur; otherwise, $\bar{\bar{s}}$ must be positive and monotonically increasing during the deformation process.

As the second stress deviation invariant enjoys such characteristics, assumption can be made that it would be expressed as a certain power of the effective stress,

$$J_2 = c\,\bar{\bar{s}}^n ,$$

where c and n are constants to be determined. By Eqn. (2-16a), then

$$\bar{\bar{s}} = \left[\frac{1}{2c}\, s'_{ij}\, s'_{ij}\right]^{1/n} .$$

In a uniaxial tension test, $\bar{\bar{s}} = s_{11}$, which implies $n = 2$ and $c = 3$, thus

$$\bar{\bar{s}} = \sqrt{3\, J_2} . \qquad (2\text{-}17)$$

The effective plastic strain $\bar{\bar{e}}^p$ is obtained by equating the plastic work per unit volume,

$$dW^p = s'_{ij}\, d\,e^p_{ij} = \bar{\bar{s}}\, d\bar{\bar{e}}^p ,$$

thus, considering Eqns. (2-17) and (2-16a),

$$d\bar{\bar{e}}^p = \frac{s'_{ij}\, de^p_{ij}}{\sqrt{\frac{3}{2}\, s'_{mn}\, s'_{mn}}}$$

which, using the corresponding flow rule, rewrites to

$$d\bar{\bar{e}}^p = \sqrt{\frac{2}{3}\, de^p_{ij}\, de^p_{ij}}\,. \qquad (2\text{-}18)$$

Drucker has shown that Eqn. (2-18) is reasonably correct for nearly any yielding function of the type $f(J_2, J_3) = 0$. Thus, a more general expression for the plastic strain increments can be obtained by introducing Eqn. (2-14) into (2-18). Presenting general and von Mises's expressions side by side, we have

$$d\bar{\bar{e}}^p = d\lambda\sqrt{\frac{2}{3}\,\frac{\partial f}{\partial s_{ij}}\,\frac{\partial f}{\partial s_{ij}}} \qquad \left(= \frac{2}{3}\,\bar{\bar{s}}\, d\lambda \right)$$

thus

$$d\lambda = \sqrt{\frac{3}{2}}\,\frac{d\bar{\bar{e}}^p}{\sqrt{\frac{\partial f}{\partial s_{ij}}\,\frac{\partial f}{\partial s_{ij}}}} \qquad \left(= \frac{3}{2}\,\frac{d\bar{\bar{e}}^p}{\bar{\bar{s}}} \right) \quad (2\text{-}19a,b)$$

and going back to Eqn. (2-14),

$$de^p_{ij} = \sqrt{\frac{3}{2}}\,\frac{\frac{\partial f}{\partial s_{ij}}}{\sqrt{\frac{\partial f}{\partial s_{mn}}\,\frac{\partial f}{\partial s_{mn}}}}\, d\bar{\bar{e}}^p \qquad \left(= \frac{3}{2}\,\frac{d\bar{\bar{e}}^p}{\bar{\bar{s}}}\, s'_{ij} \right). \quad (2\text{-}20a,b)$$

In a uniaxial test the slope of the stress-strain curve is

$$H' = \frac{d\bar{\bar{s}}}{d\bar{\bar{e}}^p}\,, \qquad (2\text{-}21)$$

so

$$d\bar{\bar{e}}^p = \frac{d\bar{\bar{s}}}{H'}$$

could alternatively be introduced in Eqns. (2-20a,b). Eqn. (2-20b) represents another form of the associated flow rule in von Mises's yield criterion. Restricting ourselves to this criterion, and equating Eqns. (2-19b) and (2-14) we have

$$s'_{mn}\left[D^{e}_{mnpq}\ s'_{pq} + 2k\frac{\partial k}{\partial e^{p}_{mn}}\right] = \frac{2}{3}\frac{\bar{\bar{s}}}{d\bar{\bar{e}}^{p}} s'_{ij}\ D^{e}_{ijrs}\ de_{rs}\ , \quad (2\text{-}22)$$

in which, by Eqns. (2-10, 11, 16b and 19b),

$$s'_{ij}\ D^{e}_{ijrs}\ de_{rs} = \frac{2}{3}\bar{\bar{s}}\ d\bar{\bar{s}} + \frac{3}{2}\frac{d\bar{\bar{e}}^{p}}{\bar{\bar{s}}} s'_{ij}\ D^{e}_{ijrs}\ s'_{rs}\ ,$$

therefore Eqn. (2-22) is simplified to

$$2k\ s'_{mn}\frac{\partial k}{\partial e^{p}_{mn}} = +\frac{4}{9}\bar{\bar{s}}^{2}\ H'\ .$$

On the other side, by the definition given in Eqn. (2-11a),

$$s'_{mn}\ D^{e}_{mnpq}\ s'_{pq} = \frac{4}{3}\ G\ \bar{\bar{s}}^{2}$$

and

$$D^{e}_{ijk\ell}\ s'_{k\ell}\ s'_{tu}\ D^{e}_{turs} = 4\ G^{2}\ s'_{ij}\ s'_{rs}\ .$$

Setting

$$S = \frac{2}{3}\bar{\bar{s}}^{2}\left[1 + \frac{H'}{3G}\right], \quad (2\text{-}23)$$

collecting the results represented by all Eqns. (2-19) and using them into the expression of the constitutive tensor, given by Eqn. (2-15), the well known formula

$$D'_{ijrs} = D^{e}_{ijrs} - \frac{2G}{S}\ s'_{ij}\ s'_{rs} \quad (2\text{-}24)$$

is obtained. Such a constitutive tensor is found to be widely employed in the literature; first introduced by Yamada[37] and subsequently modified by Tanaka[38] to account for kynematic hardening, it was rederived in matrix dressing by Zienkiewicz[23,39]. It should be noted that as only deviatoric components of stress appear in the second (subtractive) part of the left-hand side term of Eqn. (2-24), any changes in volume taking place during elastic-plastic deformation are explained solely in terms of D^{e}_{ijrs}, that is, of the elastic part of the deformation.

It should be stressed that Eqn. (2-12), with the constitutive tensor given by (2-24), is applicable to very small strain increments for, as pointed out by Dieterle[102], the equivalent stresses resulting after successive increments tend to stray away from the prescribed stress-strain curve in an exponential rather than linear manner. Dieterle reckons that an approximate alternative to (2-12), given by

$$ds_{ij} = \frac{H'}{3G} D^{e}_{ijrs} \, de_{rs}$$

allows the consideration of larger increments, but as Cook[103] points out (pg. 296), such procedure bears similitude with the secant modulus approach, and presents the same shortcomings.

Another alternative procedure based in Malvern[32] (pg. 366) by rewriting Eqn. (2-20b) in terms of (2-21), and expressing it, using the chain rule of differentiation, as

$$de^{p}_{ij} = \frac{3}{2 H' \bar{\bar{s}}} \frac{\partial \bar{\bar{s}}}{\partial s'_{rs}} ds'_{rs} \, s'_{ij} .$$

Multiplying both sides of this equation by s'_{ij}, cancelling out the equivalent stress and renaming dummy indices, it finally becomes possible to express the deviatoric stress increments in terms of the plastic strain increments and thus, by (2-20b), of the total deviatoric stresses. Total stress increments are thus finally expressed by

$$ds_{ij} = K \, de_{kk} \, \delta_{ij} + \frac{d\bar{\bar{s}}}{\bar{\bar{s}}} s'_{ij} , \qquad (2\text{-}20c)$$

K being the bulk modulus of the material at the relevant temperature, given by

$$K = \frac{E}{3(1 - 2\nu)} .$$

2.5.d - FINITE STRAIN

A constitutive equation must satisfy a series of axiomatic requirements[28,29,32,40]. Among others it must be admissible and materially objective. Admissibility means consistency with the

basic principles of Continuum Mechanics (conservation of mass and energy, balance of momenta and Clausius-Duhem inequality). Material objectivity, or material frame indifference, requires the constitutive equation to be invariant with rigid body motions of the spatial (Eulerian) coordinates. In future references the prefix "material" will be droped, but it will be understood that objectivity is required with respect to the Lagrangean coordinate system.

Eqn. (2-12) is not objective. It detects, or is affected by, rigid body rotations of a stressed body, and changes the stress tensor even when the state of stress remains unchanged. Considering, as a simple clarifying example, a bar pulled by a constant axial force whilst rotating about the X_3 axis: at one moment the bar is parallel to the X_1 axis, therefore

$$s_{11} \neq 0 \qquad \text{and} \qquad s_{22} = 0 ,$$

while later, when it is parallel to the X_2 axis,

$$s_{11} = 0 \qquad \text{and} \qquad s_{22} \neq 0 .$$

Of course, the state of stress in the bar remains unchanged during the process. The stress increments appearing in Eqn. (2-12) are not frame indifferent, and the reason is because (at finite strains) the strain increment tensor does not vanish under rigid body rotations. In an objective formulation, therefore, Eqn. (2-12) must be replaced by an alternative incremental stress-strain relation, if finite strains are to be considered. This requires the use of a frame indifferent measure of strain.

The deformation tensor (in total or incremental form) presents such an invariance, and will thus be used in an equation formally similar to (2-12), supplying a new definition of stress increments, somehow related to the stress increments given by that equation. We write

$$\Delta s_{ij}^{FI} = D'_{ijrs} \Delta \epsilon_{rs} , \qquad (2-25)$$

where the Δs_{ij}^{FI} are frame independent stress increments. The ques-

tion now is to relate these stress increments to the ones obtained from Eqn. (2-12). As Oldroyd[41] has shown, this can, in principle, be done in an infinite number of ways. A restricted number of proposed formulae is commonly mentioned in the literature[29-31], and presented as definitions of frame invariant stress increments (rates). Some of them are listed here:

$$\Delta s^{J}_{ij} = \Delta s_{ij} - s_{ik}\Delta\omega_{jk} - s_{jk}\Delta\omega_{ik} \qquad (2\text{-}26a)$$

(Jaumann[42])

$$\Delta s^{O}_{ij} = \Delta s_{ij} - s_{ik}\Delta u_{j/k} - s_{jk}\Delta u_{i/k} \qquad (2\text{-}26b)$$

(Oldroyd[41], Green[46,47])

$$\Delta s^{T}_{ij} = \Delta s_{ij} - s_{ik}\Delta u_{j/k} - s_{jk}\Delta u_{i/k} + s_{ij}\Delta u_{k/k} \qquad (2\text{-}26c)$$

(Truesdell[43-45])

$$\Delta s^{CR}_{ij} = \Delta s_{ij} + s_{ik}\Delta u_{k/j} + s_{jk}\Delta u_{k/i} \qquad (2\text{-}26d)$$

(Cotter-Rivlin[48])

Oldroyd[41] observes that the difference between any two acceptable definitions of frame indifferent stress increments (rates) consists of terms that could anyhow appear in a constitutive equation of the type of (2-25). However, he also notes that further restrictions imposed by the structural model or by the material behaviour, as verified experimentally, may lead to the necessary choice of one of the several alternatives. In the case of a visco-elastic fluid he shows that two specific definitions lead to completely different predictions for the behaviour of the fluid, one of which is the one verified experimentally.

2.6 - STRESS-STRAIN RELATION (LAGRANGEAN)

In order to give a Lagrangean equivalent to the frame indifferent Eqn. (2-25), we must relate Kirchhoff stress increments to Green strain increments. Both these definitions are obviously frame indifferent. By similarity with Eqns. (2-11, 12, 25) we assume

$$\Delta S_{ij} = D_{ijrs} \Delta E_{rs} , \qquad (2\text{-}27)$$

the task being to find an expression for D_{ijrs} . We start by writing Eqn. (2-9a) in incremental form. In those circumstances

$$\Delta S_{ij} = J X_{i/r} X_{j/s} \Delta s_{rs} + J X_{i/r} \Delta X_{j/s} s_{rs} +$$
$$J \Delta X_{i/r} X_{j/s} s_{rs} + \Delta J X_{i/r} X_{j/s} s_{rs} ,$$

and as, from Eqns. (2-8a,b),

$$\Delta X_{i/r} = - X_{i/k} \Delta u_{k/r} \qquad (2\text{-}28a)$$

and

$$\Delta J = J \Delta u_{k/k} , \qquad (2\text{-}28b)$$

these stress increment components rewrite as

$$\Delta S_{ij} = J X_{i/r} X_{j/s} \left[\Delta s_{rs} - s_{rk} \Delta u_{s/k} - s_{ks} \Delta u_{r/k} + s_{rs} \Delta u_{k/k} \right]$$

and comparing with the set of equations (2-26), we conclude that

$$\Delta S_{ij} = J X_{i/r} X_{j/s} \Delta s^{T}_{rs} \qquad (2\text{-}29)$$

and that the applicable definition of frame invariant stress increment is Truesdell's. Eqn. (2-25), therefore, rewrites to its final form

$$\Delta s^{T}_{ij} = D'_{ijrs} \Delta \epsilon_{rs} . \qquad (2\text{-}30)$$

As, from Eqn. (2-4),

$$\Delta \epsilon_{rs} = X_{i/r} X_{j/s} \Delta E_{ij} , \qquad (2\text{-}31)$$

we can rewrite (2-30) to

$$\Delta s^{T}_{ij} = D'_{ijrs} X_{p/r} X_{q/s} \Delta E_{pq}$$

which, when substituted into (2-29) and compared with (2-27) gives

$$D_{ijrs} = J\, X_{i/m}\, X_{j/n}\, X_{r/p}\, X_{s/q}\, D'_{mnpq}\,, \qquad (2\text{-}32)$$

which is the Lagrangean constitutive tensor. In this expression, D'_{mnpq} is obtained from Eqn. (2-24), and the Jacobean and coordinate derivatives from Eqns. (2-8a,b).

It should be noted that the symmetry properties enjoyed by the Eulerian constitutive tensor are conserved by Eqn. (2-32), and the Lagrangean tensor is thus also hemitropic.

2.7 - ADDITIONAL REMARKS

It should be noted that the Lagrangean constitutive tensor presented in Eqn. (2-32) is in disagreement with the expression

$$J\, X_{i/m}\, X_{j/n}\, X_{r/p}\left[D'_{mnpq}\, X_{s/q} + s_{mn}\, X_{s/p} - s_{mp}\, X_{s/n} - s_{np}\, X_{s/m}\right], \qquad (2\text{-}32a)$$

achieved by Hibbitt et al[49]. The reason for the discrepancy lies in the fact that they used Jaumann's definition of frame indifferent stress increment - Eqn. (2-26a) - instead of Truesdell's - Eqn. (2-26c) - in Eqn. (2-30). The additional terms exhibited by (2-32a), with respect to (2-32), are due to the difference between these two definitions, as Truesdell's appears naturally in the derivation of Eqn. (2-29).

We base our result in Oldroyd's remarks, presented at the end of sub-section 2.5.d . A further justification can be derived by considering infinitesimal deformation. In that case

$$X_{i/j} \cong \delta_{ij}\,, \qquad J \cong 1 \qquad \text{and} \qquad \Delta u_{i/j} \cong 0\,,$$

and Eqn. (2-32) reduces to

$$D_{ijrs} = D'_{ijrs}\,,$$

whilst Eqn. (2-26c) reduces to

$$\Delta s^{T}_{ij} = \Delta s_{ij} .$$

As should be expected, it becomes immaterial whether an Eulerian or Lagrangean description is used. The same conclusion cannot be obtained from Hibbitt's approach for, although

$$\Delta s^{J}_{ij} = \Delta s_{ij} ,$$

Eqn. (2-32a) reduces to

$$D_{ijrs} = D'_{ijrs} + s_{ij}\,\delta_{rs} - s_{ir}\,\delta_{sj} - s_{jr}\,\delta_{si} .$$

The constitutive tensor, therefore, is not conserved when the description is changed, and infinitesimal strains are considered. Besides, the Lagrangean tensor is no longer hemitropic, as it now is symmetric in the first pair of indices only.

Hibbitt and his associates[49] anticipated these conclusions and tried to justify them by arguing that when plastic deformation is considered the conventional small strain formulation is not necessarily recovered as a limiting case of the geometrically nonlinear formulation. It should be noted, however, that Eqn. (2-32a) could be used, with D^{e}_{mnpq} replacing D'_{mnpq}, to the analysis of large purely elastic deformations, as could be the case in the study of shells; even then, however, the small strain formulation would not be retrieved from Eqn. (2-32a).

We are aware of Prager's assertion[104] that only Jaumann's definition of frame invariant stress rate satisfies the condition that the yield function should be stationary when the stress rate vanishes. But he concludes the same paper by saying that this definition should therefore be "preferred". We have used Jaumann's definition at the early stages of the development of our program, but, in despite of considerable additional computational effort, no substantial discerning effect was observed with respect to comparison runs using Truesdell's definition, as introduced in the preceding section.

It is true, of course, that the comparison was extended over a small range of deformation only, due to implementation problems of the whole program; and we are also aware of the fact that Kitagawa and Tomita[91] report substantial differences when using either Jaumann's or Oldroyd's definitions. But our decision to use the more elegant and computationally more economical alternative is justified not only by its already mentioned reducibility to the infinitesimal theory when the relevant assumptions are made. The procedure is not original: previous works by Truesdell[44,45] and Green[46,47] use the definitions given by Eqns. (2-26c) and (2-26b) respectively; their results are presented and discussed by Eringen[29], and justified in terms of "mere convenience". Spencer and Ferrier[105] reason that, at least for two examples they consider (simple shear and simple torsion of incompressible materials), change from one definition to another introduces only second-order effects on the solutions, the choice becoming thus, in their words, "a matter of mathematical convenience". Hill[106] seems to agree with such conclusion when he states that the choice of a frame-invariant definition of stress rate is largely "a matter of taste and convenience".

In the previous sections dealing with finite deformation we used concepts of Truesdell's theory of hypoelasticity[44] in the analysis of plastic deformation. The similarity of hypoelastic and plastic constitutive equations allows such an extrapolation, and the close relationship between hypoelasticity and Prandtl-Reuss plasticity has already been established in a specific example by Truesdell[45]. Green extended his conclusions for both compressible[46] and incompressible[47] work-hardening materials. A comparative study is presented by Eringen[29] and additional comments can be found in Olszak et al[107].

2.8 - VIRTUAL VELOCITY EQUATION

The fundamental equation for the equilibrium of an element of a subsection of a continuum is obtained from the virtual velocity equation. The conservation of energy for an element of volume, at a certain moment of time t, is expressed, in the Eulerian description, by

$$\int_A T_i \, v_i \, dA + \int_V F_i \, v_i \, dV = \int_V s_{ij} \, V_{ij} \, dV ,$$

where T_i are the components of surface force per uni, of current surface area, and F_i are the components of body force per unit of current volume, both at time t. The remaining terms are the ones defined in Sections 2.3 and 2.4.

For the purposes of this work, however, it will be preferable to express this equation in Lagrangean form, that is, to refer it to the material coordinates and variables. By Eqns. (2-6a, 31 and 9b), and considering that the Jacobean is a measure of changes in volume, we can write, successively,

$$\int_V s_{ij} \, V_{ij} \, dV = \int_V \frac{1}{J} \, x_{i,r} \, x_{j,s} \, S_{rs} \, X_{m/i} \, X_{n/j} \, \dot{E}_{mn} \, dV$$

$$= \int_{V^o} S_{ij} \, \dot{E}_{ij} \, dV^o ,$$

where the upper dot stands for time derivative. Introducing equivalent forces T_i^o per unit initial surface area, and F_i^o per unit initial volume, defined by

$$T_i^o = T_i \frac{dA}{dA^o} \qquad \text{and} \qquad F_i^o = F_i \frac{dV}{dV^o} ,$$

we finally rewrite the equation for the conservation of energy in the required Lagrangean form

$$\int_{A^o} T_i^o \, v_i \, dA^o + \int_{V^o} F_i^o \, v_i \, dV^o = \int_{V^o} S_{ij} \, \dot{E}_{ij} \, dV^o . \quad (2\text{-}33)$$

This is the virtual velocity equation to be used as basis for the derivation of the stiffness equation required in the finite element formulation.

CHAPTER 3

A FINITE ELEMENT FORMULATION FOR THE ELASTIC-PLASTIC ANALYSIS OF PROBLEMS OF LARGE STRAINS AND LARGE DISPLACEMENTS

3.1 - REVIEW OF LITERATURE

3.1.a - INTRODUCTION: TWO CONCEPTUAL APPROACHES

The first applications of the Finite Element Method to elastic-plastic problems appeared over a decade ago and were restricted to infinitesimal strains, in general describing only the onset of plastic deformation. In those circumstances the equilibrium equations of Continuum Mechanics[28-32], in the absence of body forces, could be reduced to

$$\sigma_{ij,j} = 0 ,$$

as the distinction between Eulerian and Lagrangean derivatives becomes immaterial, and, by means of Eqns. (2-12 and 5a), rewritten to

$$D'_{ijrs} (\Delta u_{r,sj} + \Delta u_{s,rj}) = 0 . \qquad (3\text{-}1)$$

Alternatively, considering that the plastic strains do not cause change in the state of stress, i. e.

$$\Delta s_{ij} = D'_{ijrs}\,\Delta e_{rs} = D^{e}_{ijrs}\,\Delta e^{e}_{rs}$$

$$= D^{e}_{ijrs}\,(\Delta e_{rs} - \Delta e^{p}_{rs}),$$

using Eqns. (2-5a and 11a) and considering the incompressibility during plastic deformation, the equilibrium equations could be re-written to

$$\Delta u_{i,jj} + \frac{1}{1-2\nu}\Delta u_{j,ij} = 2\,\Delta e^{p}_{ij,j}. \qquad (3\text{-}2)$$

Eqns. (3-1, 2) constituted the basis of two different lines of approach followed in the earlier papers on the subject. The close relationship between them, as shown above, was only observed more recently, first in the original matrix formulation, by Marçal[50], and later in the more elegant tensor formulation in an as yet unpublished work by Blomfield[51].

The approach based on Eqn. (3-2) was proposed in 1959 by Mendelson and Manson[52] which, considering that the plastic strain increments in the equation can be treated as thermal strains, referred to it as the thermal strain approach. Subsequent papers eventually refer to the initial strain method or, in a modified form, to the initial stress approach. The underlying idea of this method, as already mentioned, is that the equations of equilibrium can be modified to compensate for the fact that the plastic strains do not cause any change in stress. Gallagher et al[53] used this approach in the analysis of stress distributions in heated plates of complex shape; their main interest was to obtain more accurate information on the factors affecting the failure processes of such structural elements. Argyris et al[54] also had structural problems in mind.

The tangent modulus approach, based on Eqn. (3-1), was first used by Pope[55] and Marçal[56], and extensively applied by Marçal and his associates[57-59]. In Ref. (59) it is referred to as

the partial stiffness method. Zienkiewicz[39] calls it the incremental elasticity or the incremental plasticity method. Again with this approach, design considerations were the main scope of earlier works. Pope[55] dealt with aircraft structures. Akyuz and Merwin[60] considered contact problems and improved the accuracy of the solutions by using a half-step Runge-Kutta-like procedure. Lee and Kobayashi[61] also considered contact problems and compared experimental with computed results; the same authors, in another work[62], dealt, however, with axisymmetric upsetting, using the same formulation. In both cases they refer to the possibilities of the finite element method for such class of problems, but remark that there are questions still to be solved, in order to improve the accuracy of the solutions, especially when large strains are present. Scharpf[63-65] also uses a finite element formulation for elastic-plastic problems, and analyses three different convergence criteria; application is made to the spreading of the plastic zone in a plate with a central straight crack but, as changes in geometry were not considered, the computation had to be interrupted when the deformation became considerable. In (65) the subject is expanded, and the tangential stiffness, initial strain and initial stress methods are again compared, by studying the convergence of each one of them in one application case.

Two papers using the tangent modulus approach deserve a closer analysis. Marçal and King[59] compare finite element solutions in certain two-dimensional stress concentration problems with known solutions obtained by other methods and by other authors, or with known experimental results. Although good agreement was obtained in general, the analysis of the deformation had to be interrupted at some stage because negative plastic strains were obtained. Yamada[37] modified their algorithm and used it to predict collapse conditions in certain categories of problems; again the procedure had limited application for the same reason mentioned above. A closer comparison of the algorithms used by Marçal and King[59] and Yamada et al[37] will be given in the next subsection.

Blomfield[51] has shown the similarity of the thermal strain and tangent modulus approaches by deriving them both in

terms of rate instead of incremental equations; results obtained in the elastic-plastic analysis of pipe bends show no significant discrepancies when one or other approach is used. Marçal[50] compared the two approaches in the case of a flat plate and stringer in tension and compared them with existing solutions. He has shown that although the constitutive tensor must be recomputed for every load increment, the tangent modulus approach can be more economical, in computation time, than the thermal strain approach. In the specific example, in order to obey the prescribed stress-strain curve, only ten increments in load were required by tangent modulus, against 2300 required by thermal strain. Marçal has also shown that, whilst the thermal strain approach is not applicable for perfect plasticity, nor even for nearly perfect plasticity, the tangent modulus method does not present such restriction. This can be envisaged easily from the analysis of Eqns. (3-1, 2). The constitutive tensor in (3-1) is expressed by Eqn. (2-24), with the denominator given by (2-23). For perfect plasticity, $H' = 0$ and the denominator is still defined; no problem arises from the use of Eqn. (3-1). In the thermal strain approach, however, the plastic strain increments are computed by an expression obtained by the substitution of Eqn. (2-21) into (2-20b), giving

$$e^p_{ij} = \frac{3}{2} \frac{\Delta \bar{\bar{s}}}{\bar{\bar{s}}\, H'} s'_{ij} ,$$

which obviously becomes undefined for perfect plasticity. To overcome this limitation, Zienkiewicz et al[39] rewrite Eqn. (2-12) in terms of the deviatoric components of stress and strain increments, ultimately obtaining

$$e^p_{ij} = \frac{3}{2} \frac{1}{\bar{\bar{s}}^2} \frac{s'_{ij}\, s'_{rs}}{\left[\frac{H'}{3G} + 1\right]} \Delta e'_{rs} ,$$

by use of Eqns. (2-24) and (2-11a).

Yamada's work[37] has influenced several Japanese investigators. Iwata et al[66] applied the same formulation to the analysis of hydrostatic extrusion and were able to describe the spreading of the plastic zone; some of their results seem to be unexpected, but in general the agreement with known (e. g. slip-line) solu-

tions can be considered satisfactory; the need for improvements in the method is stressed by the authors. Nagamatsu et al[67] studied the compression of a prismatic block, but were able to describe only the beginning of the deformation; although the plastic zone propagated over nearly the whole block, the maximum strain achieved was less than 0.13%. In a subsequent work[68] the same authors modified their formulation, introducing the updating of the geometrical matrices after each load increment. They were able to analyse the deformation for strains up to the order of 5% for full, and 4% for hollow cylinders, thus covering the elastic, elastic-plastic and fully plastic ranges. The authors claim that still larger values of strain could be considered, but they have not done so in order to save computing time. Unusually large values of computed friction coefficients are attributed by them to deffects in the analysis, to be corrected in a promised subsequent work.

Geometric non-linearities, as considered by Nagamatsu et al[68], were also treated by Argyris[54], Mallett and Marçal[69], Felippa[70] and Turner et al[71], but their solutions were restricted to small strains. Oden[72,73] imposes no such restriction, but deals with elastic and viscoelastic problems only.

Zienkiewicz et al[39] introduced what they called the initial stress approach, to overcome the computing difficulties of the tangent modulus approach, to be analysed in the next subsection, together with this new approach, and to overcome the limitations of the thermal strain approach at nearly perfect plasticity. To show the capabilities of the method, the authors present results for some stress concentration problems in civil engineering, and compare some of them with results presented in (59), showing good agreement.

A subsequent work by Nayak and Zienkiewicz[74] expands on the subject and condenses a series of results obtained by Nayak[75] in the analysis of pressure vessels, plane strain extrusion and indentation. In the extrusion case, von Mises and Tresca criteria are considered, and the results agree closely with experimental ones, presented by Johnson and Mellor[76]. Nayak's work

provides extensive review of literature and covers applications of the finite element method to a wide variety of fields: elastic-plastic problems, plate theory, complex material behaviour and analysis of large deformations in structural elements. It also covers thoroughly the state of knowledge related to each field of application.

3.1.b - THREE ALGORITHMS

Three algorithms have found wider application in the literature extending the finite element method to nonlinear problems. Two of them were proposed in the already mentioned works by Yamada et al[37] and by Marçal and King[59], and are based in the tangent modulus approach. The other one is presented in the work of Zienkiewicz et al[39] and constitutes a modification of the thermal strain approach. Nayak[75] analyses alternatives of these algorithms and we refer the interested reader to his work.

In Yamada's formulation, small load increments are prescribed, and they are adequately rated in order to exactly yield one, or a few, of the remaining elastic elements in the continuum. The procedure is schematized in Fig. 3-1 for a set of three elements. In the first graph, the first load increment is described. Points $A = B = C$ represent the original (unloaded or undeformed) situation of the three elements. An arbitrary load system is then applied, and the elastic solution is obtained, bringing the three elements to A', B' and C', respectively. In general, none of the elements will exactly yield. However, if all loads are multiplied by the factor

$$r = \min \left(\frac{k_o}{\bar{\bar{s}}} \right),$$

the minimum being taken in respect to all elements, all the incremental variables will be multiplied by this same factor (due to the linear relationships existing between them), and the state of stress and strain will now be represented by A'', B'' and C'', with C'' exactly yielding. In the second plot, points A, B, C represent

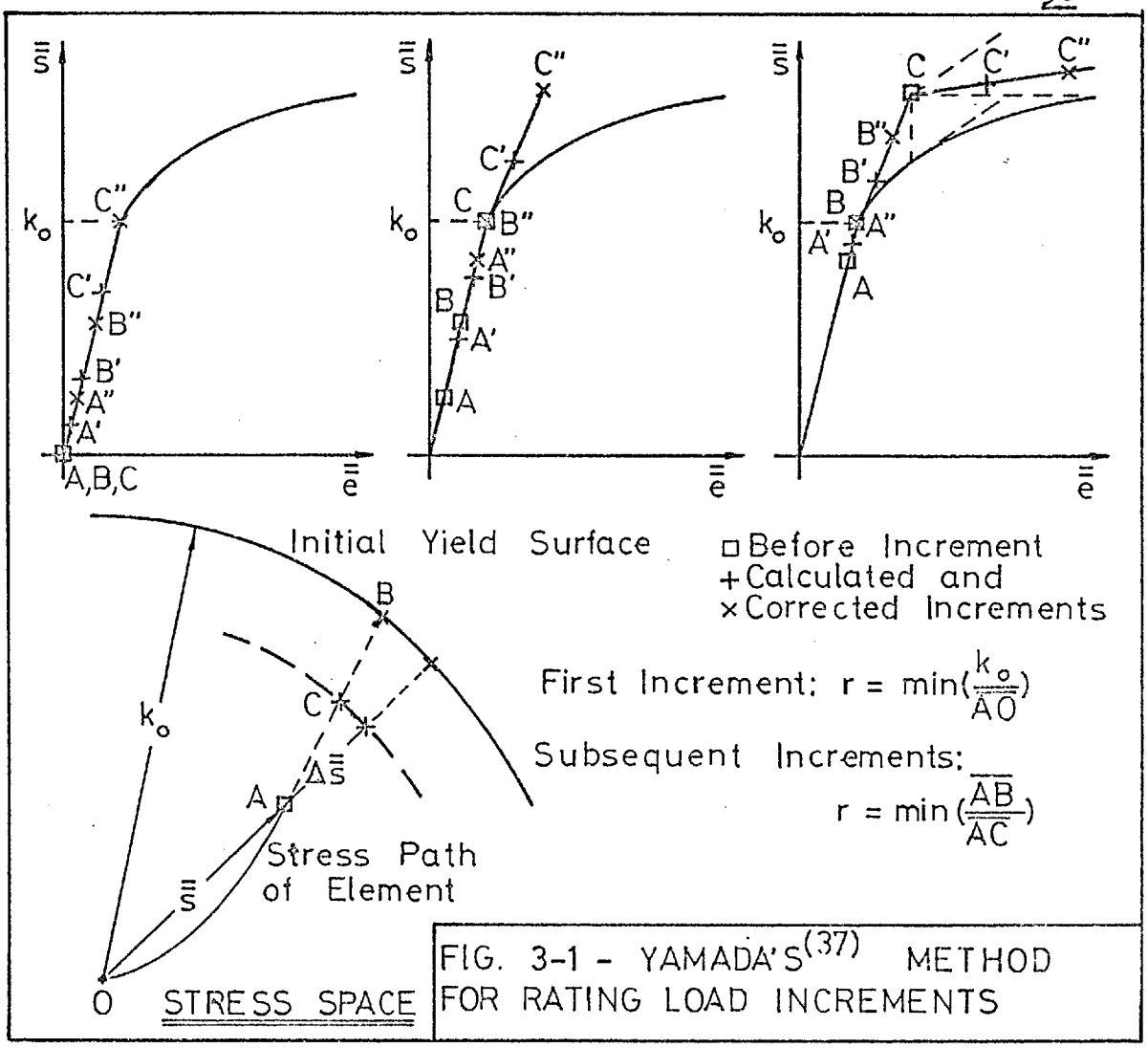


FIG. 3-1 - YAMADA'S[37] METHOD FOR RATING LOAD INCREMENTS

the situation achieved after the first load increment. A similar procedure is again applied: for some arbitrary load increments, the state of stress and strain is represented by A' , B' , C' , with C' following a tangent extrapolation to the flow curve; a correction factor is obtained, as a minimum of the correction factors computed for all elements still in the elastic range, and the new final situations, A" , B" and C" are obtained. This procedure is repeated several times, with at least one element yielding each time. Obviously, the tangential extrapolation of the flow curve, for the yielded elements, will produce substantial errors in the stresses, after a certain number of load increments. Swedlow[77] suggests that a local error at the first load increment into the plastic range (when the slope of the flow curve is maximum) can be accepted, and in subsequent increments an automatic correction can be introduced by

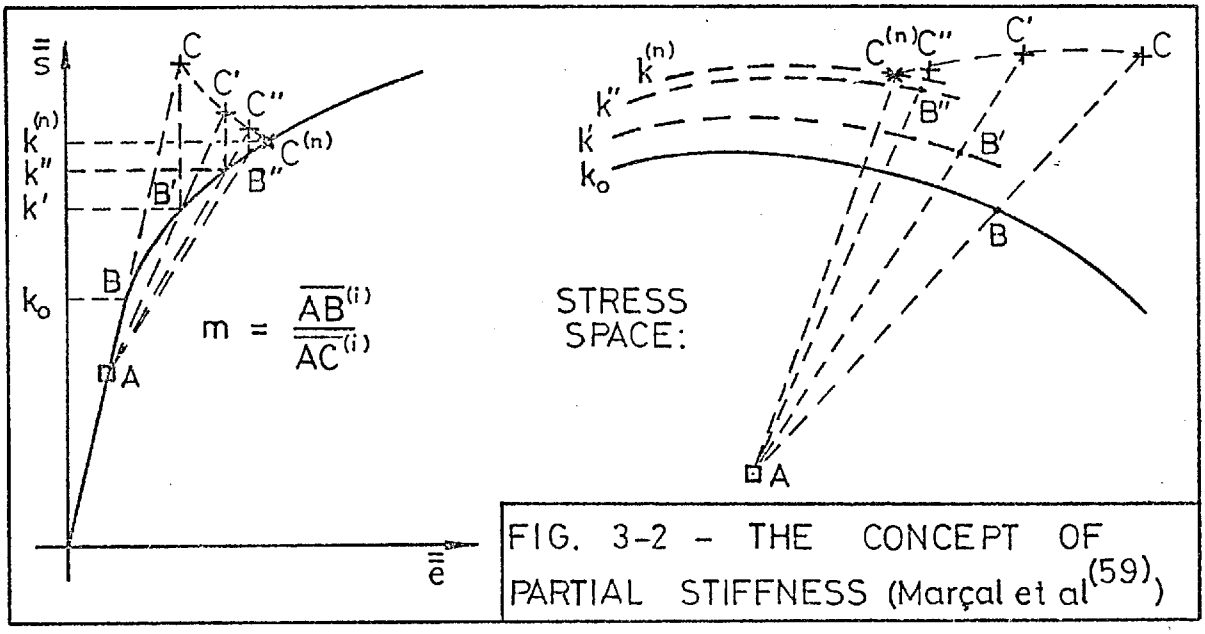


FIG. 3-2 - THE CONCEPT OF PARTIAL STIFFNESS (Marçal et al[59])

underestimating the slope, as shown for point C'' in the third plot of Fig. 3-1. The procedure is also shown in the stress space, at the bottom of Fig. 3-1, to justify the expressions for the correction factors.

Marçal and King[59] prescribe large load increments, for which several elements are expected to yield. The procedure is shown schematically in Fig. 3-2, for one element only, entering the plastic range in the next load increment. Elements staying in the elastic range, or already inside the plastic range, offer no special problem. For the element under consideration, elastic loading brings the image of the stress-strain situation for the element from A to C, well above the expected value for the deformation increment achieved. Marçal uses the relative elastic strain increment

$$m = \frac{\Delta e^e}{\Delta e^e + \Delta e^p}$$

to assemble a modified constitutive tensor

$$D''_{ijrs} = m\, D^e_{ijrs} + (1 - m)\, D'_{ijrs},$$

with which the "partial stiffnesses" are computed. The same load increment is again considered, and point C' obtained, instead of C.

The weight factor m is redefined, using the formula given in the figure, and the procedure repeated, until convergence is obtained, three or four times, according to the authors. Guha[78] claims that the process can be accelerated, and convergence obtained in only one or two iterations, by underestimating m . In his analysis of hydrostatic extrusion he does it by 15 to 20%.

Yamada's procedure can be uneconomical because of the large number of small load increments required to bring the elements into the plastic range. Marçal's, on the other hand, requires a small number of load increments, but everyone of them requires an additional iterative procedure, with a new stiffness matrix computed at each iteration. Even using Guha's acceleration, computing times may become very large.

Zienkiewicz's initial stress method[39] tries to overcome these computing drawbacks by using a thermal strain approach associated with large load increments. The method is based on the recognition that - even when ideal plasticity is considered - the increments of strain define uniquely the stress system, while the converse is not true for ideal plasticity. It is schematized in Fig. 3-3.

In this method a purely elastic solution is first obtained; because of the nonlinearity of the problem, the stresses obtained will not be the correct ones for the strain found. The excess stress components are assumed to be equilibrated by a set of forces, and the idea of the method consists in removing these excess stresses and considering the equilibrating forces as a subsequent load increment. The routine of the method can be summarized as follows:

a) For the prescribed load increments an elastic solution $(\Delta\hat{s}_{ij}, \Delta e_{ij})$ is obtained;

b) The existing stresses s_{ij} are updated, giving a set of interim stresses for which the range will be checked. If still elastic, variables are considered as definitively updated; otherwise,

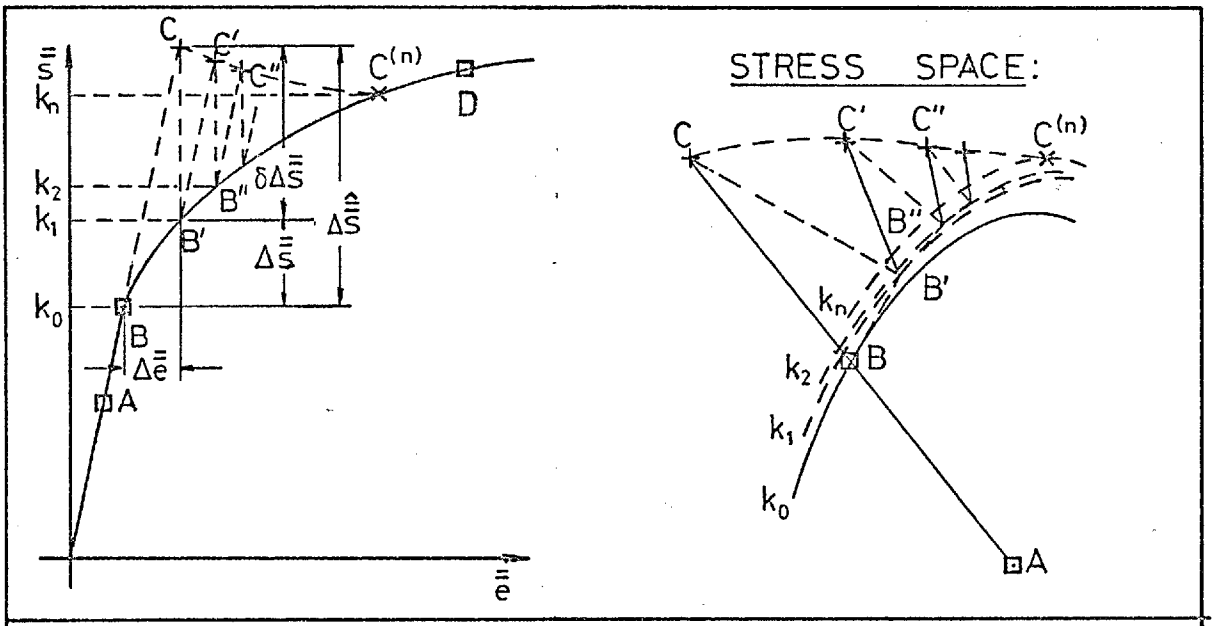


FIG. 3-3 - INITIAL STRESS METHOD (Zienkiewicz et al[39])

c) Stress increments are computed from the strain increments, according to the equation

$$\Delta s_{ij} = D'_{ijrs} \Delta e_{rs}$$

for all elements already in the plastic range (such as D in Fig. 3-3), and rated accordingly for elements for which the increment will be partially elastic and partially elastic-plastic (such as A in the figure). In any case, the differential (excess) stresses

$$\delta\Delta s_{ij} = \Delta\hat{s}_{ij} - \Delta s_{ij},$$

are calculated, stresses are updated (with Δs_{ij}), and so are the strains;

d) Using the force-stress relatioship, the forces equilibrating $\delta\Delta s_{ij}$ are obtained;

e) The procedure is repeated until convergence is reached;

f) The yield stress is updated and a new load increment considered.

The method provides a lower bound solution and can be seen, from the description given, to follow the thermal strain approach. The elastic constitutive tensor and stiffness matrix are used to solve the equilibrium equations, and the elastic-plastic constitutive tensor is only used to determine the differential stresses, or "initial stresses", as they are designated in the paper. In that way, the authors argue, there is no need to assemble a new stiffness matrix after each load increment. This will not be strictly true in a Lagrangean formulation, as can be seen immediately from Eqn. (2-32). However, a similar reasoning can be used in conjunction with the tangent modulus approach, to correct stresses extrapolating the flow curve. A set of forces equilibrating the excess stresses can be considered for a subsequent load increment, stresses being previously replaced by the expected ones. This possibility will be explored further later in this chapter.

3.1.c - RECENT TRENDS

Most of the literature reviewed so far is concerned with small strain plasticity, therefore predicting the onset of yielding and the early spreading of the plastic zone with satisfactory levels of accuracy. Larger strains can either not be tackled or, as in Nagamatsu's approach[68], require a heavy penalty in terms of computing time.

In recent years a trend towards the use of non-linear equations of Continuum Mechanics has been observed in the papers on finite element analysis, following the pioneering work by Wissmann[27]. Pian and Pin Tong[79] have compared several variational principles and applied them to plate bending analysis. Yaghmai[80] formulated a theory for the incremental analysis of large deformations and applied it to shells of revolution. Oden[81] provides a continuum mechanics theory for finite elements; most of his work is now collected in Ref. (40). Marçal[82] used incremental equa-

tions to form the basis for a general purpose program for non-linear analysis. Tanaka[38], although not using finite elements, produced an algorithm for the solution of elastic-plastic problems, considering isotropic and kinematic work-hardening; he analysed the deflection of plates under several edge conditions, using finite differences, and was able to study the onset of the elastic-plastic deformation, obtaining good agreement with experimental results, in general; discrepancies observed in the later stage of the calculation are attributed to the fact that the ratio between isotropic and kinematic work-hardening varies during deformation, whilst the formulation assumed it to remain constant. This formulation is readily prepared for implementation in finite element terms.

Hibbitt, Marçal and Rice[49] use Ref. (82) as the basic material to propose a formulation for large strains and large displacements, applicable to elastic-plastic problems, though restricted to isotropic material behaviour. However, they do not consider large strains in the sense of Lee[33]. The necessity is recognised of considering additional stiffness terms, accounting for the effect of initial displacements, initial stresses and initial loads; the first two terms appear originally in (82), and the initial load stiffness term in a work by Oden and Key[83]. The overall stiffness matrix is obtained as a linearisation of element equilibrium defined by virtual velocity equations. The development is made in a Lagrangean (initial coordinate) frame of reference, and will be shown later in this chapter. A restriction to this work, however, has already been presented in Section 2.7.

A similar approach is presented by Gordon and Weinstein[84]. They examine plane strain sheet drawing, considering smooth and friction boundary conditions, using a Lagrangean description based in a variational approach presented by Biot[85]. Only two stiffness terms are considered, and no reference is made to the effect of initial loads and initial displacements upon the stiffness, as will be the case in the present formulation and as verified, for instance, by Hibbitt et al[49]. The absence of the initial displacement term is justified by the simplified expression - incorrect

in our opinion - taken for Green's strain increments, which led, ultimately, to an infinitesimal strain formulation. The authors, however, claim to describe the progress of the yielding process in the deformation zone, and justify their results by comparing them with the ones provided by Sach's theory of drawing, at intermediate levels of the relative thickness reduction. Discrepancies at small and very large values of the relative thickness reduction are justified in terms of the inadequacy of Sach's solution at extreme situations.

A previous paper by Hofmeister, Greenbaum and Evensen[86] also considers only two stiffness terms, but uses a mixed description initial strain approach based on Felippa[70] and on a variational principle presented by Washizu[87]. In despite of the reference to Green's strains, the algorithm seems to offer little progress with respect to Nagamatsu's[68] work. Application is made to a series of stress concentration problems, and also to plate bending, but is restricted, in general - and in despite of the title of the paper - to small strains (up to 0.006 in one application example).

In recent years extensive work in the field of elastic-plastic analysis by the finite element method has been carried out by Japanese investigators, and part of it has been published in Japanese only. Some of it has been mentioned in the previous subsection. An interesting survey, together with the analysis of the typical difficulties encountered has been presented by Kudo and Matsubara[88]. Special reference must be made to an ambitious paper by Kitagawa, Seguchi and Tomita[89], which analyses the problem of a finite element formulation similar to the one presented by Hibbitt et al[49], but referred to the current configuration of the continuum. They use a convected coordinate system embedded in the body and follow approximately the same path described in (49). In their conclusions, however, it is seen that with such a frame of reference, the initial displacement stiffness term disappears (a result already advanced in (49)), but additional terms appear. One term must be added to the stiffness to account for changes in the surface of the elements during the incremental deformation,

and one term must be added to the nodal forces, to correct body forces due to change of the base vectors during the incremental deformation. It appears, however, that these terms do not represent an additional effect, neglected or disregarded in the previous literature, but are inherent to the Eulerian description. This can be justified formally by regarding that in the Lagrangean description the integrals are computed with respect to the undeformed geometry. In a further paper the authors consider a two-dimensional restriction of the formulation[90], which is then implemented in a computer program and applied to the analysis of certain stress concentration problems in notched and perforated specimens[91]. Unfortunately, this application has been published in Japanese only; however, according to the abstract[91a], it seems that the results obtained are not satisfactory in the large strain range, and it is hinted that the reason lies in the definitions of stress and strain employed. As the authors use Jaumann's definition of frame invariant stress increments, the considerations of Sections 2.6 and 2.7 of the present work could possibly apply.

Osias[92-94] also contributes to the subject and expands previous work for infinitesimal strains by Swedlow[95-96], using an Eulerian approach, placing no restriction on the amount of deformation, assuming isotropic work-hardening material. Flow is analysed as a history dependent process, for which a computing program (FIPDEF) is developed. Numerical solution is obtained for a number of problems: simple extension, simple rotation (up to 45°) and combined extension and rotation in a prismatic volume element, under plane stress and plane strain conditions, and later to the problem of necking in flat tensile bars. Results in the first case agree closely with known solutions. The necking results agree qualitatively with previous results on the subject, listed by the author.

Swedlow[97] presents a general theory of elastic-plastic flow, capable of accomodating special features like work-hardening, anisotropy, plastic compressibility and others, and analyses strategies for solving the resulting quasi-linear equations. In another paper[77], restriction is made to a von Mises work-hardening material, and the torsion of a prismatic bar is studied. The formulation is amenable to analytical or numerical integration (by the gi-

nite element, finite differences or boundary integral methods). Perfect plasticity and rigid elasticity are not covered. Computer programs based on the formulation are claimed to be economical.

Different approaches have been tried in recent papers by Zienkiewicz and his associates[98-100]. Zienkiewicz and Godbole[98] use a stream function formulation to describe large deformation in plastic and visco-plastic conditions. A finite element solution is found for the non-Newtonian flow problem, and application is made to the analysis of steady state extrusion and non-steady state punch indentation. In the extrusion case they improve results obtained by Nayak and Zienkiewicz[74,75], although at the cost of using a finer mesh; the extrusion pressure is however still above that given by the slip-line solution. The indenting pressure, in the non-steady state application, is shown to be linearly dependent on the depth of penetration, and above the small deformation or slip-line solutions. The need for refinements in practical applications is stressed by the authors, and the possibility of achieving this by simultaneously solving the temperature variation in the continuum under investigation, by not neglecting convective acceleration and by considering dynamic effects upon the visco-plastic coefficient are shown.

Zienkiewicz and Cormeau[99] derive plasticity and creep solutions using a visco-plastic model of the continuum, coupled with the initial strain method. Non-associated plasticity can be treated by this approach. Applications, however, are restricted to structural engineering problems. In a stress concentration application (perforated strip) plastic strains of the order of 0.03 are reached. The numerical stability of the procedure is analysed in a separate paper by Cormeau[100].

Gotoh[101] introduces polynomial shape functions to study the deformation of sheet metals, and applies the formulation to the analysis of hydraulic bulging. Values of strain are not presented, but the whole area of the circular sheet specimens are brought into the plastic range.

Dieterle[102] recently studied the compression of tubular rings using a finite element formulation as developed by Zienkiewicz et al[39], but introducing several simplifying features, one of which has already been referred to in Sub-section 2.5.c. Although natural strains of the order of 0.45 and good correlation with experimental results are claimed to have been achieved, the apparently loose treatment of boundary conditions, the use of a secant modulus approach and the use of large values of Poisson's ratio to improve the results seem to represent too many simplifying assumptions to retain the reliability of the solutions. It must be said, however, that the text presented in the reference is too compact and may give rise to misleading interpretation of the procedures described.

Gunasekera and Alexander[108] employ a formulation which highly resembles that of Hibbitt et al[49], being, however, described in terms of the instantaneous frame of reference, by systematic updating of nodal coordinates and recomputation of the geometrical matrices; such a procedure prescinds the consideration of an initial displacement stiffness term, as presented in (49), and as used in the formulation to be presented in Section 3.2. The authors claim to be able to obtain a solution for large deformation in the problem of the elastic-plastic expansion of a hole in a plate. However, their solution is essentially applicable to the small strain range only, for, as already pointed out elsewhere[110], they do not consider any sort of objective definition for the stress increments resulting from the constitutive equation.

Nagtegaal et al[109] study the over-stiffening effect of finite element solutions in the plastic range (as mentioned in Subsection 2.5.c) and explain it in terms of excessive kinematic constraints imposed on the modes of deformation by the element types commonly used both in two and three-dimensional analysis. They conclude that this effect can be minimised by suitable arrangements in the mesh or by the use of a new variational principle, which they introduce. The formulation thus presented and applied to specific examples is a small strain one, but in an appendix the authors introduce a generalization for finite deformation, using an Eulerian frame of reference. Unfortunately this reference came to our attention only very recently, when our work was nearly conclu-

ded, to allow for deeper consideration of such an alternative treatment. This has been done, however, by McMeeking and Rice[110], producing an apparently simpler and computationally more economical formulation than the Lagrangean one, proposed by Hibbitt et al[49] and used in this work, and much more so than the Eulerian approach proposed by Kitagawa et al[89,91]. The authors consider again the problem of necking in the tensile test, and compare their results satisfactorily with Osias's[93,94] and with known experimental results.

Lee[111] used the same formulation to predict the steady state force in extrusion, being able to predict deformation well beyond the limits achieved by Iwata et al[66]. However, it must be mentioned that Guha[78], using a Lagrangean formulation similar to our own, appears to be able to predict deformation of the same or even higher order of magnitude.

An assessment of the procedures for the numerical procedures for the solution of material and geometrically nonlinear structural analysis, as well as an extensive review of the relevant literature, up to 1973, is presented by Stricklin, Haisler and Riesemann[112]. A good evaluation of methods can also be found in Cook[103].

3.2 - FORMULATION

3.2.a - INCREMENTAL STIFFNESS EQUATION (ELEMENTAL)

In the Finite Element Method a displacement assumption is usually made, expressing displacements at any point within an element as a linear combination of the displacements at a finite number of nodal points in the same element, the coefficients to be used depending on the position of the point under consideration in the undeformed configuration of the element. Conversely, and restricting considerations to simplex elements, we can express initially

$$u_i = \alpha_{ik} X_k + \alpha_{i4},$$

and obtain the alpha-coefficients by applying this equation to the nodal points of the element. In a three-dimensional space the simplex elements are simple tetrahedra, and the determinant of the system,

$$6V^o = \begin{vmatrix} \bar{X}_1^1 & \bar{X}_2^1 & \bar{X}_3^1 & 1 \\ \bar{X}_1^2 & \bar{X}_2^2 & \bar{X}_3^2 & 1 \\ \bar{X}_1^3 & \bar{X}_2^3 & \bar{X}_3^3 & 1 \\ \bar{X}_1^4 & \bar{X}_2^4 & \bar{X}_3^4 & 1 \end{vmatrix},$$

is a measure of the volume of the undeformed element. The alpha-coefficients will thus be expressed by

$$\alpha_{ik} = a_k^j \bar{u}_i^j$$

where

$$a_k^j = \frac{c_k^j}{6V^o},$$

c_k^j being the cofactors of the terms appearing in the j^{th} row and in the k^{th} column of the determinant of the system. In these two

equations, exceptionally, a subindex is allowed to take values from 1 to 4 , but this practice will not be repeated elsewhere in this work, explicit reference being made to terms involving the cofactors of the fourth (unit) column of the determinant of the system, whenever they may appear.

The numbers assigned to the nodes belonging to an element need not form a natural sequence. However, nodes will be ordered inside an element, and the superscripts in the elemental tensor equations will denote the several nodes according to their internal ordination, whatever their external node number may be. Whenever the external node number is considered, capitals will be used as superindices. In the following, Zienkiewicz's convention, as presented in (23), will be used, by which the internal numbering may be started at any arbitrary node, the other ones being numbered clockwise, as viewed from the first one (Fig. 3-4).

The displacement assumption may now be rewritten as

$$u_i = N^j \bar{u}_i^j \tag{3-3}$$

where

$$N^j = a_k^j X_k + a_4^j , \tag{3-4}$$

with k reset to the limit of the dimension of the space, are the so-called shape functions. It is easy to prove that the values of the shape functions at a node, say ℓ , will be expressed by

$$\bar{N}^{j\ell} = a_k^j \bar{X}_k^\ell + a_4^j = \delta^{j\ell} . \tag{3-4a}$$

Furthermore, as the cofactors a_k^j are constant for a given element, the material derivatives at any point within the element will be given by

$$N^j{}_{,m} = a_k^j \delta_{km} = a_m^j , \tag{3-4b}$$

thus

$$u_{i,m} = a_m^j \bar{u}_i^j \tag{3-5a}$$

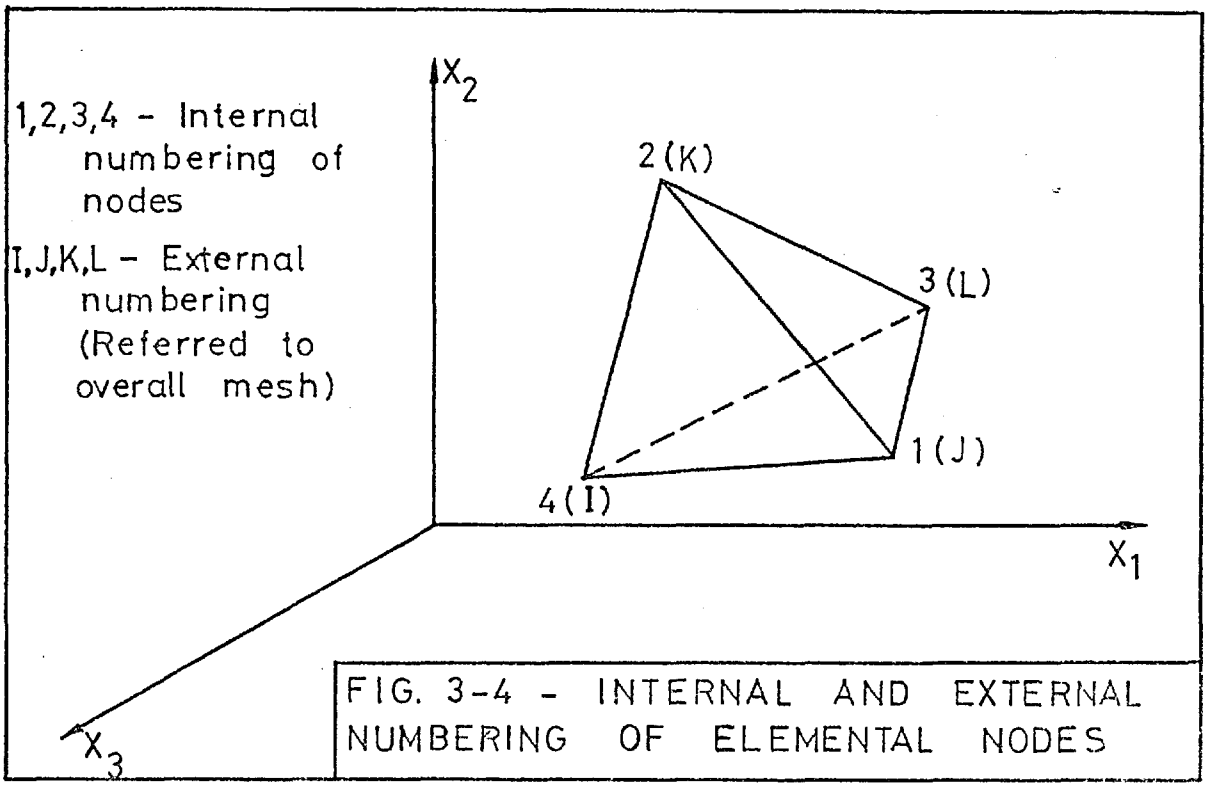


FIG. 3-4 - INTERNAL AND EXTERNAL NUMBERING OF ELEMENTAL NODES

and, in view of Eqn. (2-1),

$$x_{i,m} = u_{i,m} + \delta_{im}\,; \tag{3-5b}$$

and time derivatives of Eqn. (3-3) will be expressed by

$$v_i = N^j \bar{v}_i^j \tag{3-6a}$$

and

$$v_{i,m} = a_m^j \bar{v}_i^j\,. \tag{3-6b}$$

Finally, the time derivative of Green's strains, defined in Eqn. (2-3a), will be expressed by

$$\dot{E}_{ij} = \frac{1}{2}\left[a_j^\ell \delta_{ik} + a_i^\ell \delta_{jk} + (a_i^m a_j^\ell + a_i^\ell a_j^m)\bar{u}_k^m\right]\bar{v}_k^\ell\,,$$

therefore the Lagrangean expression for conservation of energy, Eqn. (2-33), can thus be rewritten as

$$\left\{\int_{A^\circ} T_i^\circ N^\ell \delta_{ik}\, dA^\circ + \int_{V^\circ} F_i^\circ N^\ell \delta_{ik}\, dV^\circ\right\}\bar{v}_k^\ell =$$

$$= \frac{1}{2}\left\{\int_{V^\circ} S_{ij}\left[a_j^\ell \delta_{ik} + a_i^\ell \delta_{jk} + (a_i^m a_j^\ell + a_i^\ell a_j^m)\bar{u}_k^m\right] dV^\circ\right\}\bar{v}_k^\ell\,.$$

As the velocity field is arbitrary, the overall equilibrium requires that the terms inside the curly brackets, at the left and right-hand side of the preceding equation be equated. Defining thus the "equivalent" forces $\bar{P}_k^{\ell}$, applied at the nodes of the element, in terms of the surface and body forces acting over the same element, as

$$\bar{P}_k^{\ell} = \int_{A^o} T_k^o \, N^{\ell} \, dA^o + \int_{V^o} F_k^o \, N^{\ell} \, dV^o , \qquad (3\text{-}7a)$$

the set of elemental equilibrium equations becomes

$$\bar{P}_k^{\ell} = \frac{1}{2} \int_{V^o} S_{ij} \left[a_j^{\ell} \, \delta_{ik} + a_i^{\ell} \, \delta_{jk} + (a_i^m \, a_j^{\ell} + a_i^{\ell} \, a_j^m) \, \bar{u}_k^m \right] dV^o . \qquad (3\text{-}7b)$$

Taken in incremental form, these equations rewrite as

$$\Delta \bar{P}_k^{\ell} = \int_{A^o} \Delta T_k^o \, N^{\ell} \, dA^o + \int_{V^o} \Delta F_k^o \, N^{\ell} \, dV^o \qquad (3\text{-}8a)$$

and

$$\Delta \bar{P}_k^{\ell} = \frac{1}{2} \int_{V^o} \Delta S_{ij} \left[a_j^{\ell} \, \delta_{ik} + a_i^{\ell} \, \delta_{jk} + (a_i^m \, a_j^{\ell} + a_i^{\ell} \, a_j^m) \, \bar{u}_k^m \right] dV^o + \frac{1}{2} \int_{V^o} S_{ij} \, (a_i^m \, a_j^{\ell} + a_i^{\ell} \, a_j^m) \, \Delta \bar{u}_k^m \, dV^o . \qquad (3\text{-}8b)$$

In general, surface and body forces will both depend on loads and displacements, and their increments will be expressed as the sum

$$\Delta T_i^o = \Delta_L T_i^o + \Delta_G T_i^o \qquad (3\text{-}9a)$$

and

$$\Delta F_i^o = \Delta_L F_i^o + \Delta_G F_i^o \qquad (3\text{-}9b)$$

of an increment due solely to changes in the applied loads with fixed displacements, and another increment due exclusively to changes in shape of the continuum (element) under fixed loads. The equivalent applied force increments given by Eqns. (3-8a,b) can thus be expressed, for every element, by

$$\Delta \bar{P}_k^{\ell} = \Delta \tilde{\bar{P}}_k^{\ell} + \bar{Q}_{kn}^{\ell m} \Delta \bar{u}_n^m \qquad (3\text{-}10)$$

where, from Eqns. (3-8a,b) and (3-9a,b), we have

$$\Delta\bar{\bar{P}}_k^{\ell} = \int_{A^o} \Delta_L T_k^o \, N^{\ell} \, dA^o + \int_{V^o} \Delta_L F_k^o \, N^{\ell} \, dV^o \qquad (3\text{-}11a)$$

and

$$\bar{Q}_{kn}^{\ell m} \, \Delta\bar{u}_n^m = \int_{A^o} \Delta_G T_k^o \, N^{\ell} \, dA^o + \int_{V^o} \Delta_G F_k^o \, N^{\ell} \, dV^o , \qquad (3\text{-}11b)$$

$\Delta\bar{\bar{P}}_k^{\ell}$ representing thus equivalent force increments due solely to increases in the magnitude of the applied forces, and $\bar{Q}_{kn}^{\ell m} \Delta\bar{u}_n^m$ representing incremental forces which are equivalent to the action of the existing load system under the changes in the geometry of the continuum. The stiffness term $\bar{Q}_{kn}^{\ell m}$ was first introduced by Turner et al[22], but also pointed out by Oden and Key[83], and is designated as the initial load stiffness matrix[49,40] or as the load correction matrix[83]. Specific expressions for this term will depend on the type of the loads acting over the element, as has been shown by Hibbitt et al[49]. Oden[40] provides a general but more cumbersome expression. This stiffness term is generally unsymmetric with respect to its pairs of indices, and thus introduces computational difficulties in the solution algorithm. However, if some expression can be found which directly expresses the force term represented by Eqn. (3-11b), these difficulties can be overcome.

Kirchhoff stress increments are expressed by Eqn. (2-27), with the constitutive tensor given by (2-32) and Green's strain increments expressed, from Eqns. (2-3a) and (3-5a), by

$$\Delta E_{ij} = \frac{1}{2}\left[a_j^m \delta_{in} + a_i^m \delta_{jn} + (a_i^{\ell} a_j^m + a_j^m a_i^{\ell}) \, \bar{u}_n^{\ell}\right] \Delta\bar{u}_n^m .$$

Introducing this expression into Eqn. (2-32) and that one into (3-8b), and considering the symmetries of Kirchhoff's stress increments and of the constitutive tensor - Eqn. (2-32) - it can be rewritten in the form

$$\Delta\bar{\bar{P}}_k^{\ell} = \bar{k}_{kn}^{\ell m} \, \Delta\bar{u}_n^m \qquad (3\text{-}12)$$

with the incremental stiffness matrix given, for every element, by

$$\bar{k}_{kn}^{\ell m} = {}_0\bar{k}_{kn}^{\ell m} + {}_1\bar{k}_{kn}^{\ell m} + {}_2\bar{k}_{kn}^{\ell m} \qquad (3\text{-}13)$$

where, following suitable manipulation of indices,

$$ {}^{0}\bar{k}^{\ell m}_{kn} = \int_{V^o} a^{\ell}_{i} \, D_{iknj} \, a^{m}_{j} \, dV^o , \qquad (3\text{-}14a) $$

$$ {}^{1}\bar{k}^{\ell m}_{kn} = \int_{V^o} a^{\ell}_{i} \, a^{m}_{j} \, a^{f}_{r} \left[D_{ikrj} \, \bar{u}^{f}_{n} + \bar{u}^{f}_{k} \, D_{irnj} + \bar{u}^{f}_{k} \, D_{irsj} \, \bar{u}^{g}_{n} \, a^{g}_{s} \right] dV^o , \qquad (3\text{-}14b) $$

$$ {}^{2}\bar{k}^{\ell m}_{kn} = \int_{V^o} S_{ij} \, \delta_{kn} \, a^{\ell}_{i} \, a^{m}_{j} \, dV^o . \qquad (3\text{-}14c) $$

are obtained. The term ${}^{0}\bar{k}^{\ell m}_{kn}$ is formally similar to the stiffness matrix used in small displacement analysis; Hibbitt et al[49] and Marçal[82] call it the usual small displacement stiffness matrix, whilst Oden[40] refers to it simply as the incremental stiffness matrix. The term ${}^{1}\bar{k}^{\ell m}_{kn}$ is the initial displacement[49,82] or the initial rotation[40] stiffness matrix, while ${}^{2}\bar{k}^{\ell m}_{kn}$ is the initial stress stiffness matrix[40,49].

The symmetry properties

$$ {}^{0}\bar{k}^{\ell m}_{kn} = {}^{0}\bar{k}^{m\ell}_{nk} , \qquad {}^{1}\bar{k}^{\ell m}_{kn} = {}^{1}\bar{k}^{m\ell}_{nk} $$

and

$$ {}^{2}\bar{k}^{\ell m}_{kn} = {}^{2}\bar{k}^{m\ell}_{nk} $$

are evident and will be used in the programming stage. Unfortunately, as mentioned before, similar properties are not generally enjoyed by the initial load stiffness terms.

Of course the integrals appearing in Eqns. (3-14a,b,c) may be readily obtained, as, for the simplex elements under consideration, all terms appearing in the integrands become position independent.

3.2.b - INITIAL LOAD STIFFNESS MATRIX[49]

Hibbitt et al[49] obtained explicit formulae for two particular forms of external loading, namely those of concentrated and pressure loading. They also dealt separately with the case of body forces.

It seems to us that, whatever the system of forces acting over the surfaces of the elements, it becomes simpler, especially when a fine mesh is used, to start by resolving those forces into nodal components, and use Hibbitt's formula for concentrated loads. The fact that these resolved forces act directly over the nodes simplifies the resulting expressions.

For a compressive load acting directly over an elemental node (say ℓ in the internal referential numbering) we have

$$\int_A \bar{T}_i^{\ell} \, dA = \bar{P}_i^{\ell} .$$

The corresponding part of the equivalent forces in Eqn. (3-7a), body forces being absent, and considering Eqn. (3-4a), is then

$$\bar{P}_k^{\ell} = \left| \bar{P}^{\ell} \right| \bar{n}_k^{\ell} \qquad (3\text{-}15)$$

where $\bar{n}_k^{\ell}$ are components of an unit direction vector. Clearly, according to the summation convention introduced at the beginning of Chapter 2, there is no summation intended over the index ℓ in Eqn. (3-15).

Taking this expression in incremental form,

$$\Delta \bar{P}_k^{\ell} = \Delta \left| \bar{P}^{\ell} \right| \bar{n}_k^{\ell} + \left| \bar{P}^{\ell} \right| \Delta \bar{n}_k^{\ell}$$

is obtained, and by comparison with Eqn. (3-10),

$$\Delta \bar{\bar{P}}_k^{\ell} = \Delta \left| \bar{P}^{\ell} \right| \bar{n}_k^{\ell} \qquad (3\text{-}16a)$$

and

$$\bar{Q}_{kn}^{\ell m} \Delta \bar{u}_n^{m} = \left| \bar{P}^{\ell} \right| \Delta \bar{n}_k^{\ell} . \qquad (3\text{-}16b)$$

follow. It is clear that if the direction of the force remains unchanged, there is no initial load stiffness term to consider. In general, however, it should be obtained from Eqn. (3-16b), and this is only possible if further information is supplied with respect to the way in which the components $\bar{n}_k^{\ell}$ change in magnitude. Such information is not always available, and an alternative approach must be followed, as will be described below.

The solution pattern prescribed in (49) consists in, given the set $\Delta\tilde{\bar{P}}_k^{\ell}$ and after calculating the initial load stiffness terms $\bar{Q}_{kn}^{\ell m}$, to assemble total elemental stiffness terms which correspond to the expression of Eqn. (3-13) minus the initial load stiffness terms. Instead of Eqn. (3-12), an equation relating the effective force increments $\Delta\tilde{\bar{P}}_k^{\ell}$ to the displacement increments is obtained and eventually solved (once the overall system is assembled).

In this work a different pattern will be followed. The prescribed force increments will be considered as being the total ones, that is, as corresponding to the left hand side of Eqn. (3-10). Correction to the effective force increments $\Delta\tilde{\bar{P}}_k^{\ell}$ will be made a posteriori. In other words, first we solve Eqn. (3-12) for the displacement increments and then we try to find the two components corresponding to the right hand side of Eqn. (3-10) by means of a simple iterative procedure.

To do this we rewrite Eqn. (3-10), under consideration of (3-16a,b), as

$$\Delta\tilde{\bar{P}}_k^{\ell} = \Delta\bar{\bar{P}}_k^{\ell} - \left|\bar{\bar{P}}^{\ell}\right| \Delta\bar{n}_k^{\ell} \qquad (3\text{-}17)$$

where clearly

$$\Delta\bar{n}_k^{\ell} = \frac{\bar{\bar{P}}_k^{\ell} + \Delta\bar{\bar{P}}_k^{\ell}}{\left|\bar{\bar{P}}^{\ell} + \Delta\bar{\bar{P}}^{\ell}\right|} - \frac{\bar{\bar{P}}_k^{\ell}}{\left|\bar{\bar{P}}^{\ell}\right|} . \qquad (3\text{-}18)$$

Assuming initially that $\Delta\bar{\bar{P}}_k^{\ell} = \Delta\tilde{\bar{P}}_k^{\ell}$, estimates for $\Delta\bar{n}_k^{\ell}$ can be obtained from Eqn. (3-18), and they are used in (3-17) to provide new estimates for $\Delta\tilde{\bar{P}}_k^{\ell}$, which are then introduced in (3-18), and so on. Such a procedure has shown to converge very quickly, usually in two or three steps, to a reasonable degree of accuracy. Its use avoids the need of expressing the initial load stiffness terms explicitly and does not upset the symmetry properties of the stiffness matrix.

In the applications to be considered in the next chapter, only very slow rotational movement will be considered, and the effect of body forces can thus be fully disregarded.

3.2.c - INCREMENTAL STIFFNESS MATRIX (OVERALL)

Eqn. (3-13) provides an elemental stiffness matrix. Elements, however, must not be considered individually. The displacement field must be compatible, meaning that elements must meet at the common nodal points in any deformed situation. This requirement is translated in the formulation by means of an overall stiffness matrix, covering all the elements in the continuum. Such a matrix can be obtained[23,24] by initially considering Eqn. (3-12) as extended to all nodes in the mesh, with the proviso that if a node does not belong to the element under consideration, the corresponding stiffness terms be taken as zeroes. With this convention, the overall stiffness equation

$$\Delta \bar{P}_k^L = \bar{K}_{kn}^{LM} \Delta \bar{u}_n^M \qquad (3\text{-}19)$$

can be expressed, with the total nodal force increments given by the sum of the elementary contributions, and the total stiffness matrix terms defined simply as

$$\bar{K}_{kn}^{LM} = \sum_{elem} \bar{k}_{kn}^{LM}, \qquad (3\text{-}20)$$

the summations being extended over all the elements in the mesh. In the computing stage, and to avoid unnecessarily adding up zeroes, a simple procedure can be provided in order to scan only the elements to which a particular node belongs. Of course, interelement forces will be cancelled out of Eqn. (3-19), and only external (active or reactive) forces will remain. Also, the displacement increments computed will be referred to the whole mesh, and the possibility of interelemental discontinuities or superpositions, arising from nodes presenting different displacements in adjacent elements, is removed.

3.2.d - ITERATIVE CORRECTION OF INCREMENTAL STRESSES

It has already been pointed out that the incremental solution for plastic problems will supply stresses overshooting the prescribed stress-strain relation, the error produced being cumulative and monotonically increasing. Techniques for correcting the stress field have already been analysed in Sub-section 3.1.b. The

three algorithms considered there are, however, intended for small strains, when rotations are negligible and the difference between the various definitions of stress and strain become negligible.

It seems to us that the computational disadvantages of Yamada's[37] and Marçal's[59] algorithms become more patent in a Lagrangean description, when a time consuming expression for the elemental stiffnesses is coupled with an also time consuming expression for the constitutive tensor. An ideal corrective procedure should be economical from the computing point of view, and should, therefore, require few recomputations of the stiffness terms.

This can be shown to be achieved by employing an algorithm formally similar to Zienkiewicz's initial stress method[39], but in which elastic-plastic constitutive tensors, computed at some arbitrary stage of the deformation process, and the corresponding elastic-plastic stiffness terms are used, instead of their elastic counterparts. Such an algorithm constitutes one of the several alternatives listed by Nayak[75] under the general heading of "methods of residual forces". However, the subject is not pursued further in that work, and the following, to our knowledge, will be the first application of this particular iterative procedure, which will be fully described and analysed in Section 3.3.

The reason for considering such an approach can be formally justified by referring to Fig. 3-3: if the load increments are applied under the consideration of a slope smaller than the elastic one, the differential stresses will be reduced, and the number of corrective cycles required to achieve convergence to the stress-strain curve will be smaller.

3.2.e - FRICTION CONSIDERATIONS

Friction constitutes an important factor governing the flow of material near the die/workpiece interface, in any plastic forming process, and its influence can become very complex. Exact relationships connecting the friction resistance to the other variables of the problem are not easy to express, and simplified mathematical models are usually adopted. Avitzur[113] considers and

discusses the three common descriptions of friction, and lists the relevant literature on the subject.

It is not the purpose of this work to establish a discussion on the validity or adequacy of the several friction descriptions. Instead, one will be considered, and used in connection with the application problem to be dealt with in the next chapter. It is clear that if any other description is to be preferred, only a sector of the formulation and of the computing program will be affected.

We shall consider Coulomb friction only. Coulomb's law assumes a linear relationship connecting the friction resistance and the pressure between the contacting bodies. The proportionality factor, or friction coefficient, is assumed to be constant for a given pair of materials (under constant surface and temperature conditions), and independent of velocity.

Explicit expressions affected by the adopted friction description will be presented together with the application case.

3.3 - MODIFIED INITIAL STRESS METHOD

3.3.a - INTRODUCTION

The best advantage of Zienkiewicz's initial stress method[39], which is the use of an unchanged stiffness matrix throughout the successive load increments, obtained from an also unchanged and position independent elastic constitutive tensor, is lost in the Lagrangean formulation just presented. As has been shown in Chapter 2, even the elastic constitutive tensor becomes dependent on the amount of deformation in the Lagrangean description: it is obtained by introducing the expression for D^{e}_{ijrs}, given in Eqn. (2-11a), instead of the expression for D'_{ijrs} in Eqn. (2-32). And therefore, also the stiffness terms become deformation dependent.

It follows that the constitutive tensors have necessarily to be recomputed at the beginning of each new load increment, and it is then relatively immaterial if the elastic-plastic one is computed, instead of the elastic one, as was suggested in 3.2.d.

3.3.b - DESCRIPTION OF THE METHOD

Fig. 3-5 illustrates the procedure and corrects oversimplifications introduced in Fig. 3-3, where the loci of the "new" equivalent stresses were arbitrarily assimilated with the stress-strain curve. In the modified version to be presented, the loading slopes will only coincide with the elastic one for the newly yielded or still elastic elements. A superscript $\hat{}$ will be used to denote interim values of the variables. The procedure is described as follows:

1 - Prepare initial (elastic) constitutive tensor and overall stiffness matrix.

2 - For the given load increments solve Eqn. (3-19) for the incremental displacements; compute Green strain increments ΔE_{ij}, deformation increments $\Delta \epsilon_{ij}$ and equivalent plastic strain increments $\Delta \bar{\epsilon}^{p}$ (See 3.3.c.3).

3 - If an element is still in the elastic range, compute interim stress increments $\Delta \hat{S}_{ij}$ (Eqn. (2-27))

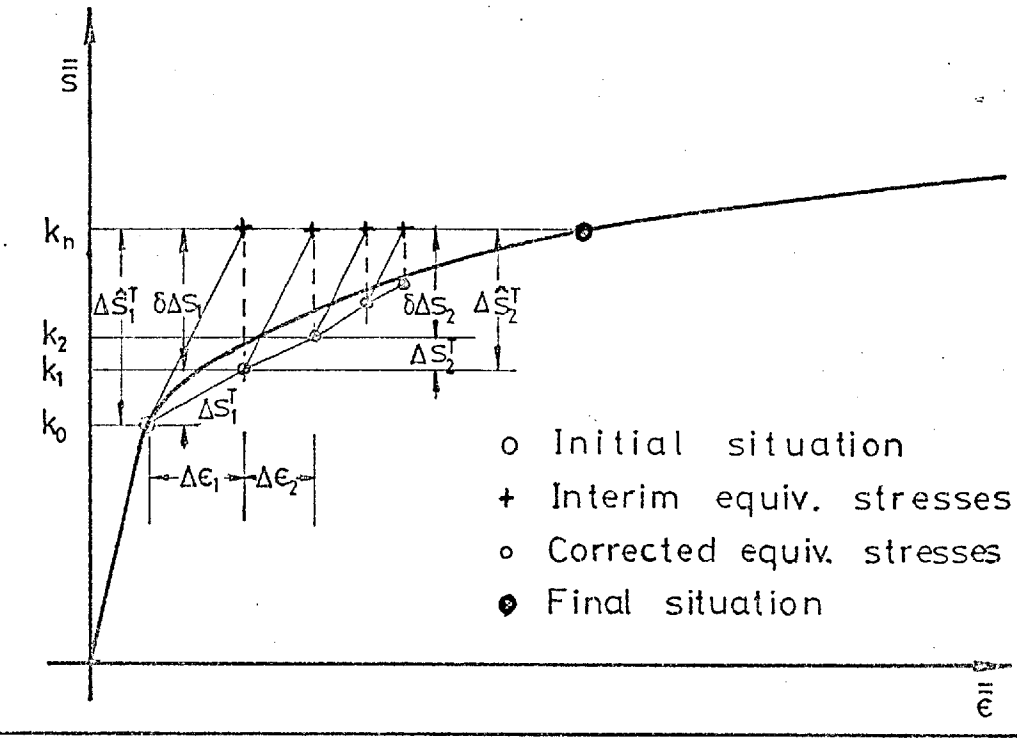


FIG. 3-5 - MODIFIED INITIAL STRESS METHOD

and $\Delta\hat{s}_{ij}^T$ (by inverting (2-29)), using the constitutive tensor produced at the beginning of the load increment; otherwise compute first $\Delta\hat{s}_{ij}^T$ (by (2-20c)), and $\Delta\hat{S}_{ij}$ afterwards (by (2-29)). Express

$$\Delta\hat{\bar{\bar{s}}} = H' \, \Delta\bar{\bar{\epsilon}}^p . \qquad (3\text{-}21)$$

4 - Compute interim stresses

$$\hat{S}_{ij} = S_{ij} + \Delta\hat{S}_{ij} \qquad (3\text{-}22a)$$

and

$$\hat{s}_{ij} = s_{ij} + \Delta\hat{s}_{ij} . \qquad (3\text{-}22b)$$

5 - Compute equivalent stress $\hat{\bar{\bar{s}}}$ and expected ordinate of the prescribed stress-strain curve $\hat{k}$.

6 - If $\hat{\bar{\bar{s}}} < 0.995\,\hat{k}$, the element is treated as elastic from the next load increment; otherwise,

6a - Compute interim slopes

$$\hat{H}' = \frac{\hat{k} - \bar{\bar{s}}}{\Delta\bar{\bar{\epsilon}}^p} \qquad (3\text{-}23)$$

and interim constitutive tensors $\hat{D}'_{ijrs}$ and $\hat{D}_{ijrs}$.

6b - Find correct stress increments Δs^T_{ij} and ΔS_{ij}, using the interim parameters obtained in step 6a.

6c - Evaluate differential stresses to be supported by body forces,

$$\delta\Delta S_{ij} = \Delta\hat{S}_{ij} - \Delta S_{ij} \qquad (3\text{-}24a)$$

and

$$\delta\Delta s_{ij} = \Delta\hat{s}^T_{ij} - \Delta s^T_{ij} . \qquad (3\text{-}24b)$$

6d - Update and store Green strains; update and store new current stresses

$$S_{ij} = \hat{S}_{ij} - \delta\Delta S_{ij} \qquad (3\text{-}25a)$$

and

$$s_{ij} = \hat{s}_{ij} - \delta\Delta s^T_{ij} . \qquad (3\text{-}25b)$$

6e - If first cycle, update nodal loads.

7 - If an element yields during the cycle under consideration, find the intermediate stress level at which yielding will begin, and recompute stresses starting from that point. That is, find an adequate rating coefficient ζ, to multiply the right hand side of Eqns. (3-24a,b), which thus rewrite as

$$\delta\Delta S_{ij} = (1 - \zeta)(\Delta\hat{S}_{ij} - \Delta S_{ij}) \qquad (3\text{-}26a)$$

and

$$\delta\Delta s_{ij} = (1 - \zeta)(\Delta\hat{s}_{ij} - \Delta s_{ij}) . \qquad (3\text{-}26b)$$

(An adequate expression for ζ will be derived in the next sub-section).

8 - Compute nodal forces which equilibrate the differential stresses. They can be expressed from Eqn. (3-8b) and are given by

$$\Delta\bar{P}^L_k = \int_{V^o} a^L_i \, \delta\Delta S_{ij} \, (\delta_{jk} + a^M_j \bar{u}^M_k) \, dV^o . \qquad (3\text{-}27)$$

9 - Check the error of the interim equivalent stress $\hat{\bar{S}}$ against the current ordinate of the stress-

strain curve $\hat{k}$. If above a prescribed limit (0.5% in this work), and if a prescribed maximum number of corrective cycles has not been achieved, repeat procedure from step 2; otherwise, replace yield stresses, equivalent stresses, slopes and constitutive tensors by the interim counterparts, recompute overall stiffness matrix and remove residual forces from existing load system. If termination criteria not satisfied, repeat procedure from step 2.

3.3.c - ADDITIONAL REMARKS

This modified procedure, as well as Zienkiewicz's[39], constitute variants of Newton-Raphson's "constant slope" method.

As has been pointed out by Argyris and Scharpf[65], the initial stress method tends to converge slowly, especially in conditions of near perfect plasticity. This drawback should, in principle, be minimised in the alternative procedure just described, except possibly at the early stages of deformation, when both procedures coincide. Fig. 3-6 justifies this statement. With the elastic extrapolations (a), the corrective stresses will represent a substantial part of the originally applied forces, the more so if the stress-strain curve is very shallow. With elastic-plastic extrapolations, as in (b), fewer iterations are required to bring the stresses to within a prescribed tolerance range.

In fact a deterioration of convergence conditions does occur when plastic deformation increases, as the updated constitutive tensors become less and less diagonally dominant. That is, the terms for which the indices

$$i = r \qquad \text{and} \qquad j = s,$$

which are originally much larger than the remaining ones, decrease in absolute value, whilst the other ones are increased. This fact is also translated into the stiffness matrix, and the iterative solution algorithm for Eqn. (3-19) tends to become ill-conditioned. Convergence requires more and more cycles, and eventually fails to occur. For this reason, it is advisable not to update the constitutive tensors in step 9, once the plastic deformation

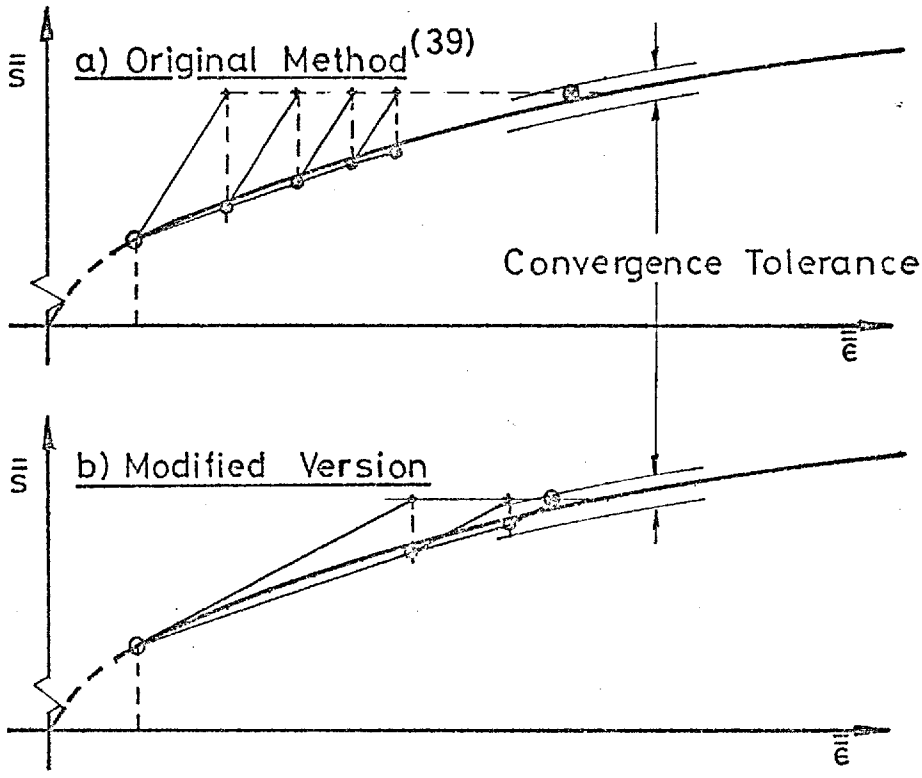


FIG. 3-6 - CONVERGENCE OF INITIAL STRESS METHODS

reaches some prescribed level.

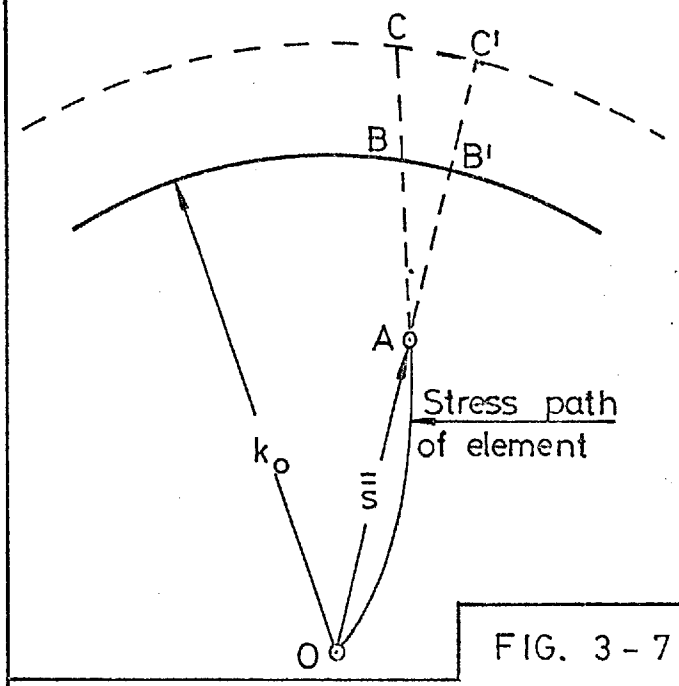
3.3.c.1 - Rating factor

Fig. 3-7 illustrates the incremental procedure for one newly yielded element in the finite element mesh. This figure is similar to the one presented by Yamada(37), reproduced here as Fig. 3-1.

In the figure, point A corresponds to the initial (elastic) situation; C and C' correspond to the initially (elastically) computed increments; and B and B' correspond to the initial yield surface. The parameter ζ, which expresses the fraction of the applied load increments which will exactly yield the element, is given by

$$\zeta = \frac{\overline{AB}}{\overline{AC}}.$$

Here, using the notation of the figure,



$\overline{OA} = \bar{\bar{s}}$ (Previous)

$\overline{OB} = k_o$

$\overline{OC} = \hat{\bar{\bar{s}}}$ (Interim)

$\overline{AC} = \overline{\overline{\Delta s}}$

$\overline{AC'} = \Delta\bar{\bar{s}}$

$\zeta = \dfrac{\overline{AB}}{\overline{\overline{AC}}}$

FIG. 3-7 - STRESS SPACE REPRESENTATION FOR ESTIMATION OF RATING COEFFICIENT ζ

$$\overline{AC} = \sqrt{\frac{3}{2}\,\Delta s_{ij}^{T'}\,\Delta s_{ij}^{T'}} = \overline{\overline{\Delta s}}$$

and

$$\overline{AB} = \frac{1}{2}\left[\Gamma + \sqrt{\Gamma^2 + 4\,\overline{\overline{\Delta s}}^2\,(k^2 - \bar{\bar{s}}^2)}\right]$$

with

$$\Gamma = \overline{\overline{\Delta s}}^2 + \bar{\bar{s}}^2 - (\bar{\bar{s}} + \Delta\bar{\bar{s}})^2 .$$

The rating coefficient is thus finally expressed by

$$\zeta = \frac{\Gamma + \sqrt{\Gamma^2 + 4\,\overline{\overline{\Delta s}}^2\,(k^2 - \bar{\bar{s}}^2)}}{2\,\overline{\overline{\Delta s}}^2} . \qquad (3\text{-}28)$$

Of course, if the relevant element remains in the elastic range during the iterative step under consideration, this parameter is simply set to one. For already plastic elements, of course, its value is zero. For a first load increment, starting from an unstressed situation, points O and A coincide, and the rating coefficient reduces simply to

$$\zeta = \frac{\overline{OB'}}{\overline{\overline{OC'}}} .$$

3.3.c.2 - Limiting the number of corrective cycles

Even the modified version of the initial stress method, as described in 3.3.b, may require a relatively large number of corrective cycles until the computed stresses fall within a prescribed tolerance range from the stress-strain curve. As Nayak[75] suggests, however, the process may be arbitrarily interrupted at any stage, provided the last set of corrective (residual) forces is subtracted from the applied forces, and thus removed from the system.

This feature has been introduced in the procedure described in the previous sub-section, in the form of a check in step 9.

3.3.c.3 - Plastic strain increment

The increment of the equivalent plastic strain increment for each yielded element is computed using[5]

$$\Delta\bar{\epsilon}^{p} = \frac{s'_{ij}\,\Delta\epsilon_{ij}}{\bar{s}\,(1 + H'/3G)} . \qquad (3\text{-}29)$$

This is clearly an essentially non-negative variable, and this fact is used in the computer program to check the validity of the results.

3.3.c.4 - Drift from stress-strain curve

If the correction of stresses - in the initial stress method - is performed using the instantaneous constitutive tensor, as prescribed by Zienkiewicz[39], a progressive drift from the prescribed stress-strain curve becomes unavoidable, as is illustrated in the first two corrective cycles in Fig. 3-5.

By correcting stresses by means of slopes defined by Eqn. (3-23) we follow Swedlow's[77] correction procedure, thus bringing the image of the corrected stresses nearer to the stress-strain curve, as illustrated in Fig. 3-5, for the last two corrective cycles.

3.4 - CONCLUSION

The preceding sections contain a formulation to be used in the incremental analysis of problems of large strains and large displacements, coupled with nonlinear material behaviour. It is thus suited for the analysis of metalworking processes. The restrictions introduced are:

a) Small elastic deformations, guaranteeing the decomposition of strain into purely elastic and purely plastic components;

b) Absence of Bauschinger effect;

c) Isothermal deformation;

d) Isotropic material behaviour.

Restriction d could be easily lifted by abandoning the symmetry properties of the constitutive tensor. The final expressions obtained in Section 3.2 would not be applicable, but alternative expressions could easily be produced. However, computing times, when using such a formulation, would be dramatically increased. Restrictions b and c might also be removable without substantial difficulty in the derivation stage, but one should expect that computing times would be again substantially affected. Restriction a is the most decisive one in the formulation; should it be lifted, a substantially new formulation would be required, and for that purpose, Lee's[33] and Freund's[114] work might prove to be of invaluable help.

CHAPTER 4

APPLICATION AND COMPUTER PROGRAM IMPLEMENTATION

4.1 - INTRODUCTION

The preceding chapter has been presented in general terms, with no restriction to any particular application case. When one is considered, a set of force and/or displacement boundary conditions has to be introduced, and eventual geometrical restrictions, such as symmetries, should preferably be considered. The latter may allow for savings in computation, by the possibility of avoiding unnecessary calculation, using the finite element mesh over part of the continuum only. The former will give more explicit expressions for the nodal forces and influence the solution of the incremental force-displacement relationship (Eqn. (3-21)), either by prescribing in advance certain nodal displacements and/or forces, or by establishing a relationship between components of these displacements and/or forces.

A particular application will also envisage a particular material, and particular ranges of strain-rate and temperature. These will define the flow stress in terms of the amount of work-hardening produced.

In the following, expressions derived in the preceding

chapter will be applied to the radial upsetting process, and the deformation of aluminium of commercial purity. The computer program for this particular application will be implemented.

For a description of the radial upsetting process we refer the reader to Section 5.1.

4.2 - MATERIAL CONSIDERATIONS

In Chapter 5 the choice of commercial purity aluminium as the test material will be justified in terms of the heating facilities available. Our aim in this section is to supply an expression for the flow stress for this particular material, in the situation of the test, in terms of the instantaneous plastic deformation produced.

The importance of using adequate stress-strain relations, and ways of obtaining them under prescribed conditions has been fully studied already. In addition to the historical work of Cook and Larke[115], a series of more recent works deals with the description of methods and testing conditions[116-122] and/or the presentation of data[119-124] for several materials. A number of papers analyses the effect of processing on the properties of the materials[125]. Suzuki et al[122] present a comprehensive collection of results, covering an extensive number of metals and alloys, considering the effect of strain, strain-rate and temperature. Mohitpour[121] considers the heat generated during deformation and presents an incremental method for obtaining stress-strain curves to large strains, at high strain-rates and sub-critical temperatures; at every step the temperature field is updated by means of a finite element technique.

A question arises as to the use of data. Swedlow[77] prefers to deal with tabular data for a discrete number of values of the plastic strain (strain-rate and temperature being assumed constant) and uses linear interpolation for intermediate values. Hockett[119] prefers to assimilate a mathematical equation to match the experimental data. Suzuki et al[122] present the results in graphical form, as do Lengyel and Mohitpour[123]; both plot also the experimental results.

A mathematical equation is perhaps more suited for analytical procedure, but the user must always be aware of the limits of validity of the equation. Hockett[119] obtains his results for commercial purity aluminium by means of a cam plastometer; he presents an extensive review of literature and selects four equations to fit the stress-strain curve, under unchanged conditions of strain-rate and temperature. They are the

$$\text{Power equation} \qquad k = A\,(\bar{\epsilon}^p)^m ,$$

$$\text{Ludwik's equation} \qquad k = A + B\,(\bar{\epsilon}^p)^m ,$$

$$\text{Swift's equation} \qquad k = A\,(B + \bar{\epsilon}^p)^m$$

and

$$\text{Voce's equation} \qquad k = A - (A - B)\,e^{m\bar{\epsilon}^p} ,$$

where A, B and m are constants, and e, in Voce's equation, is the Naperian logaritmic basis. Hockett then proceeds to fit these several equations to his tabular experimental data, using the Los Alamos General (Nonlinear) Least Squares Program, thus finding the best values for the several constants, for every one of the four forms of the stress-strain equation.

His results must be accepted, as he stresses, in global terms. The best fit is obtained in statistical terms over the whole range of strains considered (up to 0.7), but local errors can restrict the applicability of the equation. For instance, at low strain-rates (less than 11.5 s^{-1}) and at a temperature of 400°C the best fit for larger strains is supplied by Swift's equation; However, the constant B is found to be negative, which means that the flow stress drops to zero for

$$\bar{\epsilon}^p = -B$$

and assumes complex form below that value. The equation, therefore, has no signification at strains below $-B$, and the error with respect to the tabular data is substantial in the immediate vicinity above that critical value. For $\dot{\epsilon} = 0.114\ s^{-1}$, for instance, he obtains

$$k = 35.658\,(-0.000865 + \bar{\epsilon}^p)^{0.152}\ \mathrm{MN/m^2}$$

(we have converted his A constant to SI units), which matches sa-

tisfactorily his experimental curve for $\bar{\bar{\epsilon}}^p \geq 0.1$, but below that value the error becomes considerable.

We therefore decided to abandon Hockett's coefficients and to fit an equation, in Swift's form, to match his experimental data. Swift's formula contains three parameters to be defined, and the natural procedure would be to write the formula for three of the datum points, and to solve the resulting transcendental equations. Such an approach, however, does not yield satisfactory results, whatever the three-point sample may be, the reason being the presence of a marked "knee" in the data at about $\bar{\bar{\epsilon}}^p = 0.1$. The consequent approach is then to find coefficients from the several possible three-point combinations, and then to analyse the results and to suitably modify them in order to improve the fitting to the experimental data. Having done this, we found, for strain-rates of the order of 0.114 s^{-1} and temperature of 400°C,

$$k = 36.078\ (0.0417 + \bar{\bar{\epsilon}}^p)^{0.1908}\ MN/m^2 \qquad (4\text{-}1)$$

and this expression is used in the rest of this work. This equation gives

$$k_o = 36.078 \times 0.0417^{0.1908} = 19.677\ MN/m^2 \qquad (4\text{-}2)$$

for the initial yield stress. Eqn. (4-1) is plotted in Fig. 4-1, and compared with Hockett's equation, which fits the data better at higher values of strain. The discrepancies between the two equations at lower values of strain can be observed, but is shown more drastically in a logaritmic plot, as seen in Fig. 4-2.

Hockett[119] does not provide personal data for temperatures above 400°C, but he compares his results at this temperature with the ones presented by Alder & Phillips[120], for temperatures of 350 and 450°C. Although their experiments were restricted to intermediate values of strain-rate (1 to 40 s^{-1}), the agreement obtained by Hockett is good. However, Alder & Phillips's results present a high degree of scattering, which means that extrapolations to very small strain-rates become extremely unreliable, and a local comparison with Hockett's results is impossible.

A more recent work by Evans and Dunstan[126] is restricted to strain-rates above 27 s^{-1}. Although a thorough examination

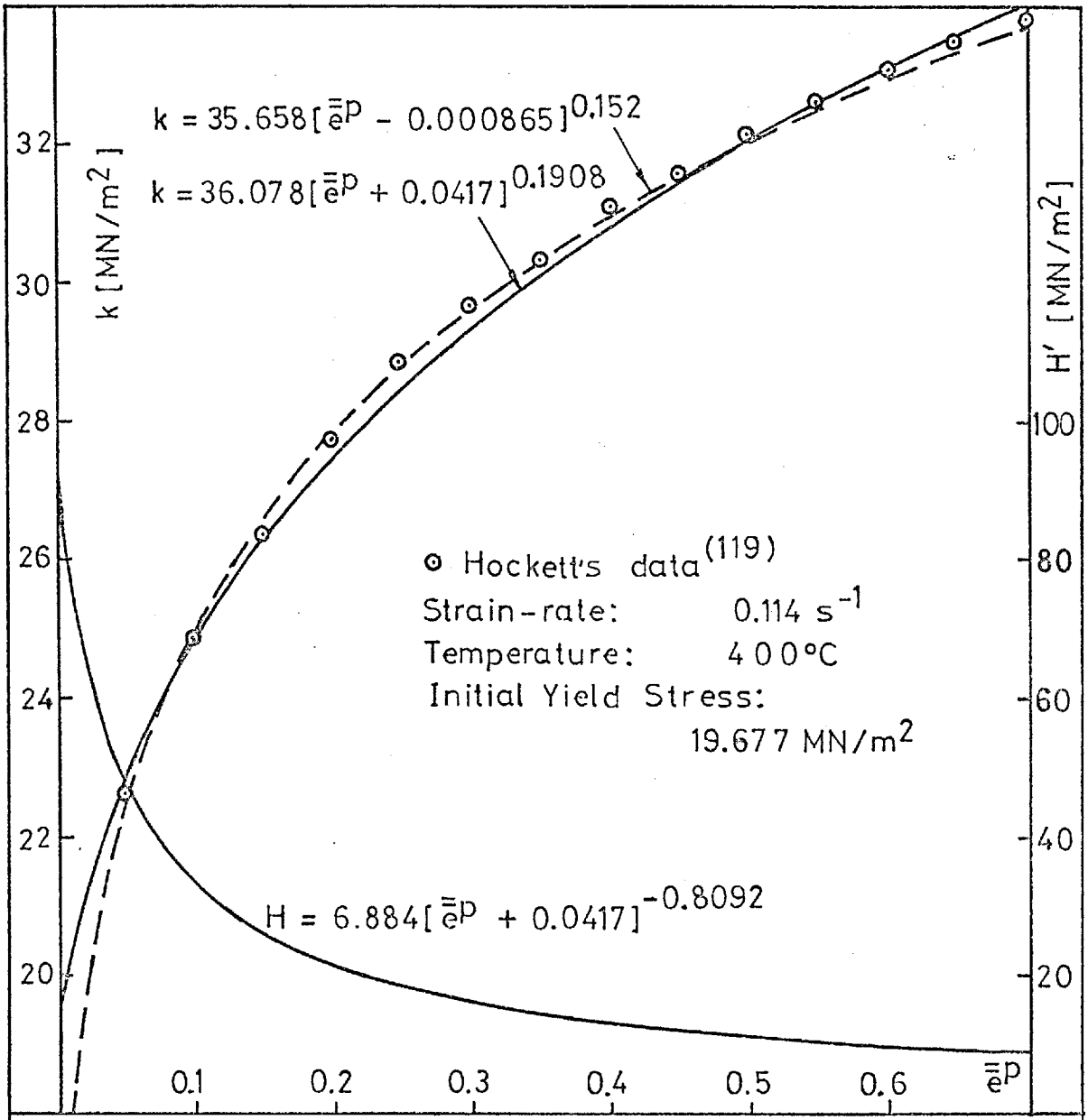
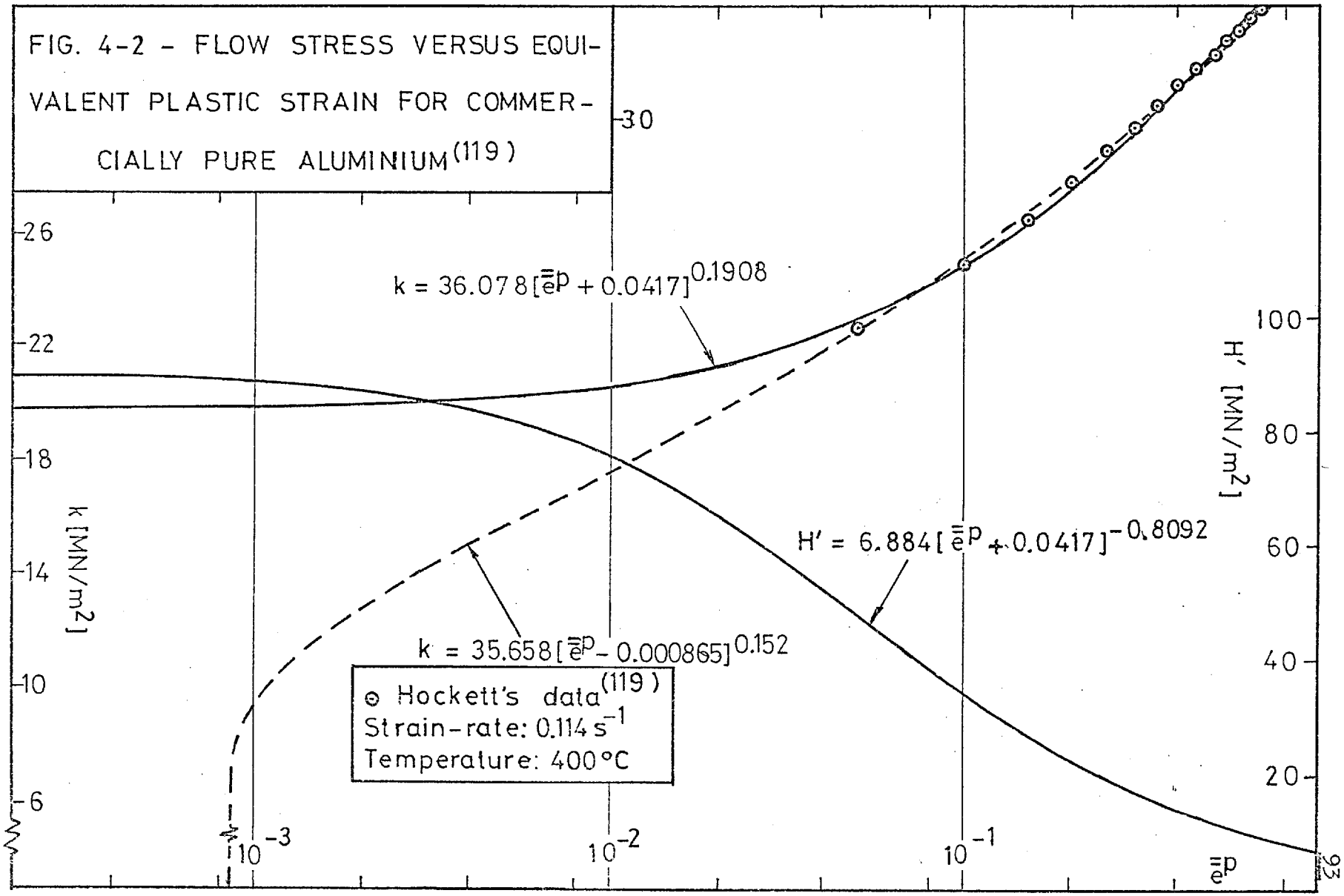


FIG. 4-1 - FLOW STRESS IN TERMS OF PLASTIC STRAIN FOR COMMERCIALLY PURE ALUMINIUM(119)

of the behaviour of the material is presented, considering loading, unloading and reloading (with varying delay times), covering temperatures up to 480°C, and backed by electron-microscopy analysis of the effect of deformation on the structure, the lack of small strain-rate data does not allow the use of their results for the purposes of this work.


FIG. 4-2 - FLOW STRESS VERSUS EQUIVALENT PLASTIC STRAIN FOR COMMERCIALLY PURE ALUMINIUM(119)
k = 36.078[ē^p + 0.0417]^0.1908
H' = 6.884[ē^p + 0.0417]^-0.8092
k = 35.658[ē^p - 0.000865]^0.152
⊙ Hockett's data(119)
Strain-rate: 0.114 s^-1
Temperature: 400 °C
k [MN/m²]
H' [MN/m²]
ē^p
10^-3
10^-2
10^-1
30
26
22
18
14
10
6
100
80
60
40
20
93

A comparison of Hockett's[119] and Alder and Phillips's data[120] for their common range of strain-rates suggests that an increase in temperature from 400 to 450°C produces a drop of the order of 20 to 25% in the flow stress. However, as mentioned before, this conclusion cannot be extrapolated reliably to very small strain-rates. On the other hand, as shown in our paper[127], presented as an Appendix to this work, the variation in temperature to be expected to occur in the deformation zone, in a radial upsetting experiment, will not be more than about 20°C, except possibly in the immediate vicinity of the roller/specimen contact surface. Neglecting such local effect, a constant temperature flow curve could be used for the whole deformation zone, with no substantial error.

4.3 - APPLICATION TO THE RADIAL UPSETTING PROCESS

When restricting the formulation presented in Section 3.2 to the radial upsetting process, the specific boundary conditions must be expressed, as well as certain specific geometrical relationships.

4.3.a - Reference Systems

In order to achieve this, we start by locating the coincident coordinate systems mentioned in Chapter 2 with respect to the undeformed specimen. As is shown in Fig. 4-3a, where the thickness of the specimen and of the roller have been intentionally and grossly exaggerated, the origins of both coordinate systems are taken at the centre of the mid-plane of the specimen. Axes X_1 , x_1 initially connect the rotation axes of specimen and roller, while axes X_3 , x_3 are coincident with the geometrical axis of the specimen. Axes X_2 , x_2 are then taken perpendicularly to those, and oriented upwards, to form left-hand systems. Both coordinate systems will be assumed to be resident in the specimen, and thus to rotate about the axes X_3 , x_3 as deformation progresses. This means that after deformation starts, the first axes will no longer intercept the rotation axis of the roller.

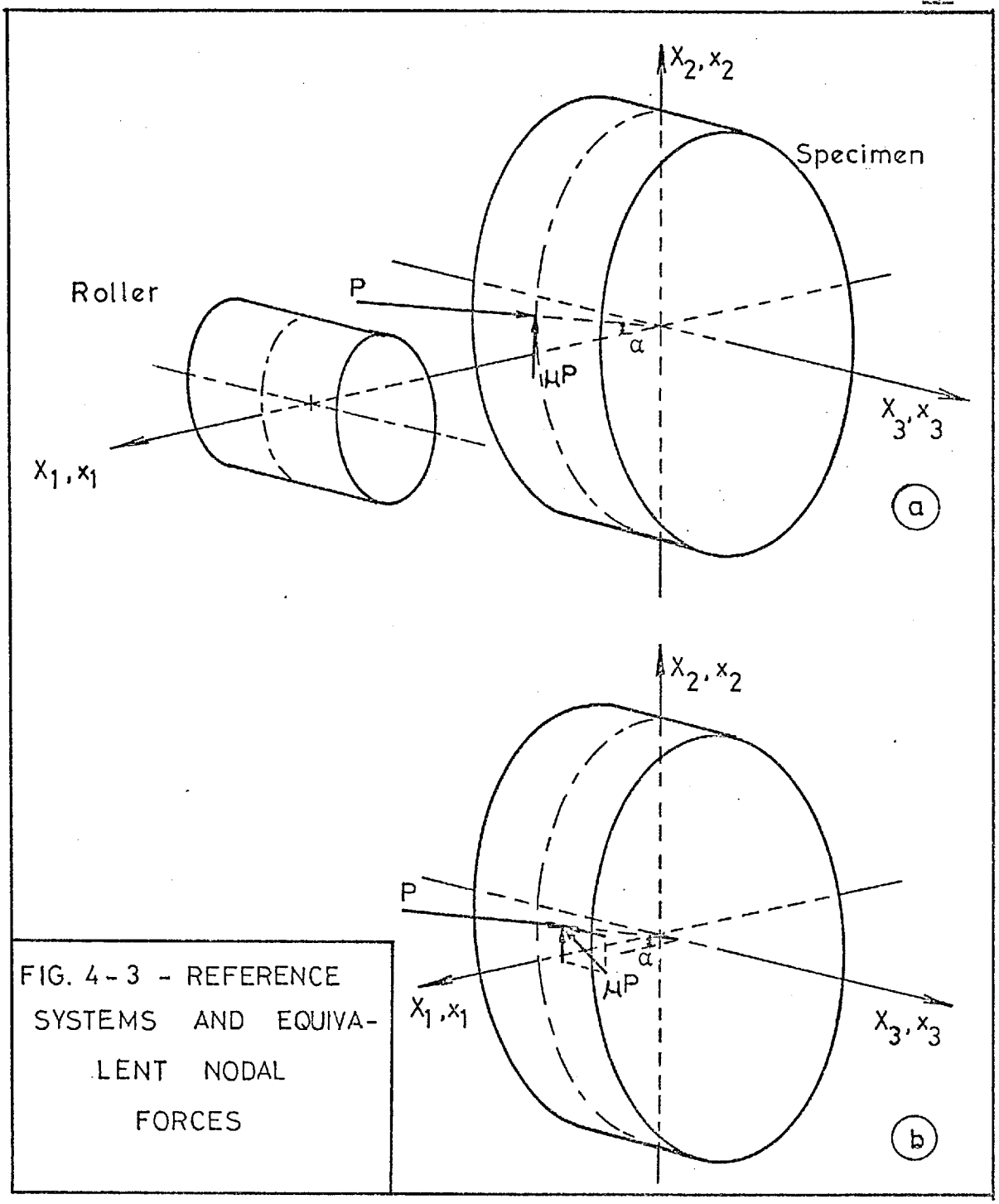


FIG. 4-3 - REFERENCE SYSTEMS AND EQUIVALENT NODAL FORCES

We now replace the set of external and friction components of nodal forces by a new set, comprising both the external (applied) and friction term.

If a force acts perpendicularly to the cylindrical mantle of the specimen, and exactly on its mid-plane (Fig. 4-3a),

the friction component will be tangential, and the effective force components will be given by

$$P_1 = - |P| (\cos\alpha + \mu \sin\alpha),$$
$$P_2 = - |P| (\sin\alpha - \mu \cos\alpha),$$
$$P_3 = 0,$$

due to the symmetry of the specimen and of the deformation process. When the force does not act on the mid-plane, the corresponding friction force will no longer lie in the mid-plane and neither will it be parallel to it (Fig. 4-3b), and will thus present an axial component. An assumption has to be made as to the magnitude of this component, and we will accept that it increases linearly with x_3, whilst the tangential component drops accordingly, falling to zero at the edge of the contact area. Under this assumption, if T is the instantaneous thickness of the specimen, the tangential and axial components of friction would be expressed respectively by

$$\mu |P| \sqrt{1 - \left(\frac{2x_3}{T}\right)^2}$$

and

$$- \mu |P| \left(\frac{2x_3}{T}\right),$$

consequently

$$P_1 = - |P| \left(\cos\alpha + \mu \sqrt{1 - \left(\frac{2x_3}{T}\right)^2} \sin\alpha\right), \quad (4\text{-}3a)$$

$$P_2 = - |P| \left(\sin\alpha - \mu \sqrt{1 - \left(\frac{2x_3}{T}\right)^2} \cos\alpha\right) \quad (4\text{-}3b)$$

and

$$P_3 = - |P| \mu \left(\frac{2x_3}{T}\right). \quad (4\text{-}3c)$$

In a general situation, if an external force has coordinate components P_1, P_2, P_3, and a normal component P_n (with respect to the contact surface), the effective total components would be expressed by

$$P_{1_{eff}} = P_1 - \mu |P_n| \sqrt{1 - \left(\frac{2x_3}{T}\right)^2} \sin\alpha , \quad (4\text{-}4a)$$

$$P_{2_{eff}} = P_2 + \mu |P_n| \sqrt{1 - \left(\frac{2x_3}{T}\right)^2} \cos\alpha \quad (4\text{-}4b)$$

and

$$P_{3_{eff}} = P_3 - \mu |P_n| \left(\frac{2x_3}{T}\right), \quad (4\text{-}4c)$$

similar expressions holding for incremental terms.

4.3.c - BOUNDARY CONDITIONS

For the sake of computing economy, only a sector of the specimen, comprising the roller/specimen interface and the plastic deformation zone, is used to house the finite element mesh. Fig. 4-4 illustrates the partially deformed specimen in a typical instantaneous situation, with the volume element housing the mesh removed. It is clear that a set of boundary conditions has to be imposed to establish the equilibrium between the removed sector and the rest of the specimen. Forces as yet unknown must be assumed as acting over the sector, on the interfaces ABCD , DCC'D' , A'B'C'D' and ADD'A' , to compensate for the effect of the rest of the specimen. Displacement boundary conditions must be imposed, which are compatible with those forces. Three different situations arise, for mid-plane nodes, for nodes in the cylindrical surface DCC'D' and for nodes in the limiting radial planes. More complex situations arise when a node belongs to more than one of those boundaries.

4.3.c.1 - Over the Mid-plane

Nodes lying on the mid-plane face of the sector (surface ADD'A' in Fig. 4-4) must not, due to the symmetry of the specimen and of the deformation process, present axial displacements. That is, we have to prescribe in advance

$$\bar{u}_3 = 0$$

and obtain an axial force component $\bar{P}_3$ which makes this condition become true. Or, in the incremental formulation, we prescribe

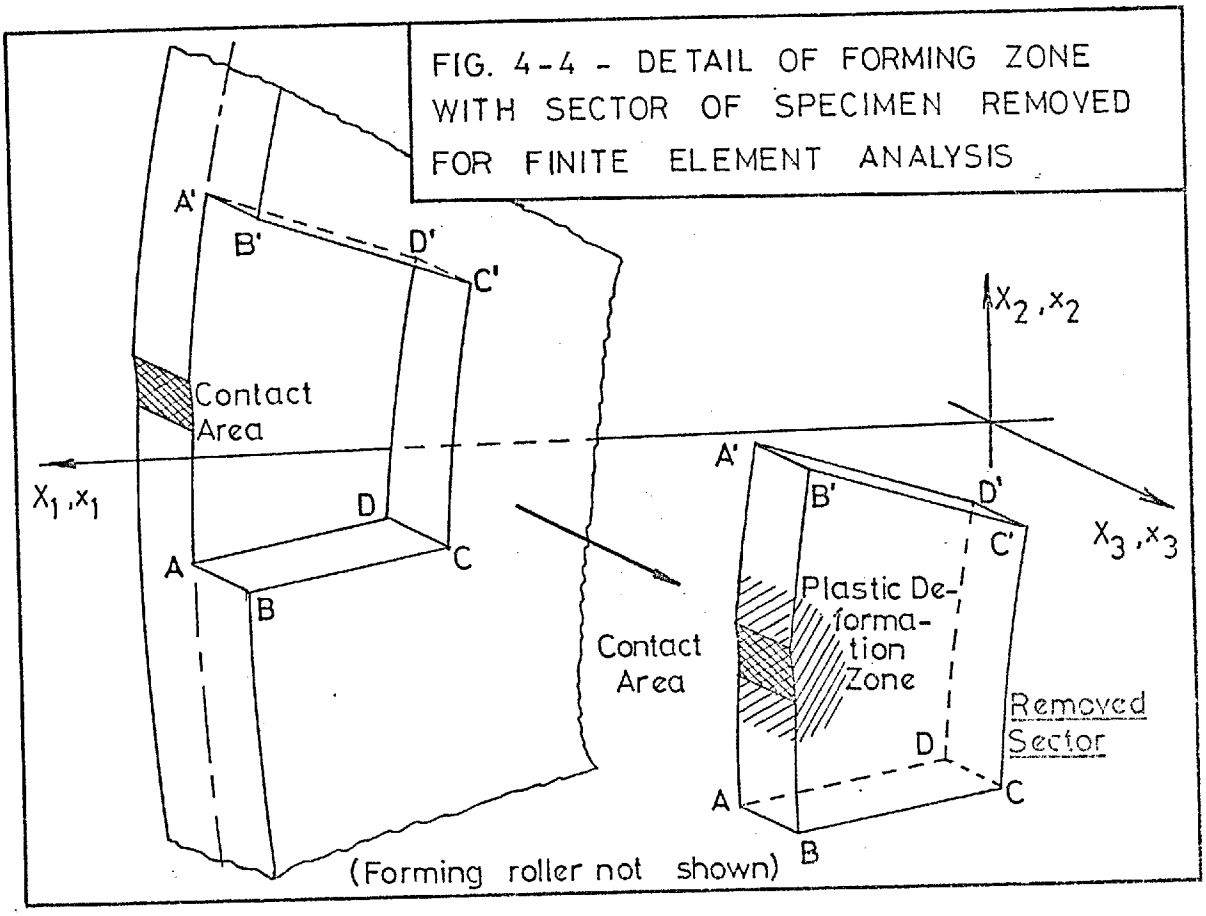


FIG. 4-4 - DETAIL OF FORMING ZONE WITH SECTOR OF SPECIMEN REMOVED FOR FINITE ELEMENT ANALYSIS

$$\Delta\bar{u}_3 = 0 \qquad (4\text{-}5)$$

and find a suitable value for the force increment (nodal reaction) $\Delta\bar{P}_3$.

4.3.c.2 - Elsewhere in the Sector/Specimen Interface

The first idea for a boundary condition in this region is to assume the interface to be sufficiently removed from the forming zone so as to lie completely in the elastic region; thus, Hertz's contact theory could be applied to express the boundary condition. However, an exact mathematical formulation becomes extremely laborious. A simple approximation which might be suggested would be to assimilate the large diameter, peripherally loaded specimen to a semi-infinite body under the action of a concentrated - or even a distributed - load, as presented, for instance, in Timoshenko and Goodier[128], pgs. 85-91. A considerable effort has been spent to implement such a boundary condition, but without successful results. In the formulation we obtained, the incremen-

tal force-displacement relationship proved to be extremely ill-conditioned, due to discontinuities introduced by the boundary condition. Convergence could only be obtained for the first load increments, and after considerable effort in the search for an adequate over-relaxation factor.

In the end we decided to abandon completely the Hertzian approach, and to express these boundary conditions alternatively by two sets of equations, one for the radial planes, and one for the cylindrical interface.

Here again, our original aim was to impose simply a rigid boundary hypothesis,

$$\bar{u}_i = 0 \qquad i = 1, 2, 3 ,$$

and consequently also

$$\Delta\bar{u}_i = 0 \qquad i = 1, 2, 3 \qquad (4\text{-}6)$$

throughout both the radial planes and the inner cylindrical mantle, with nodal reactions to be derived from Eqn. (3-19), under the consideration of (4-6). Such an assumption could be justified if the boundaries were kept sufficiently removed from the centre of pressure. This requirement imposed the use of a finite element mesh covering a very large fraction of the volume of the specimen, contained in a very large central angle, and thus becoming extremely expensive. On the other hand, if the boundaries were brought too near to the centre of pressure, the artificiality of Eqns. (4-6) became patent, giving rise to exaggerately high nodal reactions, as soon as the plastic deformation approached the lateral boundaries.

Considering the fact that the radial depth of the meshed volume was made sufficiently large to preserve the aforementioned remoteness requirement, Eqn. (4-6) was kept as boundary condition for the nodes situated in the inner cylindrical mantle.

For the radial planes ABCD and A'B'C'D', however, this condition was relaxed to allow for some sort of displacement of the boundary nodes. Several alternative formulations were ini-

tially considered and eventually abandoned for the lack of proper physical significance or simply for being grossly unrealistic. In the end, a simple condition expressed by

$$\Delta\bar{u}_2 = 0 \qquad (4\text{-}7)$$

was simply adopted, to which the condition expressed by Eqn. (4-5) was added in the case of mid-plane nodes. We do agree that such an expression would hardly be justifiable if a long-range solution were to be sought, covering a wide rotation angle of the specimen. However it can be accepted for the indentation problem (See Section 4.5) and even for the radial upsetting process if the rotation angle is kept small, as eventually happened in the applications to be described in Chapter 6.

4.3.c.3 - Contact Area

A boundary condition remains to be expressed for the nodes lying in the contact zone with the roller. We refer here to Fig. 4-5. Nodes in this location are constrained, by the geometry of the process, to present, for a given load increment, the same displacement increment $\Delta\bar{u}_\alpha$, corresponding to the direction connecting the centres of the specimen and of the roller, as shown in the figure. The assumption is not strictly true, since it does not hold for material entering or abandoning the forming zone during the load increment. These exceptions, however, represent only a small amount of the total forming zone, and can be neglected. On the other side, the forming zone is small with respect to the radius of the specimen, which allows us, in order to simplify the resulting formulation, to assimilate $\Delta\bar{u}_\alpha$ with the radial displacement increment. Thus we have

$$\Delta\bar{u}_\alpha \cong \Delta\bar{u}_r$$

and, therefore,

$$\Delta\bar{u}_r = \text{constant} \qquad (4\text{-}8)$$

will express the boundary condition for the nodes lying in the contact zone. This condition will be used to redistribute the forces acting over the contact area, and thus, to find the

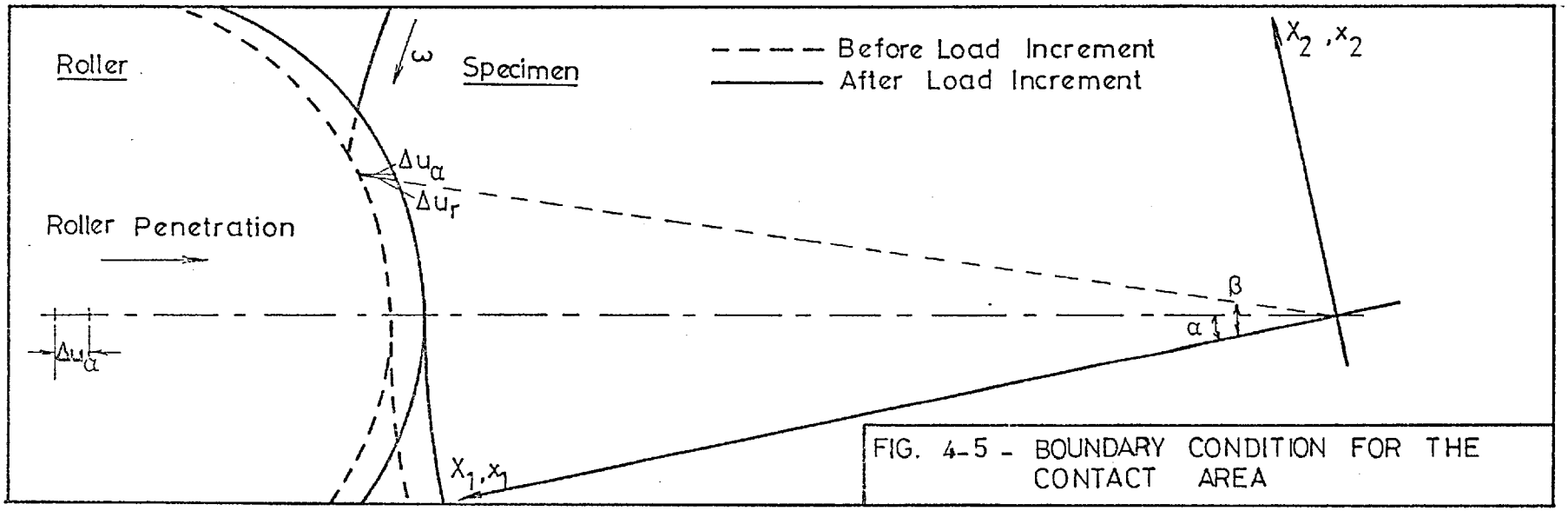


FIG. 4-5 - BOUNDARY CONDITION FOR THE CONTACT AREA

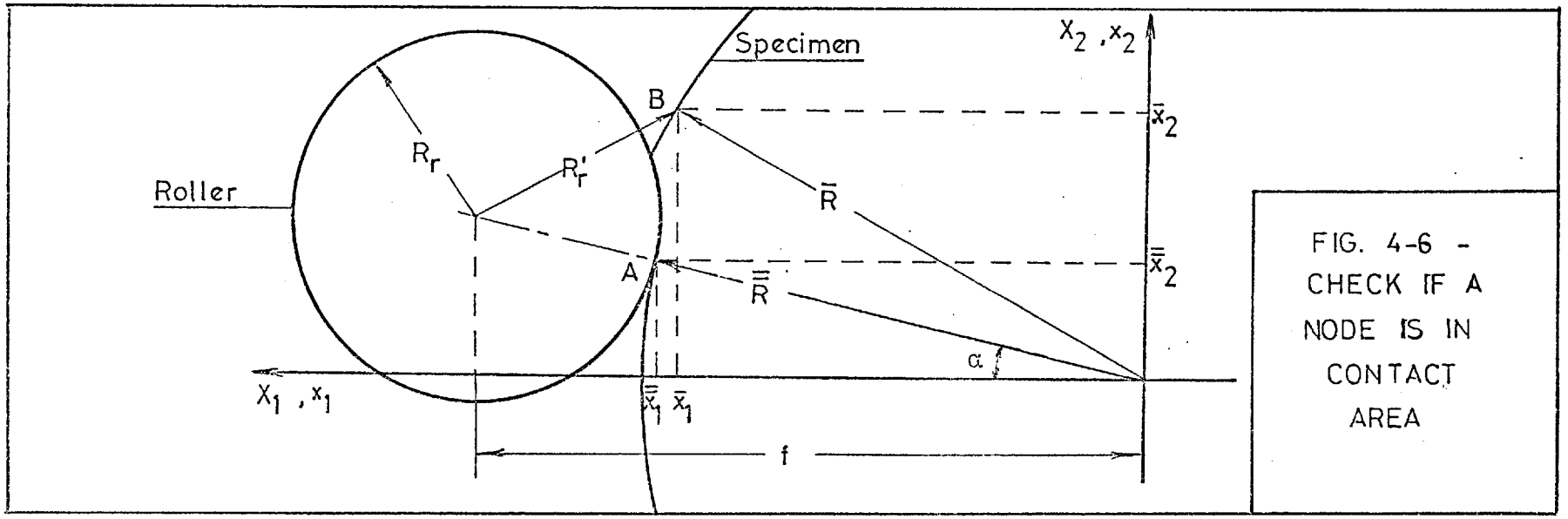


FIG. 4-6 - CHECK IF A NODE IS IN CONTACT AREA

correct load distribution, from any assumed initial distribution.

4.3.d - DELIMITATION OF THE CONTACT ARC

A procedure has been introduced to check whether - in any instantaneous situation - a node is in contact with the forming roller or not. This can be easily verified by simple geometrical relationships, obtained from Fig. 4-6. Let $A(\bar{\bar{x}}_1, \bar{\bar{x}}_2, \bar{\bar{x}}_3)$ represent the node about to leave the contact zone, and $B(\bar{x}_1, \bar{x}_2, \bar{x}_3)$ represent some arbitrary node to be checked (instantaneous coordinates will be relevant in the derivation, and are the ones used to express both points A and B). Let $\bar{\bar{R}}$ and $\bar{R}$ represent, respectively, the instantaneous radius of each of these nodes, and α be the angle by which the axes X_1, x_1 are separated from node A. The distance $\underline{f}$, indicated in the figure, is then expressed by

$$\begin{aligned} f &= (R_r + \bar{\bar{R}}) \cos\alpha \\ &= \bar{\bar{x}}_1 \left(1 + \frac{R_r}{\bar{\bar{R}}}\right). \end{aligned} \qquad (4\text{-}9a)$$

If R'_r is the distance from the axis of the forming roller to node B, then

$$\begin{aligned} R'_r &= \sqrt{(f - \bar{x}_1)^2 + (\bar{x}_2 - f \tan\alpha)^2} \\ &= \sqrt{(f - \bar{x}_1)^2 + \left(\bar{x}_2 - f \frac{\bar{\bar{x}}_2}{\bar{\bar{x}}_1}\right)^2} \end{aligned} \qquad (4\text{-}9b)$$

and obviously

$$R'_r = R_r$$

for contact, and

$$R'_r \geq R_r$$

otherwise.

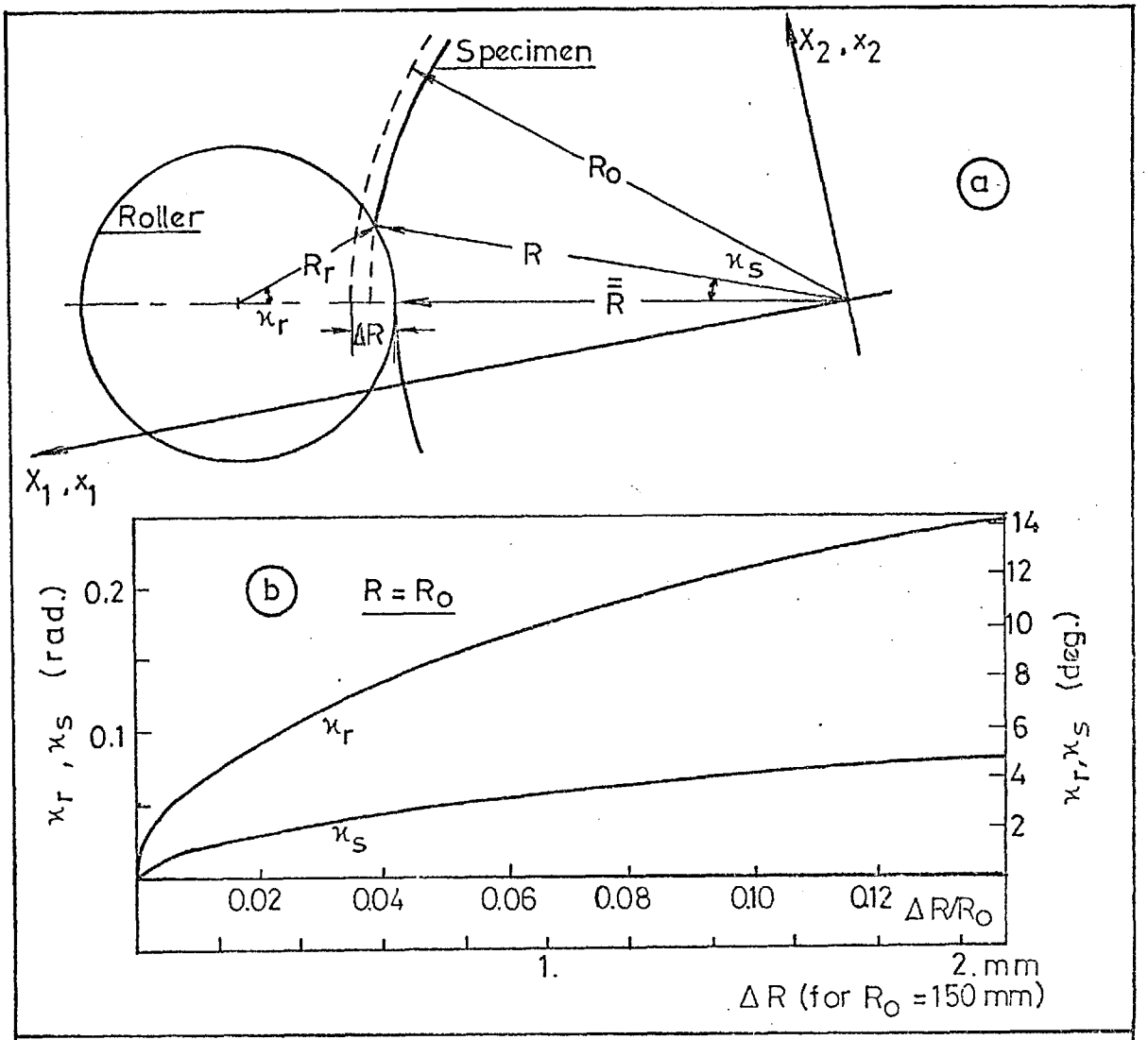


FIG. 4-7 - CONTACT ANGLES IN ROLLER AND SPECIMEN

4.3.e - CONTACT ANGLES IN ROLLER AND SPECIMEN

The contact angles in the specimen and in the roller can be obtained from Fig. 4-7 if it is assumed that the total radial reduction ΔR achieved at a given moment is known. Of course, the limits of the contact arc may not necessarily represent nodes in the finite element mesh. Two equations can be expressed from the figure, involving the contact angles:

$$R_r \sin \varkappa_r = R \sin \varkappa_s$$

and

$$R_r \cos \varkappa_r = R_o + R_r - \Delta R - R \cos \varkappa_s .$$

By squaring and adding up these expressions, the angle $\varkappa_r$ can

be eliminated and by simple mathematical manipulations

$$\cos \varkappa_s = \frac{R^2 + (R_o + R_r - \Delta R)^2 - R_r^2}{2R(R_o + R_r - \Delta R)} \qquad (4\text{-}10a)$$

can be obtained. This expression can now be introduced in the second of the original equations, giving

$$\cos \varkappa_r = \frac{R_r^2 + (R_o + R_r - \Delta R)^2 - R^2}{2R_r(R_o + R_r - \Delta R)} . \qquad (4\text{-}10b)$$

In both Eqns. (4-10a,b) R represents the instantaneous radius of the specimen, after a number of revolutions under the action of the forming roller, while R_o represents the original (undeformed) radius. At the early stages of deformation (first revolution of the specimen) they are, of course, identical. Second order effects, as the accumulation of material ahead of the forming roller, as deformation progresses, were considered negligible in this derivation.

Fig. 4-7b plots $\varkappa_s$ and $\varkappa_r$ as a function of the relative radial penetration $\Delta R/R_o$, for $R = R_o$ and $R_o/R_r = 3$.

4.4 - IMPLEMENTATION OF THE BOUNDARY CONDITIONS

4.4.a - ITERATIVE SOLUTION OF INCREMENTAL DISPLACEMENTS

It has been shown in Section 3.2 that equilibrium in this finite element formulation is expressed in the elemental form by Eqn. (3-12), and in overall terms, under the provisos mentioned in Sub-section 3.2.c, by Eqn. (3-19),

$$\Delta \bar{P}_k^L = \bar{K}_{kn}^{LM} \Delta \bar{u}_n^M .$$

If all components of the nodal force increments could be known in advance, Eqn. (3-19) would simply be used - via some suitable solution algorithm - to supply the corresponding nodal displacement increments. If the Gauss-Seidel iterative procedure is used, it would be preferable to rewrite the equation, temporarily abandoning the summation convention, in the form[25,129,133-135]

$$\sum_{n=1}^{3} \bar{\bar{K}}^{LL}_{kn}\, \Delta\bar{u}^{L}_{n} = \Delta\bar{P}^{L}_{k} - \sum_{M=1}^{L-1}\sum_{n=1}^{3} \bar{\bar{K}}^{LM}_{kn}\, \Delta\bar{u}^{M}_{n} - \sum_{M=L+1}^{N_n}\sum_{n=1}^{3} \bar{\bar{K}}^{LM}_{kn}\, \Delta\bar{u}^{M}_{n}, \qquad (4\text{-}11)$$

N_n being the total number of nodes in the mesh. This equation can now be thought of as representing a subsystem supplying the incremental displacement components for node L, in terms of newly computed displacement increments for nodes 1 up to $L-1$, and of "old" estimates of the same for nodes $L+1$ up to N_n. Talking in terms of the iterative steps, Eqn. (4-11) would give the i^{th} estimate for $\bar{u}^{L}_{n}$ in terms of the i^{th} estimate of $\bar{u}^{M}_{n}$, $M = L+1, \ldots, N_n$. In the specialized literature (as 133) this subsystem approach is known as "block relaxation".

If $\bar{\bar{F}}^{LL}_{qk}$ denotes the terms of the nodal self-flexibility matrix, obtained by the inversion of $\bar{\bar{K}}^{LL}_{kn}$, then

$$\bar{\bar{F}}^{LL}_{qk}\, \bar{\bar{K}}^{LL}_{kn} = \delta_{qk}. \qquad (4\text{-}12)$$

Adding and subtracting

$$\sum_{n=1}^{3} \bar{\bar{K}}^{LL}_{kn}\, \Delta\bar{u}^{L}_{n}$$

to Eqn. (4-11) and introducing also Eqn. (4-12), it can be rewritten to the form

$$\Delta\bar{u}^{L}_{q}\Big|_{i} = \Delta\bar{u}^{L}_{q}\Big|_{i-1} + \sum_{k=1}^{3} \bar{\bar{F}}^{LL}_{qk} \Bigg[\Delta\bar{P}^{L}_{k} - \sum_{M=1}^{L-1}\sum_{n=1}^{3} \bar{\bar{K}}^{LM}_{kn}\, \Delta\bar{u}^{M}_{n}\Big|_{i} - \sum_{M=L}^{N_n}\sum_{n=1}^{3} \bar{\bar{K}}^{LM}_{kn}\, \Delta\bar{u}^{M}_{n}\Big|_{i-1} \Bigg], \qquad (4\text{-}13)$$

the indexed auxiliary bars denoting the iterative step, or cycle, in which the incremental components involved were obtained. The whole expression involving the flexibility factors can be understood as supplying the variations in the particular incremental components, due to the iterative procedure, and expressed simply as $\delta(\Delta\bar{u}^{L}_{q})\Big|_{i}$. To accelerate convergence, an over-relaxation factor ω can be introduced (25, 129-135), giving the "block successive over-relaxation method". Eqn. (4-13) is then rewritten as

$$\Delta\bar{u}^{L}_{q}\Big|_{i} = \Delta\bar{u}^{L}_{q}\Big|_{i-1} + \omega\,\delta(\Delta\bar{u}^{L}_{q})\Big|_{i} . \qquad (4\text{-}13a)$$

Such a solution algorithm will be disturbed in the presence of displacement boundary conditions, when the incremental displacements for some nodes are prescribed in advance, or when a known relationship exists between its components, the incremental forces being then the unknowns. The immediate but clumsy way out would then be the removal of the corresponding equations, the solution of the reduced system of equations, and the return to the removed equations for the calculation of the unknown force components. A different procedure will be followed here. If the double summation terms in Eqn. (4-13) are abbreviatedly expressed as $\Delta\bar{Q}^{L}_{k}$, and if the summation convention is reintroduced, that equation rewrites to

$$\Delta\bar{u}^{L}_{q}\Big|_{i} = \Delta\bar{u}^{L}_{q}\Big|_{i-1} + \omega\,\bar{F}^{LL}_{qk}\,(\Delta\bar{P}^{L}_{k} - \Delta\bar{Q}^{L}_{k})$$

or simply

$$\delta(\Delta\bar{u}^{L}_{q}) = \omega\,\bar{F}^{LL}_{qk}\,(\Delta\bar{P}^{L}_{k} - \Delta\bar{Q}^{L}_{k}) . \qquad (4\text{-}13b)$$

If the displacement increments are prescribed in advance, the variations $\delta(\Delta\bar{u}^{L}_{q})$ should vanish, and convergence would require

$$\Delta\bar{P}^{L}_{k} \longrightarrow \Delta\bar{Q}^{L}_{k} .$$

For programming purposes a procedure is sometimes followed[25,103] in which the force increments $\Delta\bar{P}^{L}_{k}$ of boundary nodes are arbitrarily set to zero in advance, the self-flexibility terms being adequately modified so as to make (for $\omega = 1$)

$$\delta(\Delta\bar{u}^{L}_{q}) = \bar{F}^{LL}_{qk}\,(\Delta\bar{P}^{L}_{k} - \Delta\bar{Q}^{L}_{k}) = -\hat{\bar{F}}^{LL}_{qk}\,\Delta\bar{Q}^{L}_{k} . \qquad (4\text{-}14)$$

The known relations imposed by the boundary conditions will allow the computation of the modified flexibilities $\hat{\bar{F}}^{LL}_{qk}$ and - if necessary - the unknown nodal reactions can be obtained after convergence is achieved. However, the computation of these reactions can only be possible if both the old and new (modified) flexibilities are stored, as well as the internal forces $\Delta\bar{Q}^{L}_{k}$. Once the incremental displacement field has been found, Eqn. (4-14)

can be rewritten to express $\Delta\bar{P}_k^L$ in terms of these variables. Of course, in elastic (one step) problems, the reactions may not be required, and this procedure can be followed without imposing excessive storage burdens on the computer. This is not the case in the present formulation, so an alternative formulation is employed, in which the nodal incremental reactions are computed at the same time as the displacement increments. Such a procedure is described in 4.4.c .

4.4.b - OPTIMIZATION OF THE OVER-RELAXATION FACTOR

The solution of the system represented by Eqn. (3-19), with the associated boundary conditions, could be a direct or an iterative one[135,136]. It is not the purpose of this work to delve into the relative merits of the several possible alternatives of every possible solution method. This has been done elsewhere in general[129,133-135] and specific situations[136].

The solution of large, commonly sparse, linear systems by successive over-relaxation, as implemented above, is widely employed in finite element applications, and will be repeated here. A common characteristic of such applications is the arbitrariness with which values of over-relaxation are prescribed, which does not always lead to the most economical solution.

In our treatment of Eqn. (3-19) we employ a technique for improving the value of the over-relaxation factor, in order to bring it closer to the optimum one. As the stiffness matrix changes from one load increment to the next, so does the corresponding optimum over-relaxation factor, and the optimizing technique must, therefore, be used at all times.

In general the optimum over-relaxation factor is a function of the eigenvalues of the iteration matrix of the system to be solved. There are explicit expressions for that purpose. However, the task of finding reliable estimates of these eigenvalues is generally cumbersome and more time-consuming than operating with a non-optimum factor. Nevertheless, there are techniques[129-132] which allow for the optimization of the value of the over-relaxation factor during the solution process,

at relatively little additional expense and effort, and producing remarkable acceleration in the convergence process. These techniques impose certain requirements on the system matrix (in this case the overall stiffness matrix) which are not always met in practical applications, but they work satisfactorily (though not optimally) if certain of those requirements are not satisfied. That is the case of our stiffness matrix, which does not possess Young's "Property A"[129]. However, in despite of this fact, we employed the optimization technique proposed by Carré[130], and by imposing stricter controls on the newly estimated over-relaxation factors, managed to obtain very good results, with dramatic reductions in the number of cycles required for convergence (as compared with a single pre-established value). Our results seem to indicate an effective way of extrapolating Carré's technique for the case when the system does not possess "Property A". The technique - as we used it - is fully described in Appendix 1, at the end of this work.

4.4.c - IMPLEMENTATION OF THE BOUNDARY CONDITIONS

As all our boundary conditions have been expressed in terms of the vanishing of one or several of the displacement components, we follow an apparently simpler solving scheme which will be described below. In what follows, the triad (q, r, s) will be taken to represent a positive cyclic permutation of the set $(1, 2, 3)$.

4.4.c.1 - Case when one component of displacement vanishes

The relevant boundary condition rewrites, from Eqn. (4-13b), simply to

$$\bar{\bar{F}}^{LL}_{qk} \left(\Delta \bar{\bar{P}}^{L}_{k} - \Delta \bar{\bar{Q}}^{L}_{k}\right) = 0 ,$$

q being the direction along which the displacement is zero. From this equation the corresponding unknown incremental nodal reaction $\Delta \bar{\bar{P}}^{L}_{q}$ is obtained as

$$\Delta \bar{\bar{P}}^{L}_{q} = \Delta \bar{\bar{Q}}^{L}_{q} - \frac{\bar{\bar{F}}^{LL}_{qr}}{\bar{\bar{F}}^{LL}_{qq}} \left(\Delta \bar{\bar{P}}^{L}_{r} - \Delta \bar{\bar{Q}}^{L}_{r}\right) - \frac{\bar{\bar{F}}^{LL}_{qs}}{\bar{\bar{F}}^{LL}_{qq}} \left(\Delta \bar{\bar{P}}^{L}_{s} - \Delta \bar{\bar{Q}}^{L}_{s}\right) . \qquad (4\text{-}15)$$

4.4.c.2 - Case when two components of displacement vanish

Here we have two equations,

$$\bar{F}^{LL}_{qk} \left(\Delta\bar{P}^{L}_{k} - \Delta\bar{Q}^{L}_{k}\right) = 0$$

and

$$\bar{F}^{LL}_{rk} \left(\Delta\bar{P}^{L}_{k} - \Delta\bar{Q}^{L}_{k}\right) = 0,$$

from which, as above, the unknown incremental reactions

$$\Delta\bar{P}^{L}_{q} = \Delta\bar{Q}^{L}_{q} - \frac{\left(\bar{F}^{LL}_{rr}\,\bar{F}^{LL}_{qs} - \bar{F}^{LL}_{qr}\,\bar{F}^{LL}_{rs}\right)\left(\Delta\bar{P}^{L}_{s} - \Delta\bar{Q}^{L}_{s}\right)}{\bar{F}^{LL}_{qq}\,\bar{F}^{LL}_{rr} - \bar{F}^{LL}_{qr}\,\bar{F}^{LL}_{rq}} \qquad (4\text{-}16a)$$

and

$$\Delta\bar{P}^{L}_{r} = \Delta\bar{Q}^{L}_{r} - \frac{\left(\bar{F}^{LL}_{qq}\,\bar{F}^{LL}_{rs} - \bar{F}^{LL}_{rq}\,\bar{F}^{LL}_{qs}\right)\left(\Delta\bar{P}^{L}_{s} - \Delta\bar{Q}^{L}_{s}\right)}{\bar{F}^{LL}_{qq}\,\bar{F}^{LL}_{rr} - \bar{F}^{LL}_{qr}\,\bar{F}^{LL}_{rq}} \qquad (4\text{-}16b)$$

are obtained.

4.4.c.3 - Rigid nodes

In that case the unknown incremental reactions become simply

$$\Delta\bar{P}^{L}_{k} = \Delta\bar{Q}^{L}_{k}, \qquad k = 1, 2, 3. \qquad (4\text{-}17)$$

4.4.d - EXTERNALLY LOADED NODES (CONTACT AREA)

The basic problem related to the nodes lying in the contact area between forming roller and specimen is that there is no advance knowledge as to how the applied load distributes. The boundary condition expressed by Eqn. (4-8) and illustrated in Fig. (4-5) will be used to solve this problem.

Let it be assumed that the distribution of the applied load over the contact area is known at the end of a loading increment, and that the distribution in the next step is to be found. The starting point in the derivation consists in assuming an arbitrary distribution of the incremental load (eg, uniform over the contact area, for simplicity, or proportional to the current load distribution). At the end of an over-relaxation cycle such arbitrary distribution will produce a set of nodal displacement increments in which, for nodes in the contact area,

the boundary condition expressed by Eqn. (4-8) will probably be violated. The load distribution, thus, has to be altered, and this is achieved by suitably replacing the displacement increments for the relevant nodes by a new set satisfying that equation and by correcting the initially assumed load increments in terms of the deviations introduced in the computed displacement increments. The procedure is repeated at the end of each over-relaxation iteration, until convergence is obtained.

This assertion can be proved as follows. If Eqn. (4-13b) is rewritten in cylindrical coordinates - dropping the over-relaxation factor, which eventually cancels out anyway in the derivation, the first (radial) component of displacement variations would be expressed by

$$\delta(\Delta\bar{u}_r^L) = \bar{\bar{F}}_{rr}^{LL}(\Delta\bar{P}_r^L - \Delta\bar{Q}_r^L) + \delta\bar{U}_r^L,$$

where $\delta\bar{U}_r^L$ stands for all the additional terms, which are not relevant in this derivation, provided that changes in $\delta(\Delta\bar{u}_r^L)$ produce changes in $\Delta\bar{P}_r^L$ only. In that case

$$\Delta\bar{P}_r^L = \Delta\bar{Q}_r^L + \frac{1}{\bar{\bar{F}}_{rr}^{LL}}[\delta(\Delta\bar{u}_r^L) - \delta\bar{U}_r^L].$$

If $\Delta\bar{\bar{P}}_r^L$ is the true radial force increment - that is, the one for which Eqn. (4-8) is satisfied - and $\delta(\Delta\bar{\bar{u}}_r^L)$ the corresponding variation in the radial displacement, obviously also

$$\Delta\bar{\bar{P}}_r^L = \Delta\bar{Q}_r^L + \frac{1}{\bar{\bar{F}}_{rr}^{LL}}[\delta(\Delta\bar{\bar{u}}_r^L) - \delta\bar{U}_r^L]$$

holds true. Subtracting this equation from the preceding one,

$$\Delta\bar{\bar{P}}_r^L - \Delta\bar{P}_r^L = \frac{1}{\bar{\bar{F}}_{rr}^{LL}}[\delta(\Delta\bar{\bar{u}}_r^L) - \delta(\Delta\bar{u}_r^L)] \qquad (4\text{-}18)$$

is obtained.

Considering now all nodes in the contact zone, clearly

$$\sum_L \Delta\bar{\bar{P}}_r^L = \sum_L \Delta\bar{P}_r^L,$$

holds, the summation extending only to nodes in the contact

zone. Eqn. (4-18) can thus be rewritten to

$$\sum_L \frac{\delta(\Delta \bar{\bar{u}}_r^L)}{\bar{\bar{F}}_{rr}^{LL}} = \sum_L \frac{\delta(\Delta \bar{u}_r^L)}{\bar{\bar{F}}_{rr}^{LL}} .$$

As the true force increments produce the same variations in radial displacements for all nodes in the contact zone, it follows that

$$\delta(\Delta \bar{\bar{u}}_r^L) = \frac{\sum_L \frac{\delta(\Delta \bar{u}_r^L)}{\bar{\bar{F}}_{rr}^{LL}}}{\sum_L \frac{1}{\bar{\bar{F}}_{rr}^{LL}}} . \qquad (4\text{-}19)$$

This equation shows that the boundary condition (Eqn. (4-8)) will be satisfied for a radial displacement increment which corresponds to a weighted average of the computed variations in radial displacement, the weight factors being the reciprocals of the radial-radial self-flexibilities. Those can be obtained from the Cartesian components of flexibility - for a node - by

$$\bar{\bar{F}}_{rr}^{LL} = \bar{\bar{F}}_{11}^{LL} \cos^2\beta + (\bar{\bar{F}}_{12}^{LL} + \bar{\bar{F}}_{21}^{LL}) \sin\beta \cos\beta + \bar{\bar{F}}_{22}^{LL} \sin^2\beta , \qquad (4\text{-}20)$$

β being the position angle shown in Fig. 4-5. Obviously, this equation is applied irrespective of the fact that other boundary conditions may apply to the same node.

The Cartesian components of displacement variations and force increments must now be accordingly altered. The radial and tangential displacement variations relate to their Cartesian counterparts by

$$\delta(\Delta \bar{u}_r^L) = \delta(\Delta \bar{u}_1^L) \cos\beta + \delta(\Delta \bar{u}_2^L) \sin\beta$$

and

$$\delta(\Delta \bar{u}_\theta^L) = \delta(\Delta \bar{u}_1^L) \sin\beta - \delta(\Delta \bar{u}_2^L) \cos\beta .$$

If no substantial change is assumed to have occurred - due to the correction made - in the tangential component, that is, if

$$\delta(\Delta\bar{\bar{u}}^L_\theta) \cong \delta(\Delta\bar{u}^L_\theta) ,$$

the corrected Cartesian components will be expressed by

$$\delta(\Delta\bar{\bar{u}}^L_1) = \delta(\Delta\bar{u}^L_1) + [\delta(\Delta\bar{\bar{u}}^L_r) - \delta(\Delta\bar{u}^L_r)] \cos\beta \qquad (4\text{-}21a)$$

and

$$\delta(\Delta\bar{\bar{u}}^L_2) = \delta(\Delta\bar{u}^L_2) + [\delta(\Delta\bar{\bar{u}}^L_r) - \delta(\Delta\bar{u}^L_r)] \sin\beta . \qquad (4\text{-}21b)$$

These two expressions can now be introduced in Eqn. (4-13b) giving ultimately

$$\Delta\bar{\bar{P}}^L_1 = \Delta\bar{P}^L_1 + \frac{1}{\omega} \frac{[\delta(\Delta\bar{\bar{u}}^L_r) - \delta(\Delta\bar{u}^L_r)] \; (\bar{\bar{F}}^{LL}_{22} \cos\beta - \bar{\bar{F}}^{LL}_{12} \sin\beta)}{\bar{\bar{F}}^{LL}_{11} \bar{\bar{F}}^{LL}_{22} - \bar{\bar{F}}^{LL}_{12} \bar{\bar{F}}^{LL}_{21}} , \qquad (4\text{-}22a)$$

$$\Delta\bar{\bar{P}}^L_2 = \Delta\bar{P}^L_2 + \frac{1}{\omega} \frac{[\delta(\Delta\bar{\bar{u}}^L_r) - \delta(\Delta\bar{u}^L_r)] \; (\bar{\bar{F}}^{LL}_{11} \sin\beta - \bar{\bar{F}}^{LL}_{21} \cos\beta)}{\bar{\bar{F}}^{LL}_{11} \bar{\bar{F}}^{LL}_{22} - \bar{\bar{F}}^{LL}_{12} \bar{\bar{F}}^{LL}_{21}} \qquad (4\text{-}22b)$$

and

$$\delta(\Delta\bar{\bar{u}}^L_3) = \delta(\Delta\bar{u}^L_3) + \frac{[\delta(\Delta\bar{\bar{u}}^L_r) - \delta(\Delta\bar{u}^L_r)]}{\bar{\bar{F}}^{LL}_{11} \bar{\bar{F}}^{LL}_{22} - \bar{\bar{F}}^{LL}_{12} \bar{\bar{F}}^{LL}_{21}} \Big[\bar{\bar{F}}^{LL}_{31} (\bar{\bar{F}}^{LL}_{22} \cos\beta - \bar{\bar{F}}^{LL}_{12} \sin\beta) + \bar{\bar{F}}^{LL}_{32} (\bar{\bar{F}}^{LL}_{11} \sin\beta - \bar{\bar{F}}^{LL}_{21} \cos\beta) \Big] . \qquad (4\text{-}21c)$$

4.5 - FURTHER APPLICATION: THE INDENTATION PROBLEM

An interesting additional application example can be easily obtained from the formulation and from the computer program, with little additional effort. It concerns the indentation problem, when the forming roller is made to penetrate radially into the non-rotating specimen.

This application case, illustrated in Fig. 4-8, presents a second symmetry plane, which introduces an additional boundary condition (provided this plane is taken as part of the finite element mesh). The coordinate systems embedded in the specimen do not rotate any more with respect to the roller, and the condition

$$\bar{u}_2 = 0$$

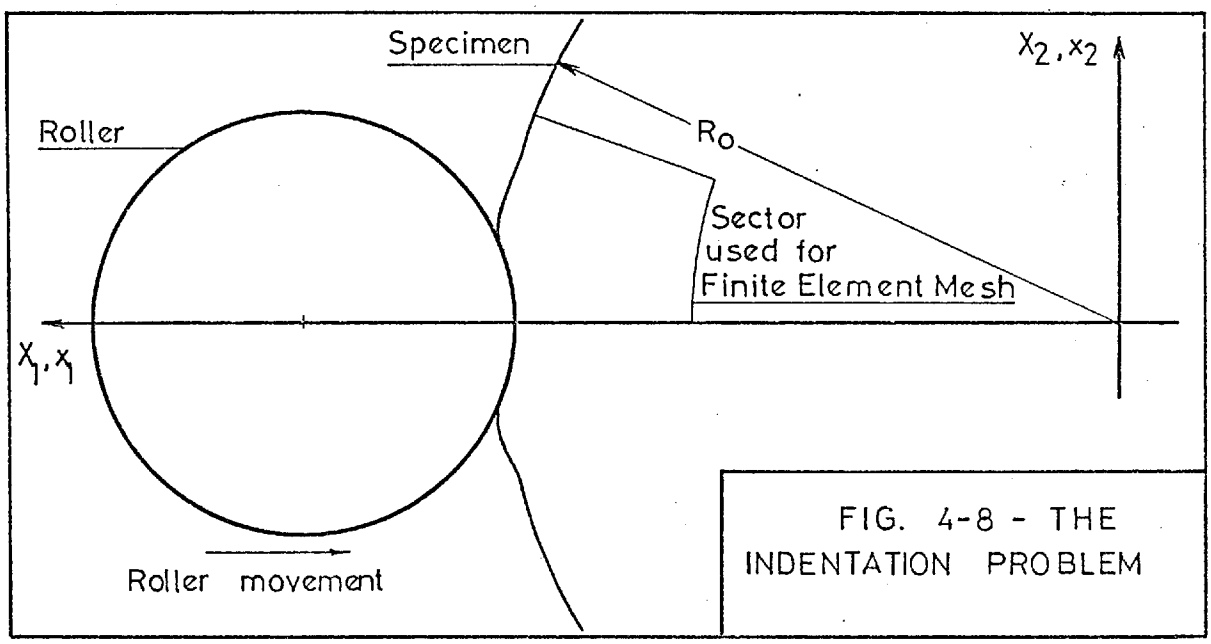


FIG. 4-8 - THE INDENTATION PROBLEM

or

$$\Delta\bar{u}_2 = 0 \qquad (4\text{-}23)$$

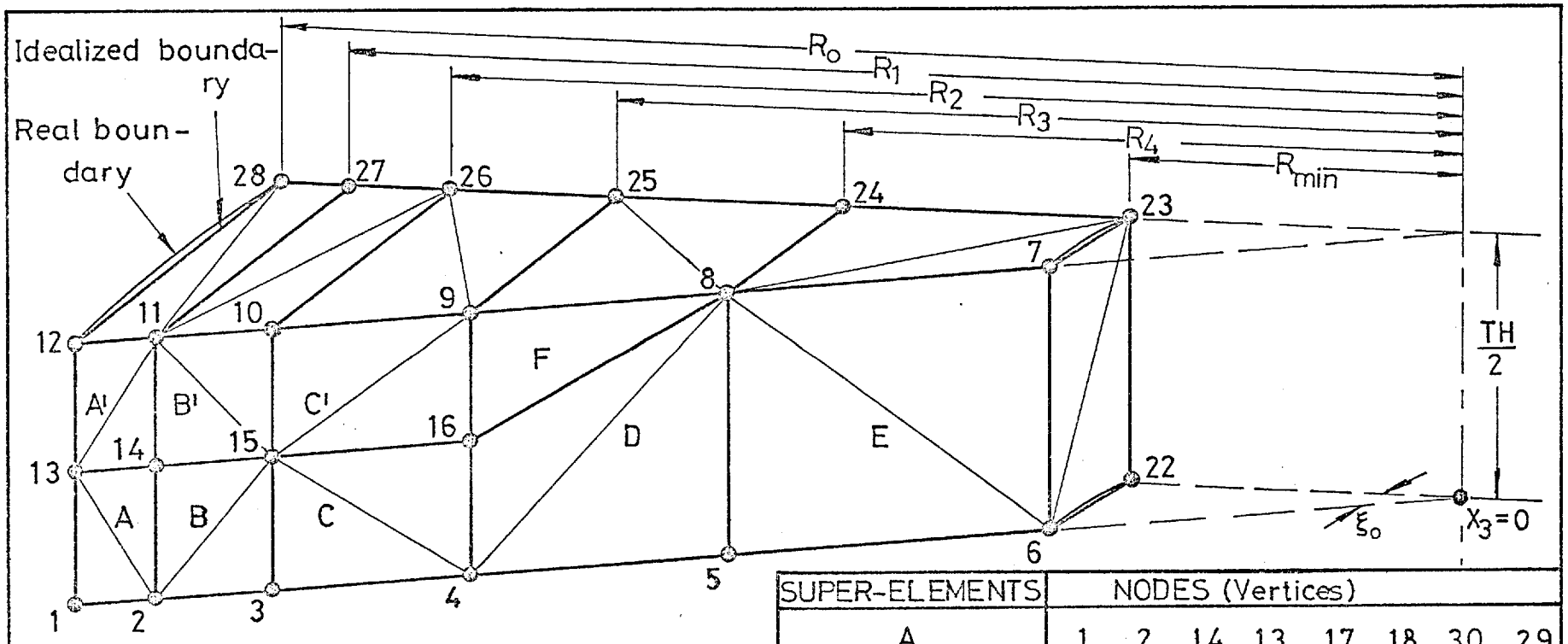
prevails over the plane $X_2 = 0$. This boundary condition must be coupled with the introduction of an unknown incremental force component $\Delta\bar{P}_2$. The treatment of this additional boundary condition, of course, follows the same scheme described in Subsection 4.4.b .

4.6 - THE FINITE ELEMENT MESH

Before introducing the computer program a word must be said about the finite element mesh it employs.

A modular mesh has been used, consisting of a certain number of repeated unit or basic blocks covering the sector detached from the specimen, shown in Fig. 4-4. A basic block covers a central angle ξ_o, which is an exact submultiple of the central angle covered by the meshed sector. Every basic block in the mesh is a mirror image of the preceding one.

If N_{nb} denotes the number of nodes, and N_{eb} the number of elements in the basic block, and if N_b is the number of basic blocks in the mesh, the total number of nodes and



SUPER-ELEMENTS	NODES (Vertices)							
A	1	2	14	13	17	18	30	29
B	2	3	15	14	18	19	31	30
C	3	4	16	15	19	20	32	31
D	4	5	8	16	20	21	24	32
E	5	6	7	8	21	22	23	24
F	8	9	16	24	25	32	—	—
C'	9	10	15	16	25	26	31	32
B'	10	11	14	15	26	27	30	31
A'	11	12	13	14	27	28	29	30

FIG. 4-9 - BASIC BLOCK AND ITS CONSTITUTIVE SUPER-ELEMENTS

elements in the mesh will be expressed by

$$N_n = (N_b + 1) \frac{N_{nb}}{2} \qquad (4\text{-}24a)$$

and

$$N_e = N_b N_{eb} . \qquad (4\text{-}24b)$$

Of course, the subindices now do not represent coordinate directions, and there is no summation involved over repeated indices.

Fig. 4-9 illustrates a basic block and its constitutive super-elements. Super-elements are either hexahedra or triangular based prisms, which can be decomposed into tetrahedral elements according to well established rules[23,24,103]. A hexahedron can be decomposed into at least five tetrahedra, or into two triangular based prisms; those can be decomposed into at least three tetrahedra.

The basic block utilized in this work has thirty-two nodes, which are shared by the adjacent basic blocks. The nine super-elements shown in Fig. 4-9 have all been divided into the minimum possible number of tetrahedral elements, that is, five for the hexahedral ones, and three for the prism. The basic block has thus forty-three elements; therefore, according to Eqns. (4-24a,b), for this specific basic block we have

$$N_n = 16 (N_b + 1)$$

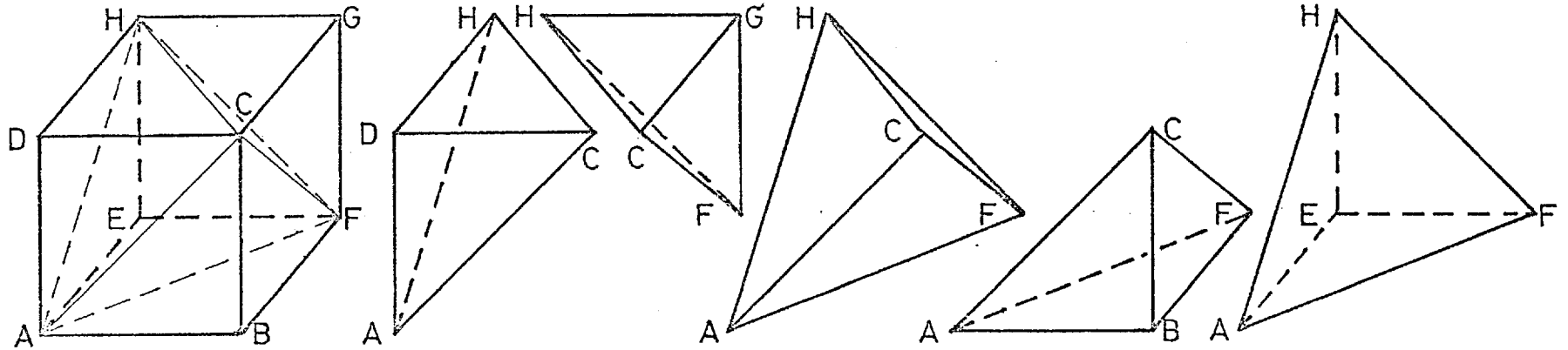
and

$$N_e = 43 N_b .$$

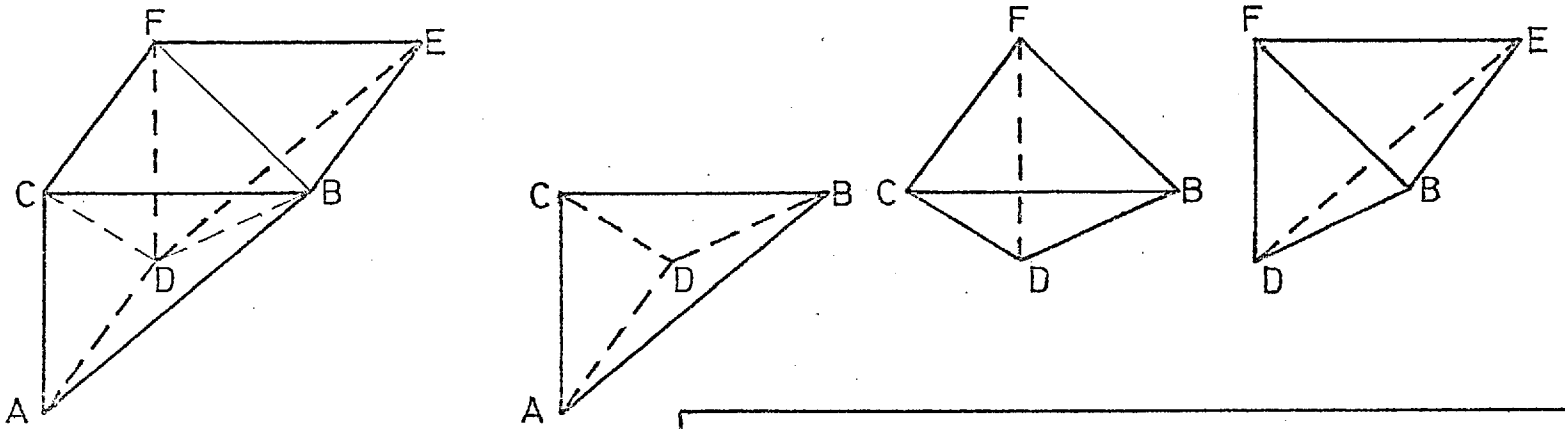
Fig. 4-10 illustrates the decomposition of the basic super-elements into their constitutive tetrahedral elements. Every hexahedral super-element in the mesh is, of course, a topologically transposed copy, or perhaps a mirror image, of super-element A ; every pentahedral super-element is similarly obtained from super-element F . In Fig. 4-10 the extreme faces, corresponding to the angular situations

$$\alpha = 0 \quad \text{and} \quad \alpha = \xi_o ,$$

have been taken as parallel for the sake of simplicity, but the



a) Hexahedral Super-elements



b) Pentahedral Super-elements

FIG. 4-10 - DECOMPOSITION OF THE SUPER-ELEMENTS INTO TETRAHEDRAL UNITS

decomposition rule is obviously not affected when a nonzero central angle is considered. The actual value of the angle ξ_o was chosen in order to produce an acceptable aspect ratio[24] for all elements in the basic block.

The several radii in Fig. 4-9, except the radius of the specimen, are left as open parameters, which can be changed in order to alter the range and fineness of the mesh; the same applies to the angle ξ_o, although in the applications a sole value,

$$\xi_o = \frac{4}{3}^{\circ},$$

was used, which met satisfactorily with the aspect ratio requirements.

The cylindrical boundaries are idealized as planes in the basic block, and therefore as broken lines in the whole meshed sector. A large number of nodes is accumulated in the nearness of the external cylindrical mantle, where stress concentrations are to be expected.

For the general radial upsetting applications the mesh used has one complete basic block situated in the negative side of the X_2 axis, and the first common interface between two adjacent basic blocks is the plane $X_2 = 0$ itself. For indentation applications the whole mesh is shifted by one whole basic block, that is, it starts at the plane $X_2 = 0$, as has already been shown in Fig. 4-8.

In the program to be introduced now, distributed loads over the faces of the mesh are rated among the adjacent nodes, accordingly to the usually adopted rules, and thereafter treated as lumped loads.

4.7 - THE COMPUTER PROGRAM

4.7.a - INTRODUCTION

A computer program has been developed for the formulation presented in Chapter 3, with the restrictions introduced in the preceding sections of this chapter. Both radial upsetting and indentation are covered. A condensed flow block diagram of the program is presented in Fig. 4-11, whilst Appendix 2, at the end of this work, gives the complete listing, including that of the subroutines. Appendix 3 presents the list of the variables utilized in the program and subroutines. This section will be concerned with the implementation of the program, the analysis of its basic features and the investigation of its possibilities and limitations.

The program was developed by the author at the Imperial College between 1972 and 1975.

4.7.b - ANALYSIS OF THE PROGRAM

The program has been called E P F E L D A , for Elastic-Plastic Finite Element Large Displacement Analysis. As is indicated in the flow block diagram of Fig. 4-11, EPFELDA can be loosely subdivided into nine modules, in which specific operations are performed. The term loosely is used here to indicate that

a) subsidiary operations, not relevant to the subdivision presented, may also be performed in each module;

b) operations specifically intended to be performed in a certain module may sometimes be repeated - for operational convenience - in another module.

A tenth module, not indicated in Fig. 4-11, concerned with the output of the complete set of input data, is listed in Appendix 2, but was not used during most of the applications, as a paper saving measure, as most of the data remained unchanged from one testing case to the next. An additional WRITE

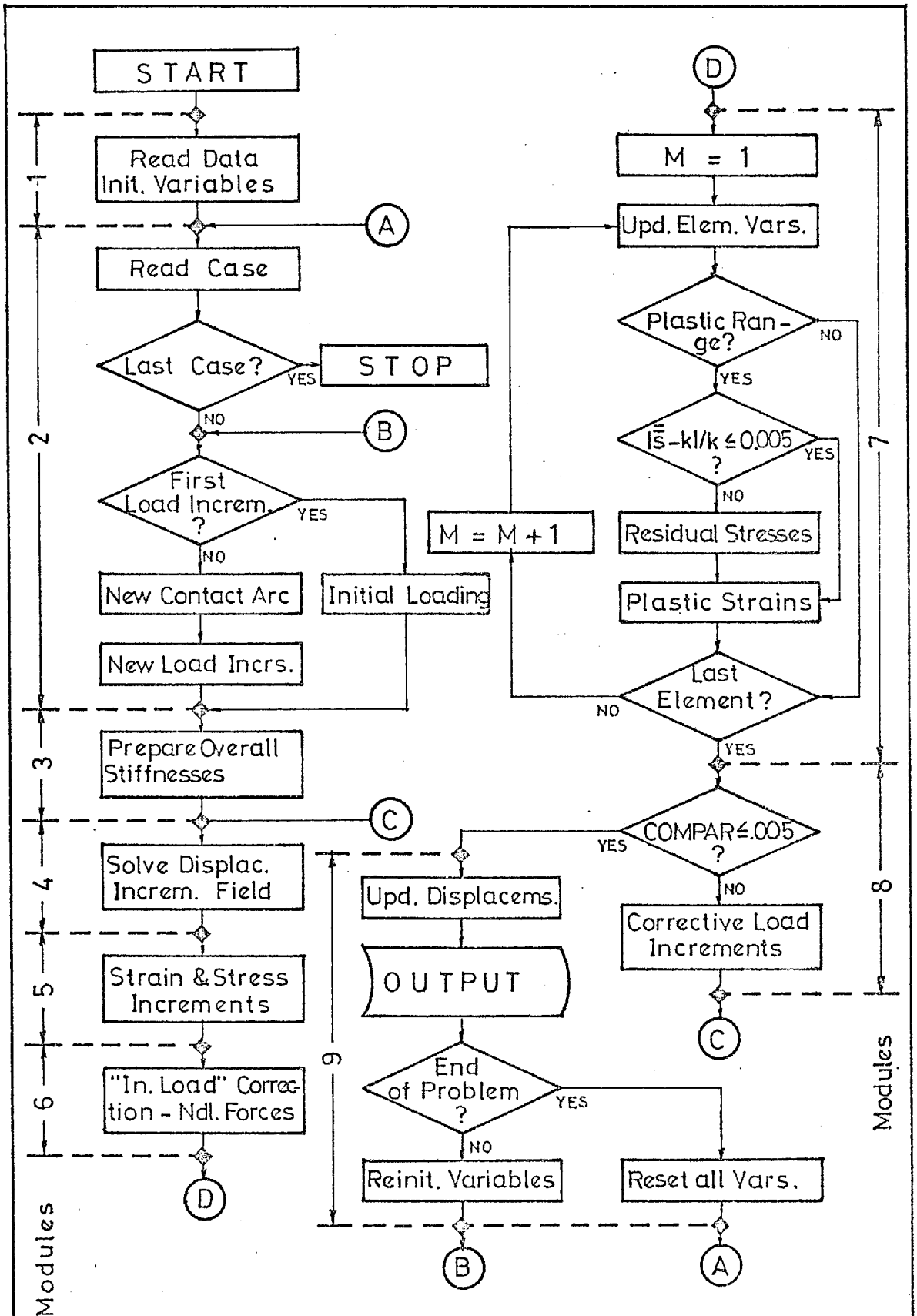


FIG. 4-11 - PROGRAM EPFELDA (Condensed Flow Block Diagram)

statement was added, instead, to Module 2, producing the output of some relevant parameters for each testing case only (angular speed of specimen and friction coefficient).

The program comprises eight subroutines and four function-subroutines, and has seven common blocks. The unlabelled common block obviously enrols the most populated arrays in the program. The intercoupling between the main program and the subroutines, and the distribution of the common blocks is shown in Table 4-1. The main program will be described in the remaining of this sub-section, and the subroutines will be described in 4.7.c .

	EPFELDA	call EPMM	call GAUSS	call FIRST	call STIFF	call TSTIFF	Common Blocks: Unlabelled	C	D	E	EM	GS	ST
EPFELDA							X	X	X	X	X	X	
COEFF	X							X					
DERIV	X					X			X	X			
DERI2	X											X	
EPMM	X									X	X		
GAUSS	X						X	X	X			X	
FIRST						X					X		X
STIFF						X						X	X
TSTIFF	X						X	X	X				X
EQST	X												
KNV	X	X		X	X								
KVN			X			X							
RATST	X												

TABLE 4-1 - Program EPFELDA : Discrimination of subroutines, function-subroutines and common blocks

4.7.b.1 - Module 1 (Data)

Module 1 concerns the entering of data, via punched cards, in groups relating to specific purposes. One group supplies parameters for the successive over-relaxation, another one defines the basic block, one supplies the material properties and testing conditions. Cylindrical components of nodal coordinates are entered for one face of the first basic block. Elements and constitutive nodes are read on for the first basic block only. For an explanation of the several input parameters we refer to the listing of program and variables (Appendices 2 and 3).

The data thus introduced are then used to compute additional but related data. The total number of nodes and of elements in the mesh are obtained from the data for the basic block and the total number of blocks; the elastic (Eulerian) matrix is generated by Eqn. (2-11a). Nodes are then scanned, and Cartesian coordinates and condition numbers (defining the position of the node with respect to the geometry of the boundaries) are computed, and some nodal variables are initialized. Finally, all the elements are scanned, their constitutive nodes are generated and geometrical data related to the elements are computed, via subroutine CØEFF, which is described in 4.7.c.1. During this scanning, other elemental variables are also initialized.

4.7.b.2 - Module 2 (Initializations)

This module bisects into two branches, one of which is only used for the first load increment, the other one being used for all subsequent ones.

In the first load increment the friction coefficient and an arbitrary initial load increment are read on. This arbitrary load is applied over the peripheral nodes lying at the azimutal position $\alpha = 0$ (Figs. 4-5,6), that is, $X_2 = 0$. Some geometrical variables are initialized. Eventually, if there are further test cases to be examined, the program may return to this branch or stop, once the current test case is concluded.

In the subsequent load increments the rotation angle is updated, as well as the list of externally loaded nodes. A new load increment is arbitrarily distributed among the nodes in the contact zone. The input parameter STEP defines the amount of load introduced per cycle. The exact distribution of the increments prescribed at this stage is immaterial, in view of the procedure described in 4.4.d .

4.7.b.3 - Module 3 (Assemble overall stiffness matrix)

In the main program this module is restricted to calling subroutine TSTIFF , which is described in 4.7.c.8, and which computes the overall stiffness matrix and the self-flexibility submatrices; these are stored in the location of the corresponding self-stiffnesses, which are not required in the over-relaxation routine. The output of this subroutine is transferred to subroutine GAUSS , via the unlabelled common block.

4.7.b.4 - Module 4 (Incremental force-displacement relation)

In the main program this module consists solely in calling subroutine GAUSS , in which the incremental force-displacement relation (Eqn. (3-19)) is solved by successive over-relaxation, the nodal reactions for the restrained boundary nodes are computed and the loading over the contact area with the roller is redistributed.

Due to the linear character of the incremental relation, a multiplying factor (RATIØ) is used to produce a desired amount of displacement increments in the contact zone (eg, rounded-off values). This factor is computed in terms of the input parameter RAT, which is initially set equal to the input parameter STP, but is progressively increased in terms of the parameter DINCR , so that progressively larger radial penetrations are achieved at the successive load increments. As deformation progresses, and more and more elements enter the plastic range, the risk of plastic instability effects increases; the multiplying factor RAT is then "moderated", by the reduction in the values of both STP and DINCR (which is actually performed in Module 9).

The vectors computed by GAUSS are transferred to the main program. Subroutine GAUSS is described in 4.7.c.5.

4.7.b.5 - Module 5 (Strain and stress increments)

Consists of a complete scanning of elements, using the incremental nodal displacements to compute Green's strain increments (Pg. 73), and those to obtain first Kirchhoff (Eqn. (2-27)) and later Truesdell (Eqn. (2-30)) and Cauchy (from Eqn. (2-26c)) stress increments.

In this module, as in module 7, the derivatives appearing in Eqns. (2-2a,b) or (3-5a,b), and in the incremental form of (3-5a,b), are computed separately, by means of subroutines DERIV (4.7.c.2) and DERI2 (4.7.c.3), respectively.

4.7.b.6 - Module 6 (Nodal updating)

This module consists of a simple scanning of the nodes. The iterative procedure described in 3.2.b, to correct the incremental forces, by purging the initial load stiffness dependent term, is applied here. Subsequently the nodal force components are updated and the functions DMU, representing the friction factor dependent part of Eqns. (4-4a,b,c) are prepared, to be used in module 4, in the next load increment.

4.7.b.7 - Module 7 (Updating elemental variables and computing residual stresses)

Again the elements are scanned and the elemental variables are updated, once the relevant increments are computed. Elements remaining in the elastic range receive no further treatment.

For elements entering, or remaining in the plastic range, the full procedure described in 3.3.b, up to step 7, is applied. The equivalent plastic strain increment (3.3.c.3) is computed, and the total plastic strain updated. The rating factor ζ (3.3.c.1) is computed by means of function-subroutine RATST. The stress and strain situation is checked against the prescribed stress-strain curve, and the residual stresses are computed (Eqn. (3-24b)) and stored, and the elemental parameter RD(M) is set from zero to unity. If all the individual RD(M)'s retain their original value, meaning that all elements are either still elastic or nearly exactly yielded, the parameter CØM-

PAR is set to zero, otherwise being set to unity.

The elastic-plastic material matrices are updated in the process by calling subroutine EPMM.

4.7.b.8 - Module 8 (Corrective force increments)

If the comparison parameter COMPAR is zero, the results from the previous module are considered satisfactory, and the execution is diverted to module 9. Otherwise, a new scanning of elements is performed and the remaining steps of the routine described in 3.3.b executed. That is, the residual stresses are used to compute the corrective load increments (Eqn. (3-27)); if the maximum prescribed number of initial stress corrective cycles (NMGØ) has been achieved, execution is carried to the next module, otherwise it is diverted to module 4 (CALL GAUSS).

4.7.b.9 - Module 9 (Output, checks and reinitializations)

This module involves the production of the report concerning each load increment, writing out the full set of results. If the displacement field has not been updated in the previous module, due to a low value of CØMPAR, this is done here. Eventual unbalanced residual forces are removed from the loading system. The radial penetration is checked against a prescribed limit, the plastic strains are checked against a prescribed maximum, plastic strain increments are checked for its sign. Any of these three checks can trigger a termination procedure: all variables are reinitialized, and execution diverted to a new test case (if any) or simply terminated. Otherwise, only the incremental variables are set to zero, and execution returned to module 2. In that case, the number of plastic elements is taken as a measure of the risk of plastic instability, being used to redefine the parameters DINCR and STP (See module 4).

4.7.c - SUBROUTINES

4.7.c.1 - CØEFF

Subroutine CØEFF is called only once for every test case; strictly speaking, it only has to be called again if the finite element mesh is changed. This subroutine computes the volumes of the elements (actually multiplied by a factor 6) and the cofactors of the volume determinant, whose expression is given in page 69. They are stored as the vector V6 and the supermatrix A, respectively; this one is constituted of 4x4 blocks representing the elemental matrices a_i^j appearing in Chapter 3. Both arrays are kept in the unlabelled common block.

The subroutine also checks if the nodes for each element have been supplied in a consistent order (the volume must be positive) and makes the necessary corrections if this does not occur. Thus, from this point of view, the order in which the elemental nodes are punched in the data cards becomes immaterial.

4.7.c.2 - DERIV

Subroutine DERIV computes the Lagrangean derivatives of displacements $u_{i,m}$ (Eqn. (3-5a) and, with them, the Eulerian derivatives of the initial coordinates $X_{i/j}$ (Eqn. (2-8)), the Lagrangean derivatives of current coordinates $x_{i,j}$, and the Jacobean of this coordinate transformation.

The elemental array $u_{i,m}$ is stored as DERU in the common block /DSP/. The coordinate derivatives and the Jacobean are stored as DXNT, DXST and XJC, respectively, in the common block /EDI/.

4.7.c.3 - DERI2

Formally similar to the first part of subroutine DERIV, this one computes the derivatives $\Delta u_{i,j}$ appearing, for instance, in 3.2.a, whenever Eqn. (3-5a) is taken in incremental form. The resulting array is stored as DEDU, and thus returned to the main program.

4.7.c.4 - EPMM

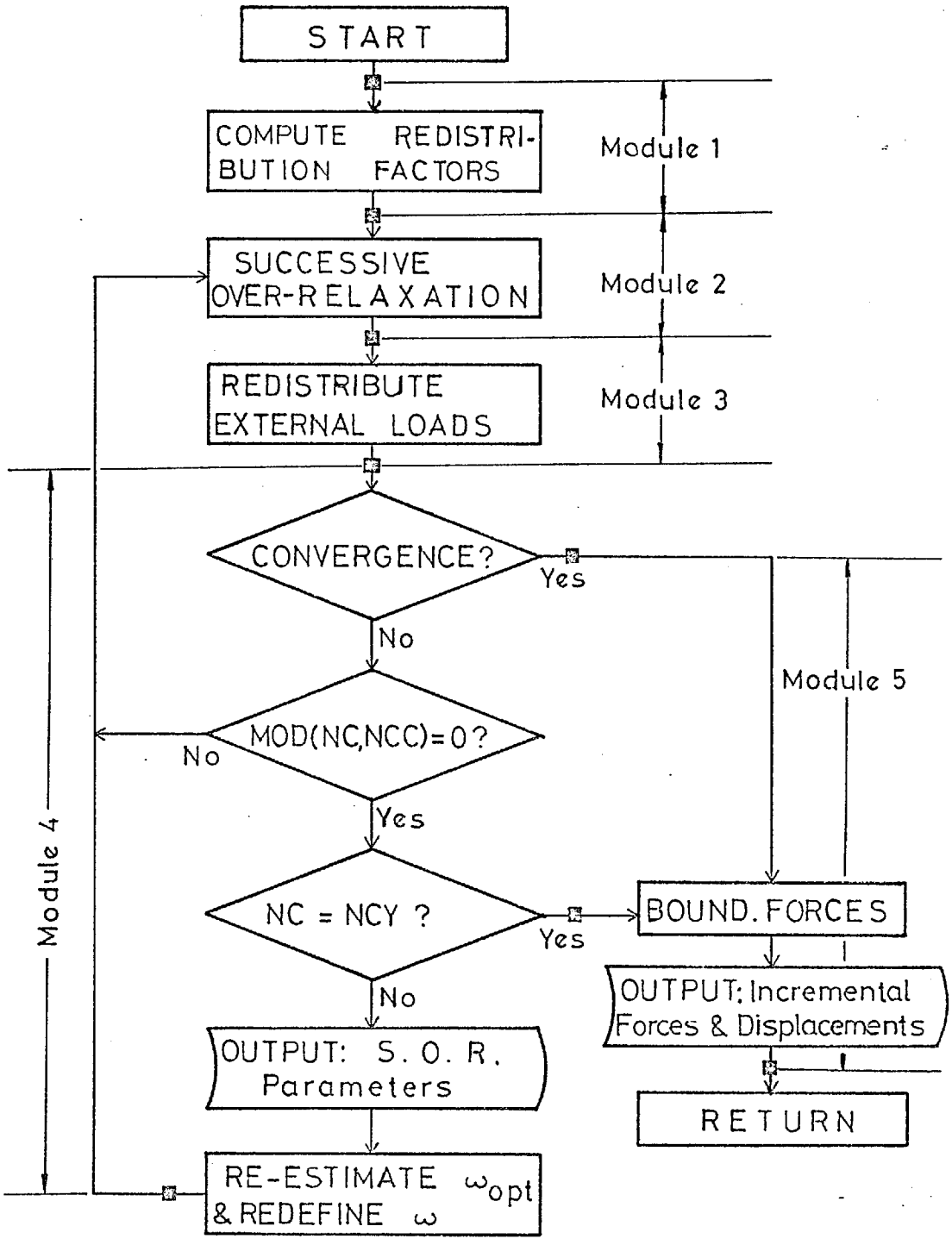
This subroutine computes the elastic-plastic Lagrangean constitutive tensor (or material matrix). In fact, the infinitesimal elastic constitutive tensor appearing in Eqn. (2-11) is entered, as matrix DE, and the elastic-plastic counterpart - Eqn. (2-24) - is first computed and stored as the array D; Eqn. (2-32) is then implemented and the Lagrangean tensor is computed, for a particular element, as DEP, and stored in the total array DT. Both DT and DE return to the main program via the common block /EMM/.

In this subroutine the symmetry properties of the intervening tensors are used to achieve economies in core and computing time. By using the integer function KNV, described in 4.7.c.9, the pairs of indices (i,j) and (r,s) in the 81 component fourth-order tensors are converted into a new single pair of local indices, and the tensors are thus computed and stored as two-dimensional arrays, more specifically as symmetrical 6x6 matrices.

4.7.c.5 - GAUSS

Subroutine GAUSS is the largest and possibly the most important one in EPFELDA. In it, basically, the boundary conditions are introduced to the radial upsetting or the indentation problem, and the incremental force/displacement relation - Eqn. (3-19) - is solved by successive over-relaxation (SOR). Fig. 4-12 presents a condensed flow block diagram for this subroutine, in which it is shown that - in the same way as we have done with the main program - it can be loosely subdivided into five basic modules.

In module 1 the nodes are scanned. For nodes belonging to the roller/specimen interface the weight (or redistribution) factors represented by Eqn. (4-19) are prepared; other nodes are left untreated. The individual numerators of the redistribution factors, which are the reciprocals of the radial-radial self-stiffnesses RADFL, are stored as CFA(N). As, in our numbering, the third node following an interfacial one is never interfacial, we use this same array and store the angle β, appearing in Eqn.



If NC = NCY, unconverged results are printed out

FIG. 4-12 - SUBROUTINE GAUSS - Condensed Flow Block Diagram

(4-20), in the position CFA(N+3). The variable SUMLD is used to store the denominator of Eqn. (4-19).

Module 2 concerns the solution of the incremental force-displacement relation proper, under consideration of the boundary conditions, exception made of the one referring to the roller-specimen interface. The expanded flow block diagram is shown in Fig. 4-13. As the method employed is widely used and well established, we will not elaborate further on the subject at this stage. It is sufficient to say that Eqn. (4-13) is implemented. The boundary conditions are introduced via Eqns. (4-15,16,17). Table 4-2 lists the possible values and the signification of the several control parameters involved in this module, and referred to in Fig. 4-13.

NBC(N)	= -1	Nodes in general (No boundary condition involved) or in the mid-plane
	0	Restrained boundary nodes
	1	Nodes in the lateral face of the specimen
	2	Node in the external cylindrical surface of the specimen
ICP(N)	= 0	Externally loaded node (In contact with the roller)
	1	Otherwise
NIF	-	Number of nodes in the interface between two adjacent basic blocks

TABLE 4-2 - Explanation of the parameters of Fig. 4-13

Module 3 concerns the redistribution of the externally applied loads, as explained in 4.4.d. The procedure is initialized in module 1, prepared in module 2 and fully applied in this module, which is also shown in expanded block diagram form in Fig. 4-14. In this figure, DDR stands for the radial displacement residual $\delta(\Delta\bar{u}_r^L)$ for one loaded node, while DDRM stands for the common corrected residual $\delta(\Delta\bar{\bar{u}}_r^L)$.

The variable FACT, defined at this stage, will be used later to define the multiplying factor referred to in 4.7.b.4.

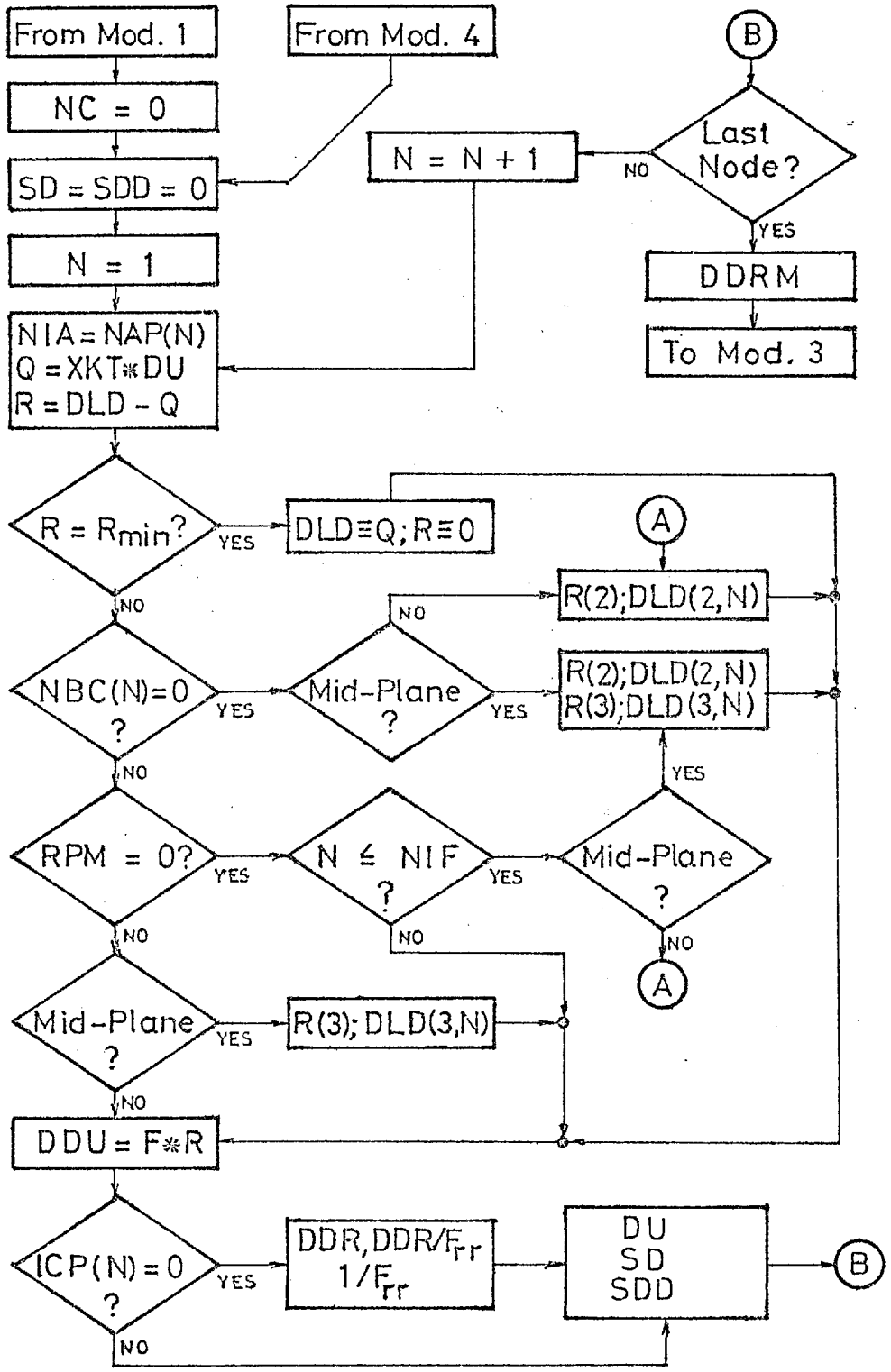


FIG. 4-13 - SUBROUTINE GAUSS (MODULE 2) - FLOW BLOCK DIAGRAM - SOR & BOUNDARY CONDITIONS

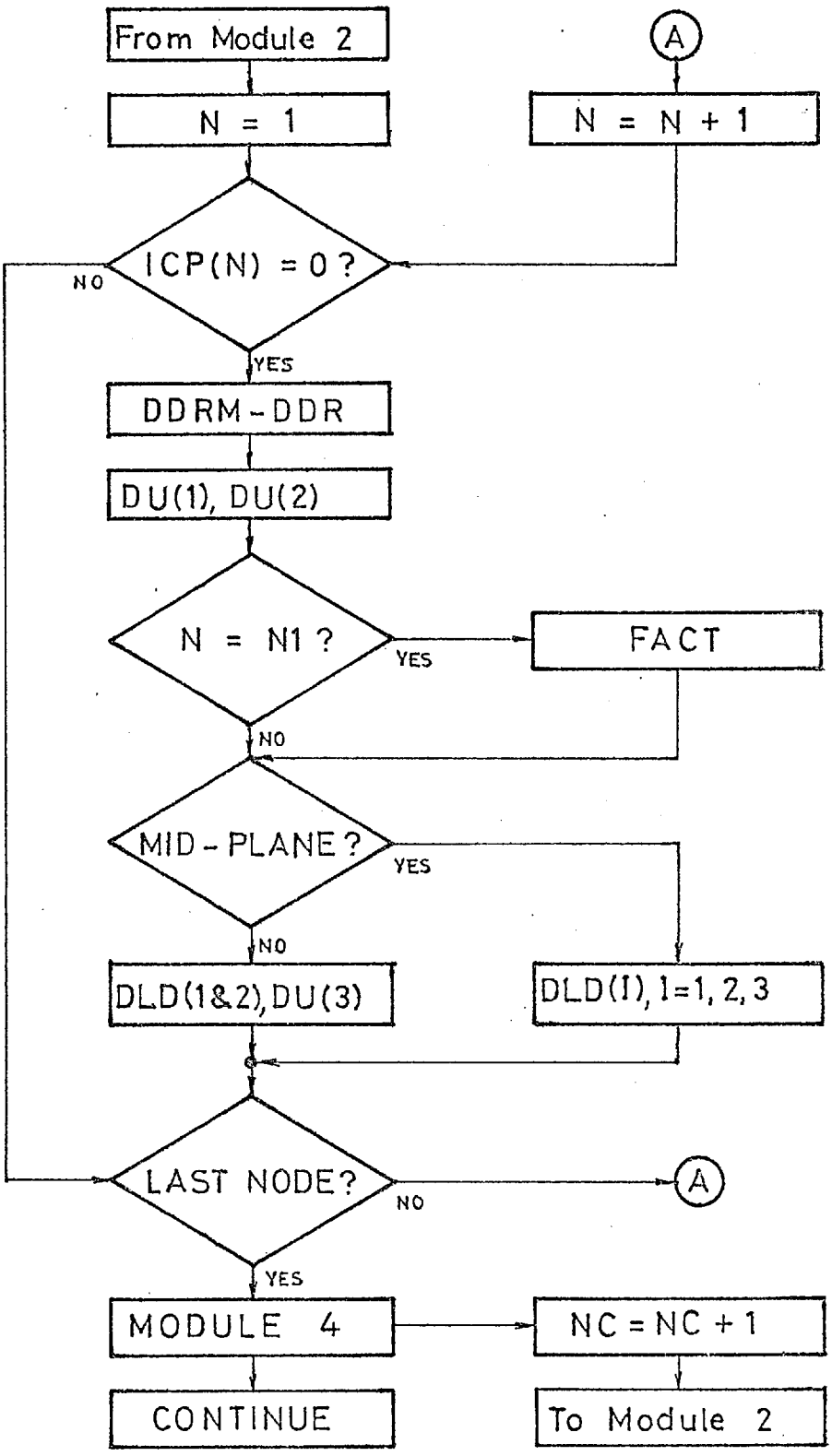


FIG. 4-14 - SUBROUTINE GAUSS (MODULE 3) - FLOW BLOCK DIAGRAM - MULTIPLYING FACTOR & LOAD REDISTRIBUTION

That is, if all displacement and force increments are multiplied by the reciprocal of FACT, the first component of displacement u_1 of any externally loaded node will attain a prescribed value RAT. Of course, this artifice can only be accepted as reasonably valid as long as FACT does not depart substantially from unity, due to the complex geometrical relations involved. Checks are therefore introduced to keep FACT within bounds, by either decreasing or increasing RAT.

It is clear that the applied loads must be intrinsically compressive in both the radial upsetting and in the indentation problem we are considering. Therefore, if a node is unloaded, there is provision introduced in this module, so as to avoid the occurrence of traction forces.

In module 4 the successive over-relaxation procedure is concluded with the check for convergence; a further procedure is introduced to redefine the over-relaxation factor, in order to accelerate convergence, using a method described by Carré[130]. A complete block diagram of this module is shown in Fig. 4-15, but the complete analysis of the procedure is left to Appendix 1.

In module 5 the final value of the multiplying factor RATIO is finally defined, displacement and force increments are corrected and the output report is produced.

Friction is also considered in this subroutine, in module 2. As only a few nodes will ever contact the roller, certain words in the array DNU, which would otherwise remain unused, are employed to store local variables involved in the consideration.

4.7.c.6 - STIFT

This subroutine prepares the elemental stiffness matrices expressed by Eqn. (3-13), by successively adding up the component terms, expressed by Eqns. (3-14a,b,c). The stiffness terms are stored in the array XK and transferred to subroutine TSTIFF via the common block /STF/, where they will be employed in the assemblage of the overall stiffness matrix, using Eqn. (3-20).

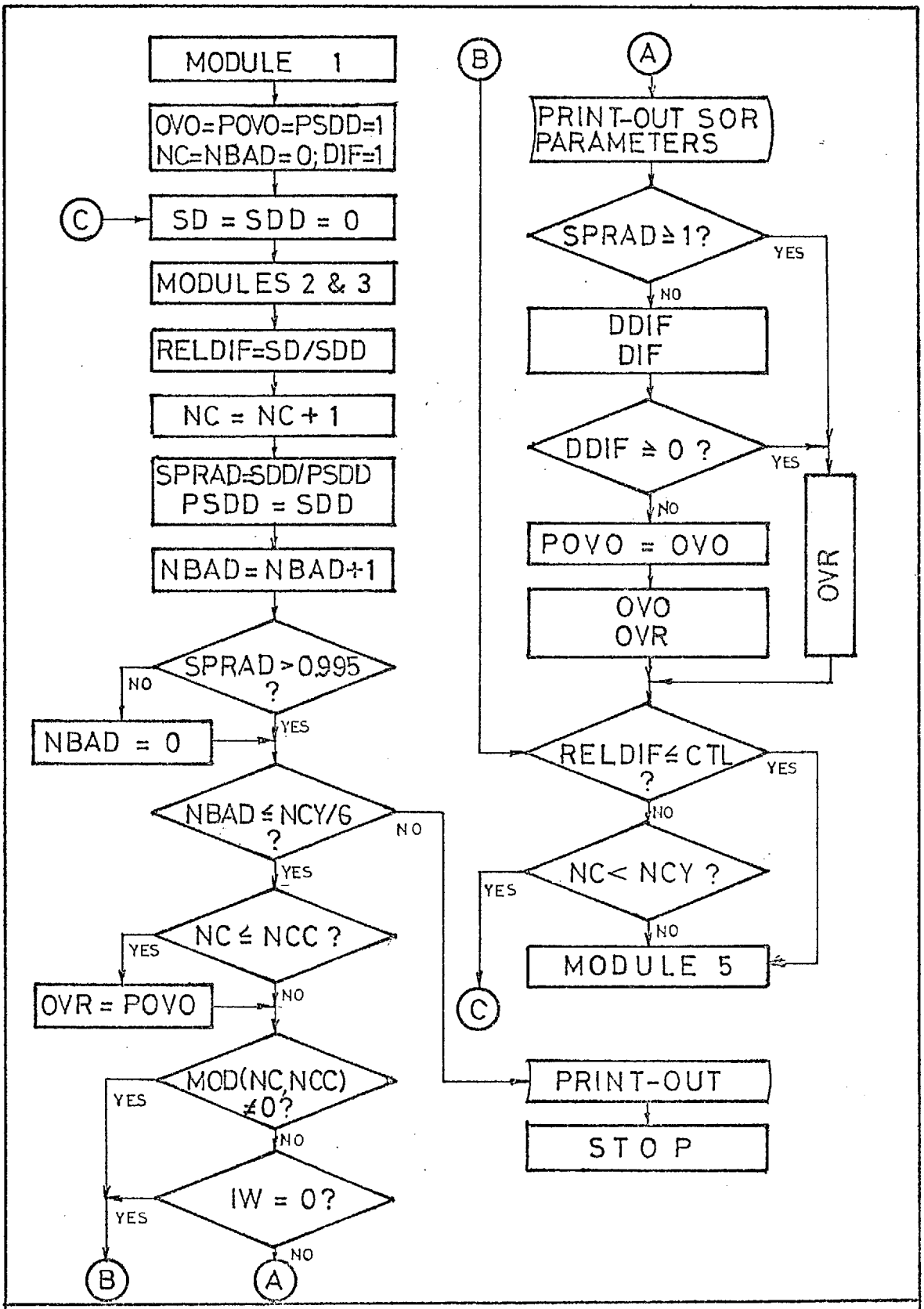


FIG. 4-15 - SUBROUTINE GAUSS (MODULE 4) - FLOW BLOCK DIAGRAM - OPTIMIZATION OF OVER-RELAXATION FACTOR

For programming purposes, XK is presented as a two-dimensional 12x12 array. The correspondence with the four-dimensional tensor expression $\bar{k}_{kn}^{\ell m}$ of Eqn. (3-13), which has 144 components, that is, the identity

$$XK(I,J) \equiv \bar{k}_{kn}^{\ell m}$$

is fully established by defining

$$\ell \equiv 1 + \text{Integer } (I - 1)/3 ,$$

$$m \equiv 1 + \text{Integer } (J - 1)/3 ,$$

$$k \equiv \text{Remainder}(I/3) ,$$

and

$$n \equiv \text{Remainder}(J/3) ,$$

and by replacing k or n by 3 if the above expressions yield a null result.

To avoid scanning the whole range of the 12x12 stiffness matrices, the symmetrically positioned components

$$XK(I,J) \qquad \text{and} \qquad XK(J,I)$$

are computed simultaneously. The parameter FLG, equaling 1 or zero, is used to avoid the duplication of the values to be stored in the main diagonal.

The initial stress stiffness term $^{2}\bar{k}_{kn}^{\ell m}$, expressed by Eqn. (3-14c), becomes zero whenever

$$k = n .$$

This fact is also considered in the subroutine, by means of the parameter

$$FLAG \equiv \delta_{kn} .$$

4.7.c.7 - FIRST

The previously analysed subroutine, although a very simple one from the programming point of view, is a very costly one in terms of the required computing time, due to the complexity of the equations involved, and of the large number of in-

ternested DØ-loops it requires. It would be totally unadvisable to use it for the first load increment, when all elements are still in the elastic range, and the derivatives $X_{i/j}$ reduce to Kronecker deltas. The expression for the component stiffnesses and for the constitutive tensor are then extremely simplified. Besides, there are no initial stresses and displacements to consider, and only the matrix represented by C_{klmn} remains nonzero in Eqn. (3-13). Substantial time can be saved by programming a routine specifically designed for this situation, and subroutine FIRST is intended to cover this purpose.

In fact, it has been given a more general scope. By disregarding only the initial displacement stiffness term in Eqn. (3-13), and introducing only the simplification represented in the formulae by the fact that

$$X_{i/j} \cong \delta_{ij}$$

at the early stages of the deformation process, we programmed FIRST so as to use it through several load increments for all elements still in the elastic range. Obviously, the elastic Lagrangean constitutive tensor is not available at this stage and must be updated after every load increment.

4.7.c.8 - TSTIFF

This subroutine starts by calling either subroutine FIRST (for elements still in the elastic range) or DERIV and STIFF (for elements already in the plastic range), and receives the elemental stiffnesses. These are then assembled into the overall stiffness matrix, according to Eqn. (3-20). The assembling techniques are described more fully elsewhere[23-24]. The resulting matrix, XKT, is then stored in the unlabelled common block. Also in this subroutine the reciprocal stiffness terms (self-stiffnesses) are stored in a local array PRØV, then inverted, producing the self-flexibilities, which are then stored in XKT, in place of their corresponding inverses.

4.7.c.9 - Function Subroutines

There are four function subroutines in EPFELDA , which perform a set of simple but widely repeated operations.

a) EQST - This real function implements Eqn. (2-17), with the second invariant given by Eqn. (2-16a), and thus returns the Eulerian equivalent stress. The six intervening components of stress are supplied in vector form.

b) KNV and KVN - These two integer functions process the indices of double-dimensioned 3x3 arrays, in order to store them or use them in vector form. Function KNV is used for symmetric arrays, as, for instance, stresses, which are converted to a 6-term vector, and thus stored, allowing for an economy in storage requirements. Function KVN is used for general tensors, as stiffnesses and flexibilities, which are converted to a nine-term vector; no storage economy is obtained, but operational advantages may occur in certain specific situations. Table 4-3 presents the results of these two functions.

J \ I	1	2	3
1	1	4	6
2	4	2	5
3	6	5	3

a) KNV(I,J)

J \ I	1	2	3
1	1	4	8
2	6	2	5
3	9	7	3

b) KVN(I,J)

TABLE 4-3 - Integer functions KNV and KVN.

Although these functions are used in most of the subroutines and in the main program, the most patent example of the advantages of its application is found in subroutines EPMM, STIFF and FIRST.

c) RATST - This real function simply implements Eqn. (3-28), thus producing the rating parameter ζ required in the method proposed in 3.3.b, to discriminate between purely elastic and elastic-plastic deformation of an element.

4.7.d - Concluding Remarks

Two points related to the program require further explanation.

In radial upsetting applications the rotational movement of the specimen must be taken into account and introduced in the program. If a very large mesh were employed, it would possibly be easy to implement such a requirement into the formulation. With a relatively coarse mesh as we use, a more cumbersome approach must be followed. It consists in artificially introducing a shift in the applied (existing) load system, from one increment to the next. The shift angle is taken as only a fraction (defined as SUB in the listing of module 2 of the main program) of the central angle ξ_o of the basic block. This implies a re-rating of the applied load with respect to the nodes currently in contact with the roller. Such re-rating, in the program, is performed indirectly, by means of the polynomial factor multiplying the variable FACT1 (also in module 2), which is later used in the preparation of the new load increments. As a consequence, as a node starts to move out of the forming region, the corresponding load increments become smaller and smaller, eventually they become negative; eventually, a next load increment simply cancels out the existing load, meaning that that particular node belongs to basic blocks which are no longer in contact with the forming roller.

In 4.7.c.5 (Subroutine GAUSS) we described how it is possible to produce a desired amount of radial reduction (or roller penetration), within certain limits, by using an adequate multiplying factor, thus exploiting the linear character of the incremental force-displacement relation. By defining the parameter RAT, used to express the multiplying factor, the way we have done in module 2 (4.7.b.2), the roller penetration, in the successive load increments, will be given values which are integer multiples of the parameter STP. Our original aim was to work with only one value of STP, but eventually several values were used (0.01, 0.02 and 0.05). Several loading rates could thus be considered. How the results were influenced will be seen in Chapter 6.

CHAPTER 5

EXPERIMENTAL WORK

5.1 - THE EXPERIMENTAL EQUIPMENT

5.1.a - INTRODUCTION

The concept of the radial upsetting process is schematized in Fig. 5.3: a spinning disc specimen, eventually heated on its periphery, comes into contact with a pressure roller. If sufficient pressure is applied, and plastic deformation produced, the net result will be a radial reduction and peripheral thickening of the disc. The specimen, for that purpose, is driven, whilst the roller may be driven or run idle, rotating about its axis exclusively by the friction effect at the contact zone. Side dies could be added in the deformation zone, in order to contain and redirect the lateral spread of material, thus imparting a definite and predetermined shape to the deformed cross-section.

As becomes clear from the concept of the process, an experimental radial upsetting rig must allow for

a) a certain range of angular velocities of the specimen, preferably with the possibility of continuous variation over the range; as this movement brings fresh material to the deformation zone, we will refer to it, from now on, as the feeding movement.

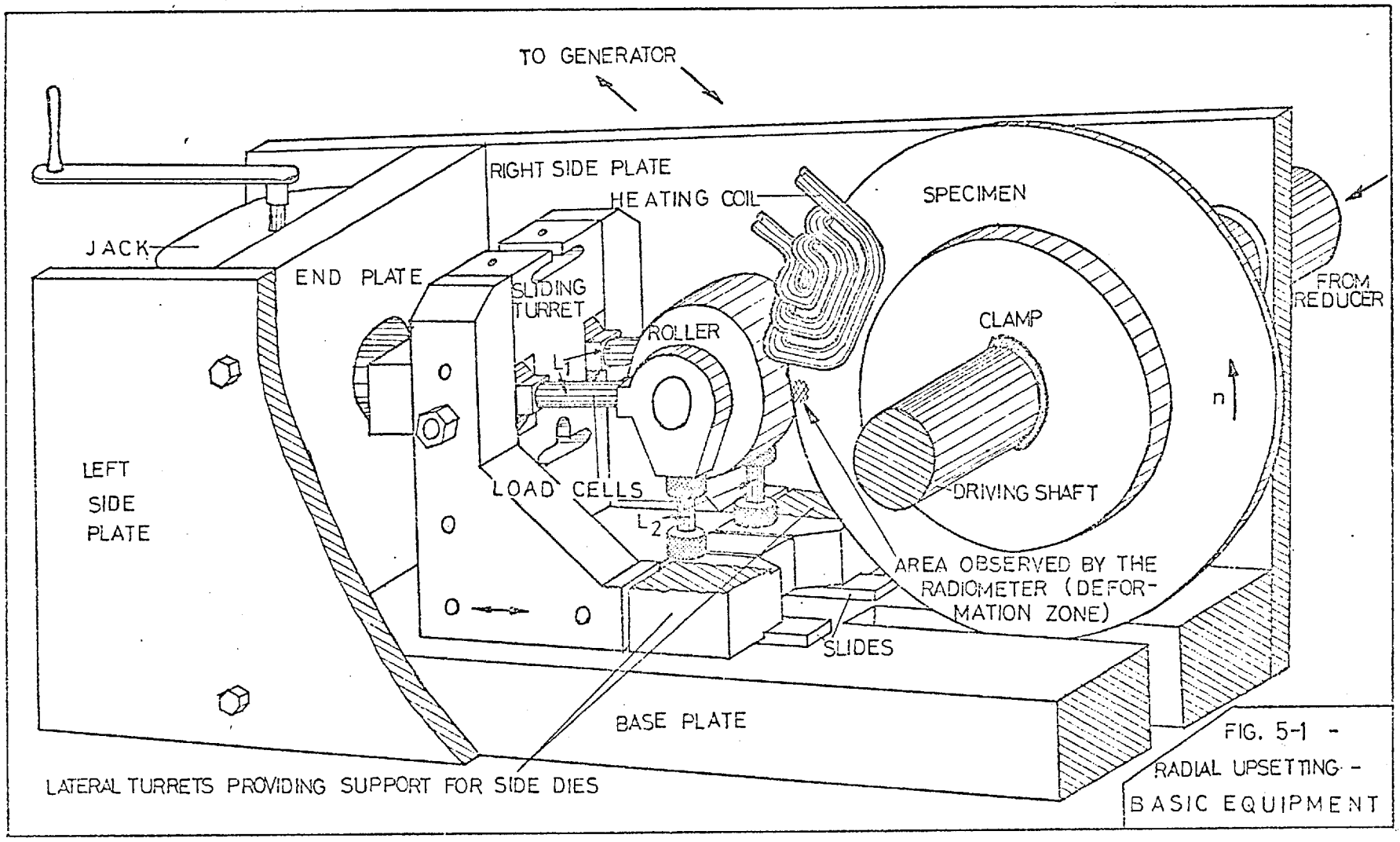


FIG. 5-1 - RADIAL UPSETTING - BASIC EQUIPMENT

b) a linear displaceability of the roller, with which the amount of radial reduction obtained per revolution of the specimen will be defined; this amount will thus be referred to as the penetration per revolution or, when no doubt arises, simply as the penetration.

c) Heating of the specimen, when hot-working is intended.

d) Measuring and control of relevant parameters.

e) Possibility of using specimens of different diameters and thicknesses.

f) Possibility of adding side dies for experiments with restricted deformation.

For the experimental work to be described, a special rig has been designed and constructed, as will be described. No side dies were used at this stage of the research, but provision has been made in the design for their inclusion in an eventual follow-up of this work. The rig has been designed to accept a very wide range of specimen diameters: 250 to 1000 mm.

The penetration movement could, in principle, be obtained manually or by some form of driving system. The manual alternative, by means of a mechanical jack and a handle, was preferred, although it is not out of the question the possibility of eventually replacing the handle by an electric motor plus reducer. In that case some form of control, possibly micro-switches, would have to be used to limit the amount of penetration per revolution.

5.1.b - BASIC EQUIPMENT

The basic equipment used in this work is shown in Fig. 5-1. The driving system for the specimen, measuring and heating facilities are not shown, and will be discussed in another section. It is now sufficient to know that induction heating was used (hence the coil in the figure) and continuous variation

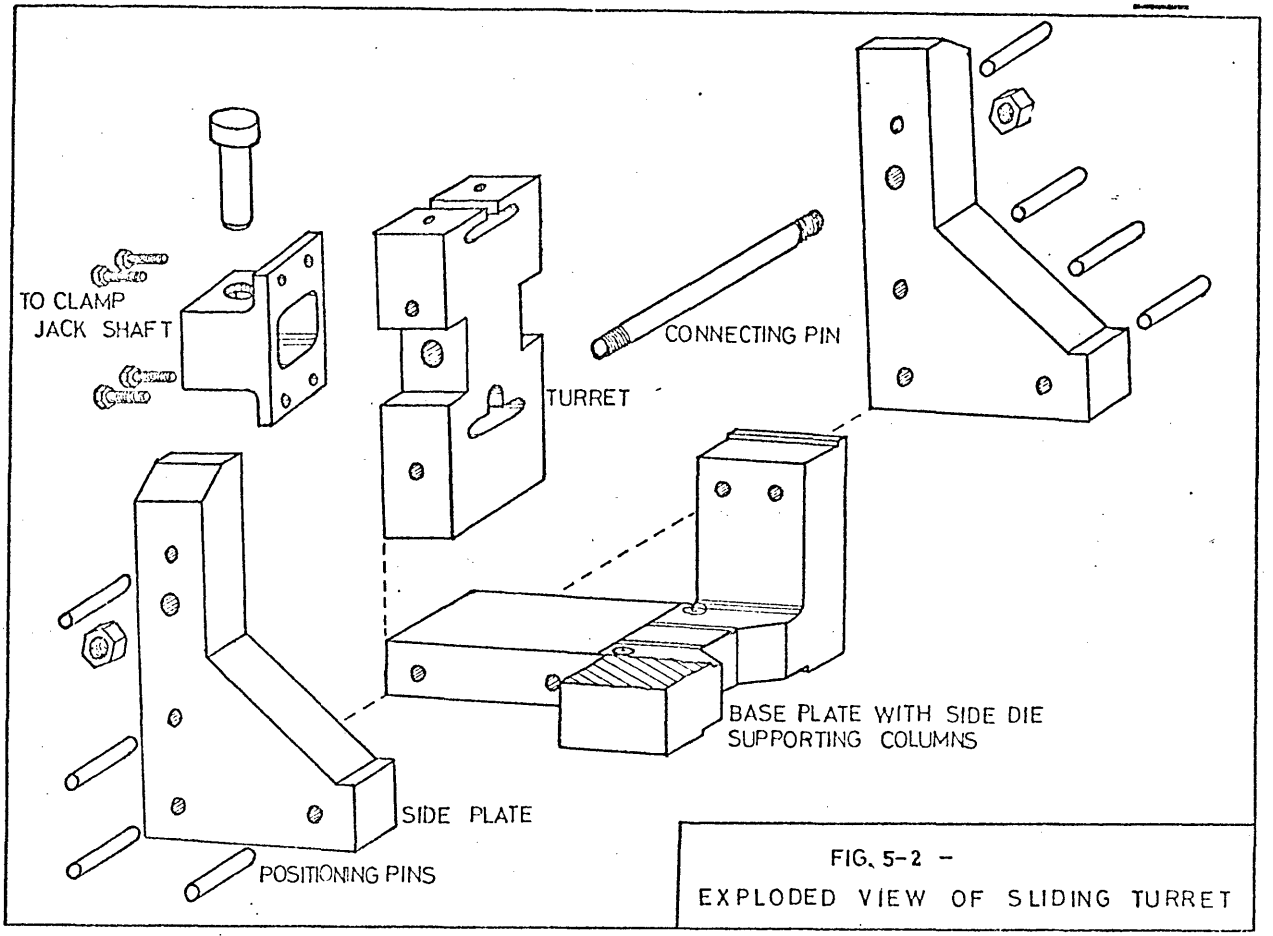


FIG. 5-2 -
EXPLODED VIEW OF SLIDING TURRET

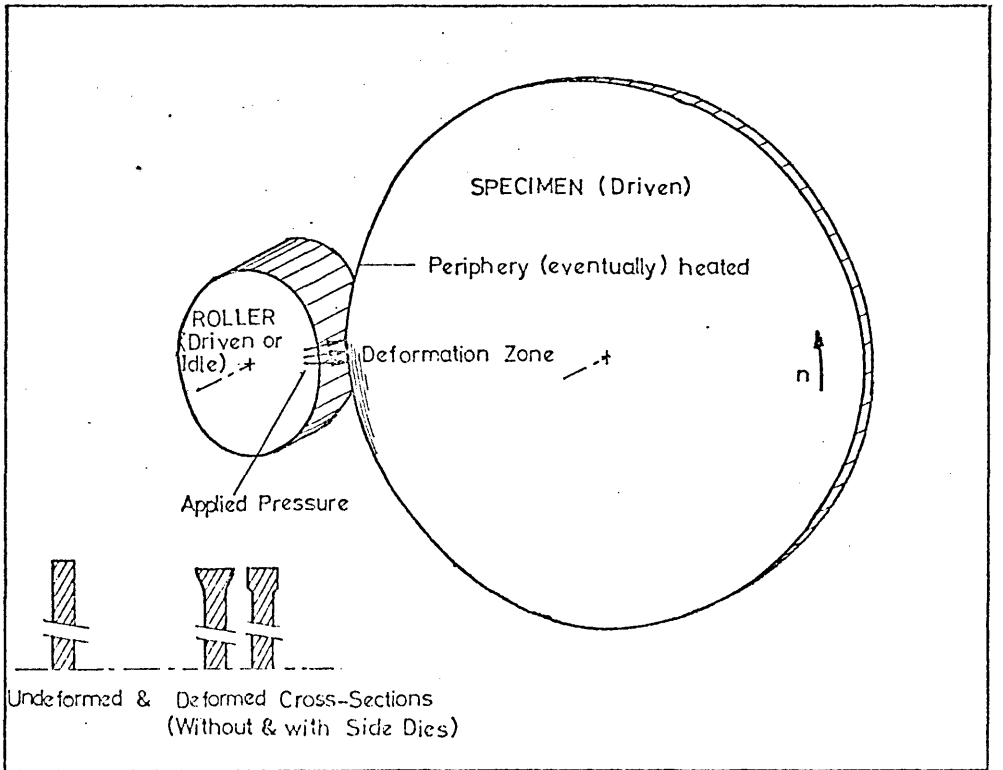


FIG. 5-3 - THE CONCEPT OF THE RADIAL UPSETTING PROCESS

of the feeding speed is possible.

The rig is a box-like construction resting over a bench (not shown in the figure), in order to bring it to a comfortable working height. A thick base plate provided with a longitudinal slot to allow for the use of specimens of larger diameters, supports two long side plates and two thick end plates (one of them not shown in the figure), giving a strong and stiff structure to which the remaining elements are attached. One of the end-plates has a permanent location, at one of the extremities of the base plate, whilst the other one can be mounted at a series of positions, allowing for a series of 50 mm displacements, to adjust for the diameter of the specimen to be used. The mechanical jack allows for a travel of 50 mm, thus justifying the amount mentioned above.

The side plates house bearings for the driving shaft, which is split in two parts, each provided with an end flange. When the specimen is clamped between these flanges, continuity is provided to the shaft. A certain amount of axial displaceability of either part of the driving shaft allows for the introduction of the specimens, covering a thickness range of up to 12.7 mm. A Hi-Torc universal joint (not shown) connects the shaft to the driving system.

The forming roller is carried by a L-shaped sliding turret, which is displaced via the jack, slides attached to the base plate acting as guides. As the relative position of the roller with respect to the sliding turret is not affected by the process (except for the elastic deformation of those elements, assumed to be negligible), the distance travelled by the sliding turret is also the distance travelled by the roller. Exclusively for machining and assembling purposes, this sliding turret has been made up of several parts, as shown in the exploded view of Fig. 5-2. Here again we have a thick base plate with two frontal side columns; the other elements are attached to this base plate by means of several positioning pins (dowels) and one connecting pin with tapped ends. The lateral undercuts in the vertical element (turret) house the extremities (bearings) of the horizontal load cells; the slots are intended to be used for additional load

cells, in future applications, when side dies are to be used. The grooves at the bottom of the U-shaped part of the base plate and the lateral columns are for this same purpose.

The roller is mounted, via needle bearings, over a very thick shaft, whose ends are anchored at the other extremity of the horizontal load cells (L1 in Fig. 5-1).

The vertical load cells (L2) can be adjusted in height and simply rest on dimpled seats in L1 and in the turret base plate. All load cells have a central portion (the load cell proper) of very thin A180 steel tubing (about 0.75 mm wall thickness for L1 and 0.63 mm for L2), heat-treated to RC 60-62, intended to receive the strain-gauges.

The forming roller is also made of A180 steel, heat treated to RC 60. All other elements are of mild steel.

The jack utilised is a Duff-Norton Jactuator, Model 1805, of the inverted type. Its characteristics are given below:

Capacity	45.0 MN (10 tons)
Worm gear ratio	24:1
Max. safe torque	20.9 Nm
Travel / worm turn (nominal)	0.365 mm (Tests with the actual jack have shown a larger specific travel, of the order of 0.397 mm average over the whole range; in the following a rounded-off value of 0.4 mm will be considered).

Figs. 5-4 to 5-6 are photographs presenting partial and overall views of the actual equipment. In Figs. 5-4 and 5-5 the induction coil and its support (which is attached to the sliding turret in operational situations) where removed to show the load cells. In Fig. 5-6 they have been replaced, and the induction generator is also visible in the background. The measuring equipment can be seen at the right-hand side of the photograph: the infra-red radiometer, to measure the temperature at the surface of the specimen, in the deformation zone; the strain-gauge bridge and related accessories; and the UV recorder. (See 5.1.d).

The specimen is driven by a 1.5 HP induction motor, via a speed reducer. This one consists of a Kopp-system continuous

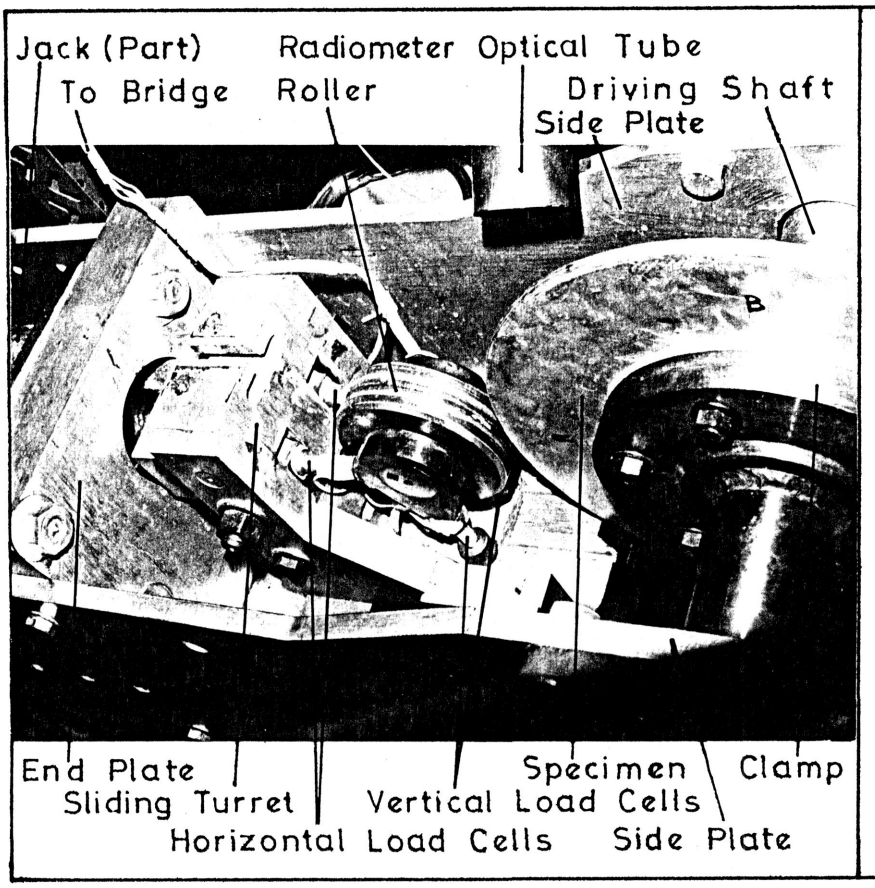


FIG. 5-4 - BASIC RADIAL UPSETTING EQUIPMENT (Heating Coil removed)

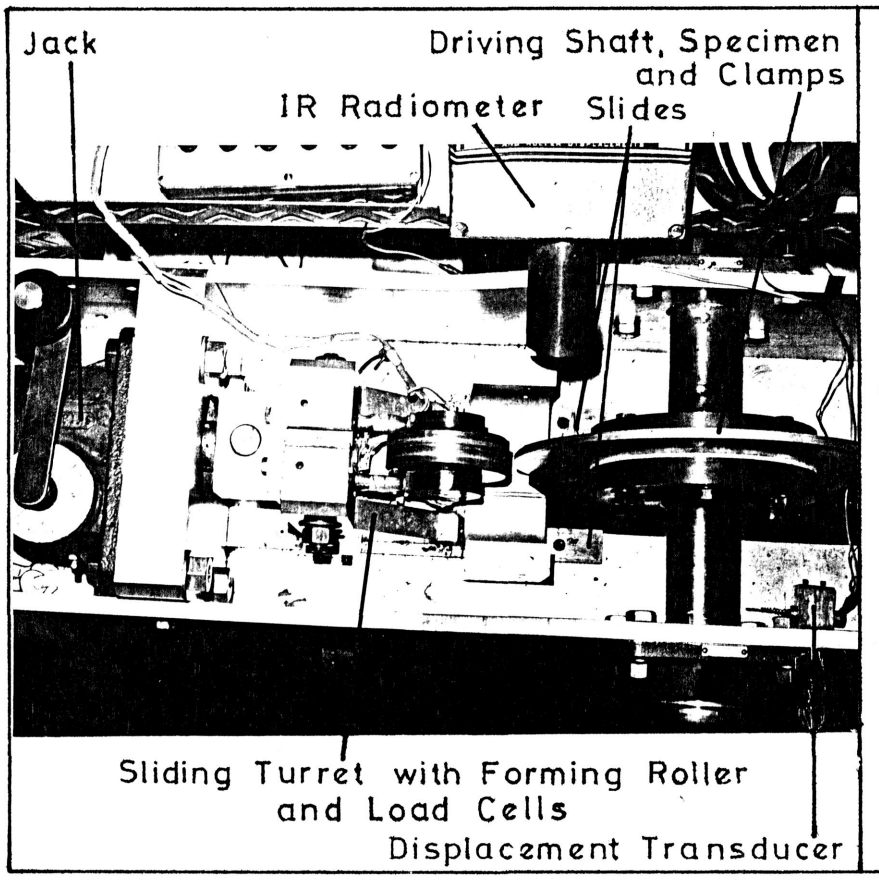


FIG. 5-5 - GENERAL VIEW OF RADIAL UPSETTING RIG (Heating Coil removed)

variator, type MSR1, with a gear ratio of 91.3:1 , supplied by Allspeeds Engng., connected, by means of an elastic coupling, to a Hainsworth worm gear reducer with a fixed gear ratio of 15:1. This one, finally, connects to the driving shaft by means of the universal joint. Fig. 5-7 schematizes the whole assembly, as the driving system does not appear in the photographs of Figs. 5-4 to 5-6, where it is hidden underneath the bench carrying the measuring equipment.

5.1.c - HEATING EQUIPMENT

Induction heating was used in the experimental work, the sole reason for this choice being the availability, in the Metalworking Laboratory of the Department, of a Radyne induction generator, model RD 300, Type G, whose characteristics are:

Power output	28 kW
Operating frequency	2-5 kHz
Power consumption	51 kVA
Power factor	0.9

Water-cooled oscilator valve

Economic considerations were taken into account, and the decision was taken of not investing in new equipment. It should be stressed, however, that induction heating is not the best answer for the radial upsetting process, the reason being the awkward shape of the induction coil required and the considerable air gaps required to allow for the eventual deformation (lateral spreading) of the material. Plasma heating could possibly offer a better solution to this problem.

The best shape for the induction coil was obtained by experimentation. It consists basically of a flat pancake coil bent two times over a specially built template, as shown in Fig. 5-8. Initially 3/16" copper tubing was used to produce the coil, but it proved to be highly unsatisfactory, by not providing a sufficient flow of cooling water. New templates, and 1/4" tubing coils were finally made. In order not to restrict the internal cross-section of the tubing at the bends, the constructional technique of filling the tube with sand prior to bending,

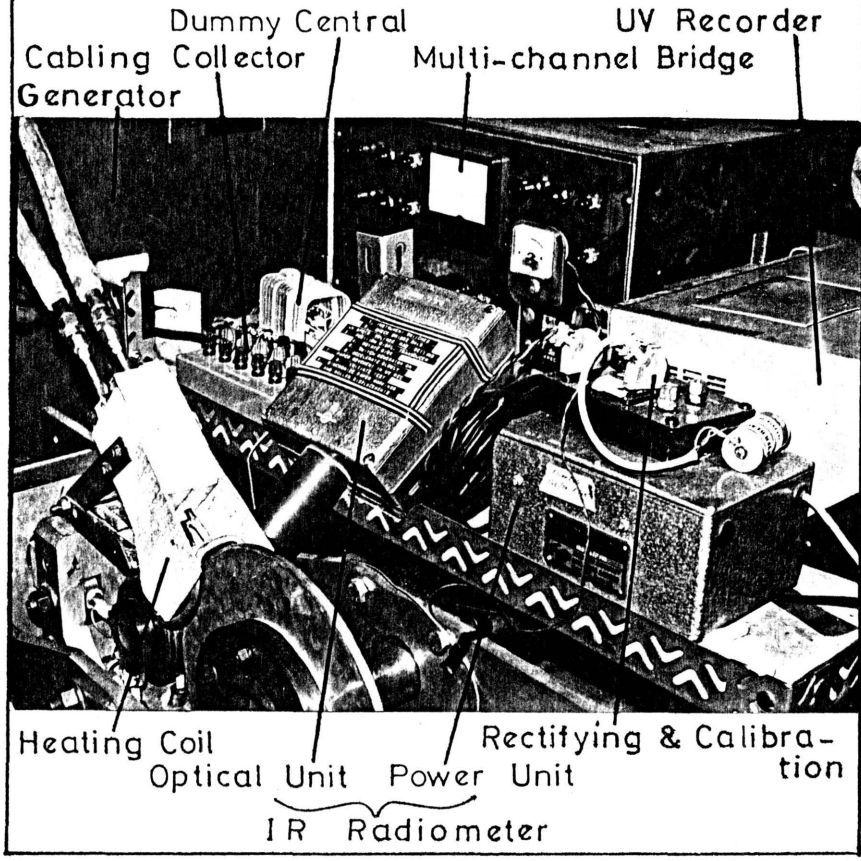


FIG. 5-6 - EXPERIMENTAL RIG AND INSTRUMENTATION

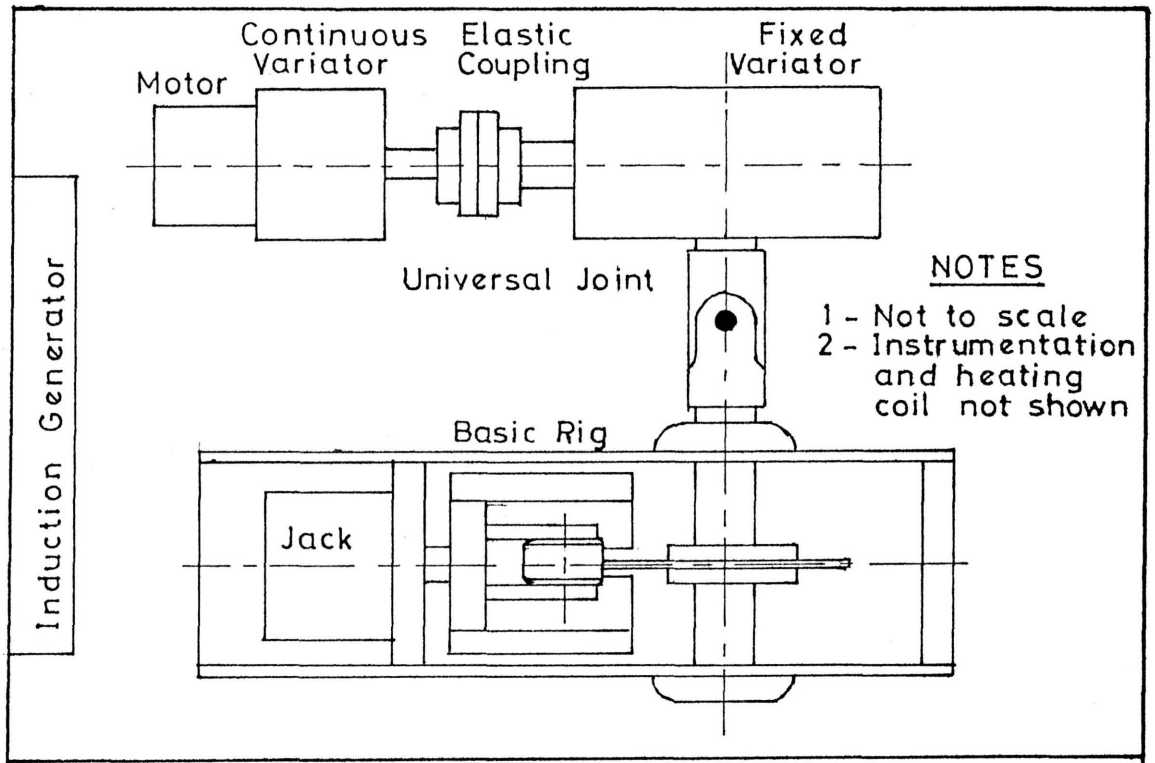


FIG. 5-7 - OVERALL ASSEMBLY FOR THE RADIAL UPSETTING PROCESS

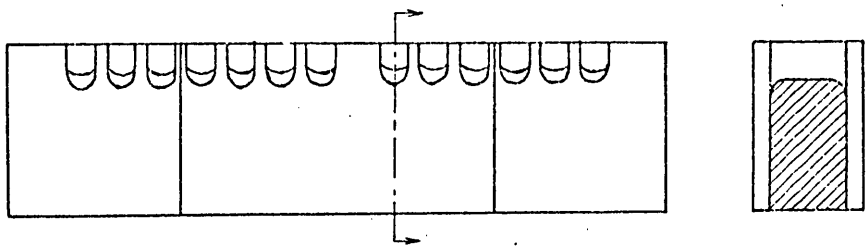
and the stopping of the ends was used. Thus, sound coils could be produced. Once the bending operations were concluded, the sand could be easily washed out with water and compressed air.

In order to mount the coil in its working position, its terminals were embedded in asbestos blocks, which could be more easily fitted to a metalic extension attached to the top of the sliding turret (Fig. 5-6). This extension could also be easily tilted with respect to the turret, by means of a simple screw, thus allowing for the adjustment of the coil for a range of specimen diametres. Two thin asbestos plates were additionally used in order to enclose the coil, as a safety measure. They can be seen in Fig. 5-6, but have been removed in the inset of Fig. 5-8. Due to the extremely small air gaps between adjacent turns of the coil, short-circuiting problems were unavoidable with an unprotected coil; however, they could be easily avoided by dressing the coil in asbestos sleeving, as can be seen, too, in the inset of Fig. 5-8.

The temperature achieved in induction heating is highly dependent on the gap between coil and the part to be heated. In order to minimize this gap, we worked with two coils. To begin deformation, a coil with a gap $G = 17$ mm (Fig. 5-8) was used; as the lateral spreading progressed, and came close to the sides of the coil, deformation was interrupted, and the coil replaced by another one, with a gap $G = 35$ mm, after what deformation was continued.

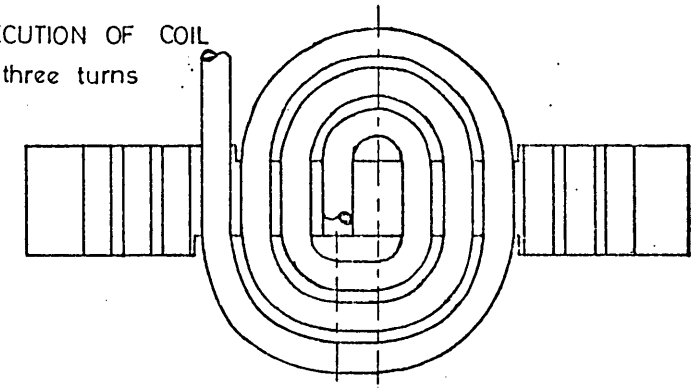
Lozinskii[137] presents data relating the depth of penetration of heating, that is, the depth at which 90% of the energy introduced has already been converted into heat, as a function of the operating frequency of the generator and of the heating temperature. These data refer to two temperatures only, and they are presented in Fig. 5-9. A practically linear behaviour can be observed, for a given temperature, if a logaritmic plot is used; it is thus easy to interpolate a possible curve for a heating temperature of 400°C, showing that for the frequency range of the Radyne generator the depth of penetration

1 - TEMPLATE



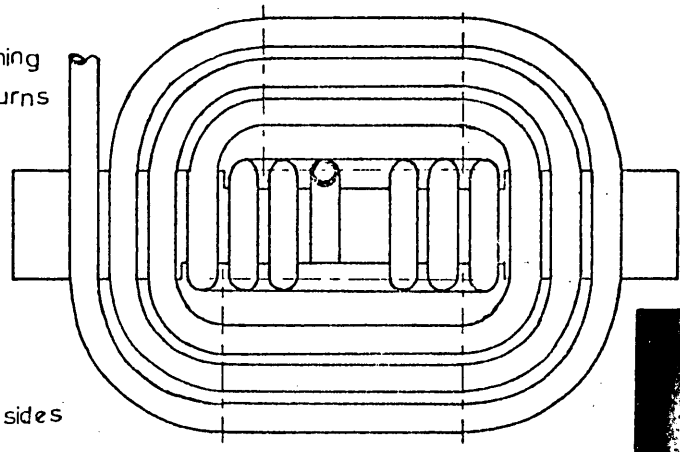
2 - EXECUTION OF COIL

a - First three turns



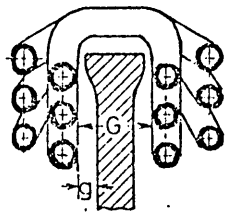
b - Bend sides

c - Remaining three turns



d - Bend sides

3 - FINAL CROSS-SECTION



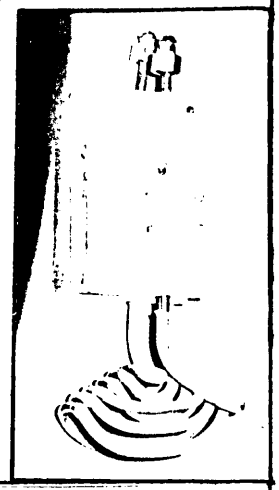


FIG. 5-8 - EXECUTION OF HEATING COIL

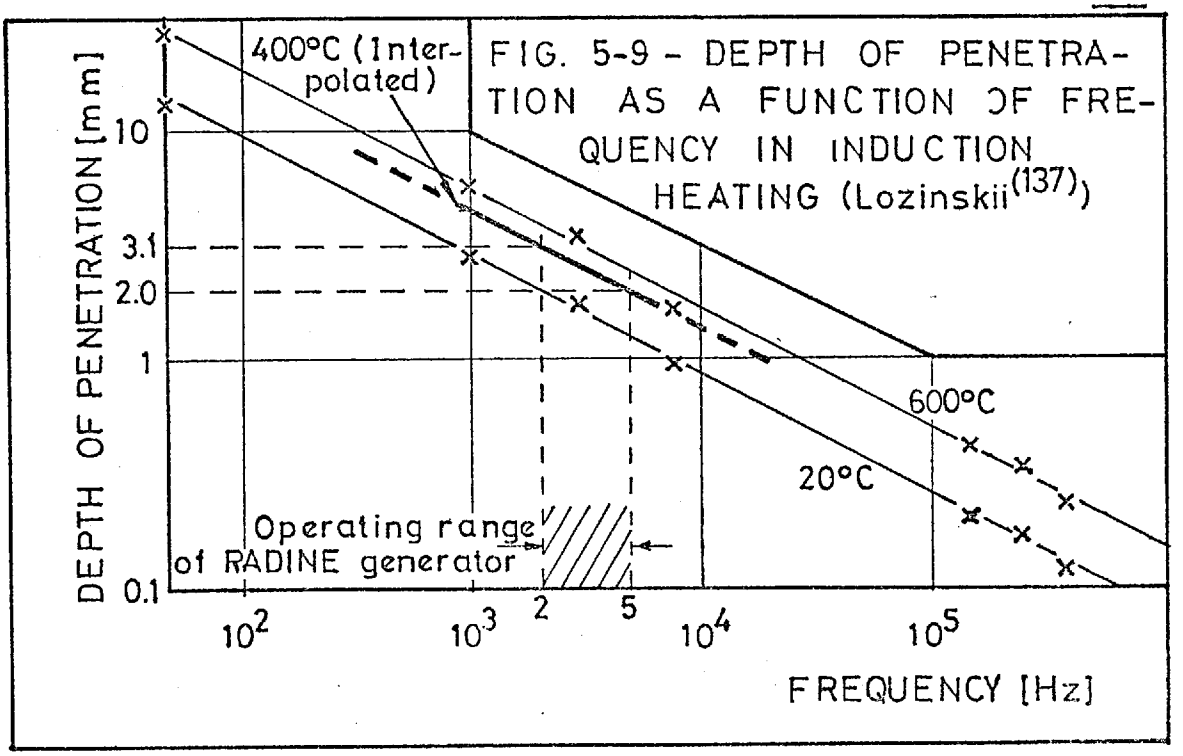


FIG. 5-9 - DEPTH OF PENETRATION AS A FUNCTION OF FREQUENCY IN INDUCTION HEATING (Lozinskii[137])

is of the order of 3 mm. As the heating coil surrounds the two faces of the specimen, which is 6.35 mm thick in the applications to be described in Section 5.2, we should expect, after sufficient time is given for conduction, that a homogeneous temperature will exist across the thickness of the specimen.

5.1.d - MEASURING EQUIPMENT

5.1.d.1 - Temperature Measurement

During hot-forming applications of the radial upsetting process there exists the need for a continuous check of the temperature in the forming zone. In the case of the deformation of aluminium, the working temperature is too low to allow the use of optical pyrometers. Thermocouples, rubbing against the specimen were tried, but the results proved to be unreliable; a non-contact solution is required to this problem, and it is supplied by the use of an infra-red radiometer, which observes moving part by means of an optical tube. Such an instrument, however must be previously calibrated for the specific operating conditions, taking into account the relative situation of the instrument with respect to the specimen, the optical tube used and the emissivity of the material to be observed[138].

A Dynalec IR-Radiometer 31, built by Hawker Siddeley Dynamics Ltd., was used in our experiments. It can measure radiation from objects at temperatures ranging from 80 to 1000°C; it is provided with a screw adaptor, capable of taking simple tube extensions to restrict the field of view, or mirror optical systems, to provide increased sensitivity with small angular fields of view. The power supply - 6.5 V DC at 100-150 mA - is provided by a main power unit, although in-built rechargeable batteries could be used alternatively. The output, corrected for room temperatures in the range from -5 to +35°C, is a 600 Hz signal supplied to the power unit (See Fig. 5-6), from where it can be collected to operate remote equipment, for instance, to drive the 1 mA DC coil meter of a UV recorder. In that case, an intermediate circuit must be introduced to supply the recorder with a signal in the adequate range[139].

The radiometer operates by focusing the infra-red radiation[140], in the wavelength range of 1.7 to 3 microns, on an infra-red cell, previously chopping it by the segments of an intersecting disc, kept at room temperature and rotated by a miniature motor (Fig. 5-10). The radiometer then compares the infrared radiation from the hot object with the radiation from the disc, such that zero output is obtained if object and disc are at the same temperature. There are four sensitivity ranges for the output, the selection being made simply by turning a knob. There is an additional knob which acts as a gain control. These two are the only external control elements of the apparatus.

In general applications, such as temperature measurements in large surface areas at close distance, simple tube stops provide a sufficiently defined field of view, without too much loss of energy of the cell. Fig. 5-11 gives the details of the optic tube we have used, the end stop being dimensioned to give the adequate field of view. Reducing the opening of this stop the field of view tends to a limiting value. If lower fields of view are required, an optic tube of more length must be used.

The field of view can be expressed by the equation

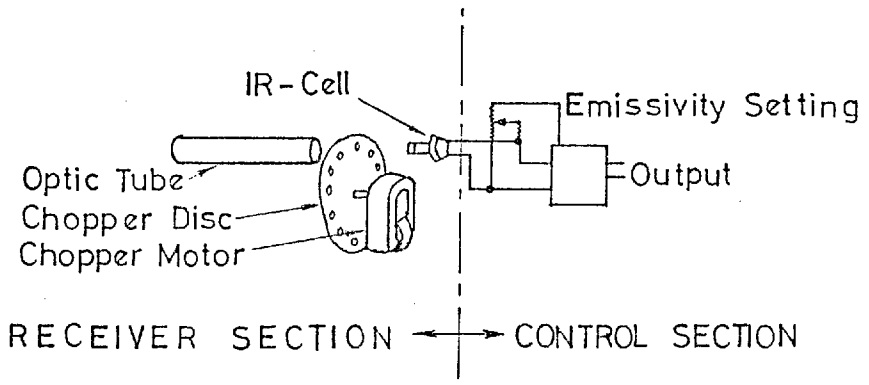


FIG.5-10 - SCHEMATIC REPRESENTATION OF THE INFRA-RED RADIOMETER[139]

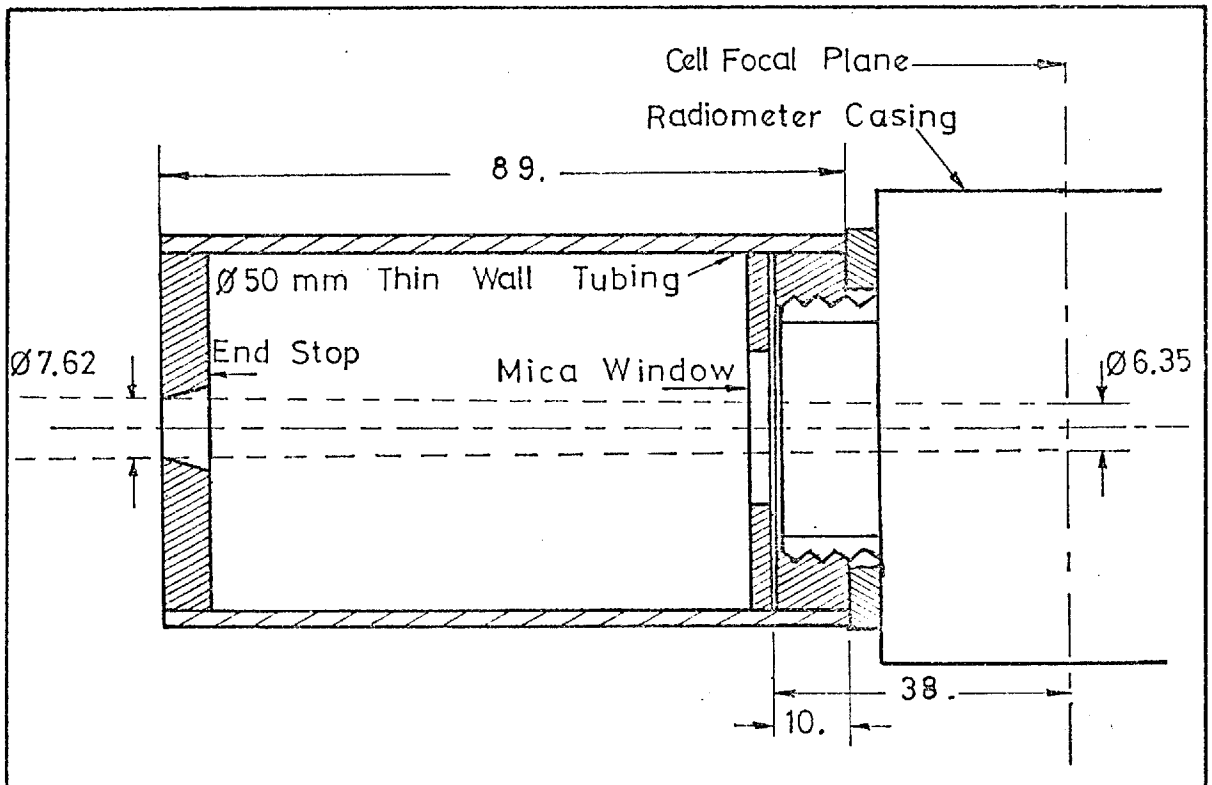


FIG. 5-11 - OPTICAL TUBE USED WITH THE INFRA-RED RADIOMETER[140]

$$\varphi = 2 \tan^{-1} \frac{D_a + D_c}{2L},$$

where D_a is the diameter of the tube opening, D_c is the cell diameter (6.35 mm in the case of the present radiometer), and L is the distance from the cell to the tube stop. In our case a field of view of the order of

$$\varphi = 8.5^{\circ}$$

was found to be satisfactory. This field of view must be fully covered by the specimen at all times during the temperature measurement.

5.1.d.2 - Strain measurement

The forces involved in the deformation by radial upsetting were measured by means of strain-gauges attached to the load cells mentioned earlier, and shown in Figs. 5-1 and 5-4 to 5-6. The gauges used were of the type EA-06-187BB-120, manufactured by Micro-Measurements Inc.. They have a resistance of 120 ohms (± 0.15 %) and they are temperature compensated for use on steel. The gauge factor and the cross-sensitivity quoted by the manufacturer are 2.09 (± 0.5 %) and + 0.5 %, the small value of cross-sensitivity being particularly useful because it minimizes the effect of the axial strain on the gauges.

The cement used was an epoxi-resin known as Eastman 910 Adhesive, supplied by Welwyn Electric Ltd.. After cementing, the gauges were coated with a polyamide lacquer known as Gage-kote #1, also supplied by Welwyn. The leads were then connected to the eight-channel Automation bridge, via a dummy central (Fig. 5-6), and from there the signal was redirected to a SE 3006 UV recorder. Fig. 5-12 gives the typical circuitry for one strain-gauge. Half of the bridge consists of high stability 120 ohm resistances, plus four way switches, ten turn variable set balance and set calibration resistances, together with a balance meter, all housed in the Automation equipment.

All the bridges were supplied by a 3 V DC constant voltage power pack, whereas their outputs were connected to the individual channels of the UV recorder, in which A100 galvanome-

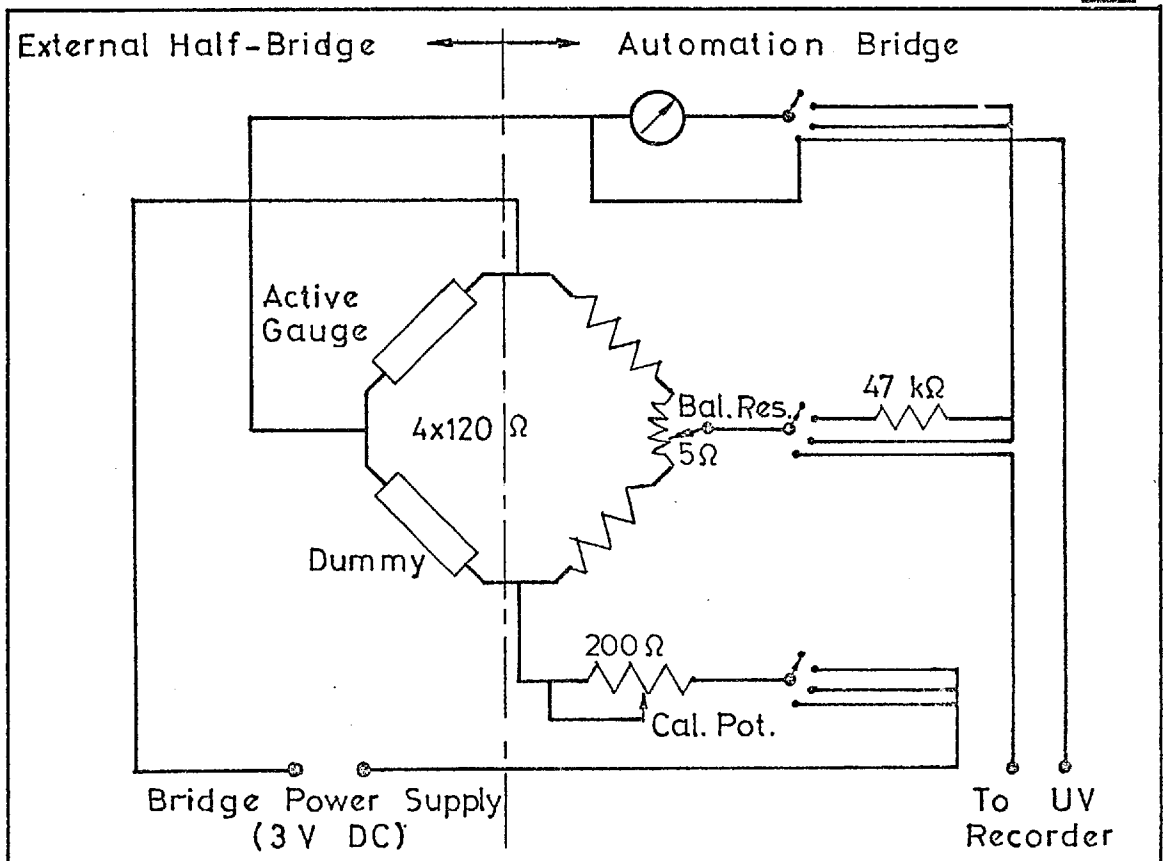


FIG. 5-12 - STRAIN-GAUGE BRIDGE

ters, supplied by SE Laboratories (also suppliers of the UV recorder) were used. The resistance and sensitivity of the galvanometers were checked by precision Wheatstone bridge and injector potentiometers. Calibration was made directly in terms of load, as will be described elsewhere.

5.1.d.3 - Displacement transducer

A displacement transducer was used to measure the displacements of the roller and/or the radial reduction in the specimen. Measurements, however, did not prove to be satisfactory, and had to be abandoned. Apparently the transducer had some defect.

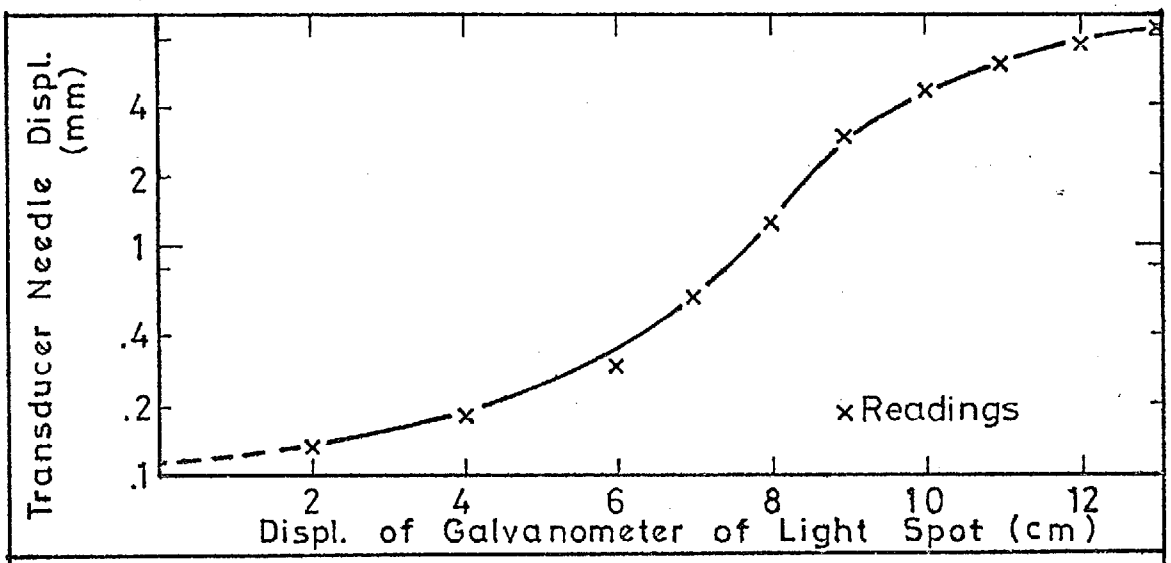


FIG. 5-13 - CALIBRATION CURVE OF DISPL. TRANSDUCER

As a matter of fact, the transducer simply did not behave linearly, as the calibration curve shows (Fig. 5-13). There is insufficient discrimination at small displacements of the needle. Fortunately, however, we controlled the amount of penetration of the roller, via the number of turns of the jack handle (sensitivity of the order of 0.1 mm) and also conducted a thorough set of measurements over both deformed and undeformed specimens.

5.1.d.4 - Outputs

The output of all measurements is given by the SE 3600 UV recorder, which is a commercial writing oscillograph suitable for laboratory and industrial use. It operates with pencil type galvanometers. The incident light from an ultraviolet light is deflected by the movement of a small mirror attached to the galvanometer suspension. The movement is caused by the torque which is produced when current passes through the coil attached to the suspension. Recording is effected by focusing the reflected spot onto sensitized printout paper. The relevant characteristics of this recorder are:

Channels : 6
Paper speeds : 8
Recording paper : 150 mm width
Longitudinal grid lines spaced at 2 mm, with every cm accentuated
Transversal grid lines: every 0.1 second, or every second, or, when required, by external command.

The galvanometers used were of the type A100, whose characteristics are:

Type: moving coil
Linearity of deflection: ±1 %
Damping: electro-magnetic
Focal length of lens: 35 cm
Natural frequency: 100 Hz
Flat frequency response: 60 Hz (± 5 %)
Nominal resistance: 35 Ω (± 10 %)
Damping resistance: 350 Ω
Maximum safe current: 10 mA (rms)
Maximum sensitivity: 0.0037 mA/cm (± 10%)
or 0.1300 mV/cm (±10%)

5.1.c - CALIBRATIONS

5.1.e.1 - Infra-red radiometer

a) Theory[138-141]

The intensity of the energy radiated by a hot body is a function of its absolute temperature Θ and its surface emissivity ε, as defined by

$$W = \varepsilon \sigma \Theta^4,$$

σ being Stefan-Boltzmann's constant. If the radiometer is calibrated against a black body source and used to measure the temperature of a body of emissivity ε, it will indicate an apparent temperature Θ_A, where

$$\Theta_A^4 = \varepsilon \Theta^4, \qquad (5\text{-}1)$$

and in order to get a correct output reading, one has to multiply the output result by a gain factor equal to $1/\varepsilon$. This can be done, in our radiometer, by means of the gain control knob, which allows for settings of emissivity between 0.2 and 1.

As the output result is supplied in the form of a current reading i (in the range from 0 to 1 mA), a relationship must be established between the current read and the temperature. For a black body we can put simply

$$\Theta = k_R \, i^{0.25} , \qquad (5\text{-}2)$$

where k_R stands for the characteristics of the electric circuitry of the radiometer and power unit, when set for reading in the R^{th} range. The same equation applies, obviously, for any body, provided the adequate value of emissivity has been set in the control knob, otherwise the apparent temperature of Eqn. (5-1) will be obtained.

The knowledge of the correct value of emissivity, therefore, allows an absolute calibration to be established, between output current and observed temperature. However, the emissivity of a material varies with the wavelength of the radiation and, therefore, with temperature. For aluminium, for instance, Reynolds[142-143] has shown how temperature and wavelength affected the spectral emissivity for both the polished and the roughened material (Fig. 5-14).

It is difficult to say the exact value of emissivity of a particular material, and how it varies with the several influencing factors, unless sophisticated experiments are made, and even then it would be out of the question to change the setting of the emissivity during an experiment, when the temperature is changing.

A relative calibration is then the best approach, as it does not require the exact value of emissivity at any moment, the calibration being obtained in terms of a ratio between a preset value of emissivity and the correct emissivity, this ra-

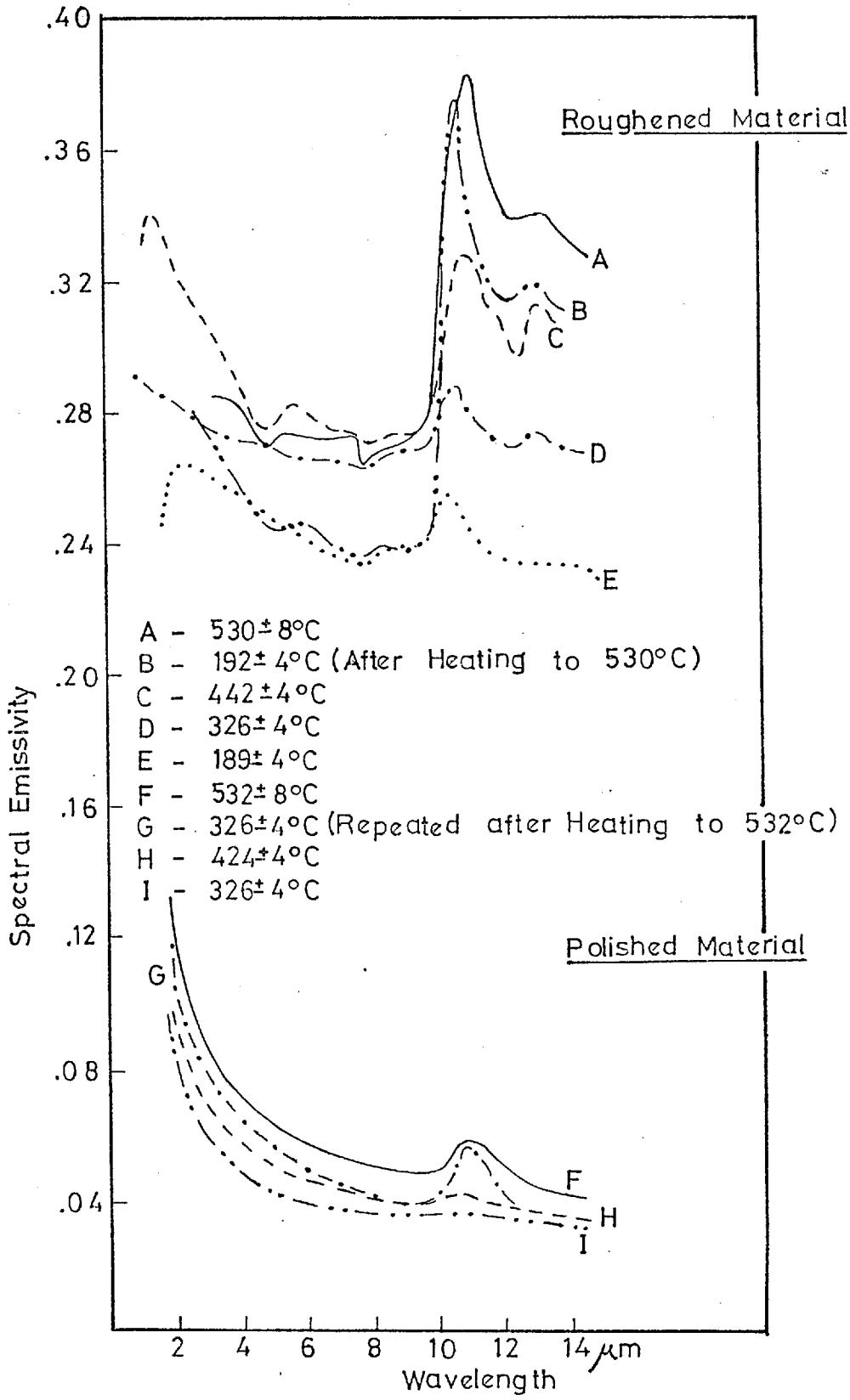


FIG. 5-14 - SPECTRAL EMISSIVITY FOR ROUGHENED AND POLISHED ALUMINIUM PLOTTED AGAINST WAVELENGTH, FOR SEVERAL VALUES OF TEMPERATURE[142-143]

tio acting as a proportionality (scale) factor, the value of which does not have to be known (nor how it varies along the temperature range), as one relates directly the currents observed as output, and the temperatures that caused them, these ones obtained by some other method. In effect, if ε is the correct value of emissivity in a certain situation, and if the gain control knob is set at ε_s, Eqn. (5-2) will be rewritten to

$$\Theta = k_R \, (i \varepsilon_s / \varepsilon)^{0.25} . \qquad (5\text{-}3)$$

b) Calibration

Our calibration has been performed in nearly working conditions, that is, with specimen and radiometer as they would be geometrically situated during the forming tests, with the infra-red cell of the radiometer at 242 mm from the forming region, tilted by 30° with respect to the horizontal plane, as shown in Figs. 5-4 to 5-6.

Our original intention was to perform the calibration with a moving specimen, the temperatures being read from a thermocouple rubbing against its surface. However, no useful results could be obtained, as the contact pressure is a determining parameter which is not easy to control adequately. The alternative we adopted was that of drilling a $\emptyset$ 1 mm hole radially into the the specimen, 0.5 mm apart from the face observed by the radiometer, and to introduce the CA 1560 F thermocouple to a depth of 12 mm, so that the junction stood at the centre of the field of view. A COMARK Electronic Thermocouple was used to read the temperatures. The specimen was heated under the coil, and both the temperature and the radiometer output current were then read, as the heat propagated by conduction inside the specimen. The emissivity control was set at 0.3, and readings were made for ranges 2 and 3, the results being shown in Fig. 5-15, in which relative temperatures were plotted, instead of the absolute ones. As the results for range 3 fall outside the forming temperature range, for aluminium, they were subsequently disregarded.

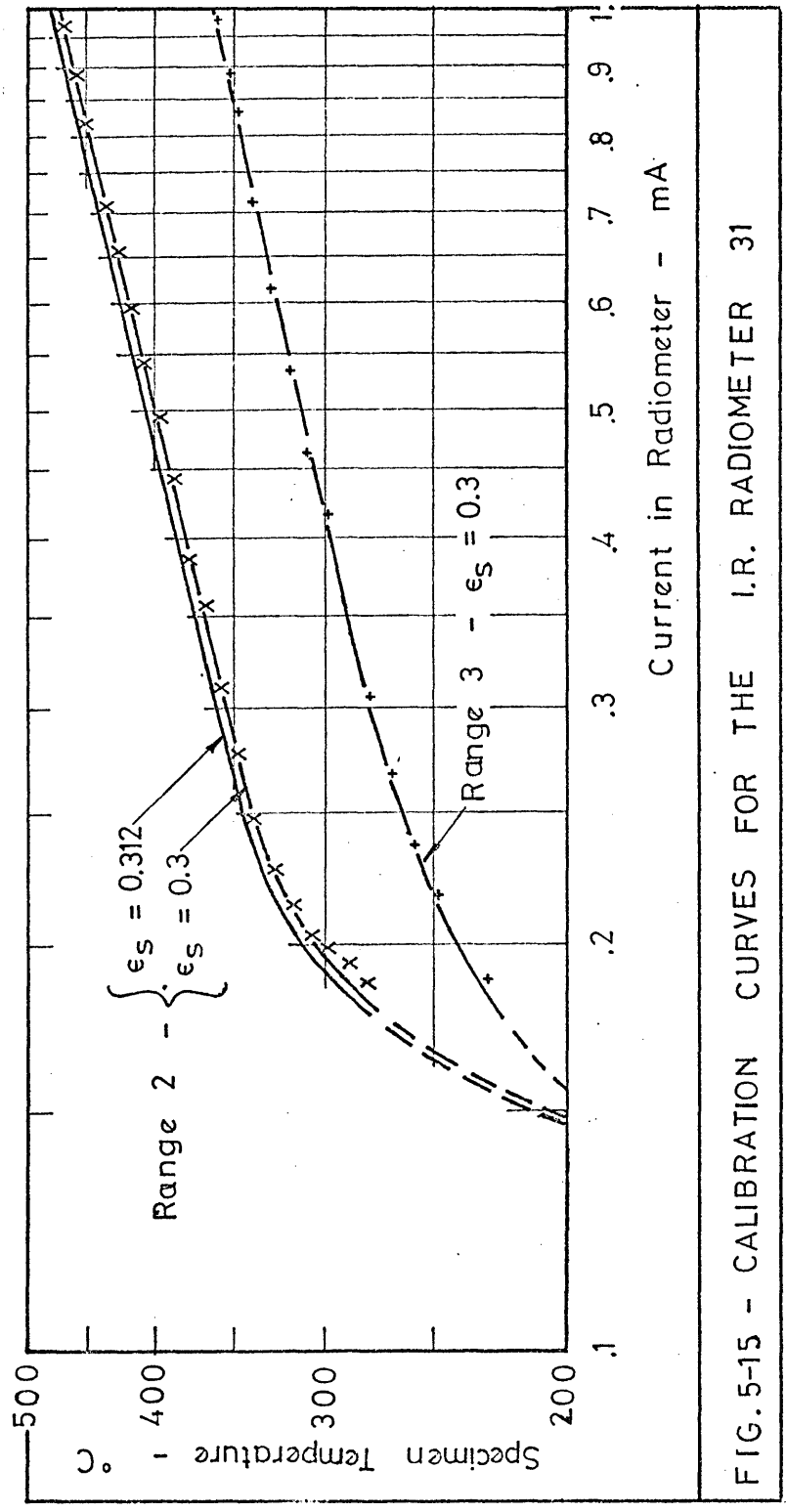


FIG. 5-15 - CALIBRATION CURVES FOR THE I.R. RADIOMETER 31

However, the curve for range 2 does not cover the entirety of the forming temperature range, as the 1 mA reading corresponds to a temperature of 473°C only. The curve can be modified, however, in order to extend it up to 480°C, or any other desired temperature level, by changing the setting of the emissi-

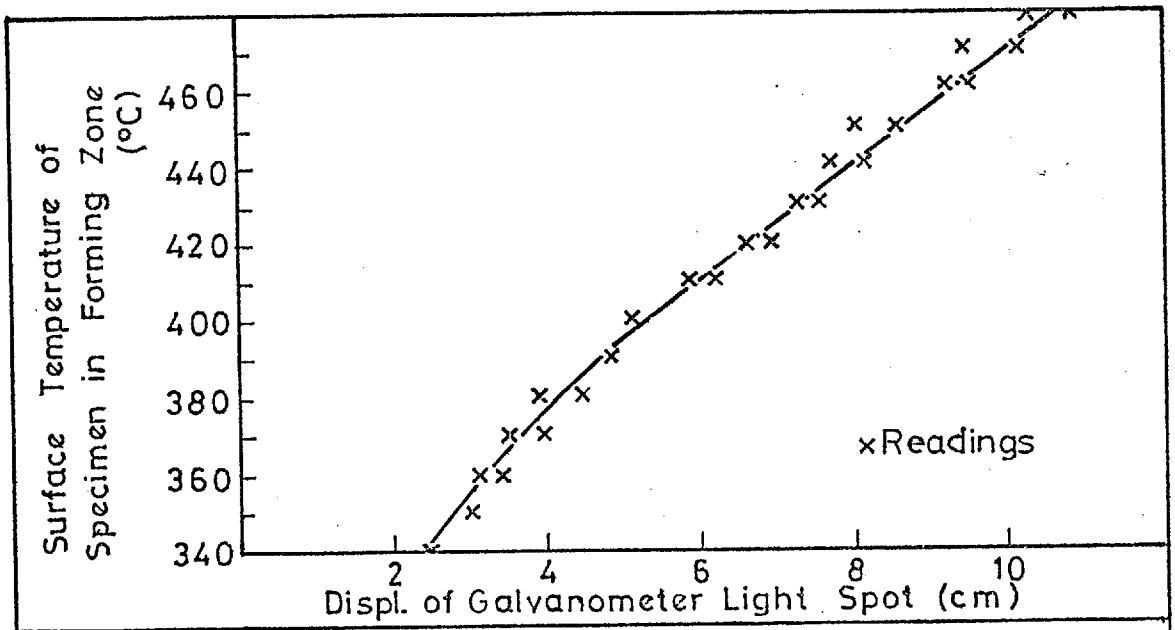


FIG. 5-16 - UV RECORDER OUTPUT VERSUS SURFACE TEMPERATURE OF SPECIMEN IN FORMING ZONE

vity level. In effect, it can be seen from Eqn. (5-3) that, if ε_1 and ε_2 are different emissivity settings, the corresponding temperatures, for identical current readings, obey the relation

$$\frac{\theta_1}{\theta_2} = \left(\frac{\varepsilon_1}{\varepsilon_2}\right)^{0.25} . \qquad (5\text{-}4)$$

The calibrating curve can thus be extended to 480°C if an emissivity setting of 0.312 is used, the curve being recomputed by means of Eqn. (5-4). The recomputed curve is also shown in Fig. 5-15, and is also confirmed experimentally. Fig. 5-16, finally, plots the calibration curve for the UV recorder.

Kleiber[144] describes a new model of radiometer in which a linearisation of the output signal is achieved by means of variable amplification over the temperature range. As a consequence, the corresponding plotting of Fig. 5-15 shows practically straight lines.

Deeper consideration into the applications of infrared radiometers for the temperature control of metalworking processes can be found in Black[145] and Reynolds[146].

c) Recorder output

At the beginning of every experiment the signal produced by the radiometer was fed to a 0 - 1 mA ampère-meter, thus giving a visual display of the temperature. The curve of Fig. 5-15 was used to produce a temperature scale which was then superimposed to this instrument. Once the adequate working temperature was reached, and before starting the actual experiment, the 600 Hz signal was transferred to an intermediate rectifying and calibrating circuit and then supplied to one of the recorder galvanometers. This intermediate circuit is shown in Fig. 5-17, the potentiometer being used to adjust the scale factor relating the recorder output with the measured temperatures. The calibration curve obtained has already been referred to and shown in Fig. 5-16. The rectifying circuit is contained in the black box on top of the power unit, in Fig. 5-6.

5.1.e.2 - Strain-gauges

Fig. 5-12 shows the typical circuit for a strain-gauge. The dividing line, in the Wheatstone bridge, shows the part of the circuit which is interior to the Automation eight-channel bridge. The 5 ohm resistance serves for balancing the bridge, and the 200 ohm potentiometer to calibrate the output supplied to the UV recorder and thus the displacement of the light spot.

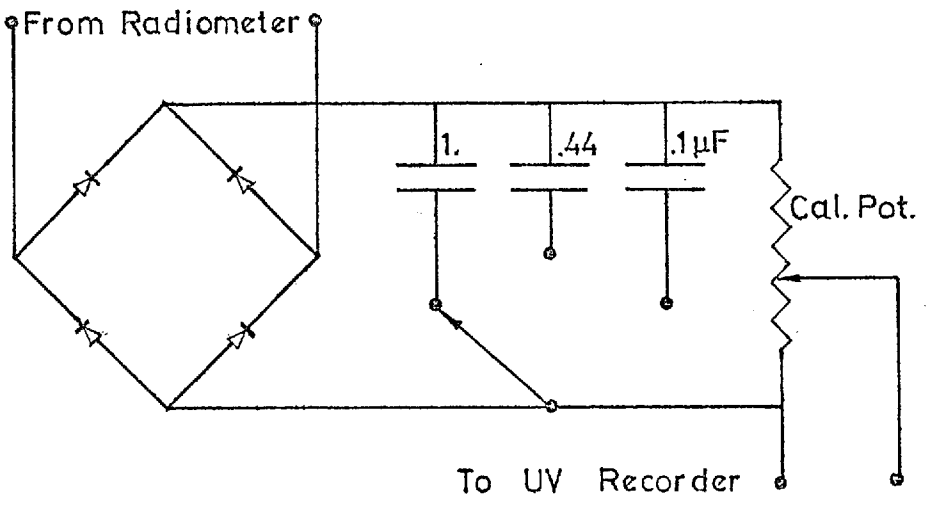


FIG. 5-17 - RADIOMETER RECTIFYING CIRCUIT

The main switch, for every channel, has three alternative "on" settings. The first one introduces a protective shunt, the second one is used for balancing the bridge and the third one is for normal operation. In that case, as becomes clear from Fig. 5-12, the signal is deflected for output (in our case, to the UV recorder).

The calibration was performed directly in terms of the axial load applied over the load cells and the displacements of the light spot of the galvanometer. It was performed over a 6000 lb Tinius Olsen press. As the display of the press is in British units, the horizontal load cells were calibrated by the application of successive increments of 40 lbs (178 N), up to a maximum load of 880 lbs (3.92 kN). Half of the values of both the step and the maximum load were used when calibrating the vertical load cells. The zero drifts were negligible. The calibration curves are given in Fig. 5-18.

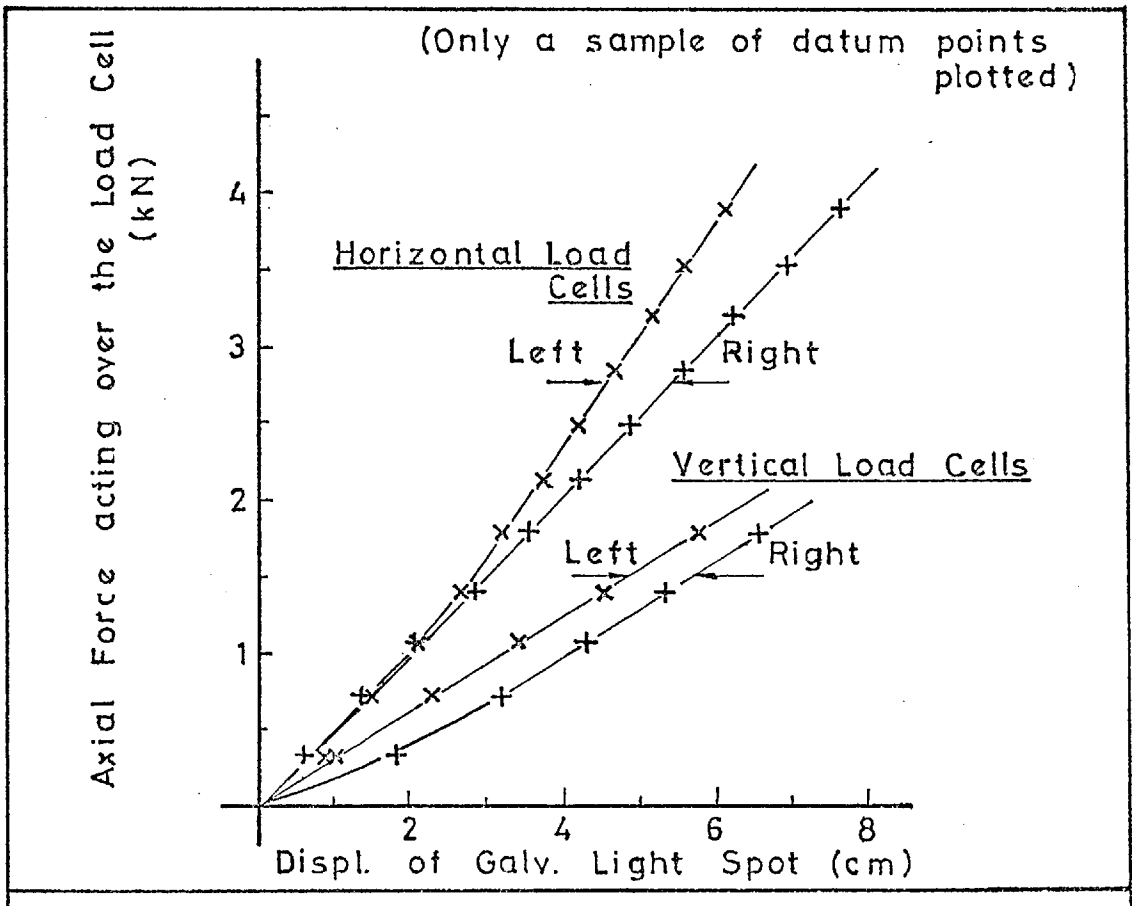


FIG. 5-18 - STRAIN-GAUGE CALIBRATIONS

5.2 - EXPERIMENTAL WORK

5.2.a - INTRODUCTION

The original plans for our research work were based on the idea of producing deformation by radial upsetting in thin mild steel discs. However, this idea had to be abandoned due to the impossibility of heating the material to an adequate working temperature with the available facilities. Under special conditions a temperature of the order of 950°C could be achieved against a prescribed temperature of 1050-1100°C. Two specimens were deformed in these conditions. Nevertheless, in order to be able to perform experiments over a wider range of temperatures, we decided to work with a different material. Preliminary experiments with aluminium and dural proved to be successful, from the heating point of view. Both could be easily heated up to the melting point. For economical reasons, aluminium of commercial purity (99% Al minimum) was preferred and adopted for our experimental work.

Some preliminary experiments were performed at room temperature over lead specimens, cast at the Metalworking Laboratory. They were 6 mm thick, with a diameter of 219 mm. However, we found that a highly nonuniform deformation pattern was obtained, due to the large grain size (Fig. 5-19). We did not have the proper facilities to produce specimens cast to a controlled grain size, and our interest in the deformation of lead was only colateral, so we abandoned experiments with this material altogether.

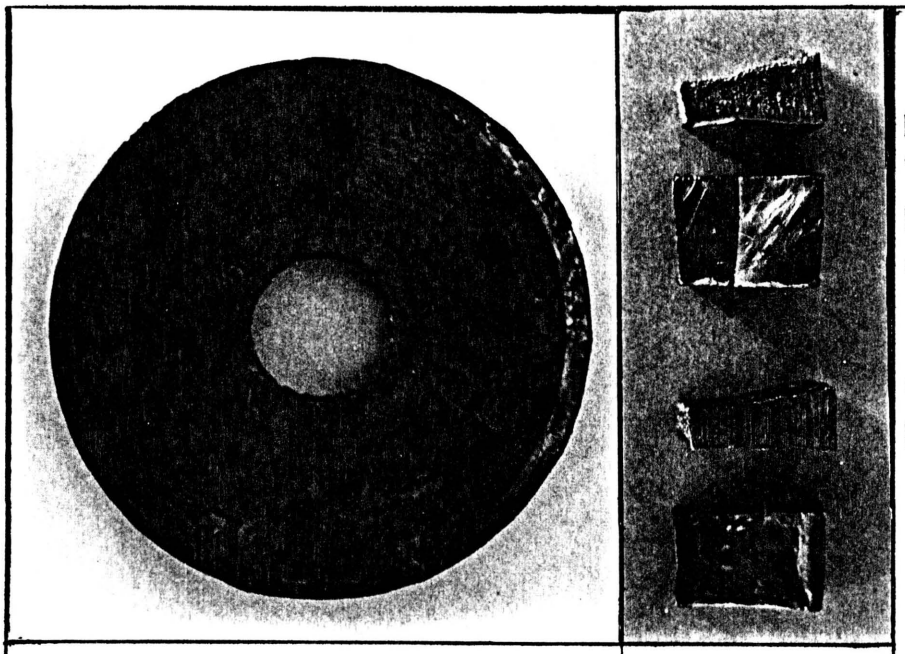
The aluminium specimens we employed had a thickness of 6.35 mm (1/4") and a diameter of 300 mm. The inner part of some of the deformed specimens was subsequently cut out and converted into 215 mm specimens, which were then tested at room temperature. The reduced size of these specimens did not allow for the use of the heating coil, because it then interfered with the clamping flanges.

Successive experiments were performed at feeding speeds of 0.5 , 1.0 , 1.5 and 2.0 rpm, with temperatures in

the forming zone varying between 400 and 450 °C. In each case, penetrations of 0.1 and 1.2 mm/revolution were used, although most of the experiments were restricted to the much lower range of 0.1 to 0.4 mm/revolution. Penetration was achieved manually, and their amount, in the first experiments, checked against the displacement transducer. A circular scale, visible in Fig. 5-5, was used to control the amount of rotation of the handle, once the backlash was removed, and thus to restrict and control the amount of penetration.

A special word must be said about the heating problem. Due to the low efficiency of the heating coil, it becomes extremely difficult to reach the desired working temperature. Although the generator was always used at full capacity, it used to take about fifteen minutes to achieve the required temperature. Of course, if the specimen was steady (non-rotating), heating took place very quickly (in about thirty seconds), but was restricted to a small portion of the periphery of the specimen. The adopted procedure was to start the rotating of the specimen at very low speed, and as the temperature reached the desired level, to slowly increase the speed, up to the intended amount. Once the correct temperature was achieved, at the also correct speed, on the other hand, care had to be taken to control the output of the generator, in order to avoid further increases in temperature. Usually an initial temperature of 400 °C was adopted, and it was then allowed to increase during the experiment up to a limit of 450 °C (although temperatures of the order of 480 °C and more were eventually registered at times). The intentional use of a continually increasing temperature during the experiment was preferred because earlier tests had shown the difficulty of keeping the temperature steady. Once the temperature started to increase, any small resetting of the generator caused sudden and substantial drops in temperature, sometimes well below the desired temperature range.

Reference must also be made to the fact that, once the lateral spread of the material, due to the nature of the deformation process, tended to fill the gap supplied by the heating coil in the first heating, the experiment was interrupted and the



a b

FIG. 5-19 - IRREGULAR DEFORMATION OF LEAD SPECIMENS

a) Specimen
b) Cut-outs

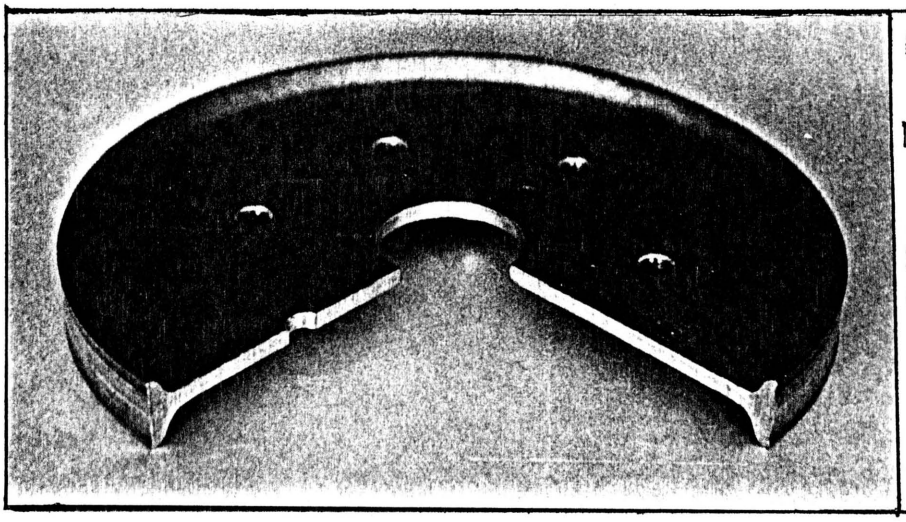


FIG. 5-20 - REGULAR DEFORMATION IN THE RADIAL UPSETTING OF ALUMINIUM

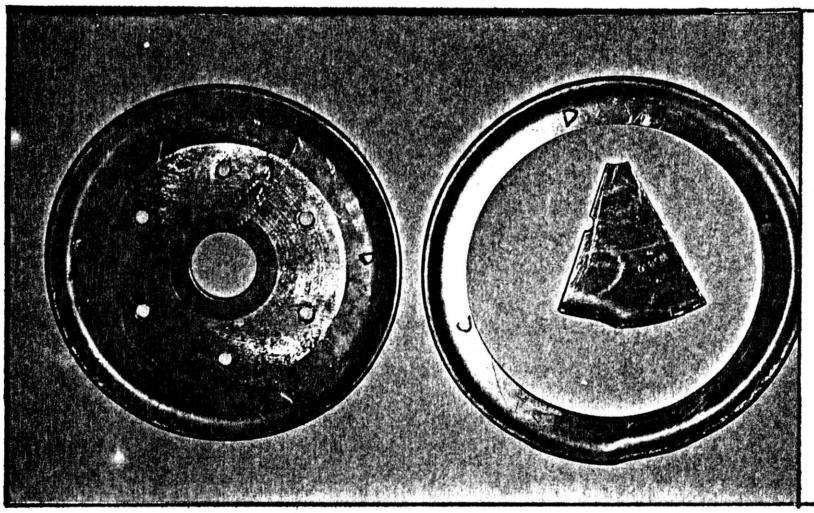


FIG. 5-21 - DEFORMED SPECIMENS AND DEFORMATION FRONT

coil substituted by another one, with a wider gap. Before restarting the experiment, the specimen had to be heated again, but this operation did not take more than five to ten minutes, as the specimen did not have time to cool down sufficiently during the substitution of the coils. Once the gap of the second coil was used out, the experiment was considered as finished.

From the technological point of view the experiments have shown that the radial upsetting process is feasible, provided that adequate conditions are used. Sound deformation can be achieved with an adequate penetration rate. Rates of the order of not more than 0.2 mm/revolution usually produced good symmetrical) deformation, as can be seen, for instance, in the example of Fig. 5-20, in which a total radial reduction of more than 40 mm has been obtained; although deformation is not perfectly symmetric, this is due to the fact that a grid was traced on the surface of one of the sides of the specimen only. The two examples of Fig. 5-21, though corresponding to more moderate deformation, are also satisfactory. Fig. 5-22 compares two examples of sound and nonsymmetrical (buckled) deformation. Intermediate values of penetration rate (up to 0.4 or 0.5 mm/revolution) produced good results depending on a series of factors: the specimen had to be perfectly plane, and be mounted perfectly perpendicularly to the axis of the forming roller. If those requirements were not met, bending effects became noticeable, usually leading to nonsymmetric deformation, as shown in the second example of Fig. 5-22. At very large penetration rates, instability by buckling was always present, leading to highly non-symmetric deformation, distributed in a wavy pattern along the circumference of the specimen, usually presenting two locations of predominantly left- and two locations of predominantly right-side deformation. However, we did not manage to observe the other deformation patterns referred to by Paramour[20], which suggests that, at least up to the 300 mm diameter range, and for the material in question, lubrication of the roller is not required, nor is it necessary to drive the roller at a predetermined speed.

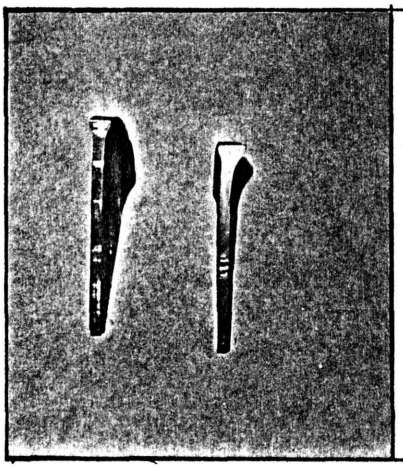


FIG. 5-22 - SOUND (SYMMETRIC) AND UNSOUND (BUCKLED) DEFORMATION IN RADIAL UPSETTING

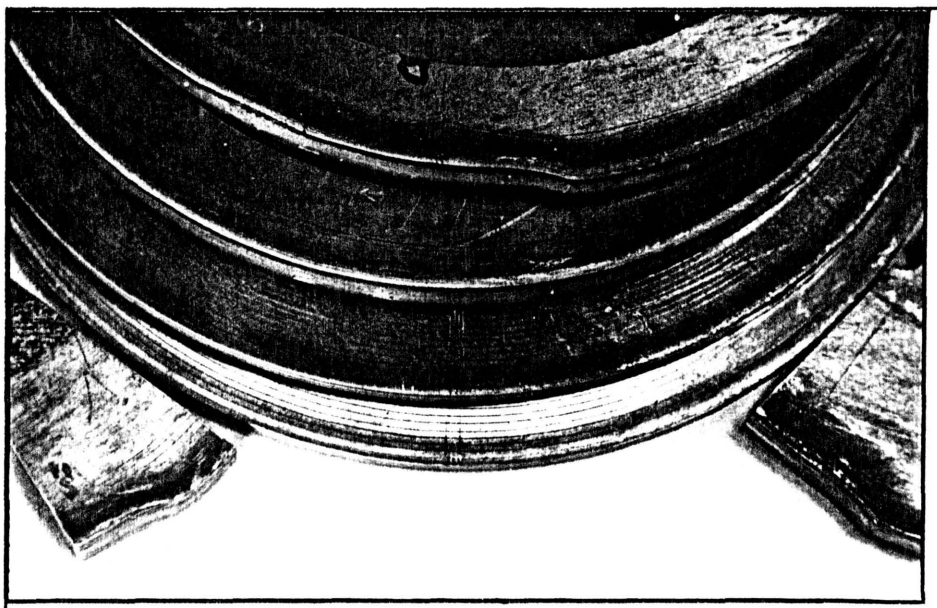


FIG. 5-23 - A SAMPLE OF SPECIMENS AT VARIOUS STAGES OF DEFORMATION

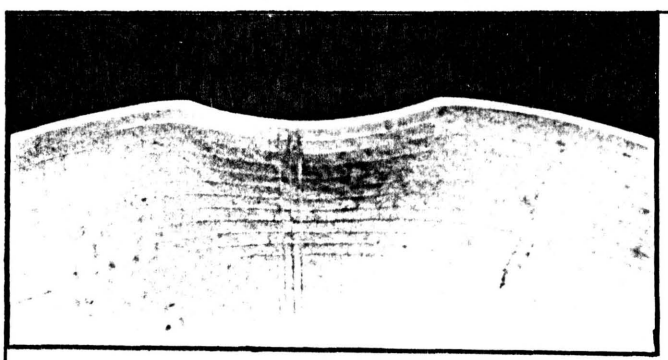


FIG. 5-24 - AN INDENTED SPECIMEN

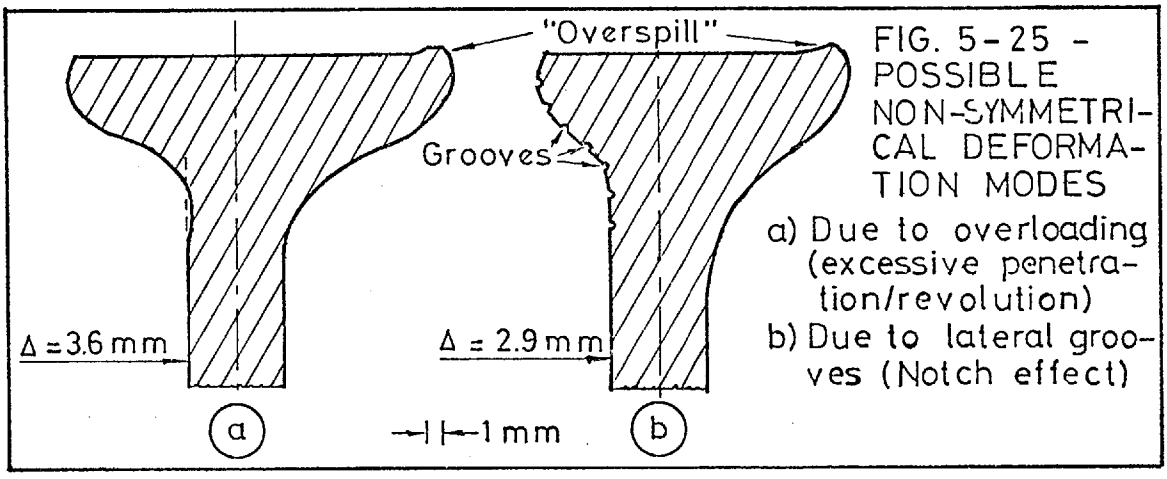


FIG. 5-25 - POSSIBLE NON-SYMMETRICAL DEFORMATION MODES
a) Due to overloading (excessive penetration/revolution)
b) Due to lateral grooves (Notch effect)

In some experiments a system of grooves was applied to one of the sides of the specimen, as can be seen in Figs. 5-23 and 5-24. Although the depth of the tracing was kept at the minimum discernible, the notch effect proved to be too substantial, especially at very large values of penetration, giving a totally different deformation mode for each side of the specimen, with smooth and deep deformation on the non-scratched side, and intense but shallow deformation on the side of the grooves, presenting a distinctly recognizable edge at one of them. Obviously, tracing is not the adequate method of producing a control grid.

Fig. 5-25 exemplifies the two nonsymmetrical deformation modes just referred to, by transcribing the cross-section of two specimens, as copied from an amplification produced in the profile projector. In the first example, sound deformation was maintained for four or five revolutions, when small penetrations were used; in the next revolution, a penetration of the order of 1.6 mm was tried, and all the material seems to have moved to one side of the specimen. The second example does not seem too much different from the preceding one; however, deformation in this case was achieved by using only small amounts of penetration/revolution (not more than 0.4 mm/rev), and non-symmetry was observed from the first revolution. The "overspill" indicated in the figure occurs when the material spreading laterally out surpasses the semithickness of the forming roller and thus ceases to be under its direct compressive action.

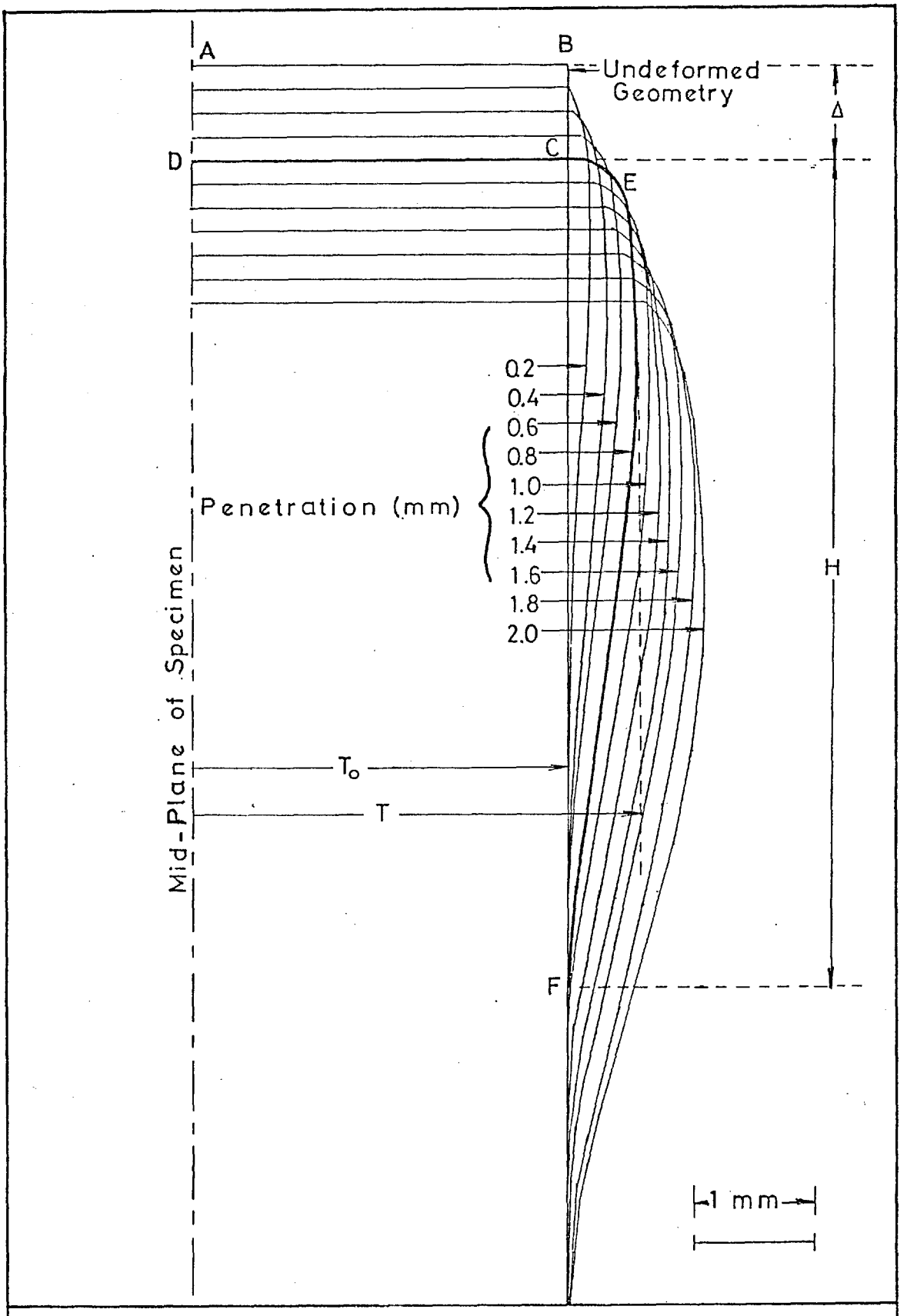


FIG. 5-26 - DEFORMATION MODES IN RADIAL UPSETTING

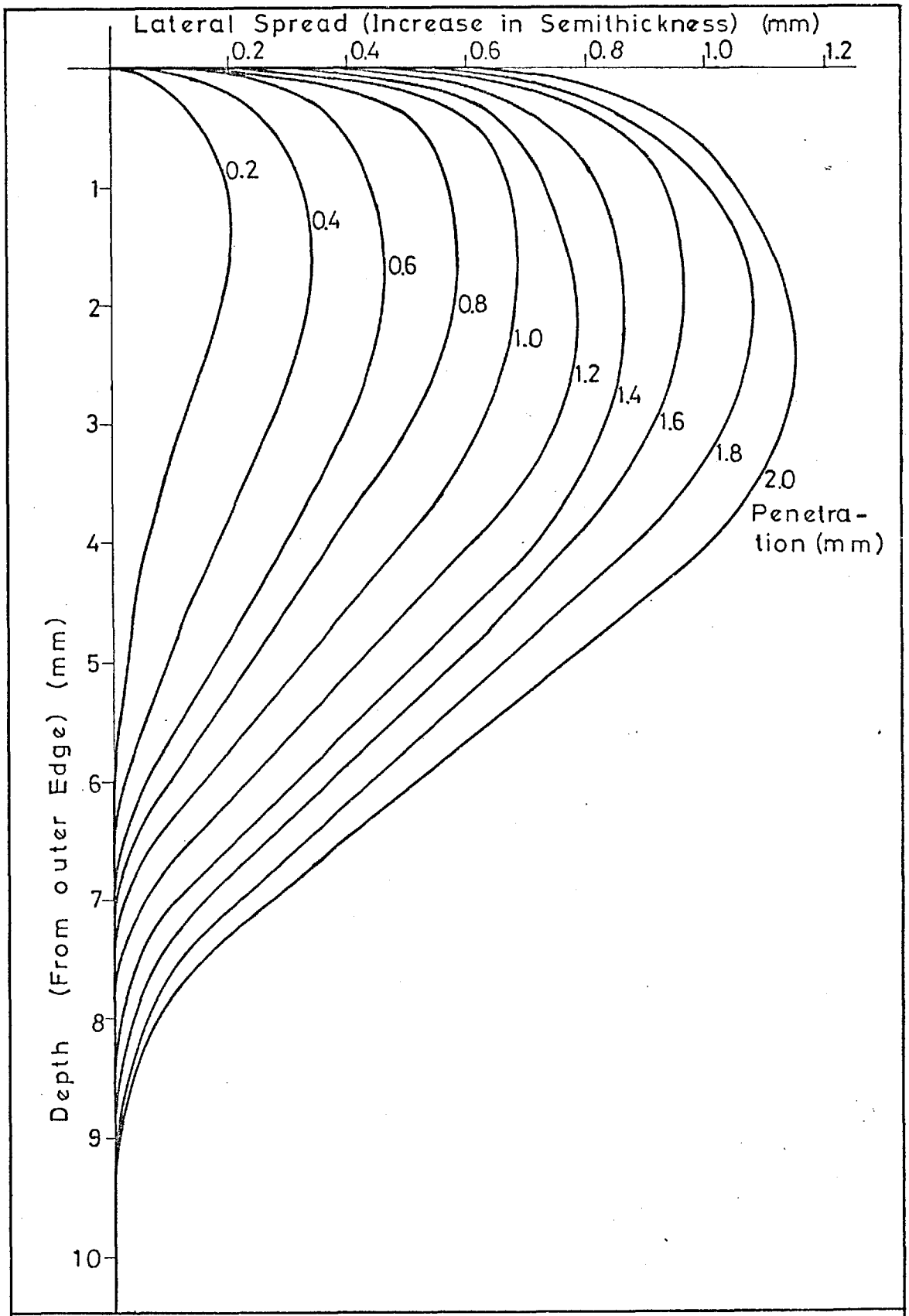


FIG. 5-27 - INCREASE IN SEMITHICKNESS IN TERMS OF PENETRATION

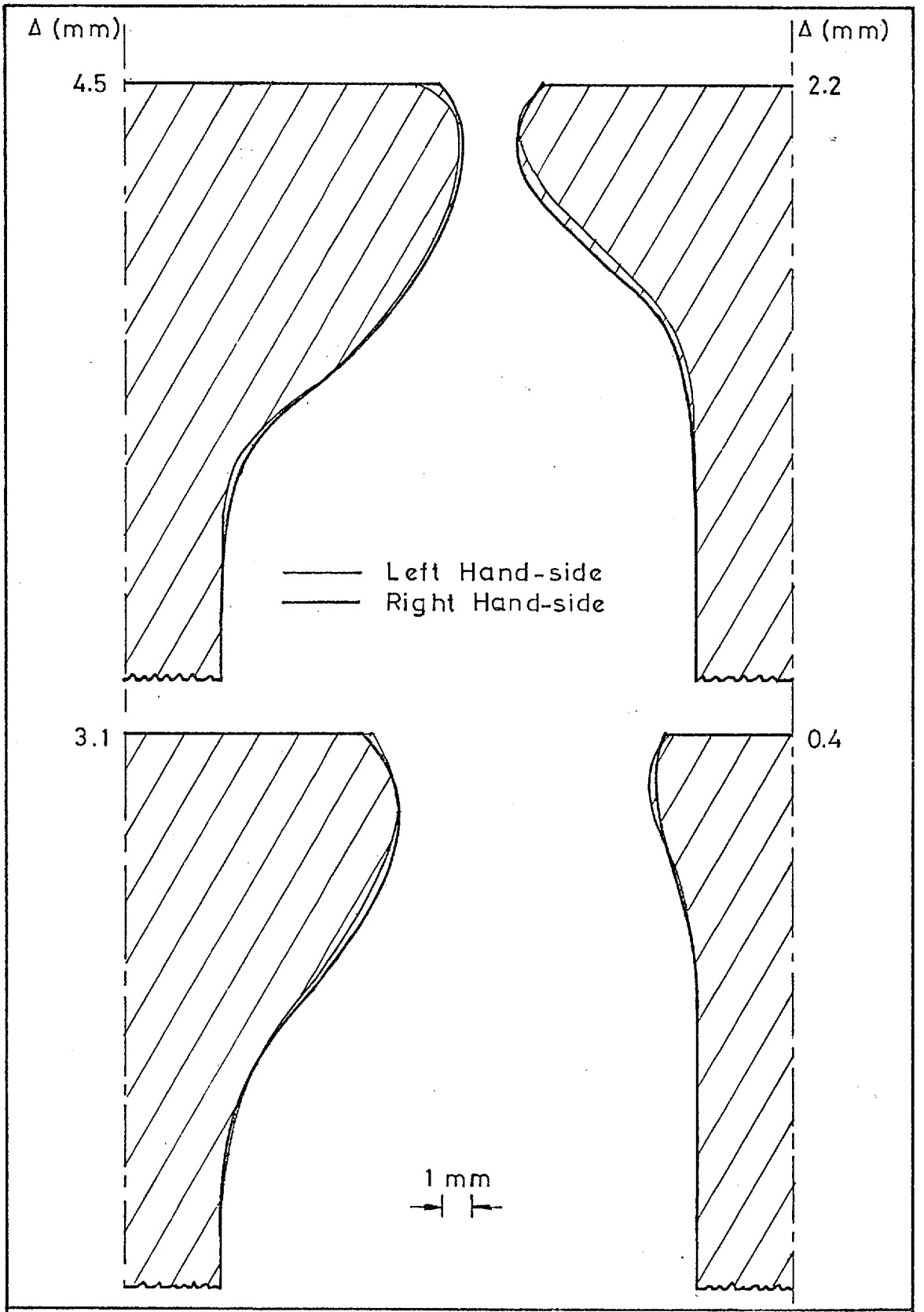


FIG. 5-28 - A MEASURE OF THE DEGREE OF SYMMETRY IN SOUND RADIAL UPSETTING

5.2.b - DEFORMATION MODE

The deformation mode normally encountered in the radial upsetting experiments is presented in Figs. 5-26 and 5-27, for a set of values of penetration. They have been obtained from 2 mm thick radial slices cut out of the deformed specimens, magnified in the profile projector. A check for the correctness of the penetration values was made, in each case, by comparing the area CEF (In Fig. 5-26), which was obtained by numerical integration, against the area ABCD, which is simply expressed by $T_o \Delta/2$. Only specimens for which these areas deviated by less than a few percent were considered acceptable.

The curves represented in both these figures are really averages obtained from a pool of not less than three sound specimens, analysed, on the profile projector, under a magnification of 15 times, both sides of the specimen being considered. Fig. 5-28 illustrates a sample of the profiles obtained (though under a magnification of five times only), showing that a reasonable degree of symmetry was obtained for the specimens taken into account for that purpose.

Linear relationships relate the parameters of the deformation (height of deformed bulge H and maximum final thickness T, shown in Fig. 5-26, to the penetration Δ. In fact, in a previous work[147], presented as Appendix 5 to this thesis, we have already used the expression

$$H = 5.4 + 1.5\Delta ,$$

which was obtained from coarse, preliminary measurements, in which the frontier of the deformed bulge was estimated by the naked eye only. By using the profile projector, under a magnification of 15 times, improved results were obtained, which are presented as Table 5-1. A least squares linear approximation can thus be obtained for both H and T, which are then expressed as

Δ mm	$\frac{T - T_o}{2}$ mm	H mm
0.2	0.196	6.0
0.4	0.334	6.6
0.6	0.455	6.8
0.8	0.580	7.0
1.0	0.680	7.2
1.2	0.780	7.8
1.4	0.860	8.4
1.6	0.956	9.0
1.8	1.075	9.2
2.0	1.148	9.4

TABLE 5-1 - Geometric parameters of the deformed bulge in radial upsetting (Fig. 5-26)

$$H = 5.85333 + 1.71515\,\Delta$$

and

$$T = 1.04191\,T_o + 1.04242\,\Delta\,.$$

Those equations, of course, are only valid for the experimental conditions of our investigation, that is, for the material tested, for the particular diametral dimensions of specimen and roller, and for the penetration range of 0.2 to 2.0 mm only. The general shape of the deformation mode seems to satisfy a cubic equation in terms of the radius, the coefficients of which would be dependent on the penetration Δ. No attempt has nevertheless been made to express these equations.

No significant change in the deformation mode was observed when changing the angular velocity of the specimen, in the range allowed by the driving and reducing system of the rig (0.25 to 1.1 rpm).

A slightly different deformation mode was obtained in the few room temperature tests we conducted. Only a qualitative comparison obviously applies, as the temperature was not the only changing parameter in the series: smaller specimens (with a diameter of the order of 210 mm) were used. Room temperature tests presented a deformation bulge spreading out more intensely in the immediate vicinity of the forming roller, but pene-

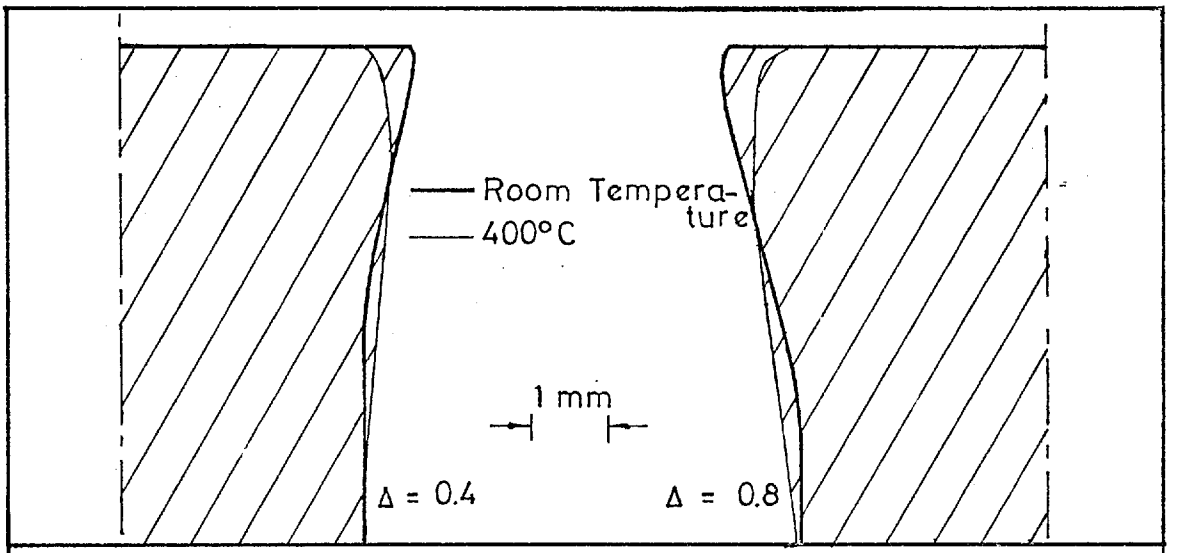
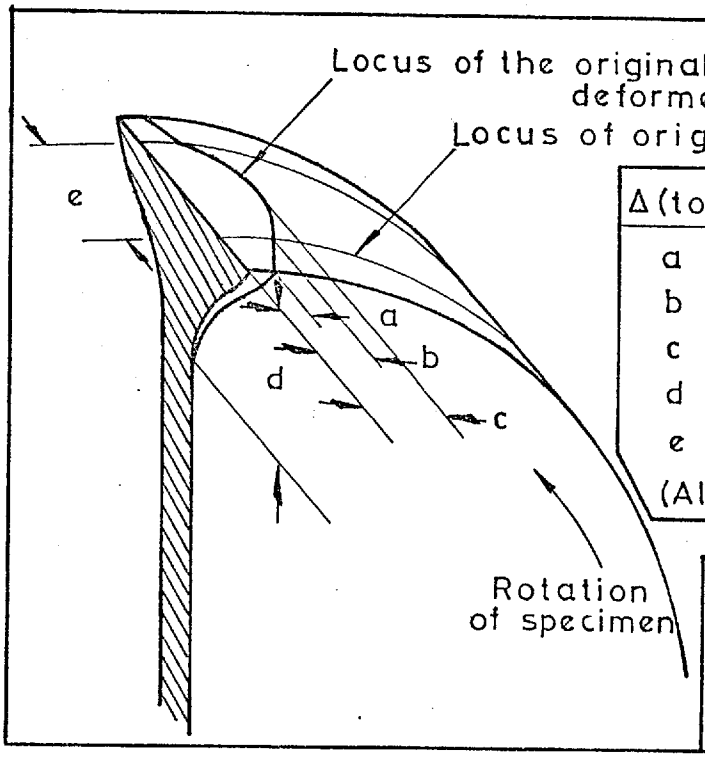


FIG. 5-29 - DEFORMATION IN HOT AND COLD RADIAL UPSETTING

trating less deeply towards the centre of the roller. Fig. 5-29 compares the hot and cold deformation modes in specific situations. These observations are consistent with common sense and also with results verified elsewhere (Appendix 4). In hot forming operations the temperature of the roller lies well below that of the specimen; this one is thus substantially cooled in the immediate vicinity of the contact area. Deformation, therefore, becomes more difficult in these surroundings. In room temperature deformation, however, such a thermal gradient does not occur; deformation predominates in the vicinity of the application of the forces, that is, near the interface. The heat eventually generated by the deformation process only reinforces this behaviour.

Our only experiment with a 1/8" (3.17 mm) thick steel specimen was conducted at a temperature of 900-950°C, which could be maitained with extreme difficulty, exploiting the full capacity of the induction generator. The deformation pattern, as sould be expected, does not differ substantially from the one verified for aluminium. However, much more force is required. In our specific application case, the reduced thickness of the specimen produced a too slender loading structure in the forming zone, and although care was taken to keep the penetration/revolution within very small values, buckling became inevitable, and a dish-like flanged disc was eventually obtained.



Δ (total)	1.3	11.5	20.2
a	0.4	2.0	2.0
b	0.5	3.0	5.5
c	0.6	3.5	12.5
d	4.0	15.0	9.0
e	6.5	8.7	15.8

(All dimensions in mm)

FIG. 5-30 - PARAMETERS OF OUT-OF-PLANE DEFORMATION IN RADIAL UPSETTING

In the preceding analysis, no mention was made to the three-dimensional nature of the deformation process under investigation. Fig. 5-30, restricted once again to the hot-working of aluminium specimens, informs about the third (tangential) component of displacement and provides additional insight into the nature of the deformation. It can be observed that the out-of-plane deformation of particles originally lying on a given radial plane of the specimen is restricted to the immediate vicinity of the contact area. Furthermore, a stretching of the original (undeformed) cylindrical mantle of the specimen is observed (compare the parameter e, in the figure, with the initial thickness - 6.35 mm - of the specimen). The out-of-plane effect is more accentuated in the vicinity of the mid-plane.

For small amounts of penetration (up to a total of the order of 0.5 mm) hardly any out-of-plane deformation is observed. A sizeable out-of-plane effect can be noticed for total penetrations of the order of 1 mm onwards, initially restricted mainly to the lateral faces of the specimen (consider especially parameters a and d, in the figure). For very large radial reductions the variations in these parameters stabilize (and even begin to decrease), whilst the remaining ones go on increasing; that is, the out-of-plane deformation becomes restricted to a layer in the vicinity of the contact area (sticking friction).

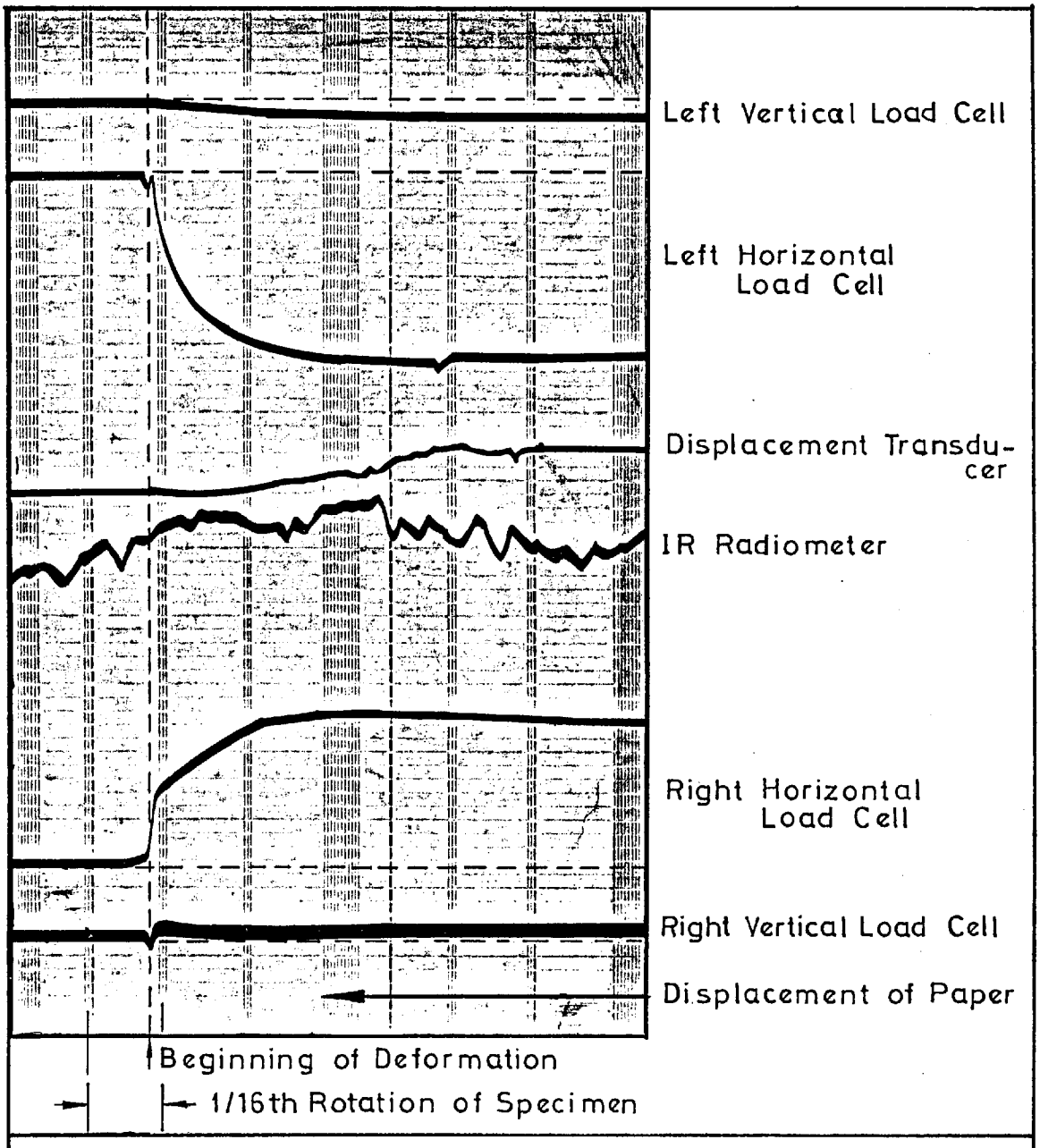


FIG. 5-31 - OUTPUT REPORT FROM UV RECORDER (TYPICAL SAMPLE)

5.2.c - FORCES IN TERMS OF PENETRATION

Fig. 5-31 presents a portion of a typical output report from the UV recorder, where the six relevant output signals (from the two horizontal and two vertical load cells, from the radiometer and from the displacement transducer) can be seen. As the output signals are faint, they have been intensified for copying purposes.

As can be seen from this figure, the vertical (tangential) components of force are extremely small, corresponding to a few percent only of the horizontal (radial) components. For this reason we have fully disregarded these components in the analysis to follow.

In all we employed twenty-two aluminium specimens. Two of those were used exclusively for the indentation tests, which will be dealt with in the next section. We do not use the records corresponding to the first ten specimens because either they were used for colateral purposes only (eg, testing the induction heating coil or calibrating the IR radiometer), or because - as should be expected in the beginning of an experimental work - extraneous factors interfered, causing the results to be meaningless.

By careful documentation of the testing conditions, coupled with the subsequent examination of the resulting flanged specimens, via, for instance, the area control already mentioned in the preceding section, a tabulation could be established for every specimen, relating the applied force to the penetration produced. The results obtained are plotted in Fig. 5-32.

It should be stressed that all data appearing in this figure refer to one-step deformation applied over a virgin (previously undeformed) specimen. Most of these specimens were subsequently used to produce further deformation, over several revolutions and using several alternative loading programmes, in order to exploit the possibilities of the radial upsetting process. Although force measurements were made, their significance is dependent not only on the penetration instantaneously produced, but also on the current geometry of the specimen, which generally varied throughout the peripheral length, due to the stepwise deformation produced during the first revolution. An interpretation of the force measurements under those circumstances becomes extremely complicated and of dubious validity.

We used this part of the experimental work, instead,

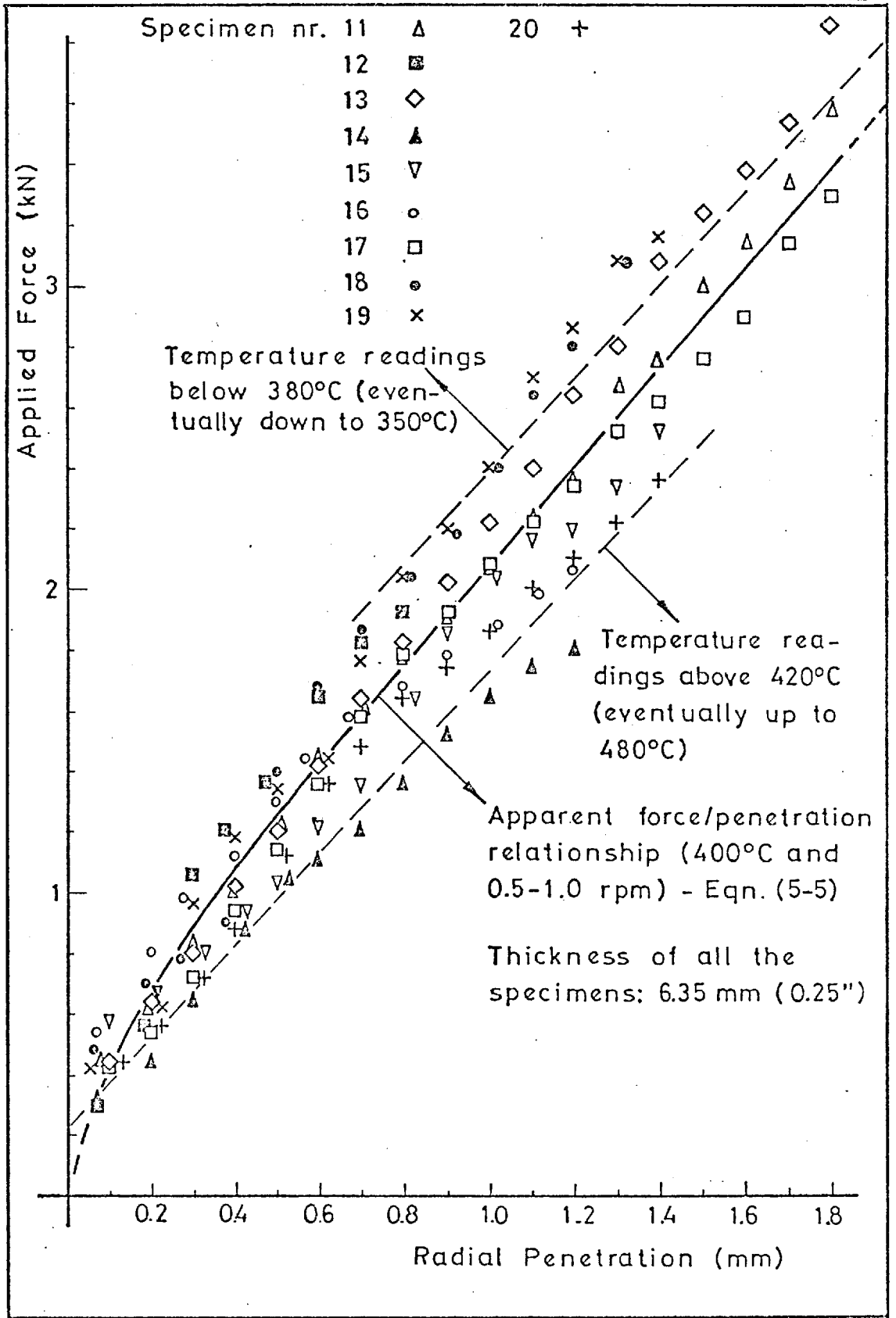


FIG. 5-32 - RELATIONSHIP BETWEEN APPLIED FORCE AND DEFORMATION (PENETRATION) ACHIEVED IN THE RADIAL UPSETTING OF COMMERCIALLY PURE ALUMINIUM

to verify the feasibility of the process, provided sensible loading programmes were maintained, up to the limit of deformation (total radial reduction of more than 40 mm) which could be achieved in our experimental rig.

In order to establish a force-displacement (penetration) relationship, isothermal conditions have to be maintained during the test, but, as we mentioned earlier in this chapter, this requirement is not easy to be achieved. Inevitable temperature variations occurred during some of the experiments.

Our intention was to conduct all tests at a temperature of $400^{\circ}C$, but for the purposes of the analysis of the experimental results, temperatures ranging from 380 to $420^{\circ}C$ were considered as satisfactory. Testing situations where the temperature fell out of this range are indicated in Fig. 5-32, and its results are not taken into account in the following analysis. Thus, the width of the range of results, for every particular value of penetration, is considerably narrowed.

Previously(147 - Appendix 5) we considered averages of the remaining data. These averaged forces seem to fit a quadratic equation in terms of the penetration. This equation can be expressed by means of the least squares method, from the tabulated data. The expression we arrived at, valid for penetrations from 0.1 to 1.8 mm, is given by

$$P \cong 0.2031 + 2.1331\,\Delta - 0.21694\,\Delta^2, \qquad (5\text{-}5)$$

with Δ taken in mm, and P given in kN. This equation is represented, in Fig. 5-32, by the thick semi-continuous line.

5.2.d - THE INDENTATION PROBLEM

A few indentation tests were also conducted, covering penetration values up to 4 mm. Two disc specimens were used for that purpose, and eight tests were performed on each of them. Some of the tests, however, had to be later disregarded, as the record of the testing conditions was not sufficiently reliable.

When indentation is considered, a problem relating to the heating of the specimen arises. As the specimen does not rotate during the experiment, the heating coil must be placed some distance away from the actual deformation zone (otherwise it would interfere with the compression roller). In order to reach an adequate temperature (by conduction) ahead of the roller, the temperature of the material immediately under the coil must be allowed to reach much higher levels. This can be easily achieved with our generator when the specimen is steady, but at the risk of melting the material under the coil before the right temperature in the deformation zone is reached.

A different approach to the heating problem would be to heat the whole periphery of the rotating specimen, as in the radial upsetting process, and once the adequate temperature is reached, to stop the specimen and to perform the experiment. During the experimental stage, the induction generator could be either switched off (and the temperature would drop during the indentation) or kept operative (and the temperature would go on increasing, but material would eventually melt under the coil). Both these alternatives indicate that the test must be performed very quickly if isothermal conditions are to be assumed and if no undesirable side effects are to occur. The first one was followed in our experiments, after a few trials with the second one proved to be unsuccessful.

Figs. 5-33 and 5-34 show the deformation mode obtained for two particular values of penetration. One quadrant of the deformation zone is shown in each case. The lateral topography of the specimen, for the purpose of drawing these figures, was ob-

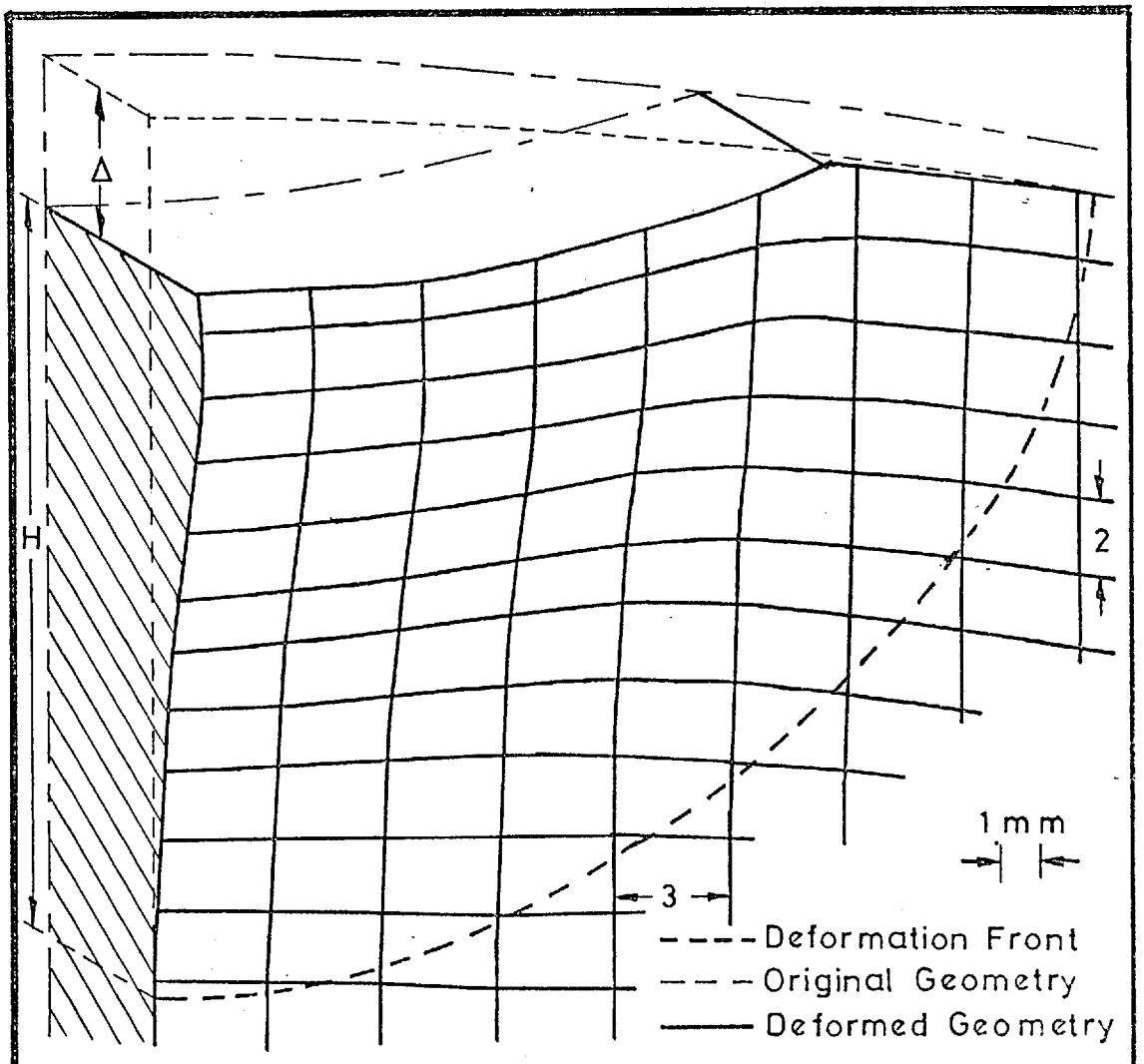


FIG. 5-33 - INDENTATION OF CYLINDRICAL SPECIMENS BY A CYLINDRICAL ROLLER - DEFORMATION MODE FOR Δ = 3.95 mm

tained by a dial gauge scanning a set of lines parallel to the radial symmetry plane, and separated by a distance of three millimetres. Readings were made at the deformed position of very shallow circumferential grooves traced on the sides of the undeformed specimen.

As can be observed from the figures, deformation is restricted to an approximately elliptical boundary, here termed as the deformation front. The maximum depth H of this deformation front (19.0 and 16.8 mm, respectively, in the case of the figures) consistently lies about 50% above the corresponding values usually found in the radial upsetting tests. This seems to be counterbalanced by the maximum increase in the semithickness

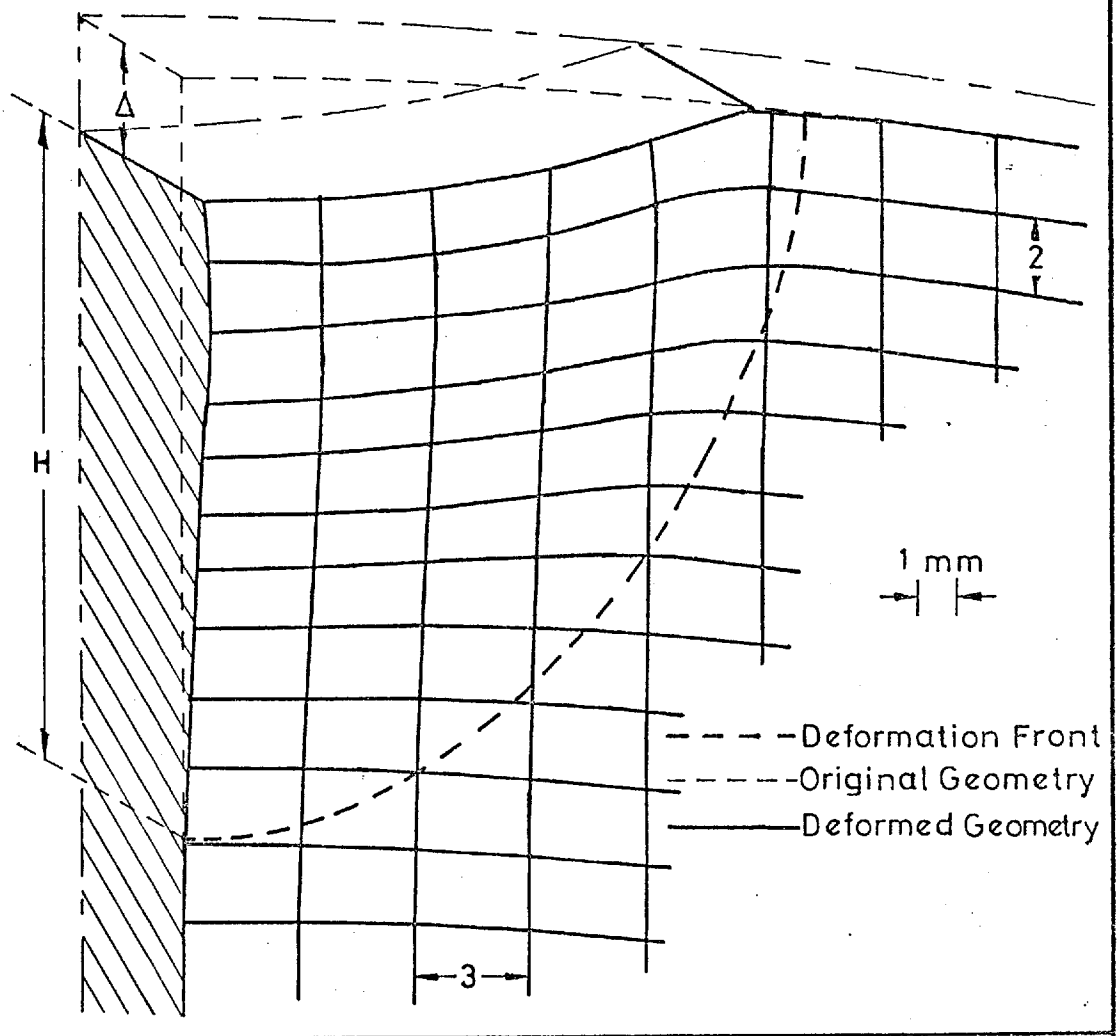


FIG. 5-34 - INDENTATION OF CYLINDRICAL SPECIMENS BY A CYLINDRICAL ROLLER - DEFORMATION MODE FOR Δ = 2.90 mm

(1.43 and 0.73 mm, respectively), which is well below the amount to be expected in radial upsetting, for the same amount of penetration. No substantial out-of-plane deformation was noticed, except perhaps around the quarters of the contact surface, and even there it did not amount to more than a small fraction of what would be expected in radial upsetting. A slight thickenning occurs in the vicinity of the cylindrical mantle of the specimen, outside the bounds of the contact surface, but no radial increase, or accumulation of material, is detected in this region. The maximum final thickness is achieved in the radial plane of symmetry, about two to four millimetres away from the forming roller (depending on penetration).

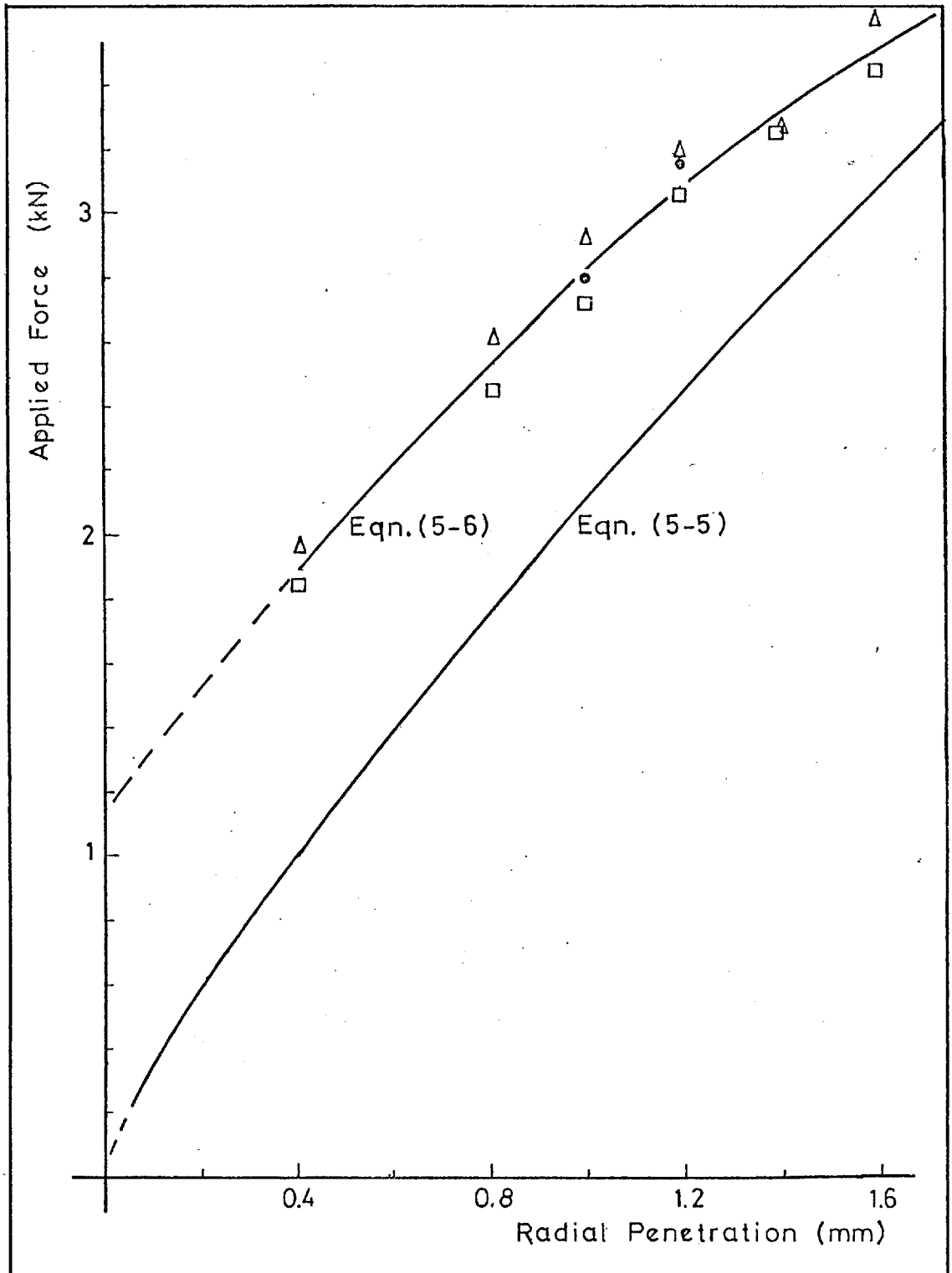


FIG. 5-35 - INDENTATION OF CYLINDRICAL SPECIMENS BY A CYLINDRICAL ROLLER - FORCE/PENETRATION RELATIONSHIP

Due to the speed requirement on the indentation tests, it becomes extremely difficult to establish a relationship between applied force and instantaneous penetration, during such a test. Instead, the force at the end of every test was recorded, together with the final value of penetration. A sample of results is plotted in Fig. 5-35. A least squares approximation of the results suggests an equation

$$P = 1.14689 + 1.98976\,\Delta - 0.32292\,\Delta^2 \qquad (5\text{-}6)$$

which, obviously, is not valid for small values of penetration.

If the results obtained for indentation are compared with those for radial upsetting (eg, the plot of Eqn. (5-6) compared with that of Eqn. (5-5)), it is observed that, for the same value of penetration, the force required for indentation is larger than that for radial upsetting. This observation should obviously be expected, as the contact area in the indentation situation is larger than in radial upsetting.

CHAPTER 6

THE FINITE ELEMENT SOLUTION

6.1 - INTRODUCTION

In this chapter the computer results obtained with the program EPFELDA , as described in Chapter 4 and in Appendices 2 and 3, are presented and compared with the experimental (Chapter 5) and upper bound (Appendix 5) ones. The behaviour and limitations are presented and analysed.

The formal procedure described in Chapter 4 has been applied using a mesh consisting of four basic blocks in the radial upsetting, and three in the indentation applications. However, due to the unsatisfactory results generally obtained, alternative solutions were eventually tried. The changes required by such alternative solutions are not incorporated in Chapter 4 nor in the listing of Appendix 2, but they will be sufficiently clarified when they are analysed in the text to follow.

Computer results are analysed from a triple point of view: the force/penetration relationship, the general mode of deformation and the obedience to the prescribed stress-strain curve are considered. Colaterally, the stability of the solutions is commented upon.

6.2 - THE RADIAL UPSETTING PROBLEM

6.2.a - INTRODUCTION

Nine sets of results will be analysed. Of those, seven follow the the procedure described in Chapter 4, from here onwards referred to as "relaxed boundary conditions", with the mesh presented in Fig. 4-9 extending to a depth of 15 mm from the external cylindrical boundary of the specimen. The two remaining sets follow the same formulation, but using a reduced mesh, with 24 nodes and 33 elements in the basic block, extending to a depth of 10 mm only.

The results are summarized in Table 6-1 and in Figs. 6-1 to 6-8.

Set	STP	Symbol (*)	Penetr. (mm)	Max. $\bar{\varepsilon}^p$	Nr. of LI	Failure	μ	Deformation Mode
A	0.01	×	0.43	0.055	8	(+)	0.0	Acceptable but not fully satisfactory
B	0.02	+	0.32	0.040	7	(+)	0.0	
C	0.04	Δ	0.38	0.046	6	(+)	0.0	
D	0.10	□	0.20	0.020	3	(+)	0.0	
E	0.02	o (§)	0.42	0.042	9	(+)	0.0	
F	0.02	∇	0.42	0.060	9	(+)	0.2	
G	0.10	◇	0.20	0.023	3	(+)	0.2	
H	(RM)	▲	1.33	0.245	11	(-)	0.0	Bad
I	(RM)	◆	1.33	0.245	11	(-)	0.4	Bad

(*) As used in Figs. 6-1 to 6-3 (RM) Reduced mesh

(§) Modified load redistribution in contact zone

(+) No convergence achieved in next load increment

(-) Time limit, with unsatisfactory result in at least the last load increment

TABLE 6-1 - FINITE ELEMENT RESULTS FOR THE RADIAL UPSETTING PROBLEM

From Table 6-1 the immediate observation arises that although the larger mesh produces reasonably satisfactory deformation mode, it tends to fail before a substantial amount of plastic deformation is achieved. Failure is due to the loss of diagonal dominance in the stiffness matrix, which leads to mo-

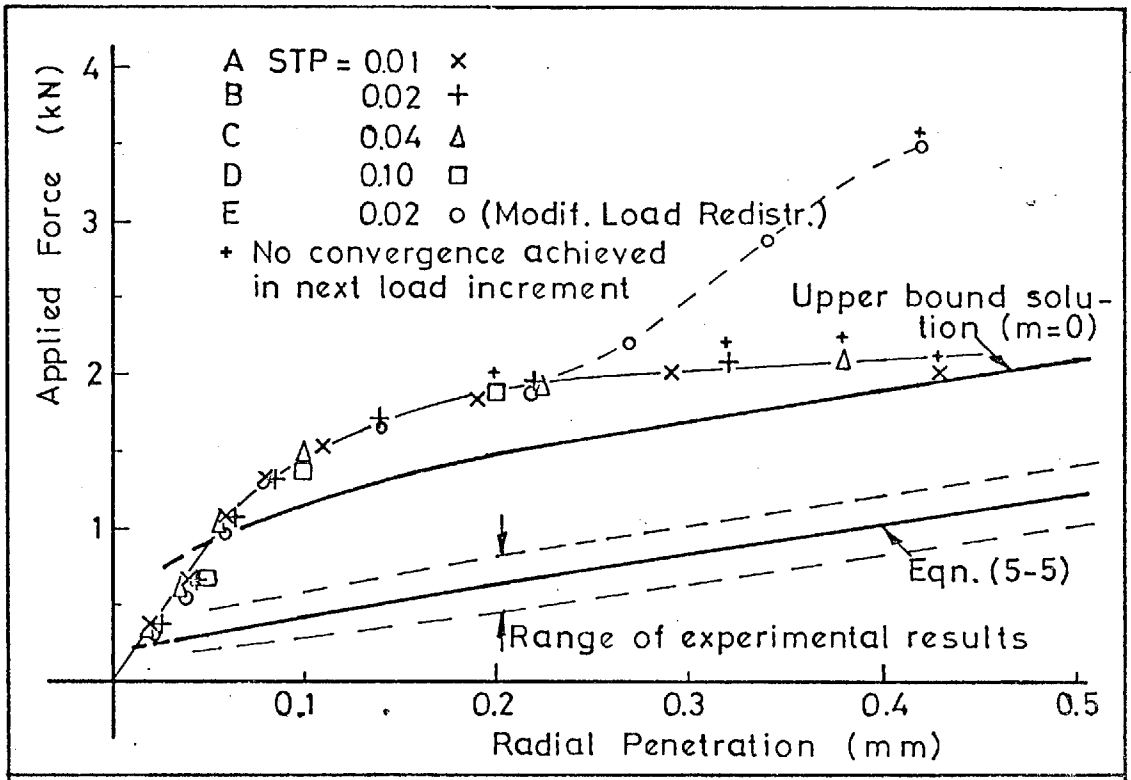


FIG. 6-1 - FORCE IN TERMS OF PENETRATION IN RADIAL UPSETTING: A COMPARISON OF FINITE ELEMENT, UPPER BOUND AND EXPERIMENTAL DATA

re difficult convergence for the incremental displacement field in every subsequent load increment, and eventually to no convergence at all for a radial penetration of a few tenths of a millimeter (depending on the value of the loading parameter STP). Larger values of plastic strain could be achieved employing the reduced mesh, but at the cost of a totally unacceptable force/penetration relation (Fig. 6-3) and a less satisfactory deformation mode.

Set E represents an alternative formulation using the larger mesh, but differing from the procedure described in Chapter 4 by the fact that the load redistribution in the contact zone (described in 4.4.d) was performed using a stricter redistribution criterion, smaller increments being prescribed for the boundary nodes about to enter or about to leave the contact zone (thus more in line with Fig. 4-5). The actual implementation of the corrected formulae, replacing those derived in Subsection 4.4.d, although extremely simple, is not presented he-

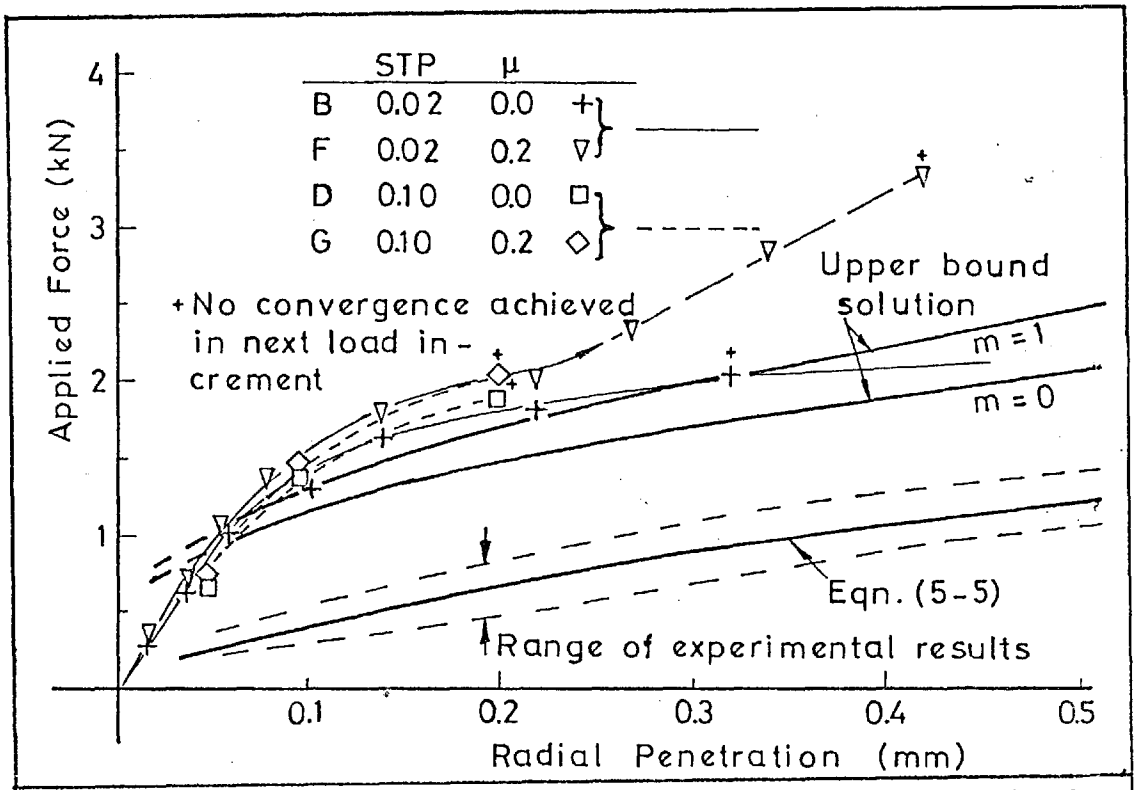


FIG. 6-2 - EFFECT OF A NONZERO FRICTION COEFFICIENT ON THE FINITE ELEMENT SOLUTION TO THE RADIAL UPSETTING PROBLEM

re, as the results did not prove to be fully satisfactory; in fact, no increase was obtained in the amount of penetration before failure, and an erratic behaviour was observed in the last three load increments, with a sudden increase in the applied force (Fig. 6-1).

6.2.b - FORCE/PENETRATION RELATIONSHIP

Figs. 6-1 to 6-3 plot the force/penetration relationships obtained for the nine sets of data listed in Table 6-1, and compares them with the experimental results (Fig. 5-32) and with the upper bound solution[147].

For the larger mesh the force required to achieve a certain level of penetration is usually well above the one verified experimentally, and slightly above the one obtained by the upper bound solution. There is an indication that for the higher values of penetration (had they been achieved), the finite element solution would lie below the upper bound one, as should be expected from a supposedly more rigorous formulation. On the other hand, the choice of the loading parameter STP does not

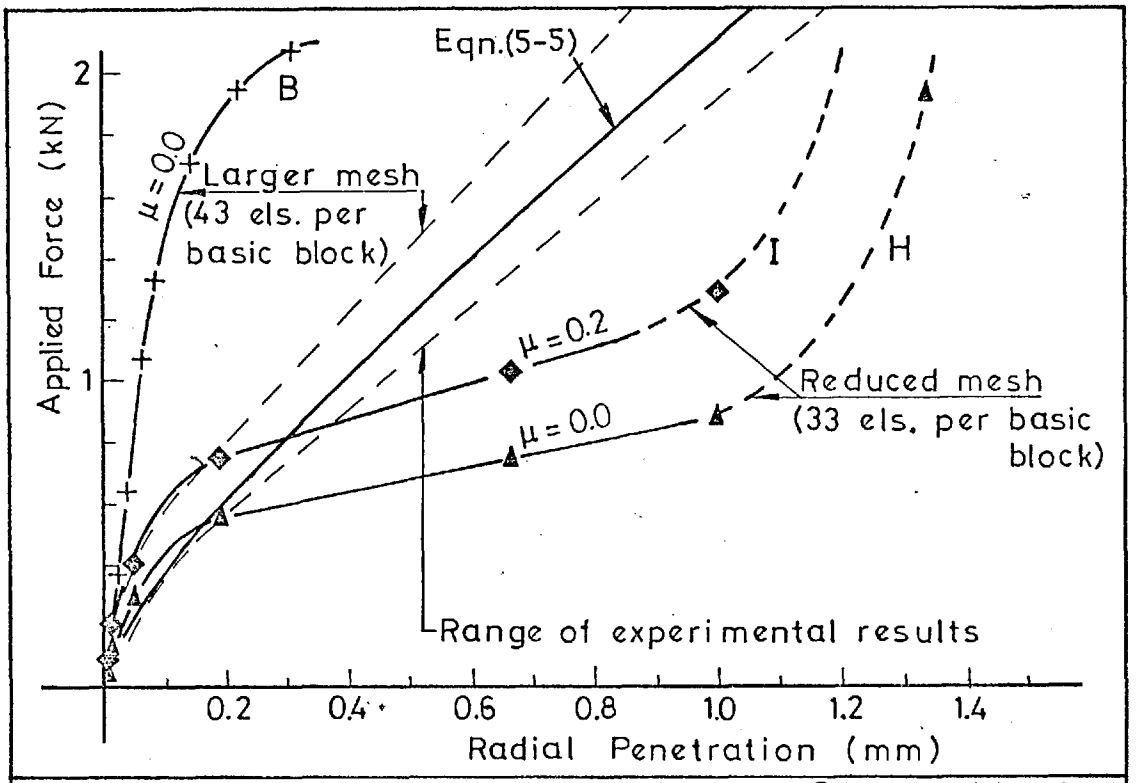


FIG. 6-3 - FINITE ELEMENT SOLUTIONS TO RADIAL UPSETTING USING A LARGE DEEP AND A SMALL SHALLOW MESH

seem to affect the order of magnitude of the forces; larger values of this parameter, however, will fail after a smaller number of load increments (Fig. 6-1 and Table 6-1).

Exception to these observations is the set E, for which an anomalous force increment was found in the last three converged load increments. The explanation for this increase seems to lie in the fact that probably larger penetration should have taken place, to equilibrate the last load increments, but this requirement was hindered by the load redistribution procedure. Possibly some error, which we have not been able to detect, arose in the derivation of the modified redistribution formulae.

The reduced mesh produced two drawbacks from the force/penetration point of view. At first, too small values of force were computed (Fig. 6-3), and after a number of load increments, an exaggerated increase in the forces was verified. Such increase, however, can be easily explained in terms of the radial spreading of the plastic zone towards the inner boundary,

which is not allowed to move.

The effect of a nonzero friction factor is analysed in Figs. 6-2 and 6-3. An unpublished result, originally intended to be included with the upper bound analysis[147], based on Kudo's comparisons between constant and Coulomb friction coefficients[148, 113], suggested that, for the amount of penetration obtained when using the larger mesh, the constant friction situation $m = 1$ corresponds to a Coulomb friction coefficient averaging 0.2. However, the results for sets F and G, for which a Coulomb factor $\mu = 0.2$ was used, suggest a slightly less drastic effect than the one obtained with the upper bound solution using $m = 1$.

6.2.c - DEFORMATION MODE

The results represented by the sets A to G did not allow a steady state situation to be reached (that is, one in which no further radial penetration is produced, and deformation is solely due to the rotational - or feeding - movement of the specimen). It is therefore not very significant to produce a direct comparison of the deformation mode obtained by the finite element solution with the one obtained experimentally. Fig. 6-4 attempts such a comparison for the maximum (final) value of penetration in the case of sets A, C and F. The radial plane considered for the finite element solution is the one corresponding to this maximum radial reduction; the computed out-of-plane deformation is also plotted.

In Fig. 6-4, as well as in the following ones, which plot deformation modes, the out-of-plane and axial displacements are plotted to an enlarged scale. For the purposes of comparison with the experimental results, curves for the adequate penetration value have been obtained by interpolation from Fig. 5-27. When plotting such data in Fig. 6-4, they were superimposed to the computed out-of-plane displacement component, otherwise the visualization would be made more difficult.

It is seen from Fig. 6-4 that the finite element solution predicts an acceptable deformation mode from the purely

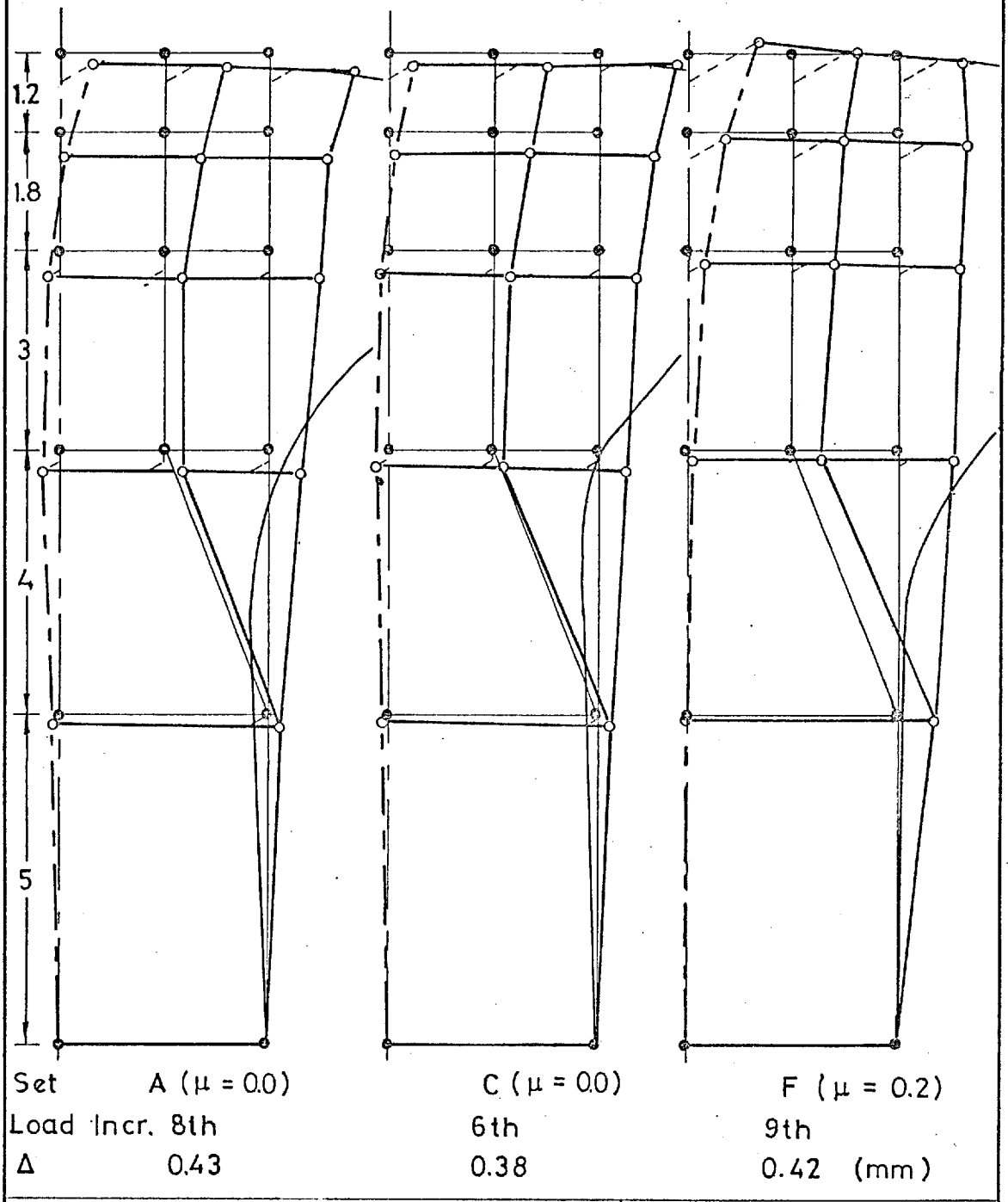


FIG. 6-4 - COMPARISON OF THEORETICAL (FINITE ELEMENT) AND EXPERIMENTAL DEFORMATION MODES

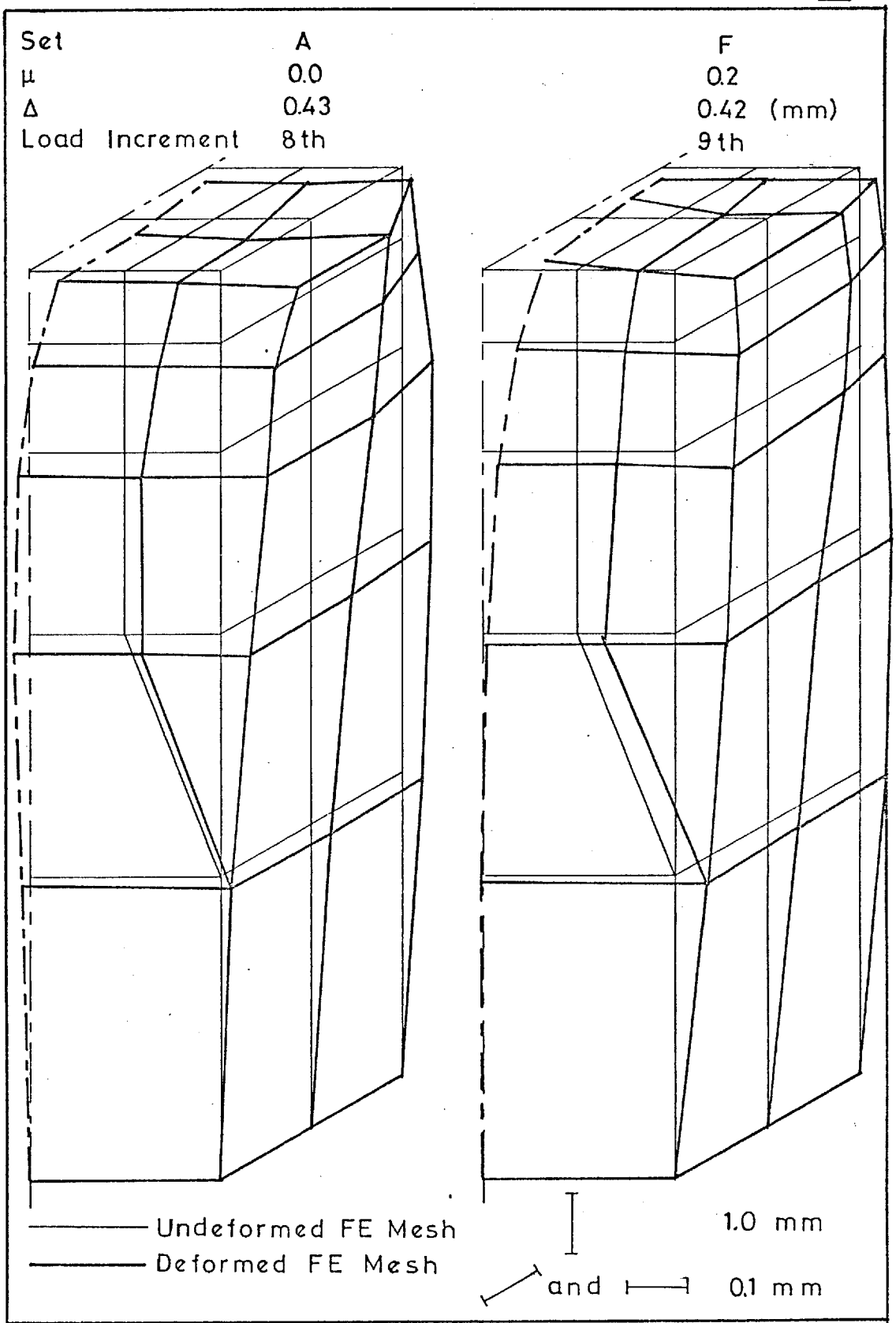


FIG. 6-5 - EFFECT OF A NONZERO FRICTION COEFFICIENT ON THE DEFORMATION MODE IN RADIAL UPSETTING

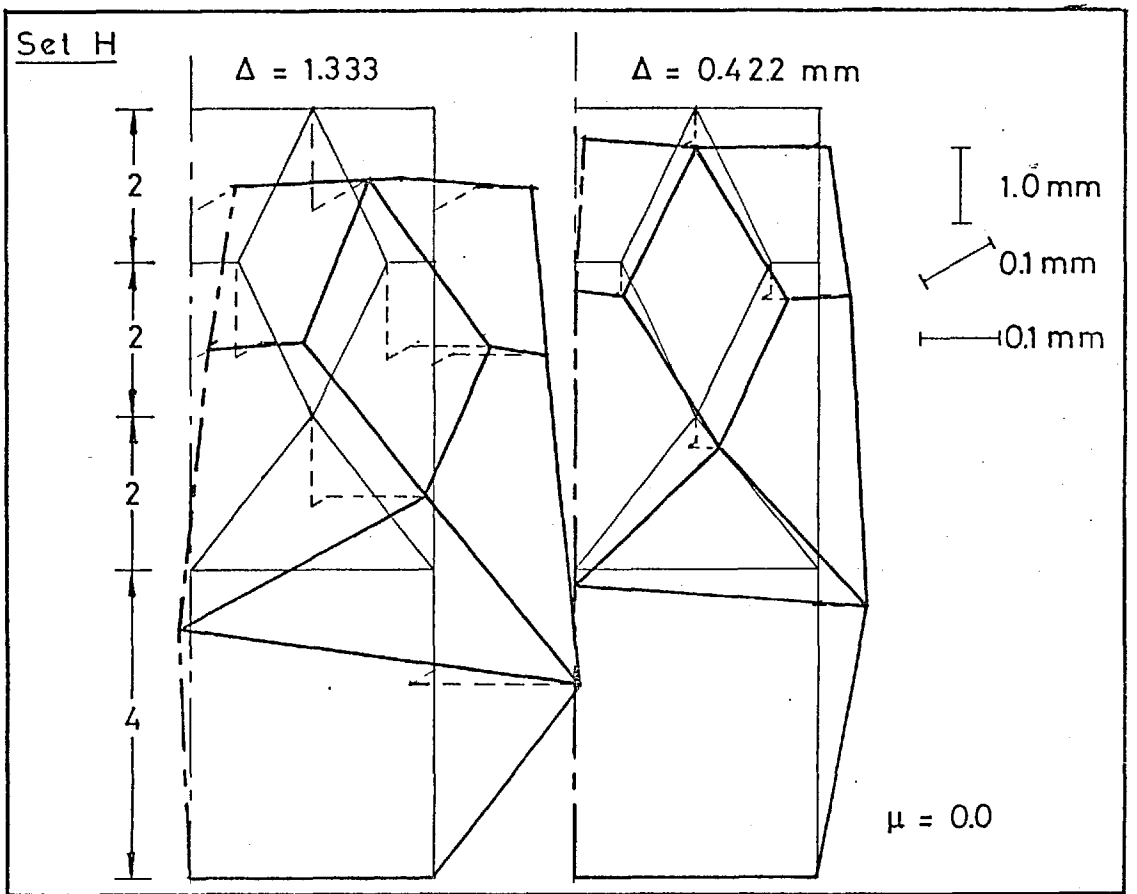


FIG. 6-6 - DEFORMATION MODE IN RADIAL UP-SETTING USING THE REDUCED MESH

qualitative point of view. In quantitative terms, however, the thickening of the specimen is predicted as much less intense than verified experimentally, especially when friction is considered. On the other hand, substantial deformation (in relative terms) is present over the whole depth of the mesh, a fact which also contradicts the experimental evidence.

The out-of-plane deformation is generally small, except when friction is considered. In that case the transversal displacements in the contact zone are predicted as nearly as twice as large than the maximum local thickening of the specimen; besides, the deformed surface tends to lag behind the original radial plane. When no friction is considered, this lagging behind is reduced to the vicinity of the contact zone; over most of the depth of the mesh it lies ahead of the original radial plane but presenting comparatively small values of displacement.

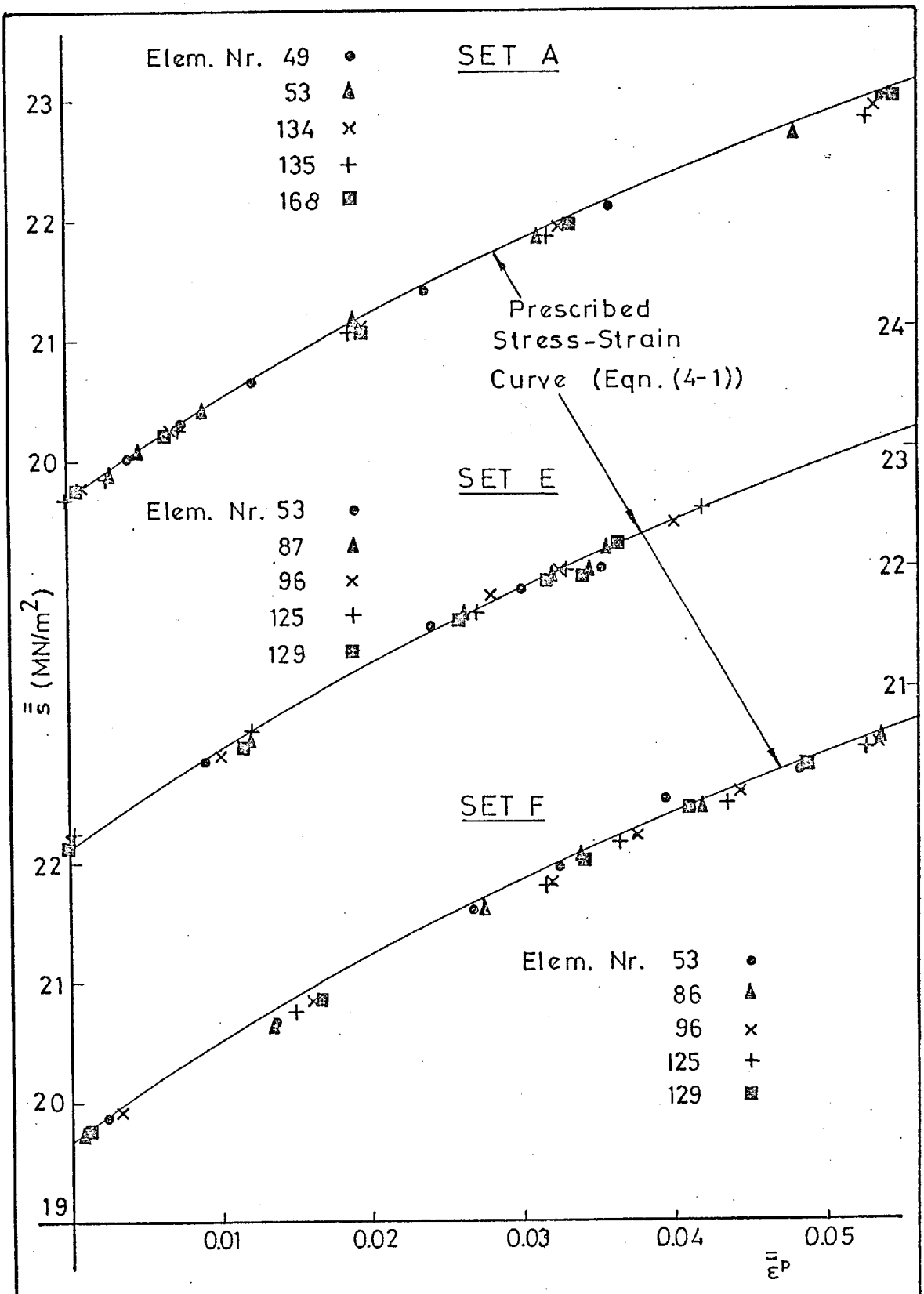


FIG. 6-7 - EQUIVALENT STRESS / PLASTIC STRAIN FOR A SAMPLE OF ELEMENTS USING THE LARGER FINITE ELEMENT MESH

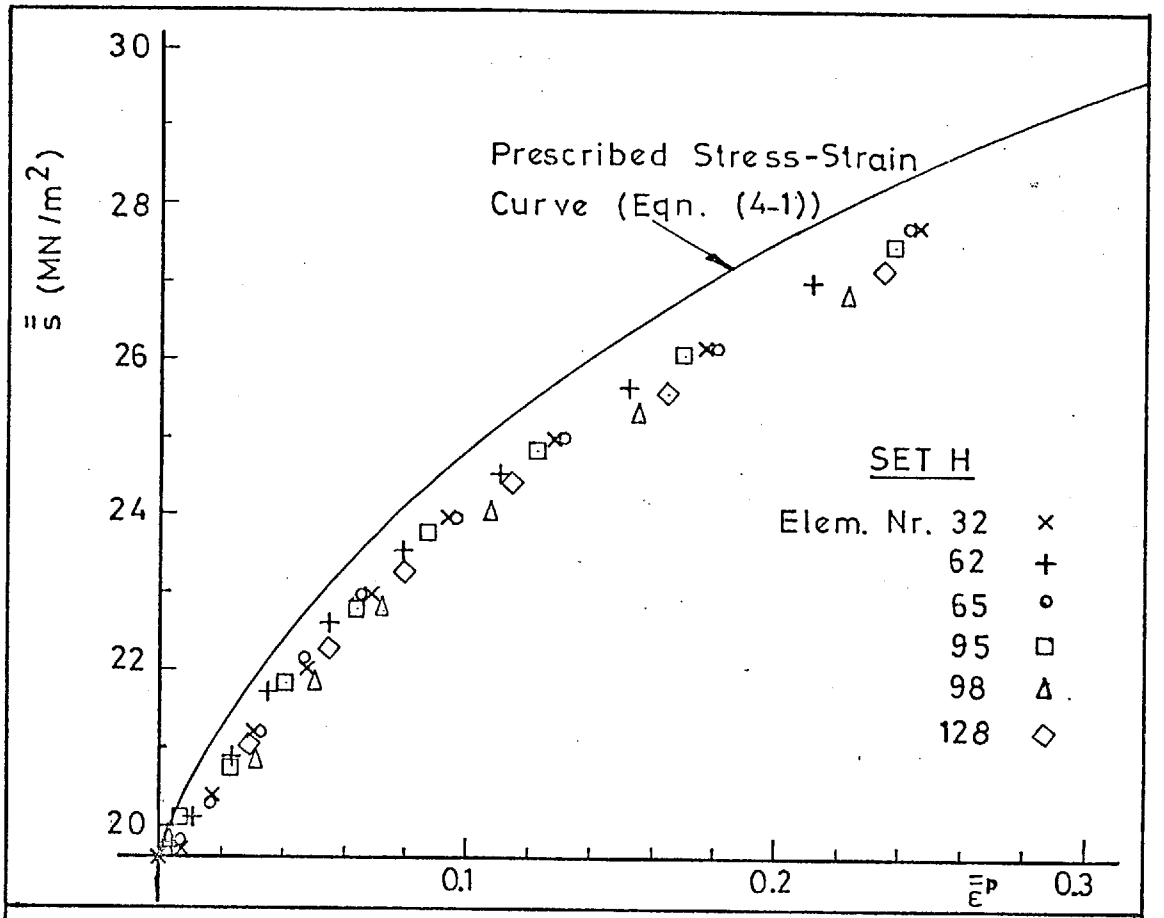


FIG. 6-8 - EQUIVALENT STRESS / PLASTIC STRAIN FOR A SAMPLE OF ELEMENTS USING THE REDUCED FINITE ELEMENT MESH

Fig. 6-5 plots the deformation mode of the part of the mesh involved in the contact arc, on both the frictionless and friction-affected situations (μ = 0.2) (Sets A and F).

Fig. 6-6 considers the frictionless case using the reduced mesh (Set H) and plots the deformation mode for two values of penetration. The lateral expansion (thickening) is again smaller than verified experimentally, but the out-of-plane deformation is much smaller than predicted when using the larger mesh. This result is apparently due to the fact that in the reduced mesh the effect of deformation becomes more directly compressive (as translated by the larger plastic strain increments). The deformation mode obtained with this reduced mesh is blatantly unsatisfactory. Maximum thickening occurs too far from the cylindrical mantle of the specimen, as becomes clear from the

analysis of the case when $\Delta = 1.333$ mm, the constancy of volume requirement is grossly violated.

6.2.d - STRESS-STRAIN CURVE

Fig. 6-7 plots the equivalent stress/plastic strain results for a sample of elements corresponding to sets A, E and F, and compares these plots with the prescribed stress-strain curve of the material at the temperature of 400°C (Fig. 4-1). Fig. 6-8 plots a sample of elements from set H.

It is observed that in all cases a very good agreement has been obtained, lying within a tolerance of less than 0.5% in the case of the larger mesh (Fig. 6-7), but slightly larger in the case of the reduced mesh (Fig. 6-8). This is due to the fact that, at the time when this case was run, a less stringent error control was used in the initial stress procedure. The larger plastic strains achieved with set H can be easily explained in terms of the fact that, for the same amount of radial penetration, the deformation was allowed to extend to a much smaller volume of material (due to the rigid boundary treatment of the inner cylindrical mantle of the finite element mesh).

6.3 - THE INDENTATION PROBLEM

6.3.a - INTRODUCTION

Eighteen sets of results were considered for the purpose of the analysis of the indentation problem. In ten of them the relaxed boundary condition situation described in Chapter 4 is employed. In the eight remaining ones, a fully rigid boundary was assumed in the interfaces between the finite element mesh and the rest of the (removed) specimen. The implementation of such a simplified boundary condition is extremely simple, but it is not presented here, nor in any of the appendices. For all the sets of results the same basic block of Fig. 4-9 was used. A mesh consisting of three basic blocks was considered, except for set V, when four were used.

The results are summarized in Table 6-2 and in Figs. 6-9 to 6-20.

Set	STP	Symbol (*)	Penetr. (mm)	Max. $\bar{\bar{\varepsilon}}^p$	Nr. of LI	Failure		Deformation Mode
J	0.10	o	0.200	0.018	3	(+)	0.0	Acceptable but not fully satisfactory
K	0.04	×	0.160	0.015	4	(+)	0.0	
L	0.02	+	0.310	0.038	7	(+)	0.0	
L'	0.02	▽	0.260	0.038	6	(+)	0.0	
L''	0.02	◇	0.820	0.083	10	(+)	0.0	
M	0.02	△(%)	0.260	0.024	6	(+)	0.0	
N	0.02	□(%%)	0.430	0.068	6	(+)	0.0	
O	0.10	•	0.200	0.018	3	(+)	0.2	As above
P	0.02	◈	0.160	0.018	5	(+)	0.2	
Q	0.02	▲(%)	0.180	0.015	5	(+)	0.2	
R	(RB)	▼	1.377	0.163	6	ST	0.0	Generally bad, especially at latter stages of the execution
S	(RB)	o	1.070	0.194	10	(+)	0.0	
T	(RB)	×(%%)	0.980	0.198	16	TL	0.0	
U	(RB)	+	1.851	0.124	3	(+)	0.0	
V	(RB)	▽(%%%)	1.941	0.185	3	SL	0.0	
W	(RB)	△	1.110	0.880	9	(+)	0.0	
X	(RB)	□	1.600	0.280	6	(+)	0.0	
Y	(RB)	•	0.340	0.040	7	(+)	0.0	

(*) As used in Figs. 6-9 to 6-11 (RB) Rigid boundary condition

(%) Modified load redistribution in contact zone

(%%) Two corrective initial load cycles allowed

(%%%) Three corrective initial load cycles were allowed, and four basic blocks were used

(+) No convergence achieved in next load increment

ST Execution halted because of unsatisfactory results (either deformation mode or excessive increase in plastic strains)

TL Time limit

SL Execution halted because of excessive increase in applied force

TABLE 6-2 - FINITE ELEMENT RESULTS FOR THE INDENTATION PROBLEM

In set M a modified load redistribution procedure, identical to the one employed with set E (in the radial upsetting applications) was applied, but without the same force increase being verified before the failure of the program.

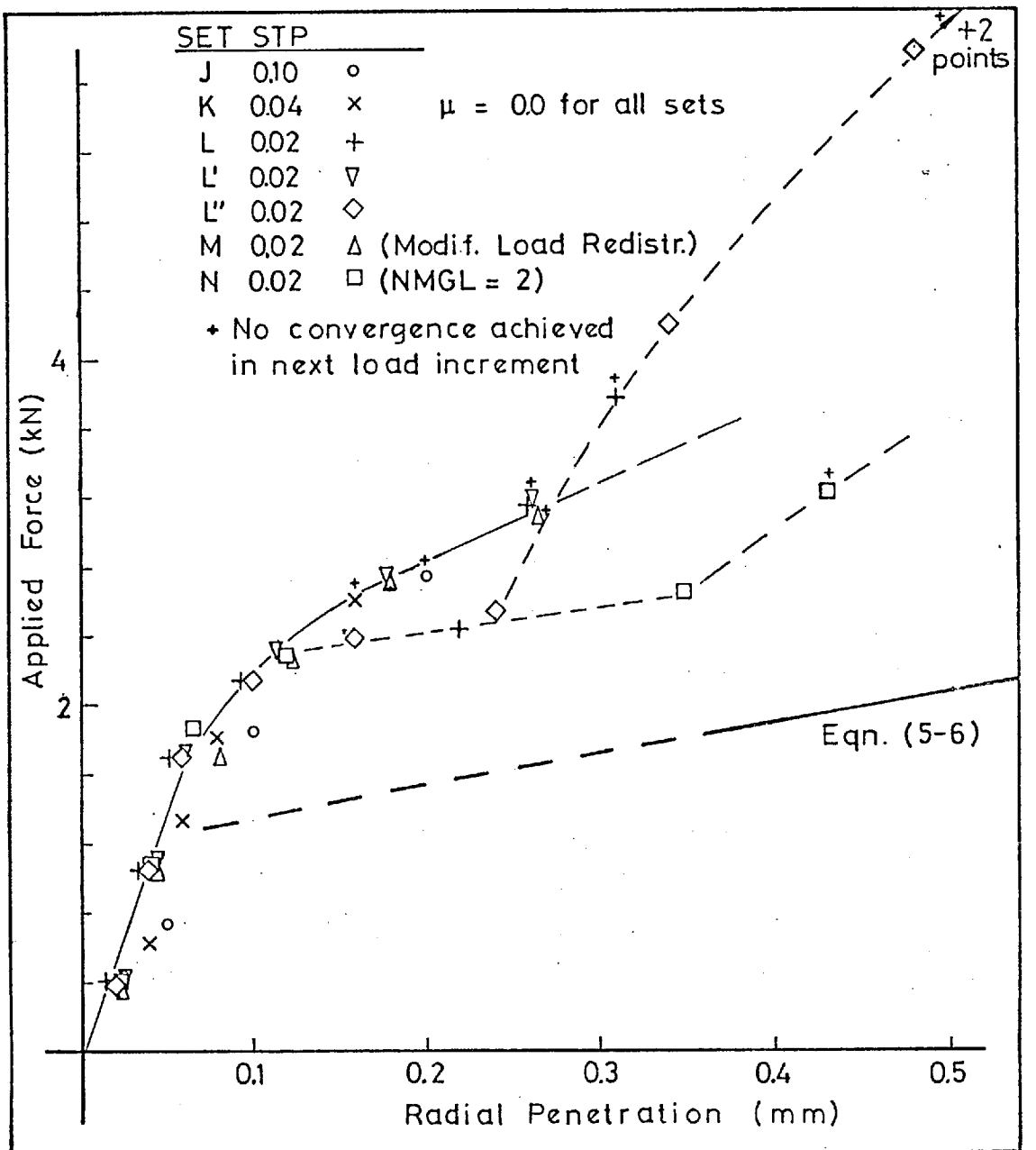


FIG. 6-9 - PREDICTED FORCE IN THE FINITE ELEMENT SOLUTION OF THE FRICTIONLESS INDENTATION PROBLEM AND COMPARISON WITH EXPERIMENTAL RESULTS

In sets N , T and V the maximum number of corrective cycles in the initial stress procedure was increased to two (N , T) and three (V) .

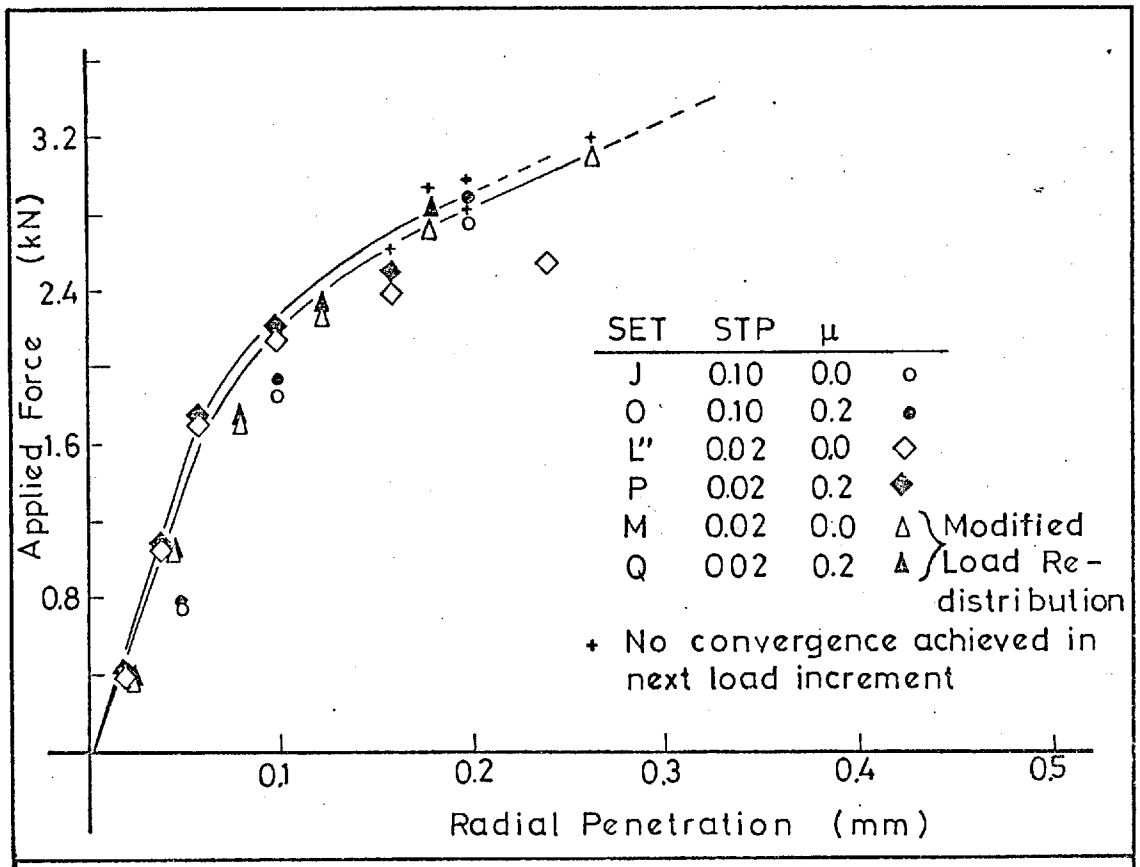


FIG. 6-10 - EFFECT OF FRICTION ON THE PREDICTED FORCE IN THE FINITE ELEMENT SOLUTION TO THE INDENTATION PROBLEM

6.3.b - FORCE/PENETRATION RELATIONSHIP

Figs. 6-9 to 6-11 plot the force/penetration relationships in the eighteen sets, and compare them with the experimental results, given in Fig. 5-35.

In Figs. 6-9 and 6-10 the relaxed boundary condition is considered. The first one covers the frictionless situation, while in the second one some frictionless results are compared with the corresponding case when μ is set to 0.2. The computed forces seem to discrepate less from the experimental ones than previously verified with the radial upsetting process; nevertheless they are still extremely high. Except for extremely large values, the loading parameter STP does not seem to influence substantially the results. A sudden increase is sometimes detected in the computed force, after a few load increments; this

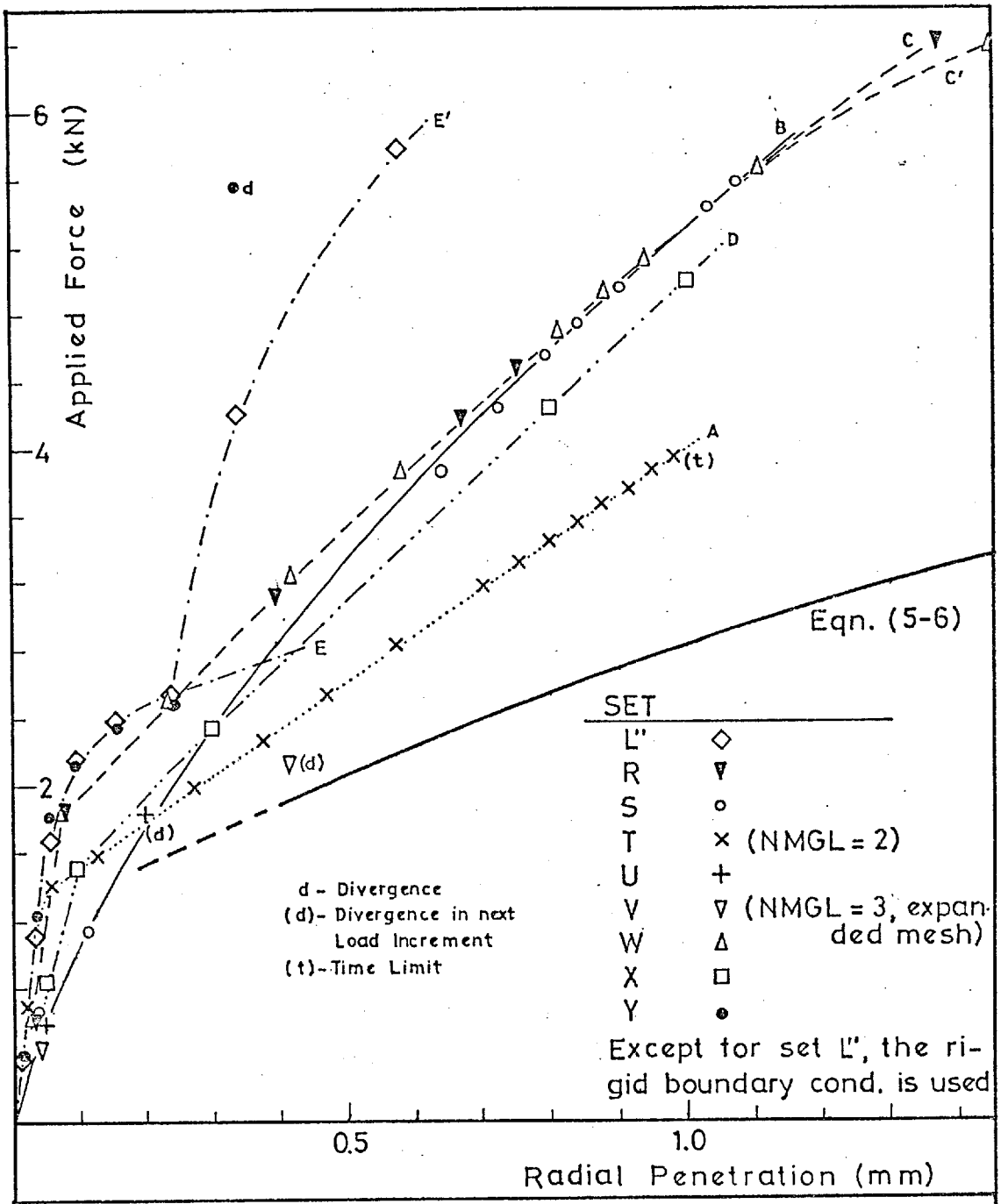


FIG. 6-11 - PREDICTED FORCE IN THE FINITE ELEMENT SOLUTION TO THE INDENTATION PROBLEM USING THE RIGID BOUNDARY CONDITION

seems to be due to the spreading of the plastic zone towards the boundaries of the finite element mesh and, therefore, to point to the inadequacy of the boundary conditions, when formulated as in Chapter 4. In the case when two corrective initial stress cycles were allowed (set N), smaller forces were encountered and the anomalous terminal increase in force took place at a sligh-

tly increased level of deformation.

When friction was considered (Fig. 6-10), a very small increase in force was predicted, as we had already found in the radial upsetting application.

Similarly to what had been observed in 6.2.b, the failure of the program occurred at an early stage of deformation, with penetrations of the order of 0.3 mm and less, usually due to the loss of the diagonal dominance of the stiffness matrix.

In Fig. 6-11, finally, results are plotted for the cases in which the rigid boundary condition was used. These cases having been run at an earlier stage of the development of the program, several alternative loading situations were used, none of them involving the loading parameter STP. They consisted mainly in prescribing a total incremental force to be rated among the nodes in the contact zone in the second load increment. In the subsequent load increments new total force increments were derived in terms of the previous one and of the deformation it produced. Such a procedure produced extremely erratic behaviour, as will be shown in the sets to be analysed, and was eventually abandoned. Sometimes extremely large force increments were unintentionally produced; the deformation mode was usually distorted by such anomalous steps, and further load increments proved to be of little - if any - significance.

Substantially deeper values of penetration were generally achieved with the rigid boundary, in comparison with the relaxed boundary situation; this is coupled, however, with substantially larger forces (paths A, B, C and D against E in Fig. 6-11) and with usually unsatisfactory deformation modes.

Sets R and S are typical examples of the application of the loading procedure described above. The force increment arbitrarily applied in the second loading step was respectively 2400 and 500 N (eventually reduced by the removal of the residual forces in the initial stress correction). In set R this was followed by two further increments of the same order of magnitude, and then by a small one followed by a large one (following path C in Fig. 6-11). For set S, paradoxically, the second loading

step was followed by a very large load increment, and then by a succession of small ones (following path B., which eventually tends to coincide with path C of set R). In set W the same initial increment of 2400 N was used, but the size of the subsequent load increments was limited. Again path C (or rather C') was followed, indicating a certain degree of consistency of the results. Considering the deformation mode, however, a curious behaviour is observed. The general pattern of deformation for both sets R and W is not fully satisfactory, as will be analysed in 6.3.c; however, a certain consistency of the results is retained throughout the several load increments. The same cannot be said, however, of set S. Following the abnormally large third load increment, a substantial spreading-out of material - or thickening of the specimen - is observed. In the subsequent load increments, paradoxically, a return of the material (negative spreading) is verified. At the last produced load increment, roughly the same lateral shape observed for sets R and W (interpolating, of course, for comparable values of penetration) seems to have been obtained.

As we have previously verified when considering the relaxed boundary condition, an increased number of corrective cycles in the initial stress procedure seems, again, to lead to reduced forces (set T); the same conclusion could not be obtained, however, from set V, when the size of the mesh was also altered. But the deformation mode obtained in either case is not satisfactory (6.3.c).

Set X corresponds to another frustrated example in which a large initial load increment led to a larger one - and to failure of the program - in the next loading step.

6.3.c - DEFORMATION MODE

The analysis of the deformation modes produced in the indentation applications is summarized in Figs. 6-12 to 6-17. In these the deformed mesh is superimposed to the original one, which is drawn in thinner lines. The undeformed mesh is drawn to a scale of 7.5:1 (Figs. 6-12 to 6-14) or 5:1 (Figs. 6-15 to 6-17).

In the deformed mesh - and in order to bring certain aspects of the deformation to an observable level, different scale factors are used for the several components of displacement: although the radial (horizontal in the figures) component is drawn to the same scale as the whole undeformed mesh, the other two components are taken as ten times larger. This produces a distortion of the deformed mesh, which, thus, does not correspond to the actual deformed shape.

As the penetrations achieved in the computer solutions lie far below the ones for which the experimental deformation mode was recorded, a comparison between computed and experimental modes is only possible in qualitative terms. Common features of the computed solutions are:

a) The deformation (thickening) of the specimen extends over the whole depth of the mesh;

b) Maximum thickening does not occur in the radial symmetry plane but rather on the immediately adjacent interblock interface. This pattern of deformation has been consistently obtained, irrespective of the boundary conditions utilised.

Neither of these observations were verified experimentally. In the experimental work the depth of deformation was found to be dependent on the level of penetration. It should be pointed out, however, that a slight reduction of the thickness of the deformed specimen in the radial symmetry plane was observed in some cases, although of a lesser order of magnitude and with a lesser degree of systematicity than in the computed results.

Figs. 6-12 to 6-14 consider the cases when the relaxed boundary condition was used. In Fig. 6-12 the deformed mode corresponding to two values of penetration for set L" is shown. In the case of a penetration of 0.48 mm (8th. load increment) a relative reduction in the size of the transversal (axial) displacement increments (not observed up to the previous load increment) begins to take place in the vicinity of the contact zone and of the radial symmetry plane. This deformation pattern is reinforced in the subsequent load increments, and is clearly visible in

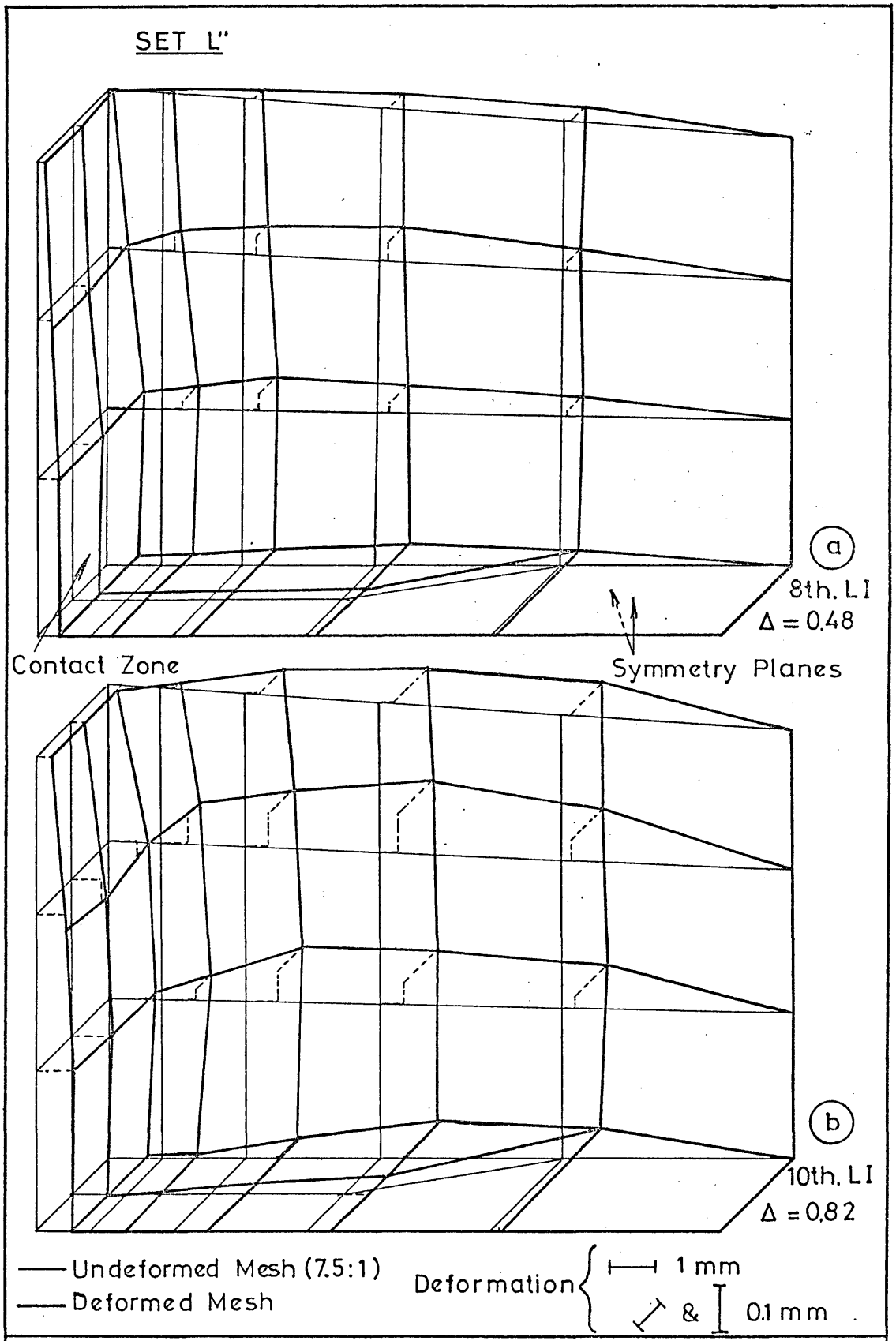


FIG. 6-12 - PREDICTED DEFORMATION MODE IN INDENTATION (BY FINITE ELEMENTS AND USING THE RELAXED BOUNDARY CONDITION)

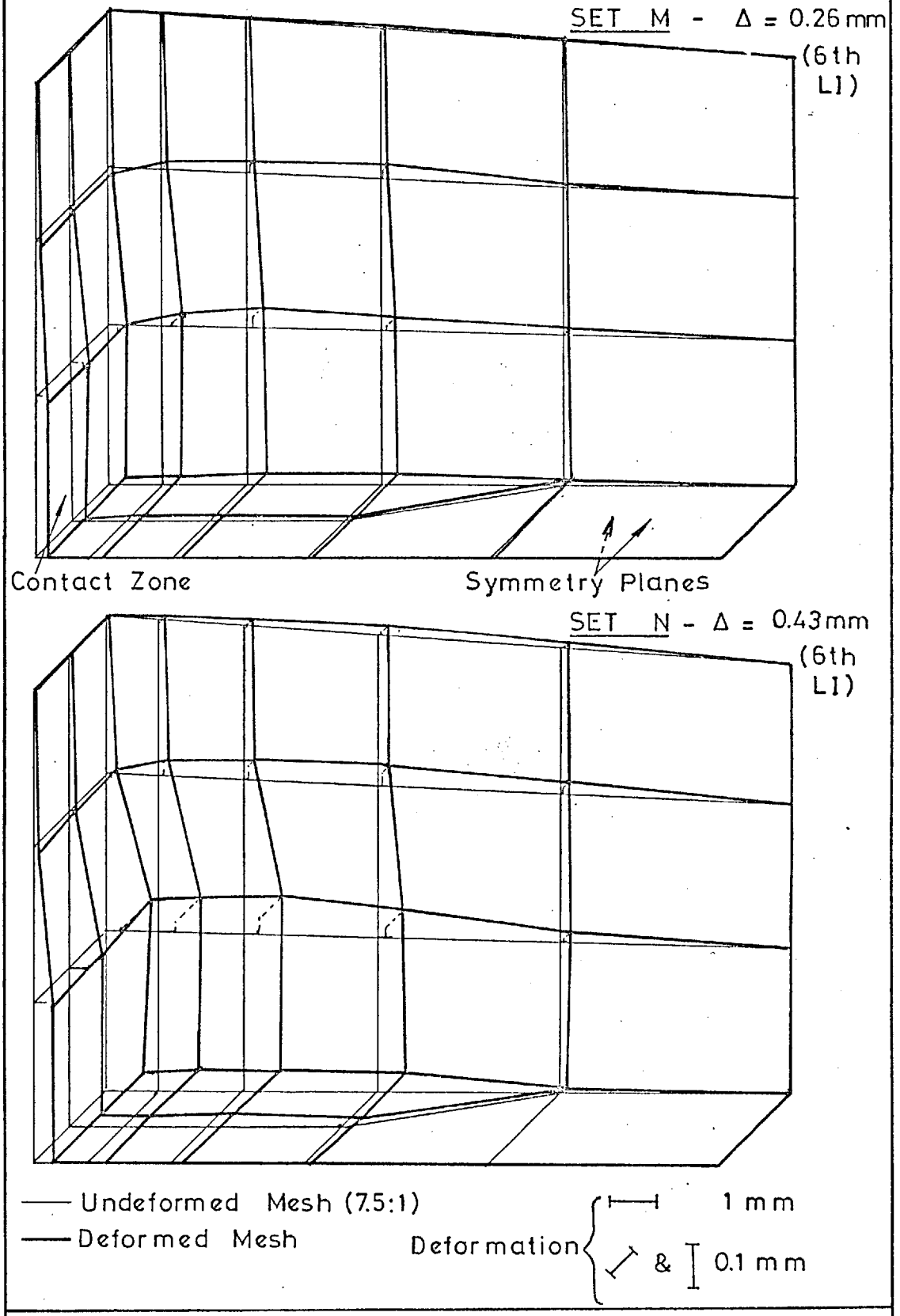


FIG. 6-13 - PREDICTED DEFORMATION MODE IN INDENTATION (BY FINITE ELEMENTS AND USING THE RELAXED BOUNDARY CONDITION) - ALTERNATIVE CASES

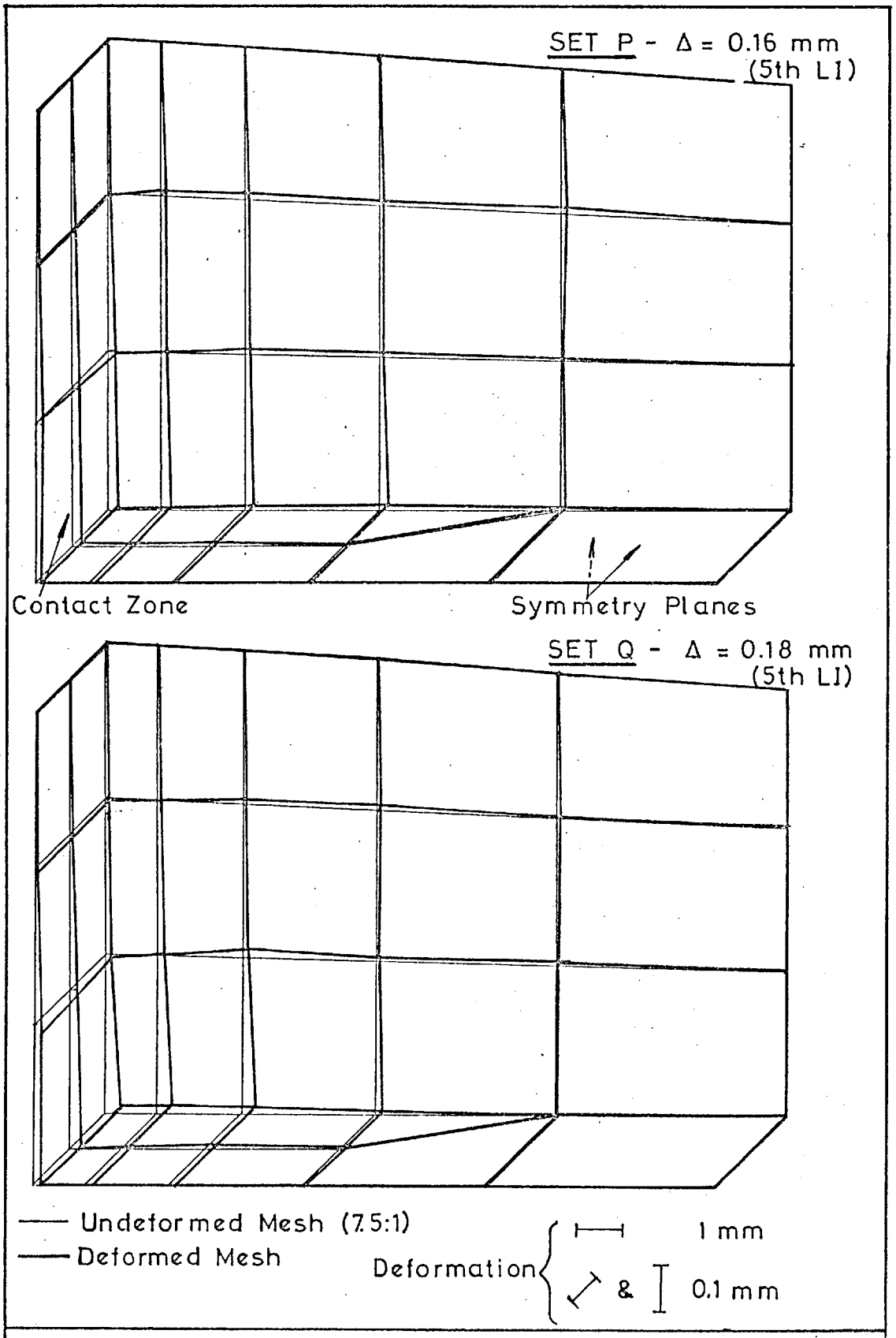


FIG. 6-14 - PREDICTED DEFORMATION MODE IN INDENTATION (BY FINITE ELEMENTS, USING THE RELAXED BOUNDARY CONDITION AND CONSIDERING FRICTION)

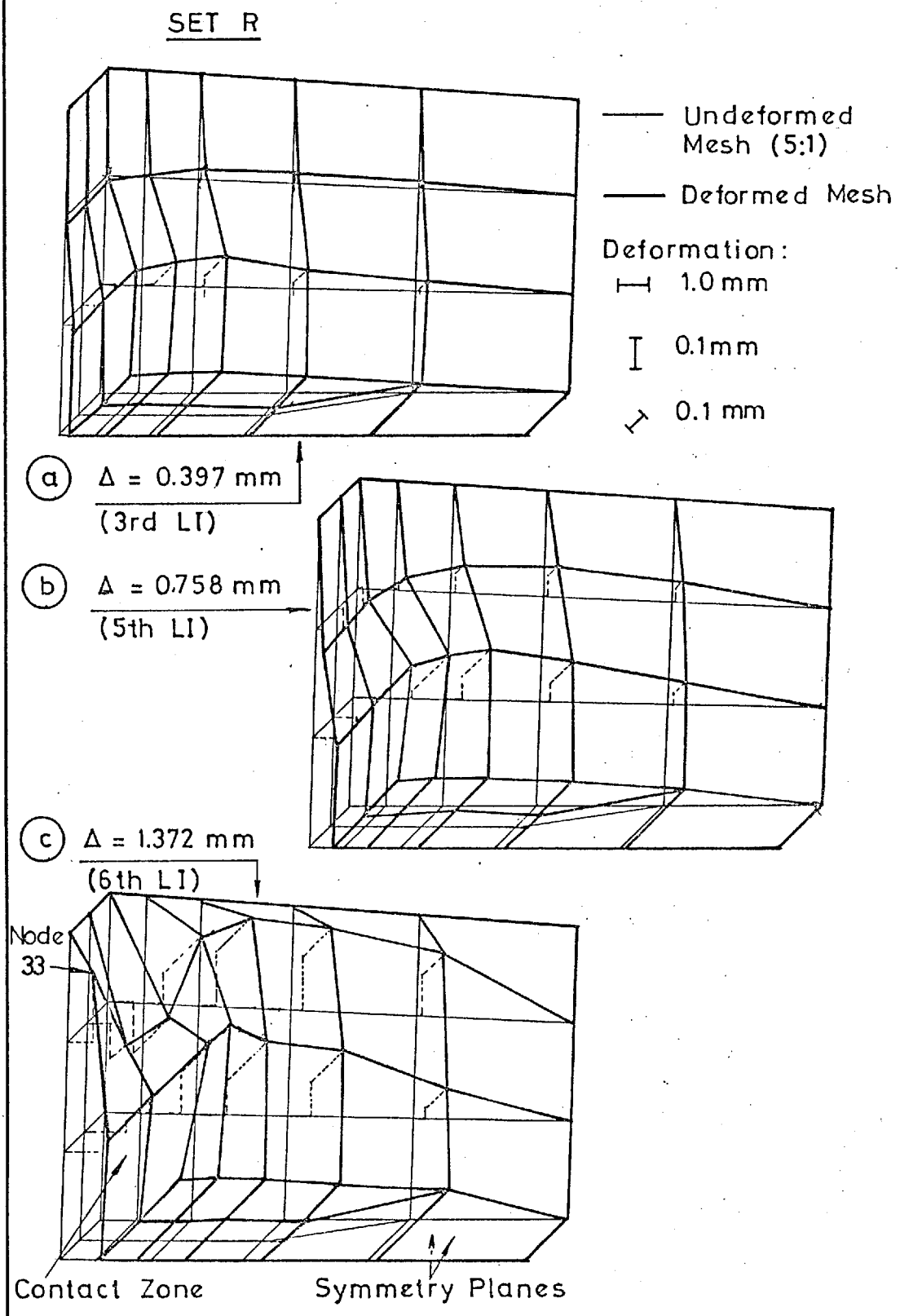


FIG. 6-15 - DEFORMATION MODE IN INDENTATION, PREDICTED BY THE FINITE ELEMENT METHOD, USING THE RIGID BOUNDARY CONDITION

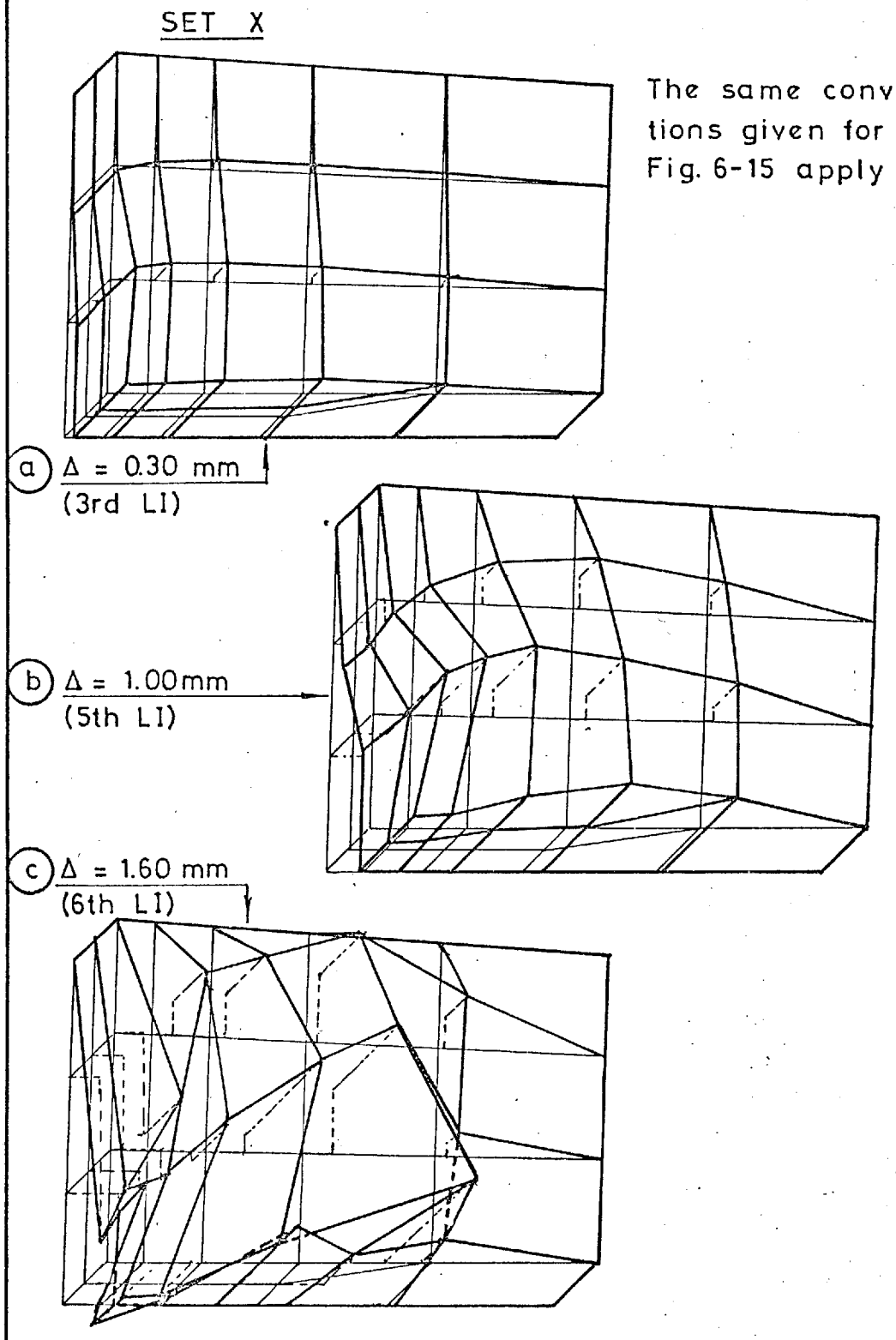


FIG. 6-16 - DEFORMATION MODE IN INDENTATION, PREDICTED BY THE FINITE ELEMENT METHOD, USING THE RIGID BOUNDARY CONDITION (Contd.)

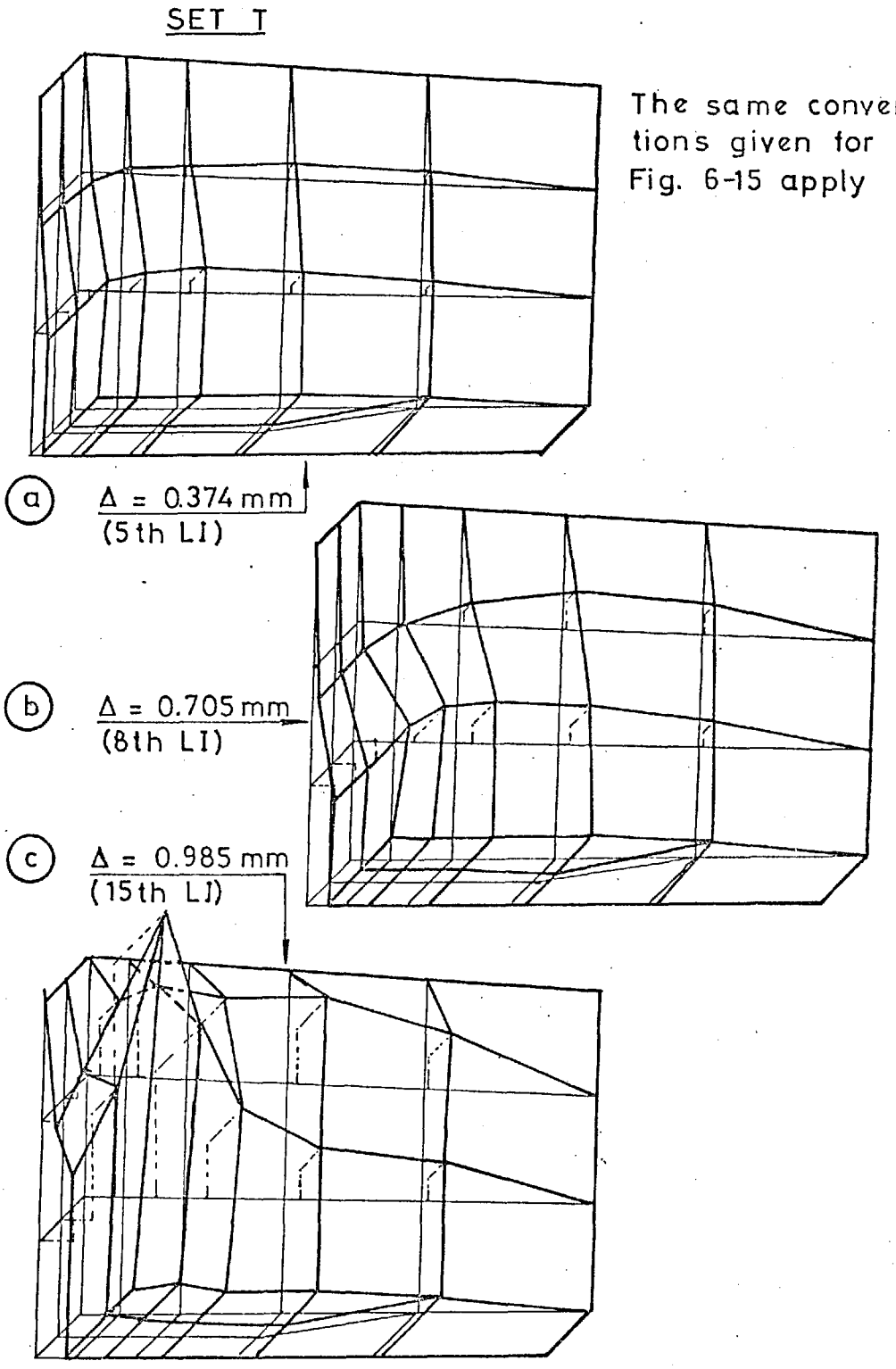


FIG. 6-17 - DEFORMATION MODE IN INDENTATION, PREDICTED BY THE FINITE ELEMENT METHOD, USING THE RIGID BOUNDARY CONDITION (Contd.)

the representation of the tenth load increment, when also a substantial amount of out-of-plane deformation is observed in all non-boundary radial planes.

The afore-mentioned effect is less noticeable in the case of set M, when the modified load redistribution procedure was used for the nodes in the contact zone, and of set N, when two corrective cycles were used in the initial stress procedure.

No definite interpretation can be drawn from the deformation modes observed when friction was considered (Fig. 6-14): the final values of penetration were too small.

The remaining figures (6-15 to 6-17) consider the sets in which the rigid boundary condition was used. Due to the larger values of penetration achieved, the deformational behaviour and the nature of failure of the program becomes more patent.

Fig. 6-15 considers a satisfactorily well-behaved case (set R) and plots the deformed mode corresponding to three values of penetration. The local effect verified in Fig. 6-12 (set L") is not found here, although it appears again in the next cases. Deformation seems to be sound up to the fifth load increment, but an excessive amount of radial displacement increment, nearly doubling the total penetration, takes place in the next load increment, and the specimen becomes heavily distorted. Obviously the real situation is not as drastic as shown in Fig. 6-15c. Scale-factor distortions have to be erradicated. However, the magnitude of the change of direction in the displacement of Node 33 (indicated in the figure) produce a patological set of strain increments for the elements to which this node belongs, leading to also patological sets of stress states, as a consequence of which the program will certainly fail in the next load increment.

The same situation is shown in more drastic overtones in Figs. 6-16 (set X) and 6-17 (set T). In both cases, sound deformation is observed up to a certain stage of execution (5th. and 8th. load increment, respectively). In the case of set X, an excessive radial reduction in the next load increment led to-

wards an overlapping deformation pattern (actually no proper overlapping occurred, but only a tendency towards it; again the difference in the scale factors is responsible for the degenerated representation). Here, several nodes underwent displacement direction reversals. A seventh load increment was actually initialized, but no convergence was achieved in the solution of the incremental force-displacement relation. To avoid or postpone such a failure mechanism, a succession of very small loading steps was tried in the case of set T, after the eighth load increment. Seven more were achieved, with a progressive worsening of the deformation mode, culminating with the patological geometry of Fig. 6-17c. From the twelfth load increment, one single element in the mesh exhibited a totally unacceptable state of stress (equivalent stress of the order of 8000 MN/m^2), although all the remaining ones behaved reasonably.

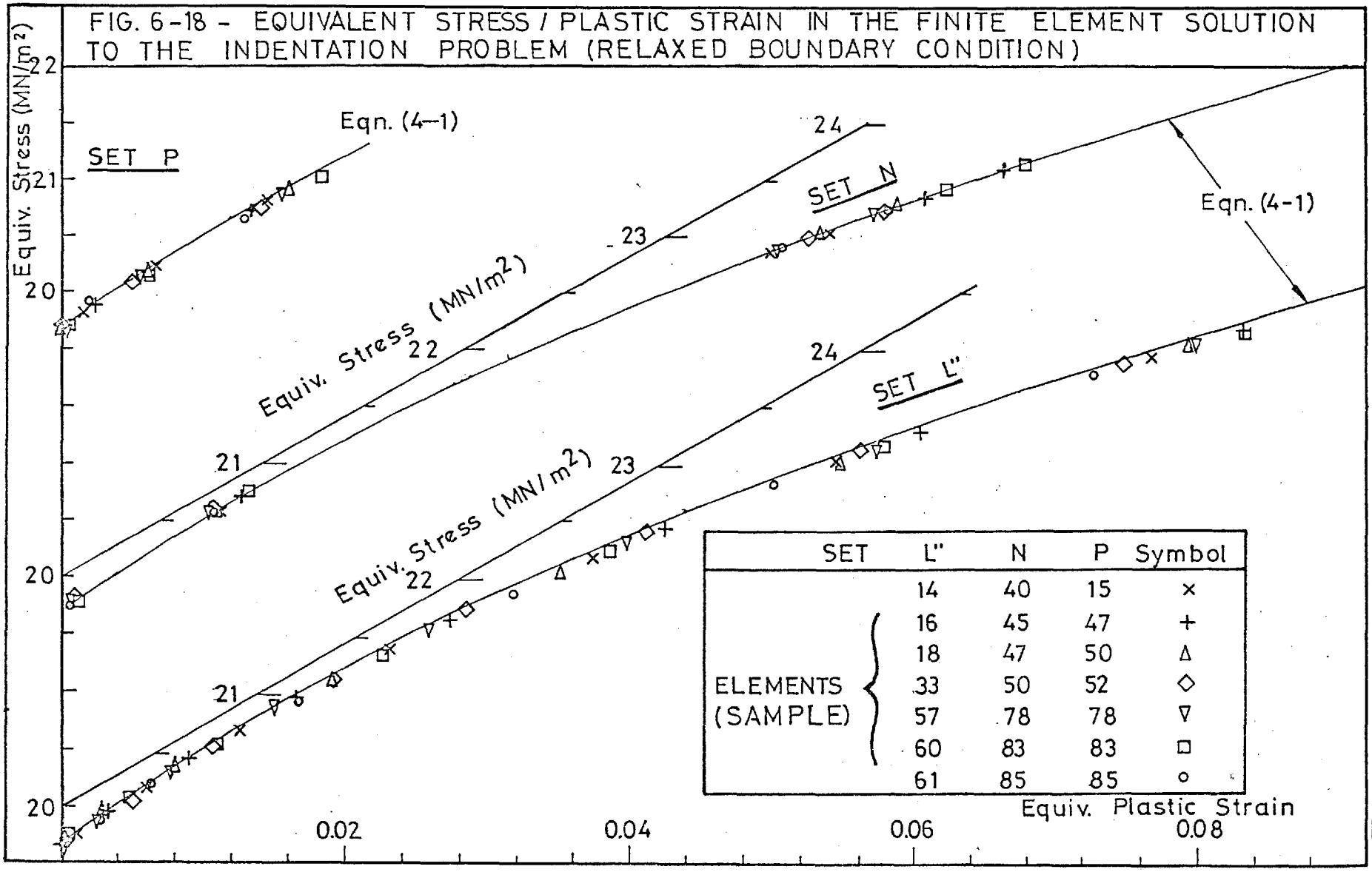
6.3.d - STRESS-STRAIN CURVE

Fig. 6-18 plots the equivalent stress / plastic strain results for a sample of elements belonging to sets L", N and P, corresponding to the relaxed boundary condition, and compares these plots with the prescribed stress-strain curve of the material at the temperature of 400°C (Fig. 4-1). Figs. 6-19 (sets S, T and X) and 6-20 (set W) plot samples of elements corresponding to the rigid boundary condition.

A close agreement is observed in all cases between computed pairs of results and the prescribed curve.

As can be seen in most of these examples, a substantial increase in plastic strain usually takes place in the last recorded load increment. This indicates a plastic instability situation which we have not been able to control adequately in EPFELDA. Failure of the program usually follows the abnormal increase in the plastic strains.

FIG. 6-18 - EQUIVALENT STRESS / PLASTIC STRAIN IN THE FINITE ELEMENT SOLUTION TO THE INDENTATION PROBLEM (RELAXED BOUNDARY CONDITION)



SET	L"	N	P	Symbol
ELEMENTS (SAMPLE)	14	40	15	×
	16	45	47	+
	18	47	50	Δ
	33	50	52	◇
	57	78	78	▽
	60	83	83	□
	61	85	85	○

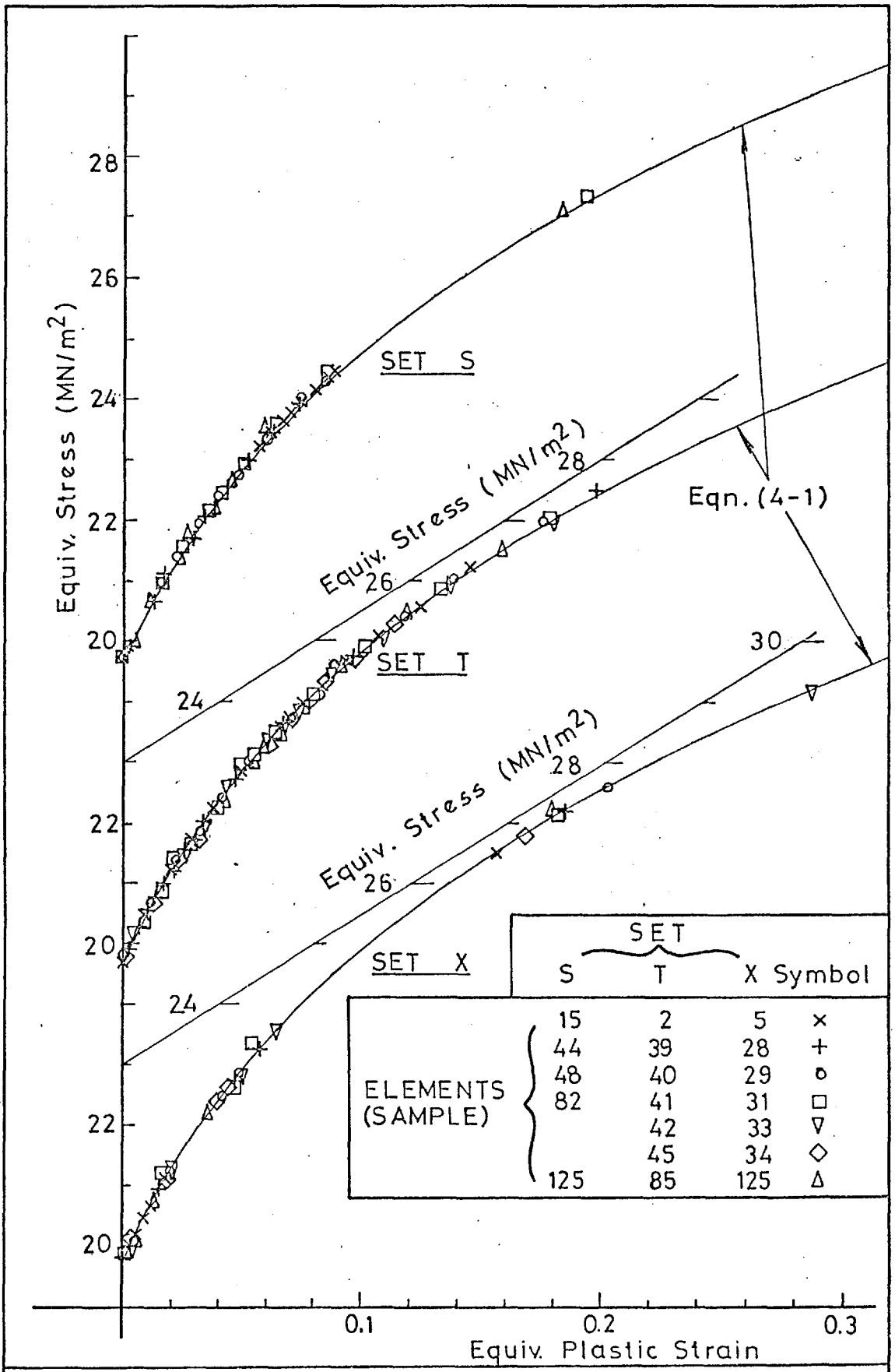


FIG. 6-19 - EQUIVALENT STRESS / PLASTIC STRAIN IN THE FINITE ELEMENT SOLUTION TO THE INDENTATION PROBLEM (RIGID BOUNDARY CONDITION)

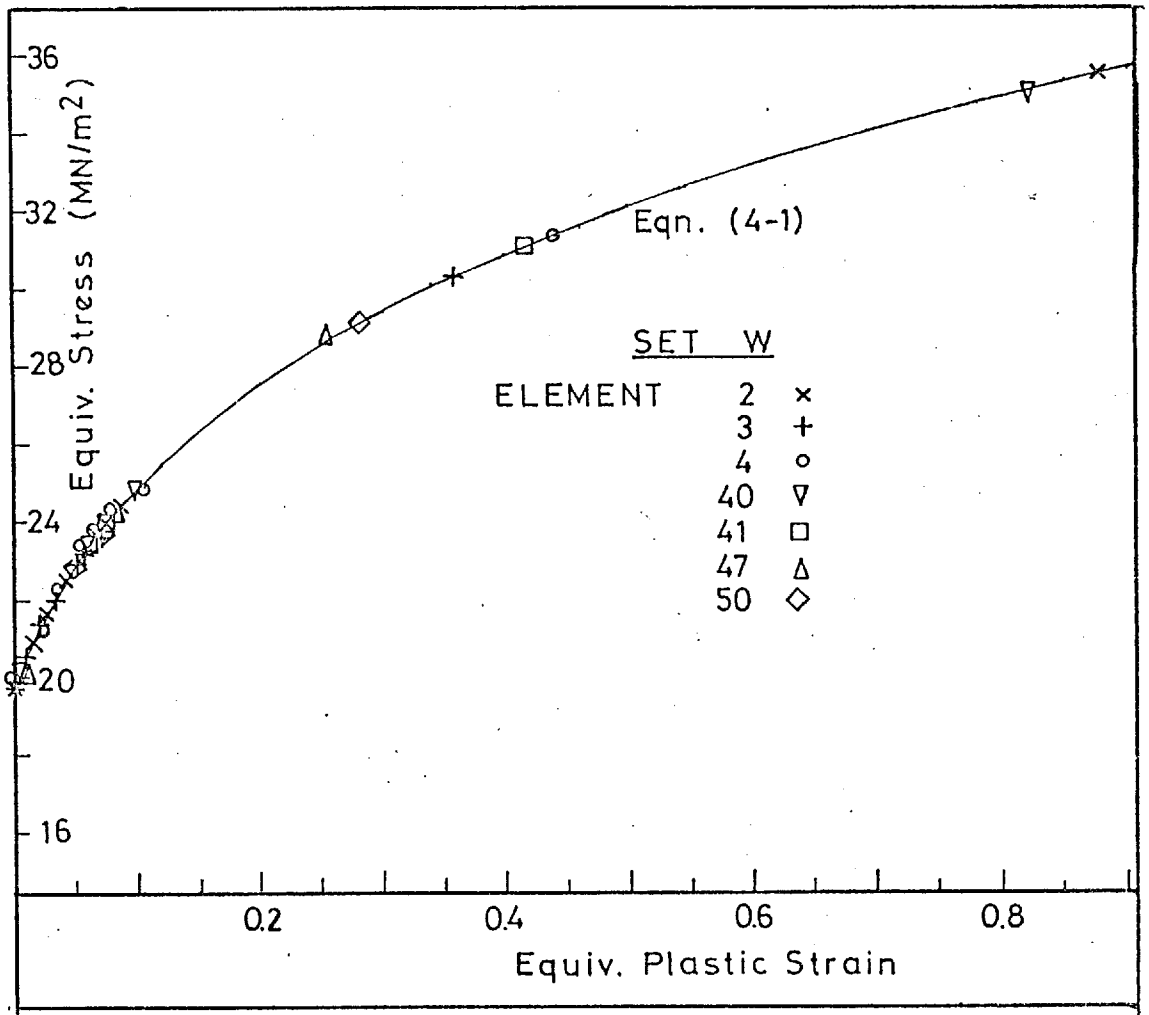


FIG. 6-20 - EQUIVALENT STRESS/PLASTIC STRAIN IN THE FINITE ELEMENT SOLUTION TO THE INDENTATION PROBLEM (RIGID BOUNDARY CONDITION) - Contd.

CHAPTER 7

DISCUSSION AND CONCLUSION

7.1 - DISCUSSION

The results produced by the application of EPFELDA to the radial upsetting and indentation problems, as described in Chapter 6, are far from satisfactory. The main criticism which could be presented is certainly the usually early failure of the program, but the nature of the results could also be questioned. Several reasons could be enumerated to explain such a poor performance. They are listed and analysed here.

a) Too compact meshes have been used

Execution of EPFELDA is highly demanding in terms of computing time. Early load increments require about eighty seconds in the indentation case (three basic blocks), and about hundred and twenty seconds in radial upsetting (four basic blocks). As the plastic zone spreads, and the assembly of the elemental stiffness matrices is gradually shifted from subroutine FIRST to STIFF, these times are increased, and may eventually be doubled (If there are more elements in the plastic range, the execution of the main program is also affected and

becomes more costly). These times are extremely high, and the addition of more basic blocks (or the increase in the number of nodes and elements in the basic block) increases them in a nearly quadratic proportion. This means that an untroubled execution of the program (no divergence problems, or other terminal mechanisms occurring) could require several minutes - or even hours - to produce a reduced number of load increments (times quoted refer to the CDC 6600 computer used in all the application sets considered in Chapter 6).

This is the main reason why we have spent so much time trying to obtain a code which would operate satisfactorily producing large deformation steps, in order to achieve a substantial amount of deformation in a reduced number of load increments. Being unable to obtain satisfactory results - and there are many reasons why the algorithm should not succeed under these conditions - we finally adopted a much more modest approach, using load increments as small as possible, in order to obtain a minimum of acceptable results.

b) The boundary conditions on the lateral and inner boundaries are not properly formulated

The introduction of these artificial boundaries to the problem was required by the need to minimize the size of the finite element mesh. Ideally these boundaries should have been kept sufficiently removed from the contact zone, in order to make sure that no element adjacent to them became plastic. As it happened, plastic deformation soon reached the boundaries of the mesh (in three or four load increments) and the exaggerated increases in force (as for sets E and F (In Section 6.2) or L" (In Section 6.3)) took place.

This spreading of the plastic zone would not have been a drawback if a proper formulation had been given to the boundary conditions, taking such fact into account. However, we have not been able to express such a rigorous approach in a simple but reliable way.

The rigid boundary assumed in some of the indentation applications is certainly a simplistic solution, and the unsa-

tisfactory deformation modes it produced (besides of excessive terminal force increases) should be no surprise. The relaxed boundary adopted later is a compromise which improved one aspect of the defficiencies, by producing more satisfactory deformation modes, without, however, solving the problem of the terminal force increases. Besides, although divergence has previously been blamed on the loss of diagonal dominance of the stiffness matrix, some colateral effect imposed by such a boundary condition should not be disregarded.

c) The load redistribution procedure in the contact zone is over-simplified

The load redistribution in the contact zone is too simplistic in the sense that, once a node is considered as lying in the contact zone, it is given the same displacement increment as the other nodes in the same zone. That this is not strictly correct for nodes just entering or about to leave the contact zone, has been made abundantly clear in Chapters 4 and 6. The modified load redistribution used with sets E, M and Q should, therefore, have produced better results. In fact this did not occur, but the reason could possibly lie somewhere else.

The load redistribution procedure, as implemented in EPFELDA, is performed in the subroutine GAUSS, during the solution of the incremental displacement field. It is possible that the two numerical algorithms interfere with each other, and a gradual erosion of the results takes place. At the same time, however, it is difficult to visualize how to redistribute the applied loads independently of the solution of the displacement field. A more refined solution algorithm, in GAUSS, seems to be the likely answer.

d) The treatment of the elastic-plastic elements by the simplified procedure - Eqn. (2-20c) - is subject to criticism

In the preceding applications of EPFELDA the elemental elastic-plastic constitutive tensors were used to produce

the elemental stiffness matrix, but not to compute the resulting stress increments. Such an approach was adopted in view of the excessive stress increments previously obtained, when using the "straight" approach, as suggested by Hibbitt et al[49]. As a consequence of these excessive increments, three possible alternatives followed - and sometimes more than one at a time:

1 - The resulting stress state did not satisfy the prescribed stress-strain curve, within a reasonable degree of accuracy, with the equivalent stress grossly overshooting the prescribed curve;

2 - The corrective (residual) forces became excessive, leading to an unacceptable unloading situation; or

3 - the successive stress states for an element presented an erratic behaviour, with the equivalent stress lying successively above and below the prescribed stress-strain curve.

This is apparently due to the nature of the constitutive tensor, which allows only for infinitesimal stress increments. Dieterle[102] came across the same problems, but solved them differently. In principle, the use of an adequate definition of frame invariant stress rate (or stress increment, in our formulation) should eliminate the need for such limitation, but in our experience this did not occur.

e) <u>The use of Truesdell's definition of frame invariant stress rates is not the adequate one</u>

The concluding statement in the preceding paragraph might be objected by regarding that, according to Prager[104], Truesdell's is not the adequate definition to be used in an elastic-plastic formulation, and that Jaumann's should be preferred. However, in the early stages of plastic deformation - and we generally did not manage to go above that level - it is quite immaterial which of the definitions - if any - is used, as the

corrections they introduce become practically negligible. They only introduce substantial differences in the results once a reasonable amount of deformation is achieved (Kitagawa et al[91]).

The question of the adequate definition to be used is quite controverted in the literature. Many investigators - as, for instance, Osias[92] or McMeeking and Rice[110] - use Jaumann's without further elaboration. Others[91] compare specific definitions without considering other alternatives. And some (Truesdell[45], Hill[106]) put the problem in terms of convenience and even taste. Prager's[104] favouring of Jaumann's in plasticity applications is the only work to categorically state the adequacy of one and the inadequacy of any of the other definitions, although a subsequent paper by Spencer and Ferris[105] argues that only second-order differences should occur if the "wrong" definition is used.

We did not use Jaumann's definition exclusively in view of the computational difficulties it introduces (nonsymmetrical constitutive and stiffness tensors). But even assuming the absolute necessity of using this one, instead of any of the other definitions, in our elastic-plastic application, the amount of the strains we eventually managed to cover did not allow for any substantial departure from the "true" or "correct" solutions to take place.

f) More corrective cycles should be allowed in the application of the initial stress method

We do agree that a larger number of corrective initial stress cycles would perhaps be desirable. Our approach, however, does not seem to us to be wrong. Increasing the number of corrective cycles means simply to increase the number of times subroutine GAUSS has to be called, and the number of times the main program has to be scanned, and thus, an increase in the computing times. Considering our initial comments regarding the size of the finite element mesh, the solution we eventually adopted was based solely in terms of the minimization of computing times.

g) The application problems are too complex

It is clear that a highly complex code as FPFELDA should havee been initially applied to a simple and well known two-dimensional or axially symmetric deformation process. Four immediate advantages arise from such an approach:

1 - The formulation would become much simpler;

2 - Literature would be available on the process, either in the form of known theoretical solutions, or of reports on experimental work (or both), thus supplying reliable comparison elements;

3 - Computer requirements would be drastically reduced, from the point of view of both core and computing time; and

4 - Boundary conditions would possibly be clearly defined and easily implemented.

Such conclusions are trivial, and we are directly to blame if we did not follow this road. The possibility of working with a novel deformation process, instead of simply adding more information about a known one, seemed too attractive, at the beginning of our work, to be disregarded. However, we do intend to try, in the near future, some sort of simpler application.

7.2 - CONCLUSION

Two main suggestions could be proposed for future work on the lines of this thesis.

It seems that the well defined initial advantages of the Lagrangean formulation (systematic reference to the undeformed geometry and, therefore, the initial production, once and for all, of the shape functions) is more than offset by the innumerable drawbacks and difficulties which appear in its subsequent implementation. The complex tensor relations expressing both the constitutive and the stiffness tensors become extremely elaborated and time consuming, from the computing point of view.

The initial disadvantages of the Eulerian formulation, as hinted by Hibbitt et al[49] and effectively referred to by Kitagawa et al[89], on the other hand, seem to have been adequately overcome in subsequent and more simple formulations (Osias[92], Nagtegaal et al[109], McMeeking and Rice[110] and Lee[111]). These approaches, especially McMeeking's, should be considered as preferable to the Lagrangean formulation here presented.

A very powerful possibility of reducing the execution costs of the program could possibly lie in the use of more complex isoparametric elements. In that case the equations expressing the stiffness matrix would have to be numerically integrated over the volume (or area, in two-dimensional applications) of the element. But as the displacement field would no longer vary linearly across the elements, a variable state of stress and strain would exist within them, and a more realistic mapping of the real continuum could be achieved, with a substantially smaller number of elements. Isoparametric elements have been used extensively by Zienkiewicz and his associates[74,75,98,99,100]. Guha[78], in despite of quite satisfactory results using simplex elements, seems to be favouring the use of isoparametric ones.

REFERENCES

1. LANGE, K., "Gesenkschmieden von Stahl". Springer Verlag, Berlin (1958).
2. BLASS, E., Zur Theorie des Walzprozesses. Stahl und Eisen, 2, 283-293 (1882).
3. TRESCA, H., Sur l'écoulement des corps solides soumis à des fortes pressions. C. R. Acad. Sci. Paris, 59, 754-764 (1864) and 62, 809 (1867).
4. GEIRINGER, H., Beitrag zum Vollständigen ebenen Plastizitätsproblem. Procs. 3rd. Int. Congr. Appl. Mech., 2, 185-190 (1930).
5. HILL, R., "The Mathematical Theory of Plasticity". Oxford Univ. Press, Oxford (1950).
6. JOHNSON, W., R. Sowerby and J. B. Haddow, "Plane Strain Slip Line Fields", Arnold, London (1972).
7. LANGE, K. (Ed.), "Lehrbuch der Umformtechnik", Vol. 1. Springer, Berlin (1972).
8. THOMSEN, E. G., and J. T. Lapsley, Jr., Experimental stress determination within a metal during plastic flow. Procs. Soc. Exptl. Stress Anal., 11, 59-68 (1954).
9. THOMSEN, E. G., C. T. Yang and S. Kobayashi, "Mechanics of plastic Deformation in Metal Processing". Macmillan, New York (1965).
10. PUGH, H. Ll. D. (Ed.), "The mechanical Behaviour of Materials under Pressure". Elsevier, London (1967).

11. ALEXANDER, J. M., and B. Lengyel, "Hydrostatic Extrusion". Mills & Boon, London (1971).

12. PRAGER, W., Recent developments in the mathematical theory of plasticity. J. Appl. Phys., 20, 235 (1949).

13. DRUCKER, D. C., A more fundamental approach to plastic stress-strain relations. Procs. 1st. U. S. Nat. Congr. Appl. Mech., 487-491 (1951).

14. CREUS, G., and H. Helman, Relaciones tensión-deformación en el rango plástico. Publ. Nr. 63, CNEA, Buenos Aires (1971) (Text prepared for the 7th Panamerican Course in Metalurgy).

15. FINLAYSON, B. A., and L. E. Scriven, The method of weighted residuals: a review. Appl. Mech. Reviews, 19, 735-747 (1966).

16. STECK, E., Ein Verfahren zu näherungsweise Berechnung des Spannungs- und Verformungszustandes bei Umformvorgängen. Annals of the CIRP, 17, 251-258 (1969).

17. HELMAN, H., "Hydrostatic Extrusion of bimetallic Composites". Ph. D. Thesis, Imperial College, London University (To be presented in 1976).

18. HELMI, A., and J. M. Alexander, Geometric factors affecting spread in hot flat rolling of steel. J. Iron and Steel Inst., 206, 1110-1117 (1968).

19. SLATER, R. A. C., N. K. Barooah, E. Appleton and W. Johnson, The rotary forging concept and initial work with an experimental machine. Procs. Inst. Mech. Engs., 184 (Part 1), Nr. 32, 577-592 (1969-70).

20. PARAMOUR, M. D., "Plasticity of Edge-rolling". M. Sc. Thesis, Imperial College, London University (1971).

21. ARGYRIS, J. H., Energy theorems and structural analysis. Aircraft Engng., 26, 347-356, 383-387, 394 (1954) and 27, 80-94, 125-134, 145-158 (1955).

22. TURNER, M. J., R. W. Clough, H. C. Martin and L. J. Topp, Stiffness and deflection analysis of complex structures. J. Aeron. Sci., 23, 805-823, 854 (1956).

23. ZIENKIEWICZ, O. C., "The Finite Element Method in Engineering Science". Mac Graw-Hill, London (1971).

24. DESAI, C. S., and J. F. Abel, "Introduction to the Finite Element Method". Van Nostrand/Reinhold, New York (1972).

25. BLOMFIELD, J. A., "Applications of Finite Element Techniques to Fracture Mechanics". Text prepared for the Welding Institute Course at the Imperial College, London (1972).

26. ARANTES E OLIVEIRA, E. R., Theoretical foundations of the finite element method. Int. J. Sols. Structs., 4, 929-952 (1968).

27. WISSMANN, J. W., Non-linear structural analysis: tensor formulation. Procs. 1st. Conf. on Matrix Meths. in Struct. Mech., AFFDL-TR-66-80, 679-696 (1966).

28. ERINGEN, A. C., "Mechanics of Continua". Wiley, New York (1967).

29. ERINGEN, A. C., "Nonlinear Theory of Continuous Media". McGraw-Hill, New York (1962).

30. PRAGER, W., "Introduction to Mechanics of Continua". Ginn, Boston (1961).

31. FUNG, Y. C., "Foundations of Solid Mechanics". Prentice-Hall, Englewood Cliffs (1965).

32. MALVERN, L. E., "Introduction to the Mechanics of a Continuous Medium". Prentice-Hall, Englewood Cliffs (1969).

33. LEE, E. H., Elastic-plastic deformation at finite strain. J. Appl. Mech., 36, 1-6 (1969).

34. GREEN, A. E., and P. M. Naghdi, A general theory of an elastic-plastic continuum. Arch. for Rat. Mech. and Analysis, 18, 251-281 (1965).

35. DRUCKER, D. C., Plasticity. Procs. 1st. Symposium in Naval Struct. Mech., 407-455, Pergamon Press (1960).

36. KOITER, W., Stress-strain relations, uniqueness and variational theorems for elastic-plastic materials with a singular yield surface. Quart. Appl. Math., 11, 350-354 (1953).

37. YAMADA, Y., N. Yoshimura and T. Sakurai, Plastic stress-strain matrix and its application for the solution of elastic-plastic problems by the finite element method. Int. J. mech. Sci., 10, 343-354 (1968).

38. TANAKA, M., Large deflection analysis of elastic-plastic circular plates with combined isotropic and kinematic hardening. Ing. Archiv, 41, 342-356 (1972).

39. ZIENKIEWICZ, O. C., S. Valliapan and I. P. King, Elasto-plastic solutions of engineering problems, "initial stress", finite element approach. Int. J. Num. Meths. Engng., 1, 75-100 (1969).

40. ODEN, J. T., "Finite Elements of Nonlinear Continua". McGraw-Hill, New York (1972).

41. OLDROYD, J. G., On the formulation of rheological equations of state. Procs. Roy. Soc., 200 (A), 523-541 (1950).

42. JAUMANN, G., Geschlossenes System physikalischer und chemischer Differentialgesetze. Sitzungsbericht Akad. Wiss. Wien (IIa), 120, 385-530 (1911).

43. TRUESDELL, C., Corrections to "The mathematical foundations of Elasticity and Fluid Dynamics". J. Rat. Mech. and Anal., 2, 603-609 (1953).

44. TRUESDELL, C., Hypoelasticity. J. Rat. Mech. and Anal., 4, 83-133 and 1019-1020 (1955).

45. TRUESDELL, C., Hypoelastic shear. J. Appl. Phys., 27, 441-447 (1956).

46. GREEN, A. E., Hypoelasticity and plasticity. Procs. Roy. Soc., 234 (A), 46-59 (1956).

47. GREEN, A. E., Hypoelasticity and plasticity II. J. Rat. Mech. and Anal., 5, 725-734 (1956).

48. COTTER, B. A., and R. S. Rivlin, Tensors associated with time-dependent stress. Quart. Appl. Math., 13, 177-182 (1955).

49. HIBBITT, D. H., P. V. Marçal and J. R. Rice, A finite element formulation for problems of large strain and large displacement. Int. J. Sols. Structs., 6, 1069-1086 (1970).

50. MARÇAL, P. V., Comparative study of numerical methods of elastic-plastic analysis. AIAA Journal, 6, 157-158 (1968).

51. BLOMFIELD, J. L., A review of the methods for calculating elastic-plastic strains in general and in particular in pipe bends and shells of revolution. To be published (1971).

52. MENDELSON, A., and S. S. Manson, Practical solution of plastic deformation problems in the elastic-plastic range. NASA TR-28 (1959).

53. GALLAGHER, R. H., J. Padlog and P. P. Biljaard, Stress analysis of heated complex shapes. ARS Journal, 32, 700-707 (1962).

54. ARGYRIS, J. H., S. Kelsey and H. Kamel, Matrix methods of structural analysis: a précis of recent developments. AGARD-ograph 72 (1964), Pergamon Press (1963) (edited by Fraeijs de Veubeke).

55. POPE, G. G., A discrete element method for the analysis of plane elasto-plastic stress problems. Royal Aircraft Establishment, TR 65028 (Feb. 1965), later published in The Aer. Quarterly, 17, 83-104 (1966).

56. MARÇAL, P. V., The elastic-plastic straining of some shells of revolution with special reference to expansion bellows. Ph. D. Thesis, Univ. of London (1965).

57. MARÇAL, P. V., and C. E. Turner, Elastic-plastic behaviour of axisymmetrically loaded shells of revolution. J. Mech. Eng. Sci., 5, 232 (1963).

58. MARÇAL, P. V., A stiffness method for elastic-plastic problems. Int. J. mech. Sci., 7, 229-238 (1965).

59. MARÇAL, P. V., and I. P. King, Elastic-plastic analysis of two-dimensional stress systems by the finite element method. Int. J. mech. Sci., 9, 143-155 (1967).

60. AKYUZ, F. A., and J. E. Merwin, Solution of non-linear problems of elasto-plasticity by the finite element method. AIAA Journal, 6, 1825-1831 (1968).

61. LEE, C. H., and S. Kobayashi, Elastoplastic analysis of plane strain and axisymmetric flat punch indentation by the finite element method. Int. J. mech. Sci., 12, 349-370 (1970).

62. LEE, C. H., and S. Kobayashi, Analyses of axisymmetric upsetting and plane strain side-pressing of solid cylinders by the finite element method. J. Eng. for Ind., 93, 445-454 (1971).

63. SCHARPF, D. W., Die Frage der Konvergenz bei der Berechnung Elastoplastisch deformierbarer Tragwerke und Kontinua. Doctoral Thesis, Stuttgart Univ. (1969).

64. ARGYRIS, J. H., D. W. Scharpf and J. B. Spooner, Die elasto-plastische Berechnung von allgemeinen Tragwerken und Kontinua. Ing. Archiv, 38, 326-352 (1969).

65. ARGYRIS, J. H., and D. W. Scharpf, Methods of elastoplastic analysis. ZAMP, 23, 517-552 (1972).

66. IWATA, K., K. Osakada and S. Fujino, Analysis of hydrostatic extrusion by the finite element method. J. Eng. for Ind., 94, 697-703 (1972).

67. NAGAMATSU, A., T. Murota and T. Jimma, On the non-uniform deformation of block in plane strain caused by friction. Bull. of the JSME, 13, 1385-1402 (1970) and 14, 314-330 (1971).

68. NAGAMATSU, A., T. Murota and T. Jimma, On the non-uniform deformation of material in axially symmetric compression caused by friction. Bull. of the JSME, 14, 331-347 (1971) and 15, 1339-1347 (1972).

69. MALLETT, R. H., and P. V. Marçal, Finite element analysis of nonlinear structures. J. Struct. Div. of ASCE, 94, 2081-2105 (1968).

70. FELIPPA, C. A., Refined finite element analysis of linear and nonlinear two-dimensional structures. Ph. D. Thesis, Univ. of California (1966).

71. TURNER, M. J., E. H. Dill, H. C. Martin and R. J. Melosh, Large deflection analysis of complex structures subjected to heating and external loads. J. Aero. Space Sci., 27, 97-106 (1960).

72. ODEN, J. T., Numerical formulation of nonlinear elasticity problems. J. Struct. Div. of ASCE, 93, 235-255 (1967).

73. ODEN, J. T., On a generalization of the finite element concept and its applications to a class of problems in nonlinear viscoelasticity. Developments in Theoretical and Applied Mechanics, 4, Pergamon Press (1968) and Procs. 4th. South-eastern Conf. on Theoretical and Applied Mechanics (March 1968).

74. NAYAK, G. C., and O. C. Zienkiewicz, Elasto-plastic stress analysis: a generalization for various constitutive relations, including strain softening. Int. J. Num. Meths. Engng., 5, 113-135 (1972).

75. NAYAK, G. C., "Plasticity and large Deformation Problems by the Finite Element Method". Ph. D. Thesis, Univ. of Wales, Swansea (1971).

76. JOHNSON, W., and P. B. Mellor, "Plasticity for Mechanical Engineers". Van Nostrand, London (1972).

77. SWEDLOW, J. L., A procedure for solving problems of elastic-plastic flow. Comps. and Structs., 3, 879-898 (1973).

78. GUHA, R. M., "Finite Element Deformation Analysis of Hydrostatic Extrusion". Ph. D. Thesis, Imperial College, London Univ. (To be presented in late 1976).

79. PIAN, P. H. H., and Pin Tong, Basis of finite element methods for solid continua. Int. J. Num. Meths. in Engng., 1, 3-28 (1969).

80. YAGHMAI, S., "Incremental analysis of large deformations in mechanics of solids with applications to axisymmetric shells of revolution". Ph. D. Thesis, Univ. of California (1969), NASA CR-1350 (1969).

81. ODEN, J. T., A general theory of finite elements. Int. J. Num. Meths. Engng., 1, 205-221 and 247-259 (1969).

82. MARÇAL, P. V., Finite element analysis of combined problems of nonlinear material and geometric behaviour. Procs. ASME Joint Computer Conf. on Computational Approach to Applied Mechanics, 133-149, Chicago (1969).

83. ODEN, J. T., and J. E. Key, Numerical analysis of finite axisymmetric deformations of incompressible elastic solids of revolution. Int. J. Sols. Structs., 5, 497-518 (1970).

84. GORDON, J. L., and A. S. Weinstein, A finite element analysis of the plane-strain drawing problem. Procs. 2nd. North-American Metalworking Research Conf., 194-208, Univ. Wisconsin, Madison (May 1974).

85. BIOT, M. A., "Mechanics of incremental Deformations". Wiley, New York (1965).

86. HOFMEISTER, L. D., G. A. Greenbaum and D. A. Evensen, Large strain, elasto-plastic finite element analysis. AIAA Journal, 9, 1248-1254 (1971).

87. WASHIZU, K., "Variational Methods in Elasticity and Plasticity". Pergamon Press, New York (1968).

88. KUDO, H., and S. Matsubara, The use of finite element method in the analysis of plastic deformation of some metal forming processes. Keynote paper to 24th. CIRP General Assembly, Tokyo (1974). See addit. note, pg. 233.

89. KITAGAWA, H., Y. Seguchi and Y. Tomita, An incremental theory of large displacements and its finite element formulation. Ing. Archiv, 41, 213-224 (1972).

90. KITAGAWA, H., and Y. Tomita, Note on incremental stress-strain relations of elasto-plastic materials referred to a convected coordinate system. ZAMM, 52, 183-186 (1972).

91. KITAGAWA, H., and Y. Tomita, An incremental finite element analysis of two-dimensional large strain and large displacement problem for elasto-plastic flow (In Japanese). Trans. JSME, 40, 663-670 (1974)

91a. Id., ibid., Abstract of the previous paper. Bull. of the JSME, 17, 1523 (1974).

92. OSIAS, J. R., Finite deformation of elasto-plastic solids. NASA CR-2199 (1973).

93. OSIAS, J. R., and J. L. Swedlow, Finite elasto-plastic deformation, I - Theory and numerical examples. Int. J. Sols. Structs., 10, 321-339 (1974).

94. OSIAS, J. R., and J. L. Swedlow, Finite elasto-plastic deformation, II - Necking in tensile bars. Report SM-73-4, Dept. Mech. Eng., Carnegie Mellon Univ. (1973).

95. SWEDLOW, J. L., Character of the equations of elastic-plastic flow in three independent variables. Int. J. Non-linear Mech., 3, 325-336 (1968).

96. SWEDLOW, J. L., Approaches to non-linear problems: the example of plasticity. Procs. ASME Joint Computer Conf. on Comput Approach to Appl. Mech., 191-199, Chicago (1969).

97. SWEDLOW, J. L., A review of developments in the theory of elasto-plastic flow. NASA CR-2321 (Nov. 1973).

98. ZIENKIEWICZ, O. C., and P. N. Godbole, Flow of plastic and visco-plastic solids with special reference to extrusion and forming processes. Int. J. Num. Meths. Engng. 8, 3-16 (1974).

99. ZIENKIEWICZ, O. C., and I. C. Cormeau, Visco-plasticity, plasticity and creep in elastic solids - a unified numerical approach. Int. J. Num. Meths. Engng., 8, 821-845 (1974).

100. CORMEAU, I., Numerical stability in quasi-static elasto-visco-plasticity. Int. J. Num. Meths. Engng., 9, 109-127 (1975).

101. GOTOH, M., A finite element analysis of general deformation of sheet metals. Int. J. Num. Meths. Engng., 8, 731-741 (1974).

102. DIETERLE, K., "Faltenbildung als Verfahrensgrenze beim Stauchen von Hohlkörpern". Bericht Nr. 30, Institut für Umformtechnik (Univ. Stuttgart), Verlag Girardet, Essen (1975).

103. COOK, R. D., "Concepts and Applications of Finite Element Analysis". John Wiley, New York (1974).

104. PRAGER, W., An elementary discussion of definitions of stress rate. Quart. Appl. Mech., 18, 403-407 (1961).

105. SPENCER, A. J. M., and J. E. Ferrier, Some solutions for a class of plastic-elastic solids. Symp. on Foundations of Plasticity (ed. by A. Sawczuk), 9-24, Noordhoff, Leyden (1973). Also discussion on this paper in "Problems of Plasticity", ed. by A. Sawczuk, 518-520, Noordhoff, Leyden (1973).

106. HILL, R., Some basic principles in the mechanics of solids without a natural time. J. Mech. Phys. Sols., 7, 209-225 (1959).

107. OLSZAK, W., Z. Mroz and P. Perzyna, "Recent Trends in the Development of the Theory of Plasticity", Pergamon Press, London (1963).

108. GUNASEKERA, J. S., and J. M. Alexander, Matrix analysis of the large deformation of an elastic-plastic axially symmetric continuum. Symp. on Foundations of Plasticity (ed. by A. Sawczuk), 125-146, Noordhoff, Leyden (1973).

109. NAGTEGAAL, J. C., D. M. Parks and J. R. Rice, On numerically accurate finite element solutions in the fully plastic range. Comp. Meths. in Appl. Mech. and Engng., 4, 153-177 (1974).

110. McMEEKING, R. M., and J. R. Rice, Finite element formulations for problems of large elastic-plastic deformation. Int. J. Sols. Structs., 11, 601-616 (1975).

111. LEE, E. H., Personal communication.

112. STRICKLIN, J. A., W. E. Haisler and W. A. von Riesemann, Evaluation of solution procedures for material and/or geometrically nonlinear structural analysis. AIAA J., 11, 292-299 (1973).

113. AVITZUR, B., "Metal Forming: Processes and Analysis". Mc-Graw Hill, New York (1968).

114. FREUND, L. B., Constitutive equations for elastic-plastic materials at finite strains. Int. J. Sols. Structs., 6, 1193-1207 (1970).

115. COOK, M., and E. C. Larke, Resistance of Copper and Copper Alloys to homogeneous Deformation in Compression. J. Inst. Metals, 71, 371-390 (1945).

116. PAWELSKI, O., Ueber das Stauchen von Hohlzylindern und ihre Eignung zur Bestimmung der Formänderungsfestigkeit dünner Bleche. Arch. Eisenhüttenwesen, 38, 437-442 (1967).

117. KROK, T. V., "Development of a technique for obtaining stress-strain curves for metals at high strain-rates on the USI High-energy Rate Forging Machine". M. Sc. Thesis, London University, 1967. See also Lengyel, B., & T. V. Krok, Application of HER Forging Machine, Metal Forming, 36, 172-176 (1969).

118. LENGYEL, B., and D. C. Stamelos, On the stress-strain curves of materials for hydrostatic cold extrusion. CIRP Annals, 19, 219-224 (1971).

119. HOCKETT, J. E., On relating the flow stress of aluminium to strain, strain-rate and temperature. Trans. Met. Soc. of AIME, 239, 969-976 (1967).

120. ALDER, J. F., and V. A. Phillips, The effect of strain-rate and temperature on the resistance of aluminium, copper and steel to compression. J. Inst. Metals, 83, 80-86 (1954-55).

121. MOHITPOUR, M., "Effects of strain-rate, friction and temperature distribution in high speed axisymmetric upsetting". Ph. D. Thesis, London University, 1972.

122. SUZUKI, H., S. Hashizume, Y. Yabuki, Y. Ichihara, S. Nakajima and K. Kenmochi, Studies on the flow stress of metals and alloys. Report of the Inst. Ind. Sc., Univ. Tokyo, 18, Nr. 3, Serial 117, 139-240 (1968).

123. LENGYEL, B., and M. Mohitpour, Dynamic stress-strain data to large strains. J. Inst. Metals, 100, 1-5 (1972).

124. LENGYEL, B., and L. E. Culver, Properties of materials extruded by orthodox hydrostatic extrusion. J. Inst. Metals, 97, 97-103 (1969).

125. STüWE, L. P., Die Fliesskurven vielkristalliner Metallen und ihre Anwendung in der Plastizitätsmechanik. Z. Metallkunde, 56, 633-642 (1965).

126. EVANS, R. W., and G. R. Dunstan, The hotworking and subsequent restoration of commercial purity aluminium. J. Inst. Metals, 99, 4-14 (1971).

127. BLASS, A., and B. Lengyel, Temperature distribution in the radial upsetting of a flat disc. Procs. 2nd. North American Metalworking Res. Conf., Univ. of Wisconsin, Madison, pgs. 60-72, May 1974.

128. TIMOSHENKO, S., and J. N. Goodier, "Theory of Elasticity". McGraw-Hill, New York, 1951.

129. YOUNG, D. M., "Iterative Solution of Large Linear Systems". Academic Press, New York, 1971.

130. CARRÉ, B. A., The determination of the optimum accelerating factor for successive over-relaxation. Computer J., 4, 73-78 (1961).

131. REID, J. K., A method for finding the optimum successive over-relaxation parameter. Computer J., 9, 200-204 (1966).

132. KULSRUD, H. E., A practical technique for the determination of the optimum relaxation factor of the successive over-relaxation method. Comm. Assoc. Comput. Mach., 4, 184-187 (1961).

133. MARTIN, D. W., and G. J. Tee, Iterative Methods for linear Equations with symmetric positive definite Matrix. Comp. J., 4, 242-254 (1961).

134. ENGELI, M., Th. Ginsburg, H. Rutishauser and E. Stiefel, "Refined iterative Methods for Computation of the Solution and the Eigenvalues of self-adjoint Boundary Value Problems". Mitt. Inst. für angew. Math., Eidgenossische Techn. Hochsch. Zürich, 8, Birkhäuser Verlag, Basel/Stuttgart (1959).

135. WESTLAKE, J. R., "A Handbook of numerical Matrix Inversion and Solution of linear Equations". J. Wiley, New York (1968).

136. BAIOCCHI, I., "Numerical Analysis of Three-dimensional Wave Guide Structures". M. Phil. Dissertation, University College, London University, Feb. 1976.

137. LOZINSKII, M. G., "Industrial Applications of Induction Heating". Pergamon Press, London, 1969.

138. KANYAB, S., "Measurement of Surface Temperatures during the Extrusion of Aluminium". M. Sc. Thesis, Imperial College, London University, 1966.

139. Radiometer 31 Application Report, Issue B. Hawker Siddeley Dynamics Limited.

140. Radiometer 31 Instruction Sheet. Hawker Siddeley Dynamics Limited.

141. WOOLVET, G. A., and J. M. Alexander, A Radiation Pyrometer for Temperature Measurement in the hot Extrusion of Aluminium. J. Inst. Metals, 92, 430-431 (1963/4).

142. REYNOLDS, P. M., Spectral Emissivity of 99.7% Aluminium between 200 and 540°C. Brit. J. Appl. Phys., 12, 111-114 (1961).

143. REYNOLDS, P. M., Brit. Non-Ferrous Mets. Res. Assoc. Research Report No. A1374 (1962).

144. KLEIBER, H., Das Messen der Temperatur mit einem Strahlungspyrometer. Industrie Anzeiger, 92, 436-437 (1970).

145. BLACK, P. J. S., A Pyrometer for the continuous Measurement of the Temperature of Aluminium Extrusions. J. Inst. Metals, 94, 384-387 (1966).

146. REYNOLDS, P. M., Measurement of Aluminium Extrusion Temperatures: collaborative Work's Trials of a commercial Lead Sulphide-cell Instrument. J. Inst. Metals, 94, 379-383 (1966).

147. LENGYEL, B., and A. Blass, Radial Upsetting of Flanges. To be presented to the 4th. North-Amer. Metalworking Research Conf., Columbus, Ohio (May 1976), and to be publ. in the Proceedings of that Conference.

148. KUDO, H., Some analytical and experimental Studies of axi-symmetric Cold-forging and Extrusion, Parts I and II. Int. J. mech. Sci., 2, 102-127 (1960-61) and 3, 91-117 (1961).

NOTE - Kudo and Matsubara's paper[88] has since been published in the CIRP Annals, 23, 219-225 (1974).

NOMENCLATURE

N.1 - REVIEW OF CONVENTIONS

The generalised summation convention, as proposed by Wissmann[27] is used (See Section 2.1). Commas and strokes are used to represent derivatives with respect to initial and current coordinates, respectively (See also Section 2.1).

The prefixes d and Δ are used throughout to denote infinitesimal or small increments of a variable.

The superfix $\hat{}$ is used to represent interim values of the variable to which it is imposed.

The superfix $^{=}$ is used to represent either

a) Equivalent values of a variable (stresses and strains);
b) Variables related to a node about to leave the contact zone, in a radial upsetting situation; or
c) Corrected incremental variables, regarding the redistribution of applied loads in the contact area.

No confusion arises from this triple convention, as the three circumstances do not occur simultaneously.

A superindex ^{o} denotes a variable referred to the undeformed geometry of the continuum.

A dash (') denotes deviatoric components of stress.

Barred variables (eg $\bar{u}_i^j$) refer to a node.

N.2 - LIST OF VARIABLES

A, A° - Area of a surface, current and original (undeformed); in Chapter 3 the surface is the boundary of an element

A, B, m - In Chapter 4, parameters of the strain-hardening stress-strain equations

a, b, c, d, e - In Chapter 5, parameters of the out-of-radial plane deformation

a_k^j - Shape function derivatives

c, n - In Chapter 2, parameters of generalised definition of effective or equivalent stress

c_k^j - Cofactors of the volume-determinant of an element

D_a, D_c, L - In Chapter 5, parameters of the optical tube of the IR radiometer

D_{ijrs} - Component of the elastic-plastic Lagrangean constitutive tensor

D^e_{ijrs} - Idem, of the elastic constitutive tensor

D'_{ijrs} - Idem, of the elastic-plastic Eulerian constitutive tensor

D''_{ijrs} - Idem, of the modified constitutive tensor, in Marçal's "partial stiffness" approach[59]

$d\ell$, $d\ell^\circ$ - Distance between two infinitesimally close points, in the instantaneous and undeformed geometry, respectively

dT, dT_i - In Chapter 2, force acting over an infinitesimal area of a continuum, and its Cartesian components

$d\bar{\bar{s}}$ - Infinitesimal increment in the equivalent stress

dW^p - Plastic work per unit volume

$d\beta$, $d\beta^\circ$ - Angle subtended by three infinitesimally close points in the deformed and undeformed geometry of the continuum respectively

$d\lambda$ - Parameter in Drucker's corollary (See 2.5.b)

E, G, ν - Parameters of elastic deformation (Young's modulus, shear modulus and Poisson's ratio)

e - In Chapter 4, basis of Naperian logaritms

e^e, e^e_{ij} - Elastic strain and component of elastic strain

e^p, e^p_{ij} - Plastic strain and component of plastic strain

E_{ij}, e_{ij} - Strain components, in Green and Cauchy's sense

$\dot{E}_{ij}$ - Green's strain rate

f - In Chapter 2, yield (or loading) function; in Chapter 4, distance from the axis of the roller to that of the specimen in an instantaneous situation

$\bar{F}^{LL}_{qk}$ - Nodal components of self-flexibility

f, g, i, j, k, ℓ, m, n, p, q, r, s, t, u, L, M - Dummy and free indices in the several tensor expressions

F_i, F^o_i - Components of body force per unit volume in the deformed and undeformed situation

G - In Chapter 5, air gap between specimen and coil

H - In Chapter 5, depth of deformed bulge

H' - Slope of the equivalent stress - equivalent plastic strain increment curve

i - In Chapter 5, output current from IR radiometer

J - Jacobean of the transformation from current to original coordinates (for one element in the mesh)

J_2 - Second invariant of stress deviation

K - Bulk modulus of specimen material

k - Instantaneous and local flow stress of specimen material

k_o - Initial yield stress of specimen material

$\bar{K}^{LM}_{kn}$ - Components of total stiffness tensor (matrix)

$\bar{k}^{\ell m}_{kn}$, $\bar{k}^{LM}_{kn}$ - Components of elemental stiffness tensor (matrix), with the upper indices referred to, respectively, the elemental (internal) and to the overal numbering of the nodes

$^{0}\bar{k}^{\ell m}_{kn}$ - Incremental stiffness tensor (matrix) for one element

$^{1}\bar{k}^{\ell m}_{kn}$ - Elemental initial displacement stiffness tensor (matrix)

$^{2}\bar{k}^{\ell m}_{kn}$ - Elemental initial stress stiffness tensor (matrix)

k_R - Characteristic parameter corresponding to the R^{th} setting of sensitivity in the IR radiometer

m - In Chapter 3, Marçal's correction coefficient[59]; in Chapter 6, constant friction factor

n - In Chapter 5, angular velocity of specimen, in rpm

n_j, n_j^o - Direction cosines of externally applied load, respectively referred to the instantaneous and initial geometry of the continuum

N^j, $\overline{N}^{j\ell}$ - Elemental shape function of node j; its value at node ℓ

N_b - Number of basic blocks in the finite element mesh

N_e - Number of elements in whole finite element mesh

N_{eb} - Number of elements in the basic block

N_n - Number of nodes in whole finite element mesh

N_{nb} - Number of nodes in the basic block

P - In Chapters 5 and 6, total applied force

$|P|$, $|\overline{P}^{\ell}|$ - Magnitude of applied load, generical and acting over node ℓ

$|P_n|$ - Normal component of load acting over a boundary

P_i, $\overline{P}_i^{\ell}$ - Component of applied load, generical and nodal

$P_{i_{eff}}$ - Effective component of external load

$\overline{Q}_{kn}^{\ell m}$ - Elemental initial load stiffness tensor (matrix)

r - In Chapter 3, Yamada's rating factor[37]

R - Radial coordinate of a boundary node

R_o - Radius of undeformed specimen

R_r - Radius of forming roller

R'_r - Distance from axis of forming roller to a boundary node in the finite element mesh

S - Denominator in the expression of the elastic-plastic constitutive tensor

S_{ij}, s_{ij} - Stress components, in Kirchhoff and Cauchy's sense

$\overline{\overline{s}}$ - Equivalent stress

T_i, T_i^o - Components of surface force per unit area in the deformed and undeformed situation

T_{ij} - Component of Lagrange stress

T, T_o - Instantaneous (maximal) and original thickness of specimen

u_i - Component of displacement

V, V^o - Volume of an element in current and undeformed situation

v_i - Component of velocity

V_{ij} - Component of the rate of deformation tensor

W - In Chapter 5, energy radiated from a hot body

X_i, x_i - Components of Cartesian coordinates, referred to undeformed and deformed configuration, respectively

α - In Chapter 4, a generical angular variable; also the angle separating axis x_1 from a point about to leave the contact zone

α_{ik} - Coefficients in displacement hypothesis

β - Central angle defining the position of a point in the contact zone

δ_{ij}, $\delta^{k\ell}$ - Kronecker deltas

$\delta(\Delta\bar{u}_q^L)$ - Cartesian component of displacement variation

$\delta(\Delta\bar{u}_r^L)$ - Radial component of displacement variation

$\delta(\Delta\bar{u}_\theta^L)$ - Tangential component of displacement variation

Δ - Roller penetration into specimen

$\delta\Delta s_{ij}$, $\delta\Delta S_{ij}$ - Differential stress increments in the initial stress procedure

Δ_G, Δ_L - Prefixes identifying increments in variables depending exclusively on changes in the shape of the continuum and on changes in the applied loading system, respectively

$\Delta\bar{P}_k^\ell$, $\Delta\tilde{\bar{P}}_k^\ell$ - Components of nodal force increments, respectively total and due solely to increases in the magnitude of the applied forces, in the elemental equilibrium equation

$\Delta\bar{P}_k^L$ - Components of total force increments in overall stiffness equation

$\Delta\bar{Q}_k^L$ - Internal force increments in iterative solution of stiffness equation

Δs_{ij}^{FI}, Δs_{ij}^{CR}, Δs_{ij}^{J}, Δs_{ij}^{O}, Δs_{ij}^{T} - Frame invariant definition of stress increments: generical, Cotter-Rivlin, Jaumann, Oldroyd and Truesdell's, respectively

$\delta\overline{U}_r^L$ - A residual in the expression for $\delta(\Delta\overline{u}_r^L)$

Δu_α - Incremental displacement component in the direction defined by the angle α

Δu_r, Δu_θ - Radial and tangential components of incremental displacement, respectively

ε - In Chapter 5, surface emissivity of specimen material

ε_{ij} - Component of the deformation tensor (also the infinitesimal strain tensor)

ε_{ijk} - Component of the permutation tensor

ε_s, ε_1, ε_2 - Particular values of the surface emissivity

Γ - Intermediate variable in the derivation of the expression for the rating coefficient ζ

ζ - Rating coefficient for stress increments

$\varkappa_r$, $\varkappa_s$ - Contact angles in roller and specimen, respectively

λ, μ - In Chapter 2, Lamé's constants

μ - In Chapter 4, Coulomb friction coefficient

ν - Poisson's ratio

ξ_o - Central angle of basic block in the finite element mesh

Θ, Θ_A - Temperature in deformation zone; particular value of this temperature

σ - In Chapter 5, Stefan-Boltzmann's constant

φ - In Chapter 5, field of view of optical tube of IR radiometer

Ω_{ij} - Component of spin tensor

ω_{ij} - Component of rotation tensor

ω - Over-relaxation factor

APPENDIX 1

OPTIMIZATION OF THE OVER-RELAXATION FACTOR

A-1 - INTRODUCTORY NOTE

For reasons of mere convenience we introduce matrix notation in this appendix; and we will express matrices in bold type. Also for reasons of convenience we present the list of the variables used throughout this appendix separately, at the end of it; reference numbers, though, are referred to the sequence presented in pgs. 231 and 232.

A-2 - SUCCESSIVE OVER-RELAXATION METHOD[129,130,134]

A common final product of the numerical methods usually employed in Engineering is the solution of a set of linear algebraic equations of the form

$$\sum_{j=1}^{N} a_{ij}\, x_j = b_i , \qquad i, j = 1, 2, \ldots, N , \qquad (A\text{-}1)$$

where the coefficients

$$a_{ij} = a_{ji}$$

and

$$a_{ij} \neq 0$$

whenever $i = j$. Eqn. (A-1) could be rewritten in matrix form as

$$\mathbf{A}\,\mathbf{x} = \mathbf{b} , \qquad (A\text{-}2)$$

where **A** is a symmetric positive definite matrix whose elements are the coefficients a_{ij}, and **x** and **b** are vectors.

Such a system, whether considered in its algebraic or matrix form, can be solved by several alternative direct or iterative methods. Westlake[135] reviews these methods and Baiocchi[136] compares them in a specific application problem. Martin and Tee[133] and Engeli et al[134] restrict themselves to iterative methods. Young[129] restricts his book still further, to the analysis of a class of iterative methods.

An iterative method starts with an arbitrary estimate $x^{(o)}$ of the vector x, and derives a convergent sequence $x^{(k)}$, $k = 1, 2, \ldots$, of improved estimates, via some specific algorithm, which is repeated as often as necessary. Convergence is decided by some specified criterion. The error vector after a given cycle is given by

$$e^{(k)} = x - x^{(k)} . \qquad \text{(A-3)}$$

One of the simplest possible iterative methods is Gauss-Seidel's, in which the equations in the system (A-1) are scanned in a prescribed sequence, one variable being improved at a time, and the improved estimates being immediately used in the algorithm's next step. That is, an iterative scheme

$$x^{(k+1)} = x^{(k)} + \delta x^{(k+1)}$$

with

$$\delta x_i^{(k+1)} = \frac{1}{a_{ii}} \left\{ b_i - \sum_{j=1}^{i-1} a_{ij}\, x_j^{(k+1)} - \sum_{j=i}^{N} a_{ij}\, x_j^{(k)} \right\} \qquad \text{(A-4)}$$

is followed.

Such an algorithm, though simple, does not usually converge (or "relax" the successive values of the residual components of the vector $\delta x^{(k+1)}$) with sufficient speed to be considered of value. A simple alternative to the method consists in replacing the iteration equation by

$$x^{(k+1)} = x^{(k)} + \omega\, \delta x^{(k+1)} \qquad \text{(A-5)}$$

with the residual vector expressed from Eqn. (A-4), and where ω

is a suitably chosen positive real number. If $\omega < 1$, the algorithm "under-relaxes", and if $1 < \omega < 2$, it "over-relaxes" the residuals. Under-relaxation does not accelerate convergence, but it can provide convergence (even if a very large number of cycles is required) in the case of ill-conditioned matrices, when the usual methods would possibly fail. Over-relaxation usually accelerates convergence.

By replacing the residual term of Eqn. (A-5) by its expression given in (A-4), the equation can eventually be rearranged to the form

$$\sum_{j=1}^{i-1} (a_{ii}\,\delta_{ij} + \omega\, a_{ij})\, x_j^{(k+1)} = \sum_{j=1}^{N} (a_{ii}\cdot\delta_{ij} - \omega\, a_{ij})\, x_j^{(k)} + \omega\, b_i \,. \qquad \text{(A-6)}$$

If the matrix $\mathbf{A}$ is thought of as decomposed in the form

$$\mathbf{A} = \mathbf{D} - \mathbf{L} - \mathbf{U},$$

in which $\mathbf{D}$ is a diagonal matrix, $\mathbf{L}$ is a strictly lower-triangular and $\mathbf{U}$ a strictly upper-triangular matrix, it is easy to visualize Eqn. (A-6) as representing a matrix relation

$$\mathbf{x}^{(k+1)} = \mathbf{M}\,\mathbf{x}^{(k)} + \mathbf{c},$$

where

$$\mathbf{M} = (\mathbf{D} - \omega\,\mathbf{L})^{-1}\,((1-\omega)\,\mathbf{D} + \omega\,\mathbf{U}) \qquad \text{(A-7)}$$

and

$$\mathbf{c} = (\mathbf{D} - \omega\,\mathbf{L})^{-1}\,\mathbf{b}\,.$$

Matrix $\mathbf{M}$ is the SOR (for successive over-relaxation) matrix corresponding to the system given by Eqns. (A-1) or (A-2). It now becomes easy to show, from Eqn. (A-3), that the error vector can be expressed by the recurrence relation

$$\mathbf{e}^{(k+1)} = \mathbf{M}\,\mathbf{e}^{(k)},$$

and for the method to converge, that is, for

$$\lim_{k\to\infty} \mathbf{e}^{(k)} = 0$$

to hold for any arbitrary initial vector $\mathbf{e}^{(o)}$, it is necessary

for all the eigenvalues of M to lie within the unit circle. The object of using a relaxation factor other than unity (Method of Gauss-Seidel) is to reduce the spectral radius, that is, the largest of the absolute values of all the eigenvalues λ_i of M. We shall denote this spectral radius by ρ_M. Thus

$$\rho_M = \max |\lambda_i| .$$

Ideally a value of ω exists which minimizes ρ_M. Under these circumstances, the rate of convergence (average), expressed by

$$R = - \log \rho_M ,$$

is a maximum.

In a general situation it is extremely difficult to estimate the optimum value ω_o of the over-relaxation factor, or, conversely, the spectral radius ρ_M. Nevertheless, Young has shown(See 129 or 134) that if the matrix A of Eqn. (A-2) has "Property A", an expression can be found to express ω_o in terms of the eigenvalues μ_i of A.

The matrix A is said to possess Property A if it can, by suitable reordering of rows and columns, be brought to the form

$$A = \begin{bmatrix} D_1 & A_1 \\ D_2 & A_2 \end{bmatrix} ,$$

in which D_1, D_2 are diagonal matrices, and A_1, A_2 are arbitrary rectangular matrices. Young(129) has shown that if matrix A possesses Property A, then a relationship exists between the eigenvalues of matrices A and M, this relationship being expressed by

$$(\lambda_i + \omega - 1)^2 = \lambda_i \omega^2 \mu_i^2 . \qquad (A-8)$$

From Eqn. (A-8) it becomes clear that ω_o must satisfy the relation

$$\omega_o^2 \rho_A^2 - 4 (\omega_o - 1) = 0 ,$$

from which

$$\omega_o = \frac{2}{1 + \sqrt{1 - \rho_A^2}} \qquad (A-9)$$

follows. It is clear, from this expression, that the optimum over-relaxation factor will satisfy the inequality

$$1 < \omega_o < 2 .$$

Engeli et al[134] have shown that

a) In the Gauss-Seidel method the eigenvalues λ_i are given, from Eqn. (A-8), by

$$\lambda_i^2 = \lambda_i \mu_i^2 .$$

One root of this equation is clearly zero, and the other one gives

$$\lambda_i = \mu_i^2 .$$

Half of the eigenvalues (at least) vanish, and the remaining ones are positive and real.

b) As ω goes on increasing towards ω_o, the real eigenvalues become smaller, tending to the value $\omega - 1$. They then become complex, and increase in absolute value as $\omega - 1$. The largest eigenvalue, which defines the spectral radius, and thus the rate of convergence, is real.

c) As ω continues increasing (above ω_o), all the eigenvalues become complex and of absolute value $\omega - 1$.

These conclusions can be reached from the analysis of Eqn. (A-8). The general nature of the dependence of the eigenvalues λ_i (and thus, of the spectral radius ρ_M) on ω is shown in Fig. A-1.

A-3 - ESTIMATION OF ω_o

Several methods have been proposed for the estimation of the optimum over-relaxation factor. Some of them are based on the "a priori" determination of the spectral radius ρ_A, or at least on the establishment of bounds for this radius and, thus, for ω_o. These methods are usually elaborated, and the computing effort involved usually offsets any advantage that may eventually occur by solving the system with a good estimate of the over-relaxation factor.

This is the reason why "simultaneous" methods have been devised, in which improvements are introduced in the over-relaxa-

tion factor at the same time as the problem is solved. Solution is started with an arbitrary value of over-relaxation, and from time to time a new value is estimated according to some suitable norm. Carré[130], Reid[131] and Kulsrud[132] propose methods along these lines. Of those, Carré's seems to us to be the best one, because it is both simple and efficient in its objective.

Defining the displacement vector

$$\delta^{(k+1)} = x^{(k+1)} - x^{(k)},$$

then

$$\delta^{(k+1)} = M\,\delta^{(k)},$$

and if $n^{(k+1)}$ is some norm of the vector $\delta^{(k+1)}$, as, for instance, the arithmetic sum of the moduli of its components, then

$$\lim_{k\to\infty} \frac{n^{(k+1)}}{n^{(k)}} = \rho_M. \qquad \text{(A-10)}$$

If the execution is started with $\omega = 1$, then $\rho_M = \rho_A^2$, and Eqn. (A-9) follows. It is not necessary, of course, to start with $\omega = 1$. Substituting ρ_A in Eqn. (A-9) by μ_i, expressed from Eqn. (A-8), an estimate for the optimum over-relaxation factor, expressed by

$$\omega_e = \frac{2}{1 + \sqrt{1 - \dfrac{(\rho_M + \omega - 1)^2}{\rho_M\,\omega^2}}} \qquad \text{(A-11)}$$

is obtained. This equation gives the estimate ω_e in terms of ρ_M for any value of ω in the range $0 < \omega \leqslant \omega_o$. The equation becomes meaningless if $\omega > \omega_o$, due to the complex nature of all the eigenvalues, but this fact will simply be stated without proof.

Carré's method consists in the periodic reevaluation of the spectral radius by means of Eqn. (A-10), and its use in Eqn. (A-11). The norm $n^{(k)}$ is, of course, used in the convergence criterion of the solution algorithm, so very little additional effort is required to implement the method. As ω_o can only be approached from below, Carré starts with a small value of ω. Actually, one cycle is performed with $\omega = 1$, and the next

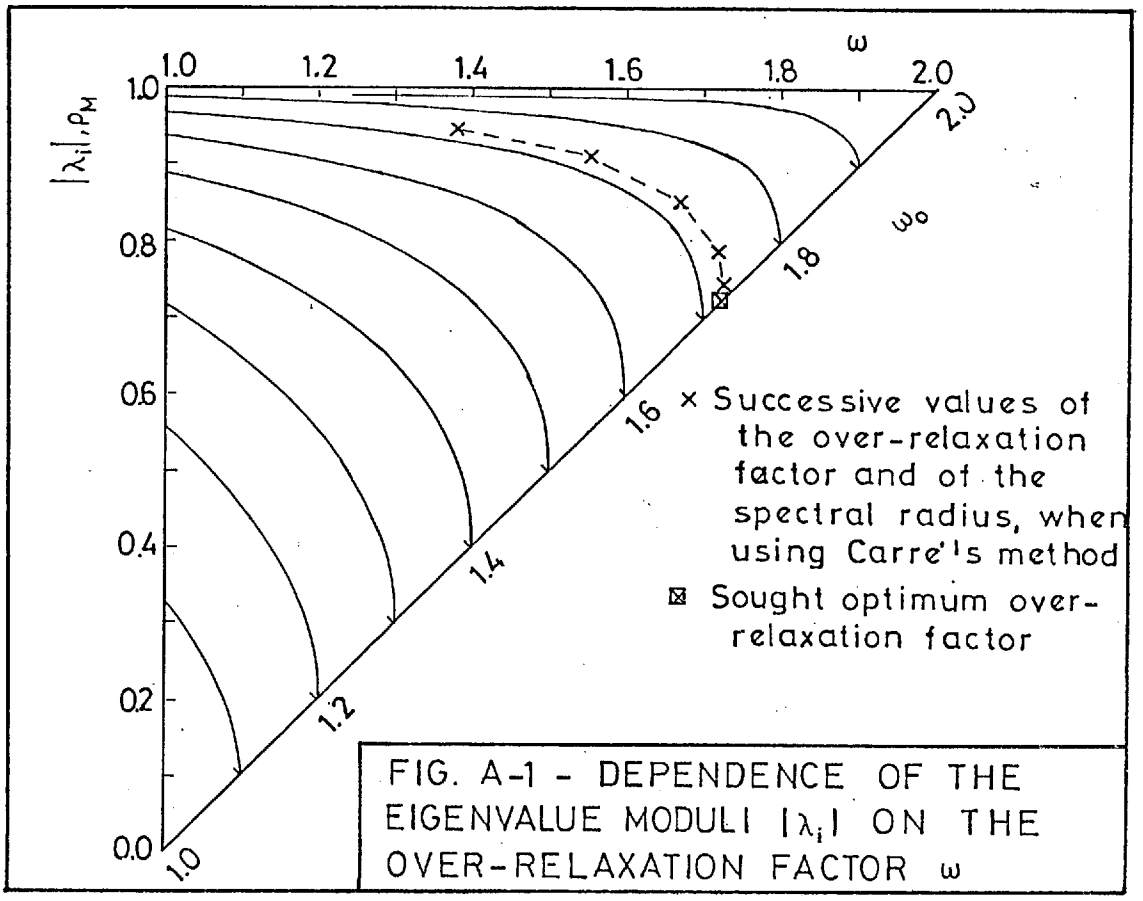


FIG. A-1 - DEPENDENCE OF THE EIGENVALUE MODULI $|\lambda_i|$ ON THE OVER-RELAXATION FACTOR ω

twelve with $\omega = 1.375$, when the first estimate ω_e is made, and ω is replaced. After every subsequent twelve cycles, new estimates are made, and the over-relaxation factor replaced.

As ω_e is only an estimate of ω_o, it could possibly occur that, at some stage, $\omega_e > \omega_o$. If the over-relaxation factor ω were to be replaced by this estimate, the method would fail in the next correction (The radicand in the denominator of Eqn. (A-11) becoming negative). To avoid this possibility, Carré replaces ω by a reduced estimate, given by

$$\omega_r = \omega_e - (2 - \omega_e)/4.$$

By using this method, a point can be plotted in a graph like the one presented in Fig. (A-1), at the end of every twelve cycles, that is, immediately before every correction in the over-relaxation factor. The loci of these plots should ideally follow a path belonging to the family of lines contained in the triangular graph. The consecutive plots become closer to each other as the optimum over-relaxation factor is approached. The locus of the values of ω_o for any system whose matrix A possesses Pro-

perty A lies on the hypothenuse of the triangle (Fig. (A-1)). This statement follows directly from Engeli's second conclusion, which we have previously mentioned.

There are other refinements to Carré's method, as, for instance, the use of Aitken's acceleration in the preliminary estimations of ρ_M, which will not be considered here, as, for reasons to be stated later, they had to be either set aside or replaced in our utilization of the method.

Carré suggests applying the method until a very small variation

$$\Delta\omega_e < 0.05\,(2 - \omega_e)$$

is obtained in the estimated values, when a good estimate of the the optimum ω_o is considered as found.

It should be mentioned that as convergence is approached, the norm $n^{(k)}$ becomes extremely small and the relative effect of truncation errors increases, and the estimates of the spectral radius become less reliable. Thus, the estimates ω_e may start to oscillate after a number of corrections has been made. Carré stops correcting the over-relaxation factor if such a situation is reached.

A-4 - BLOCK RELAXATION (SBOR)

The specific problem involved in our finite element analysis is not strictly put in terms of Eqns. (A-1) or (A-2). According to Eqn. (4-13), we obtain the three nodal components of displacement from a subset of equations. That is: the overall system is subdivided into subsystems, one for every node in the mesh, and those are then successively solved. Instead of simply dividing by the successive elements of the main diagonal of matrix A (As in Eqn. (A-4)), a more complex equation is employed for the residual displacements, involving the inverses of whole submatrices (the flexibilities in our specific case).

In other words, the system represented by Eqn. (A-2) is re-expressed in a more involved form, with the partition of the vectors $\mathbf{x}$ and $\mathbf{b}$ into subvectors $\mathbf{x}_i$ and $\mathbf{b}_i$ ($i = 1, 2, \ldots, n$) and the corresponding partition of A into submatrices A_{ij}.

The system is then rewritten as

$$\sum_{j=1}^{n} A_{ij}\, x_j = b_i \qquad (i = 1, 2, \ldots, n).$$

These equations are used to provide a sequence of approximations $x_i^{(k)}$ to the subvector x_i, in what is known in the literature as the Successive Block Over-relaxation method (SBOR)[133] although some authors refer to it as the Group Over-relaxation method[129]. It is easy to express the improved estimates for a subvector as

$$x_i^{(k+1)} = x_i^{(k)} + \omega A_{ii}^{-1} \left[b_i - \sum_{j=1}^{i-1} A_{ij}\, x_j^{(k+1)} - \sum_{j=i}^{n} A_{ij}\, x_j^{(k)} \right], \quad \text{(A-11)}$$

which is equivalent to Eqn. (4-13) and corresponds to Eqns. (A-4) and (A-5) in a comparison with the simpler SOR method.

Strictly speaking, we are faced here with a new iterative method, and the applicability of Carré's algorithm could be questioned. However Young[129], by extending the concept of Property A, shows that there is no cause of concern, as, provided the matrix possesses "Property $A^{(\pi)}$", relations similar to the ones presented in the preceding sections remain, thus guaranteeing the validity of the optimizing algorithm.

A matrix A, resulting from the assemblage of a set of submatrices A_{ij} is said to have, or possess, Property $A^{(\pi)}$ if its related matrix B possesses Property A. This related matrix B is defined as an $n \times n$ matrix whose terms are

$$b_{ij} = 0 \qquad \text{if } A_{ij} \text{ is a null matrix,}$$

and

$$b_{ij} = 1 \qquad \text{otherwise.}$$

A-5 - THE SPECIFIC PROBLEM

From the material presented in the two previous sections we are able to conclude that Carré's method can be applied to our specific problem if the intervening stiffness matrices possess Property $A^{(\pi)}$, defined above. The related matrix B is simply redefined here as an $N_n \times N_n$ (N_n being the total number of nodes in the finite element mesh) such that

$b_{ij} = 1$ if nodes i and j are interconnected, and

$b_{ij} = 0$ otherwise.

Young[129] presents the flow block diagram of a simple computer program to check if a matrix possesses Property A, and if it is consistently ordered (pgs. 159-161). We have so far avoided to mention the concept of consistent ordering, and for the sake of simplicity will continue doing so in the rest of this chapter; as this concept only applies to matrices possessing Property A, it will become irrelevant in the following derivation. We produced the program and checked a series of alternative finite element meshes. Due to the high level of interconnection of the nodes, unavoidable in three-dimensional meshes, no related matrix could be produced, which exhibited sufficient sparsity to possess Property A. As a consequence, all the finite element meshes we experimented with led to stiffness matrices which did not possess Property $A^{(\pi)}$; and thus, finally, we concluded that Carré's optimizing method was not strictly applicable to our problem.

However, we were faced with very bad convergence conditions in the preliminary runs of EPFELDA, with 300 to 500 cycles being required to a convergence criterion of 10^{-5} in the indentation applications (three basic blocks, 64 nodes, 182 unknowns and equations); in radial upsetting applications (four basic blocks, 80 nodes, 240 unknowns and equations) the situation was even worse. Moreover, although experimental runs with certain trial values of the over-relaxation factor eventually produced improvements in the convergence situation, these results were restricted to a load increment, and not usually repeated in the next.

Under these circumstances we decided to try Carré's method, in despite of the knowledge of its strict inapplicability to our specific problem. Initial results were disastrous, but the reasons for that could be easily traced to a series of factors:

a) A starting value of 1.375 for the over-relaxation

factor, as suggested by Carré, consistently led to bad results; smaller initial values, however, produced encouraging, though not fully satisfactory results.

b) Too large variations $\Delta\omega_e$ were sometimes computed, and this usually resulted in trouble in the next cycles; if $\Delta\omega_e$ was kept small, however, these problems were less frequent.

c) There seemed to exist a critical value of over-relaxation, above which the method failed completely, and SBOR diverged, although successives re-estimates indicated a much larger value of ω_o.

This third observation, although not essential in this specific application, seems to confirm Ostrowski's assertion that there exists a fixed number ε, situated between 0 and 1, such that relaxation methods tend to converge for $\varepsilon < \omega < 2 - \varepsilon$, but may fail outside this range (See Ostrowski, A. M., On the linear iteration procedures for symmetric matrices. Rendiconti Matt. Applic., 13, 140 (1954)).

As a consequence of these observations, and by a systematic analysis of unsatisfactory results, we eventually managed to establish patterns, to assess the relative importance of the intervening factors and, by trial and error, to introduce improving modifications in Carré's algorithm. Such modifications eventually led to an interesting discovery which deserves a deeper mathematical approach. It seems (at least on the basis of the matrices involved in EPFELDA) that even if a matrix does not possess Property $A^{(\pi)}$, Carré's method can be successfully applied if the loci of the optimum over-relaxation factors is assumed as shifted from the hypothenuse of the triangular graph of Figs. A-1 and A-2, to an inner line like, for instance, PQ in Fig. A-2.

Specific considerations will be presented in the next section, on the alterations we have introduced in Carré's method. We recognize that a rigorous mathematical explanation for the realization mentioned above is not at hand, and also that this result may be purely coincidental, eventually not being verified with different matrices. We do hope to come back to this subject in the near future, and to study it from a mathematical point of view.

A-6 - THE SPECIFIC ALGORITHM

Fig. A-2, which depicts a part of the triangular graph of Fig. A-1, plots a sample of early results obtained with the help of a modified Carré algorithm, but not involving any delimitation of the maximum value of the over-relaxation factor. The first two values are not shown, as they plot outside the range of the figure. Corrections were performed after every tenth cycle, and the initial value of over-relaxation was taken as 1.0 . A maximum increase

$$\Delta\omega_e = 0.1875$$

was allowed in the first correction, and variations in the subsequent corrections were not allowed to exceed 75% of the previous variation. As a consequence, a given set of the first values of over-relaxation were sometimes repeated in several load increments, as the estimated variations $\Delta\omega_e$ became usually large (and if accepted as such led to inevitable failure). In the vicinity of convergence, however, this pattern of prefixed values was definitely broken, as can be clearly seen in the figure.

To correct the assignment of a bad value of over-relaxation, a modifying procedure may eventually be introduced. The norm, in a converging process, is an essentially decreasing parameter; therefore, if an increase is verified in the norm, we reduce the over-relaxation factor for the next ten increments, according to the equation

$$\omega_{red} = (1 + \omega)/2 .$$

It is observed from Fig. A-2 that convergence usually occurs once the line PQ is crossed. Over-relaxation factors under which convergence occurred are enclosed in a circle, in the figure. It is also observed that the successive pairs (ω , ρ_M) plot satisfactorily according to the family of curves of the graph, except in the vicinity of the line PQ .

Sample A presents a well-behaved pattern, with the successive variations $\Delta\omega_e$ becoming smaller and smaller, and all results being consistent with a common estimate of ω_o (of the order of 1.805). Convergence, however, was achieved under ω =

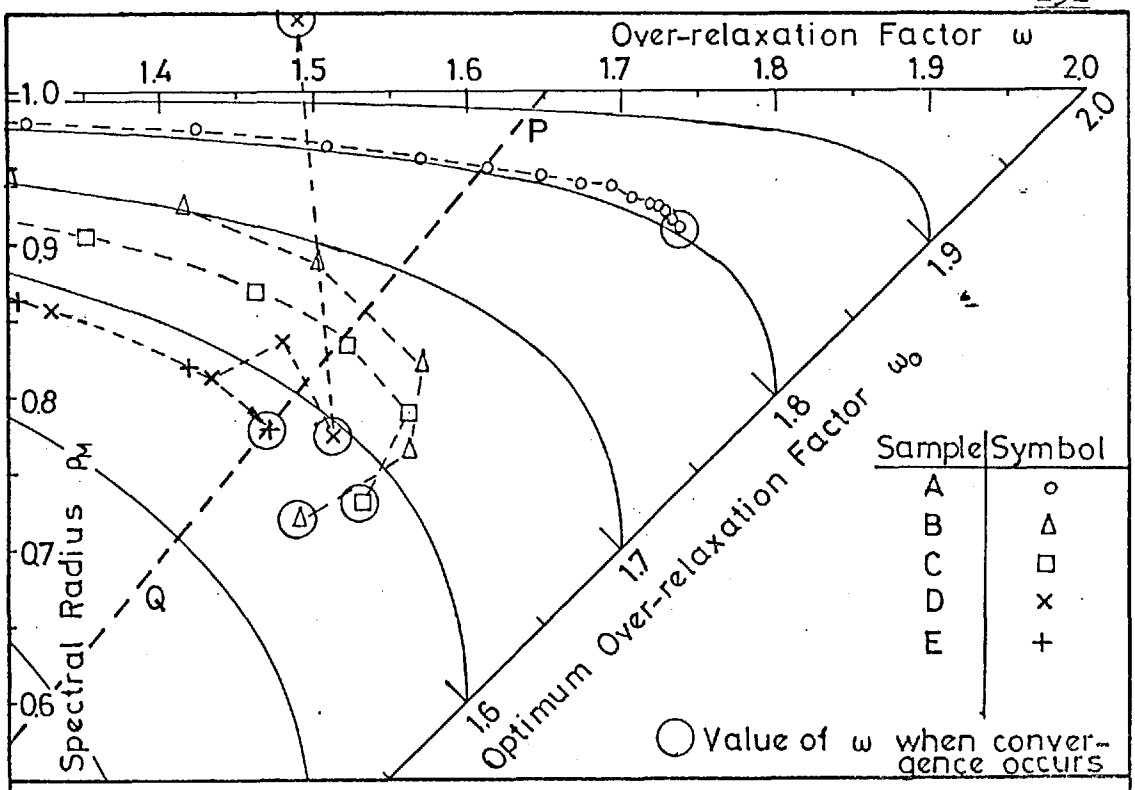


FIG. A-2 - A SAMPLE OF RESULTS OF THE APPLICATION OF CARRÉ'S METHOD FOR THE OPTIMIZATION OF THE OVER-RELAXATION FACTOR

1.740 . (Oddly, though, when bounds were removed on the increases in ω , the SBOR method failed as soon as ω crossed the value of 1.76 , with the production of very large spectral radii, actually larger than unity, and, as a consequence, divergence.

Sample B discrepates from the expected behaviour from about $\omega = 1.41$, with the spectral radii dropping exaggerately through four corrections in ω. Eventually, a negative increase in ω is computed. A similar but less drastic performance is presented by sample C.

Sample D presents an oscillating terminal behaviour, culminating with the production of a very large spectral radius. The situation, however, was already very close to convergence (to 10^{-5}) and, in despite of the high spectral radius, this was finally achieved.

Sample E , finally, compares with sample A , but convergence occurred at a much smaller value of over-relaxation (and spectral radius).

In view of these results, and of the fact that trouble commonly occurred once the plots fell to the right-hand side of the line PQ, tentatively expressed by the equation

$$\omega = 0.8375 + 0.8125\ \rho_M,$$

we simply imposed this line as a boundary not to be crossed, and the equation above as an upper-bound for the successive corrections of the over-relaxation factor.

Under such a restriction, a marginal improvement was achieved in the successful cases, but the percentage of failed cases reduced substantially.

Convergence, in the early stages of deformation, under the use of the optimizing routine, could be achieved in 60 to 70 cycles, in both the indentation and radial upsetting applications. As deformation progressed, more cycles became necessary, but the worst of all situations required only 240 cycles, which compares favourably with the 300 to 500 cycles mentioned earlier.

A-7 - NOMENCLATURE

- $\mathbf{A}$ - A symmetric, positive definite system matrix
- A_{ij} - A submatrix of $\mathbf{A}$ in the SBOR method
- A_1, A_2 - Submatrices of $\mathbf{A}$ in the definition of Property A
- a_{ij} - The elements, or components, of the matrix $\mathbf{A}$
- $\mathbf{B}$ - The matrix related to $\mathbf{A}$ in the definition of Property $A^{(\pi)}$
- $\mathbf{b}$ - Right-hand side vector in a linear algebraic system
- $\mathbf{b}_i$ - Subvector of $\mathbf{b}$
- b_i - Component of $\mathbf{b}$
- b_{ij} - Component of $\mathbf{B}$
- $\mathbf{c}$ - A vector in the SOR method
- $\mathbf{D}$ - A diagonal matrix containing the diagonal terms of $\mathbf{A}$
- D_1, D_2 - Diagonal matrices in the definition of Property A
- $e^{(k)}$ - Error vector after k^{th} SOR cycle
- i, j - Indices
- k - Cycle counter in the SOR and SBOR methods
- $\mathbf{L}$ - Strictly lower triangular matrix with the corresponding elements of matrix $-\mathbf{A}$
- $\mathbf{M}$ - The SOR matrix related to $\mathbf{A}$

N - Rank of matrix A

N_n - Total number of nodes in the finite element mesh

n - Index of the subdivision of A into submatrices

$n^{(k)}$ - Norm of the SOR method

R - Average rate of convergence

U - Strictly upper-triangular matrix with the corresponding elements of matrix -A

$x, x^{(k)}$ - Solution vector and its k^{th} estimate by the SOR method

$x_j, x_j^{(k)}$ - Solution subvector and its k^{th} estimate by the SBOR method

x_j - An element (component) of vector x

$x_j^{(k)}$ - An element (component) of vector $x^{(k)}$

$\Delta\omega_e$ - Variation from the current estimate of the optimum over-relaxation factor to the previous one

δ_{ij} - Kronecker delta

$\delta^{(k)}$ - k^{th} displacement vector

$\delta x^{(k)}$ - Residual vector

ε - A real number

λ_i, μ_i - Eigenvalues of the matrices A and M, respectively

ρ_A, ρ_M - Spectral radii of the matrices A and M, respectively

ω - Over-relaxation factor

ω_e, ω_o - Estimated and correct value of the optimum over-relaxation factor

ω_r - New value of over-relaxation, after a Carré correction

ω_{red} - Reduced value of over-relaxation, in case of an increase in the value of the norm

APPENDIX 2

EPFELDA

LISTING OF PROGRAM, FUNCTIONS AND SUBROUTINES

Main Program

```
      PROGRAM EPFELDA(INPUT,OUTPUT,TAPE5=INPUT,TAPE6=OUTPUT)
C
C     ELASTIC-PLASTIC FINITE ELEMENT LARGE DISPLACEMENT ANALYSIS
C           DEVELOPED IN THE SECOND SEMESTER OF 1971
C                    PROGRAM WRITTEN BY ARNO BLASS
C
      DIMENSION  DLD(3,96), DEQE(215), A(4,3,215), AL   (4,3), NBC(96),
     1           DMU(3,96), EQPS(215), D(6,6,215), DE   (6,6), RN (96),
     2           DU (3,96), EQS (215), CS (6,215), DEDU (3,3), W  (96),
     3           U  (3,96), HD  (215), DCS(6,215), DXST (3,3), NMP(96),
     4           X  (3,96), V6  (215), DGS(6,215), DERU (3,3), NAP(96),
     5           XLD(3,96), ND(4,215), DKS(6,215), DXNT (3,3), ICP(96),
     6           DC (3,96), XKSE  (6), XKS(6,215), CSE(6), NANP(19,96),
     7         LN(4), XL(3), PCS   (6), YELD1(215), DCE(6), RD    (215)
      COMMON     XD(173,96),NANP,NAP,ICP,DLD,XLD,NBC,RN,DMU,ND,
     1           XKS,CS,EQS,A,V6              /CRD/ X
     2           /GSS/ DU                     /EDI/ DXNT,DXST,XJC
     3           /EMM/ DE,D                   /DSP/ U,DERU
      DATA       PI /3.1415926536/
C
C     READ DATA AND COMPUTE ADDITIONAL DATA
C
      READ(5,1) OVS,TOL,NCY,NCC,IW
    1 FORMAT(2E10.2,3I5)
      READ(5,2) E, XNU
    2 FORMAT(2E13.5)
C
      READ(5,3) YIELD,CF1,CF2,TEMP                          (MODULE 1)
    3 FORMAT(4E10.4)
C
```

Main Program

```
      READ(5, 4) NEB, NIF, NBL, NSUB
    4 FORMAT(4I5)
      READ(5,5) ((ND(I,M),I=1,4),M=1,NEB)
    5 FORMAT((8(1X,4I2)))
C
      YFUN = YIELD*CF1**(-CF2)
      CSI  = PI/135.
      CSTM = CSI*FLOAT(NBL)
      NND = NIF*(NBL + 1)
      NEL = NBL*NEB
      NLL = 1
C
C     GENERATE INDICES FOR REFLEXIVE BASIC BLOCK
C
      IF(NBL.EQ.1) GOTO 11
      DO 8 M = 1, NEB
      L1 = M + NEB
      DO 7 I = 1, 4
      ND(I,L1) = ND(I,M)
    7 IF(ND(I,L1).LE.NIF) ND(I,L1) = ND(I,L1) + 2*NIF
    8 CONTINUE
C
C     GENERATE INDICES FOR THE REMAINING ELEMENTS AND NODES
C         IN THE SPECIMEN
C
      IF(NBL.LE.2) GOTO 11
      M = 2*NEB
      DO 10 NB = 3,NBL
      L1 = NIF*(NB - 1)
      DO 10 NE = 1, NEB
      M = M + 1
      DO 10 I = 1, 4
   10 ND(I,M) = ND(I,NE) + L1
   11 CONTINUE
C
C     NODAL COORDINATES WILL BE CALCULATED BY MEANS OF DATA
C         TO BE FEEDED, FOR EVERY BASIC BLOCK
C
      READ(5,12) R0, RR, TH, RPM
   12 FORMAT(4F10.3)
      SUB = FLOAT(NSUB)
      DTIME = 1.
      IF(RPM.LT.1.E-50) GOTO 14
      DTIME = 30.*CSI/PI/RPM/FLOAT(NSUB)
      NLL = 2
   14 CONTINUE
      RANG = 0.
      NMD = NBL + 1
C
C     FORM ELASTIC (EULERIAN) MATRIX
C
      G = E/(2.*(1. + XNU))
      G1 = 2.*G*XNU/(1. - 2.*XNU)
      G2 = 2.*G*(1. - XNU)/(1. - 2.*XNU)
      G3 = 3.*G
      BULK = E/3./(1. - 2.*XNU)
```

(MODULE 1)

```
      DO 15 I = 1, 3
      DO 15 J = I, 3
      IJ = KNV(I,J)
      DO 15 K = 1, 3
      DO 15 L = 1, 3
      KL = KNV(K,L)
      DE(IJ,KL) = 0.
      IF(IJ.LE.3.AND.KL.LE.3)  DE(IJ,KL) = G1
      IF(IJ.LE.3.AND.IJ.EQ.KL) DE(IJ,KL) = G2
      IF(IJ.EQ.KL.AND.KL.GT.3) DE(IJ,KL) = G
   15 CONTINUE
C
      DO 16 NI = 1, NMD
      NMP(NI) = 1 + NIF*(NI - 1)
   16 CONTINUE
C
C
C     GENERATE NODAL COORDINATES AND INITIALIZE
C        VALUES FOR STRESSES AND STRAINS
C
      RMIN = RO
      DO 45 NN = 1, NIF
      READ(5,42) N, RN(N),TEC
   42 FORMAT(I5,2F10.3)
      RMIN = AMIN1(RMIN,RN(N))
C
      DO 45 M = 1, NMD
      NF = N + NIF*(M - 1)
      IF(NF.GT.NND) GOTO 45
      CAN = CSI*FLOAT(M - NLL)
      X(1,NF) = RN(N)*COS(CAN)
      X(2,NF) = RN(N)*SIN(CAN)
      X(3,NF) = TEC*TH/2.
      RN(NF) = RN(N)
   45 CONTINUE
   46 DR = 0.
C
C     FORM SHAPE FUNCTION VALUES, FOR THE ELEMENTS
C     INITIALIZATIONS
C
      DO 50 M = 1, NEL
      CALL COEFF(ND(1,M),A(1,1,M),V6(M))
      DEDE(M) = EWS(M) = EQPS(M) = 0.
      HD(M) = G3
      YELD1(M) = YIELD
      DO 50 I = 1, 6
      CS(I,M) = XKS(I,M) = 0.
      DO 50 J = 1, 6
      D (I,J,M) = DE(I,J)
   50 CONTINUE
C
C    WRITE INPUT DATA AND CONTROL PARAMETERS
C
      IF(IW.EQ.0) WRITE(6,26)
      IF(IW.EQ.1) WRITE(6,27)
   26 FORMAT(///25H THE INPUT ARE NOT OUTPUT)
```

(MODULE 1)

(MODULE 0 - Data Output)

```
   27 FORMAT(///21H THE INPUT ARE OUTPUT)
      IF(IW.EQ.0) GOTO 56
      WRITE(6,21)
   21 FORMAT(1H1/////
     1        40X,46H ELASTO-PLASTIC ANALYSIS OF LARGE DEFORMATIONS /
     2        40X,46H ---------------------------------------------- /
     3        40X,46H ---------------------------------------------- ////)
C
      WRITE(6,22)
   22 FORMAT(40X,36H FLANGE FORMING IN AN ALUMINIUM DISK /
     1        40X,38H ANALYSIS BY THE FINITE ELEMENT METHOD //////
     2        40X,38H ARNO BLASS - IMPERIAL COLLEGE - 1972  ///
     3        40X,30H SUPERVISOR - DR. BELA LENGYEL )
C
      WRITE(6,23) NEL, NND, NEB, NBL, NMD, RR, RO, TH
      WRITE(6,24) NCY, NCC, TOL, CSIM, CSI
      WRITE(6,28) TEMP, YIELD, YFUN, CF1, CF2
   23 FORMAT(1H1/////
     1        26H TOTAL NUMBER OF ELEMENTS ,I12/
     2        26H TOTAL NUMBER OF NODES    ,I12/
     3        28H ELEMENTS IN THE BASIC BLOCK,I10/
     5        29H TOTAL NUMBER OF BASIC BLOCKS,I9 /
     6        32H TOTAL NUMBER OF MID-PLANE NODES,I6 ///
     7        25H RADIUS OF FORMING ROLLER,F13.2,4H MM. /
     8        25H RADIUS OF SPECIMEN      ,F13.2,4H MM. /
     9        25H THICKNESS OF SPECIMEN   ,F13.2,4H MM. ///)
C
   24 FORMAT(17H ITERATION LIMIT,I21,7H CYCLES /
     1        32H INTERVAL FOR PROGRESS OF OUTPUT,I6,7H CYCLES /
     2        23H CONVERGENCE TOLERANCE ,E22.5 /
     8        29H TOTAL  CENTRAL  ANGLE       ,F12.5,6H RADS. //
     9        29H CENTRAL ANGLE OF BASIC BLOCK,F12.5,6H RADS. ////)
C
      WRITE(6,25) E, XNU, DTIME, RPM
   25 FORMAT(17H YOUNGS MODULUS ,F26.2,7H MN/MSQ /
     1        17H POISSONS RATIO ,F26.2 /
     4        17H TIME INCREMENT  ,F26.2,6H SECS.///
     5        17H SPEC. VELOCITY  ,F26.2,4H RPM/)
   28 FORMAT(20H TESTING TEMPERATURE, F22.3,14H DEG. CELSIUS  //
     1        13H YIELD STRESS,F29.3,7H MN/MSQ //
     2        33H MATERIAL OBEYS STRESS-STRAIN LAW //
     3   14H EQ. STRESS = ,F7.4,2H*(,F7.4,16H + EQ. STRAIN)**,F6.4// )
C
C     OUTPUT THE ARRAY DATA
C
      WRITE(6,29)
   29 FORMAT(1H1/////
     1        33X,16H ELEMENTAL NODES,20X,20H INITIAL COORDINATES,8X,
     2                                    16H MID-PLANE NODES /
     3        33X,16H ---------------,20X,20H ------------------,8X,
     2                                    16H ---------------  ///
     5        19X,51H ELEMENT  I-NODE   J-NODE   K-NODE   L-NODE    NODE
     6           41H    FIRST  SECOND   THIRD     ORDER  NODE    /)
      DO 40 M = 1, NEL
      IF(M.GT.NMD) GOTO 32                          (MODULE 0)
      WRITE(6,30) M,(ND(I,M),I=1,4),M,(X(J,M),J=1,3),M,NMP(M)
   30 FORMAT(15X,6I9,2X,3F8.4,1X,2I7)
```

```
      GOTO 40
   32 IF(M.GT.NND) GOTO 36
      WRITE(6,34) M,(ND(I,M),I=1,4),M,(X(J,M),J=1,3)
   34 FORMAT(15X,6I9,2X,3F8.4)
      GOTO 40
   36 WRITE(6,38) M,(ND(I,M),I=1,4)
   38 FORMAT(15X,5I9)
   40 CONTINUE
      WRITE(6,39) (M,V6(M),((A(I,J,M),I=1,4),J=1,3),M=1,NEL)
   39 FORMAT(/////
     1        25X,32H ELEMENTAL VOLUMES AND COFACTORS /
     2        25X,32H ---------------------------------- //
     1        (2X,I3,3X,F10.5,3X,12F9.5))
C
C     P   R   O   G   R   A   M
C     ========================
C
   56 READ(5,57) APL, CFC, PRESC, STEP, NMGL
   57 FORMAT(4F10.3,I5)
C
C     TEST FOR END OF PROBLEM
C
      IF(APL.LE.0.) GOTO 1000
C
C     RATE APPLIED LOAD OVER CONTACT AREA
C
C     INITIALIZATION
C
      WRITE(6,58) RPM, CFC, CSI, STEP
58 FORMAT(////20X,23H PARAMETERS OF PROBLEM //
  1       20X,23H ---------------------- //
  2       20X,30H ANGULAR ROTATION OF SPECIMEN ,F6.3,4H RPM /
  3       20X,30H COULOMB FRICTION COEFFICIENT ,F6.3 /
  4       20X,30H CENTRAL ANGLE OF BASIC BLOCK ,E10.4,5H RADS //
  5       20X,30H APPROX. INIT. LOAD INCREMENT ,F6.1,2H N //)
      DO 49 N = 1, NND
      NBC(N) = -1
      IF(ABS(X(3,N)-TH/2.).LT.0.01) NBC(N) = 1
      IF(ABS(RN(N)-RO).LT.0.01)     NBC(N) = 2
      IF(ABS(RN(N)-RMIN).LT.0.01)   NBC(N) = 0
      IF(RPM.LT.1.E-50.AND.N.LE.NIF) GOTO 43
      IF(N.LE.NIF)                  NBC(N) = 0
   43 IF(N.GT.NND-NIF)              NBC(N) = 0
      DO 47 I = 1, 3
      DMU(I,N) = 0.
   47 DLD(I,N) = DU(I,N) = XLD(I,N) = U(I,N) = 0.
      ICP(N) = 1
      W(N) = 0.
   49 CONTINUE
      NM = 1
      COMPAR = 1.
      TIME = 0.
      N1 = NMP(NLL)
      PREV = 0.
      F = RO + RR
      N3 = N1 + NIF - 4
      N4 = N3 - 1
```

(MODULE 0)

(MODULE 2)

Main Program

```
      DLD(1,N1) = DLD(1,N4) = - 0.125*APL
      DLD(1,N3) = - 0.25*APL
      DMU(2,N1) = CFC
      DMU(2,N3) = CFC/2.
      DMU(3,N3) = - CFC*SQRT(3.)/2.
      DMU(3,N4) = - CFC
      ICP(N1) = ICP(N3) = ICP(N4) = 0
      DINCR = STP = 0.01
      IPN = 30
      STI = TH/2.
      GOTO 72
C
C     SUBSEQUENT STAGES
C
   60 NS = MOD(NM-1,NSUB)
      SN = FLOAT(NS)
      PREV = APL
      DINCR = 1.5*DINCR*0.975**NM
      FACT1 = STEP/APL
      FACT2 = FACT1/10.
      IF(RPM.LT.1.E-50) GOTO 63
      DEN = (SUB - 3.)*SUB*SUB - 6.*SUB - 8.
      C1 = 12./DEN
      C2 = 2.*(SUB*SUB - 8.*SUB - 2.)/DEN
      FACT1 = STEP/APL*(1. - C1*SN*SN - C2*SN)
      FACT2 = STEP/APL - FACT1
      IF(NS.NE.0) GOTO 63
      NS = NSUB
      N1 = N1 + NIF
      RANG = RANG + CSI
   63 XI1 = X(1,N1) + U(1,N1)
      XI2 = X(2,N1) + U(2,N1)
      RI  = SQRT(XI1*XI1 + XI2*XI2)
      F = XI1*(1. + RR/RI)
      NI = N1
      DO 70 N = NI, N3
      IF(RN(N).LT.R0-2.) GOTO 70
      XE1 = X(1,N) + U(1,N)
      XE2 = X(2,N) + U(2,N)
      RDS = SQRT((F-XE1)*(F-XE1) + (XE2-F*XI2/XI1)*(XE2-F*XI2/XI1))/RR
      IF(RDS.LT.1.01) GOTO 62
      DLD(1,N) = DLD(2,N) = DLD(3,N) = 0.
      ICP(N) = 1
      IF(N.EQ.N1) N1 = N1 + NIF
      GOTO 70
   62 IF(N.LE.NI+NIF) GOTO 64
      FACT1 = (1. - 100.*(RDS - 1.))*STEP/APL
      FACT2 = 0.
   64 DO 65 I = 1, 2
      DLD(I,N) = DLD(I,N) + FACT1*XLD(I,N)
   65 DLD(I,N+NIF) = DLD(I,N+NIF) + FACT2*XLD(I,N)
   66 ICP(N) = ICP(N+NIF) = 0
      IF(N+NIF.LE.NND-NIF) GOTO 70
      XE1 = X(1,N+NIF) + U(1,N+NIF)
      XE2 = X(2,N+NIF) + U(2,N+NIF)
      RDS = SQRT((F-XE1)*(F-XE1) + (XE2-F*XI2/XI1)*(XE2-F*XI2/XI1))/RR
      IF(RDS.LT.1.005) STOP
```

(MODULE 2)

```
      DLD(1,N+NIF) = DLD(2,N+NIF) = DLD(3,N+NIF) = 0.
      ICP(N+NIF) = 1
   70 CONTINUE
C
C     ICP(N) = 0  MEANS CONTACT WITH ROLLER
C
   72 NMG = 0                                              (MODULE 2)
      WRITE(6,73)
   73 FORMAT(5X,28H LOAD INCREMENT INITIALIZED  )
      RAT = - FLOAT(IFIX(DINCR/STP))*STP
C
C
C     FORM TOTAL STIFFNESS MATRIX FOR THE WHOLE SYSTEM
C                                                          (MODULE 3)
      CALL TSTIFF(NEL,NND,HD)
C
C     COMPUTE DISPLACEMENT INCREMENT COMPONENTS BY
C         PERFORMING SUCCESSIVE OVER-RELAXATION            (MODULE 4)
C              ITERATIONS FOR THE ENTIRE SYSTEM
C
   74 CALL GAUSS(NCC,NCY,OVS,TOL,NIF,NND,NM,NMG,N1,RMIN,RPM,RAT,     IW)
C
C
C     COMPUTE GREEN'S STRAIN INCREMENTS
C                                                          (MODULE 5)
      DO 125 M = 1, NEL
      DO 98 I = 1, 4
      LN(I) = ND(I,M)
      DO 98 J = 1, 3
   98 AL(I,J) = A(I,J,M)
      CALL DERIV(LN,AL)
      CALL DERI2(LN,AL,DEDU)
  100 DO 112 I = 1, 3
      DO 112 J = 1, 3
      IJ = KNV(I,J)
      DGS(IJ,M) = DKS(IJ,M) = 0.
      DGS(IJ,M) = DGS(IJ,M) + (DEDU(I,J) + DEDU(J,I))/2.
      DO 111 K = 1, 3
  111 DGS(IJ,M) = DGS(IJ,M) +
     1    (DEDU(K,I)*DERU(K,J) + DEDU(K,J)*DERU(K,I))/2.
  112 CONTINUE
C
C     COMPUTE STRESS INCREMENTS AND INTERIM STRESS VALUES
C
      DO 115 I = 1, 6
      DO 113 K = 1, 3
      DO 113 L = 1, 3
      KL = KNV(K,L)
  113 DKS(I,M) = DKS(I,M) + D(I,KL,M)*DGS(KL,M)
  115 XKSE(I) = DKS(I,M)
      DO 120 I = 1, 3
      DO 120 J = I, 3
      IJ = KNV(I,J)
      CSE(IJ) = 0.
  114 DO 116 K = 1, 3
      IK = KNV(I,K)
      JK = KNV(J,K)
```

```
      FACT = DXST(I,K)/XJC
      DO 116 L = 1, 3
      KL = KNV(K,L)
  116 CSE(IJ) = CSE(IJ) + FACT*DXST(J,L)*XKSE(KL)
     1                  + (CS(IK,M)*DEDU(J,L) + CS(JK,M)*DEDU(I,L)
     2                  - CS(IJ,M)*DEDU(K,L))*DXNT(L,K)
      DCS(IJ,M) = CSE(IJ)
  120 CONTINUE
  125 CONTINUE
      WRITE(6,127)
  127 FORMAT(5X,18H ELEMENTS SCANNED )
C
C     UPDATE FORCES AND COMPUTE FRICTION FUNCTION
C
      NI = N1
      DO 148 N = 1, NND
      IF(NMG.NE.0) GOTO 144
      NF = 0
      IF(W(N).LT.0.001) GOTO 140
  135 DO 136 I = 1, 3
      DC(I,N) = XLD(I,N)/W(N)
  136 XL(I) = XLD(I,N) +        DLD(I,N)
      WP = SQRT(XL(1)*XL(1) + XL(2)*XL(2) + XL(3)*XL(3))
      DO 138 I = 1, 3
  138 DLD(I,N) = DLD(I,N) - W(N)*(XL(I)/WP - DC(I,N))
      NF = NF + 1
      IF(NF.LE.2) GOTO 135
  140 DO 142 I = 1, 3
  142 XLD(I,N) = XLD(I,N) + DLD(I,N)
  144 IF(ICP(N).NE.0) GOTO 148
      IF(CFC.LT.1.E-5) GOTO 148
      IF(NMG.NE.NMGO) GOTO 148
      IF(N.NE.NI) GOTO 146
      NB = N + NIF/2. - 1
      NE = N + NIF - 4
      DO 145 NF = NB, NE
      IF(ICP(NF).NE.0) GOTO 145
      STI = AMAX1(STI,X(3,NF)+U(3,NF))
      NI = NI + NIF
      GOTO 146
  145 CONTINUE
  146 FACT1 = (X(3,N) + U(3,N))/STI
      FACT1 = AMIN1(1.,FACT1)
      FACT2 = SQRT(1. - FACT1*FACT1)
      DMU(1,N) = - CFC*FACT2*SIN(RANG)
      DMU(2,N) =   CFC*FACT2*COS(RANG)
      DMU(3,N) = - CFC*FACT1
  148 DLD(1,N) = DLD(2,N) = DLD(3,N) = 0.
      WRITE(6,150)
  150 FORMAT(5X,15H NODES SCANNED )
      NMGO = NMGL
      IF(COMPAR.LT.0.005) NMGO = NMG
      COMPAR = 0.
C
C     COMPUTE CORRECTED VALUES FOR STRESSES
C
      DO 188 M = 1, NEL
```

(MODULE 5)

(MODULE 6)

(MODULE 7)

```
      PHD = HDL = HD(M)
      RATEQ = RD(M) = 0.
      DO 160 I = 1, 6
      DCE(I) = 0.
      PCS(I) = CS(I,M)
  160 CSE(I) = PCS(I) + DCS(I,M)
      DO 161 I = 1, 4
      LN(I) = ND(I,M)
      DO 161 J = 1, 3
  161 AL(I,J) = A(I,J,M)
      EQE = EQST(CSE)
      PEQS = EQS(M)
      IF(HDL.LT.G) GOTO 165
      RATEQ = RATST(YELD1(M),PEQS,PCS,DCS(1,M))
  165 CONTINUE
      RATEQ = AMIN1(RATEQ,1.)
C
C     COMPUTE CORRECTED VALUES FOR ALMANSI STRAINS
C
      DEQIN = 0.
      IF(HDL.LT.G) GOTO 177
      IF(EQE.GT.0.99*YELD1(M)) GOTO 177
      DO 175 I = 1, 6
      CS (I,M) = CSE(I)
  175 XKS(I,M) = XKS(I,M) + DKS(I,M)
      EQS(M) = EQE
      IF(NMG.NE.NMGO) GOTO 188
      R = 0.
      GOTO 187
  177 CALL DERIV(LN,AL)
      CALL DERI2(LN,AL,DEDU)
      DO 178 I = 1, 3
      DO 178 J = I, 3
      IJ = KNV(I,J)
      CS (IJ,M) = CSE(IJ) = PCS(IJ) + RATEQ*DCS(IJ,M)
      XKS(IJ,M) = XKS(IJ,M) + RATEQ*DKS(IJ,M)
      DCS(IJ,M) = (1. - RATEQ)*DCS(IJ,M)
      DKS(IJ,M) = XKSE(IJ) = 0.
      DO 178 L = 1, 3
      DO 178 K = 1, 3
      LK = KNV(L,K)
  178 DCE(IJ) = DCE(IJ) + DXNT(L,I)*DXNT(K,J)*DGS(LK,M)
      DENOM = YELD1(M)*(1. + HDL/G3)
      CH = (CSE(1) + CSE(2) + CSE(3))/3.
      DO 179 I = 1, 3
  179 DEQIN = DEQIN + ((CSE(I) - CH)*DCE(I) +
     1                 2.*CSE(I+3)*DCE(I+3))/DENOM*(1. - RATEQ)
      EQPS(M) = EQPS(M) + DEQIN
      DEQE(M) = DEQE(M) + DEQIN
C
C     THIS IS THE ALMANSI PLASTIC STRAIN INCREMENT VECTOR
C         FOR THE POST-YIELDED ELEMENTS
C
      YCOMP = YFUN*(CF1 + EQPS(M))**CF2
      HDL = CF2*YCOMP/(CF1 + EQPS(M))
      IF(RATEQ.GT.0.999) GOTO 186
      HDLC = HDL
      PHLC = PHD                                  (MODULE 7)
      EQE = EQST(CSE)
```

```
      IF(DEQIN.LE.1.E-6) GOTO 180
      HDIF = (EQE - YELD1(M))/(DEQIN + 1.E-7)
      HDLC = AMAX1(10.,HDL - HDIF)
      PHLC = AMAX1(10.,PHD - HDIF)
  180 REL = PHLC/HDLC
      FACT = HDLC*DEQIN/EQE
      DCSH = BULK*(1. - RATEQ)*(DCE(1) + DCE(2) + DCE(3))
      DO 182 I = 1, 3
      DO 182 J = I, 3
      IJ = KNV(I,J)
      CSE(IJ) = 0.
      IF(IJ.GT.3) GOTO 181
      CSE(IJ) = CSE(IJ) + DCSH - FACT*CH
  181 CSE(IJ) = CSE(IJ) + FACT*CS(IJ,M)
      CS (IJ,M) = CS (IJ,M) + CSE(IJ)
      IF(PHD.LT.G) DCS(IJ,M) = REL*CSE(IJ)
      DCS(IJ,M) = DCS(IJ,M) - CSE(IJ)
      DO 182 K = 1, 3
      IK = KNV(I,K)
      JK = KNV(J,K)
      DO 182 L = 1, 3
  182 CSE(IJ) = CSE(IJ) - DXNT(L,K)*(PCS(IK)*DEDU(J,L) +
     1              PCS(JK)*DEDU(I,L) - PCS(IJ)*DEDU(K,L))*(1. - RATEQ)
      DO 184 I = 1, 3
      DO 184 J = I, 3
      IJ = KNV(I,J)
      DKS(IJ,M) = XKSE(IJ) = 0.
      DO 183 K = 1, 3
      DO 183 L = 1, 3
      KL = KNV(K,L)
      XKSE(IJ) = XKSE(IJ) + XJC*DXNT(I,K)*DXNT(J,L)*CSE(KL)
  183 DKS(IJ,M) = DKS(IJ,M) + XJC*DXNT(I,K)*DXNT(J,L)*DCS(KL,M)
  184 XKS(IJ,M) = XKS(IJ,M) + XKSE(IJ)
      RD(M) = COMPAR = 1.
  186 EQS(M) = EQST(CS(1,M))
      YELD1(M) = YCOMP
      IF(NMG.NE.NMGO) GOTO 188
      IF(EQS(M).GE.0.99*PEQS) GOTO 185
      R = 0.
      HD(M) = G3
      GOTO 187
  185 CONTINUE
      HD(M) = HDL
      R = G3/EQS(M)/EQS(M)/(1. + HDL/G3)
  187 CALL EPMM(CS(1,M),R,M)
  188 CONTINUE
      WRITE(6,190)
  190 FORMAT(5X,26H PLASTIC ELEMENTS SCANNED )
      IF(COMPAR.LT.0.005) GOTO 210
C
C     COMPUTE CORRECTIVE LOAD INCREMENTS
C
      DO 206 M = 1, NEL
      IF(RD(M).LT.0.01) GOTO 206
      FACT = V6(M)/6.
      DO 198 L = 1, 4
      LN(L) = ND(L,M)
```

(MODULE 7)

(MODULE 8)

```
      DO 198 J = 1, 3
  198 AL(L,J) = A(L,J,M)
      DO 204 L = 1, 4
      L1 = LN(L)
      DO 204 K = 1, 3
      DO 204 I = 1, 3
      FACTA = FACT*AL(L,I)
      IK = KNV(I,K)
      DLD(K,L1) = DLD(K,L1) + FACTA*DKS(IK,M)
      DO 204 N = 1, 4
      L2 = LN(N)
      DO 201 J = 1, 3
      IJ = KNV(I,J)
      FACTB = FACTA*AL(N,J)
  201 DLD(K,L1) = DLD(K,L1) + FACTB*DKS(IJ,M)*U(K,L2)
  204 CONTINUE
  206 CONTINUE
      WRITE(6,208)
  208 FORMAT(5X,27H CORRECTIVE LOADS COMPUTED )
      DO 209 N = 1, NND
      DO 207 I = 1, 3
      U(I,N) = U(I,N) + DU(I,N)
      IF(NMG.EQ.0) DU(I,N) = 0.
  207 CONTINUE
      IF(ABS(RN(N)-RMIN).LT.0.01) GOTO 209
      IF(ABS(X(3,N)).GT.0.001) DLD(3,N) = 0.
      IF(ICP(N).EQ.0) GOTO 209
      DLD(1,N) = 0.
      IF(RPM.LT.0.001.AND.N.LE.NIF) GOTO 209
      DLD(2,N) = 0.
  209 CONTINUE
      IF(NMG.EQ.NMGO) GOTO 210
      NMG = NMG + 1
      GOTO 74
C
C
C     OUTPUT THE COMPUTED RESULTS,, FOR EVERY TIME INCREMENT
C
C
  210 WRITE(6,212) NM
  212 FORMAT(////30X,I2,17HTH LOAD INCREMENT  /
     1           30X,19H================== ////
     3    16X,4HNODE,16X,13HDISPLACEMENTS,33X,11HNODAL LOADS,
     4    //42X,2HMM,42X,2H N //)
  215 APL = 0.
      DO 224 N = 1, NND
      W(N) = 0.
      DO 217 I = 1, 3
      XLD(I,N) = XLD(I,N) - DLD(I,N)
      U(I,N) = U(I,N) + DU(I,N)*(1. - COMPAR)
      DLD(I,N) = 0.
  217 W(N) = W(N) + XLD(I,N)*XLD(I,N)
      IF(ICP(N).EQ.0) APL = APL - 2.*XLD(1,N)
      W(N) = SQRT(W(N))
      ICP(N) = 1
  218 FORMAT(15X,I5,3E15.5,60X,I5)
  219 FORMAT(15X,I5,7E15.5,I5)
      IF(W(N).GT.0.001) GOTO 222
  221 WRITE(6,218) N,(U(I,N),I=1,3),N
      GOTO 224
```

(MODULE 8)

(MODULE 9)

```
  222 WRITE(6,219) N,(U(I,N),I=1,3),(XLD(J,N),J=1,3),W(N),N
  224 CONTINUE
      PDR = DR
      DR = ABS(X(1,N1)*U(1,N1) + X(2,N1)*U(2,N1))/RN(N1)
      DDR = (DR - PDR)/DR
      WRITE(6,225) APL, DR
  225 FORMAT(////15X,20H APPLIED LOAD        ,E15.5,2H N //
     1           15X,20H RADIAL PENETRATION ,E15.5,3H MM )
      WRITE(6,227)
  227 FORMAT(////3X,3HEL.,13X,30HTRUE STRESSES IN ELEMENTS, IN  ,
     1     8H(MN/MSQ),15X,6HEQUIV.,5X,25HPLASTIC STRAIN     SLOPE  //
     2     10X,7HCS(1,1),3X,7HCS(2,2),3X,7HCS(3,3),3X,
     3      7HCS(1,2),3X,7HCS(2,3),3X,7HCS(3,1),5X,6HSTRESS,5X,
     4         15HTOTAL    INCREM.,13X,3HEL. ///)
      NEQ = NYL = NYLIM = 0
      DO 250 M = 1, NEL
      HDL = CF2*YELD1(M)/(CF1 + EQPS(M))
      IF(HDL.LT.EQS(M)) NYL = NYL + 1
      IF(EQS(M).GT.1.25*YELD1(M)) NEQ = 3
      IF(EQPS(M).GE.0.3) NYLIM = NYLIM + 1
      IF(EQPS(M).NE.0.) GOTO 229
      WRITE(6,228) M,(CS(I,M),I=1,6),EQS(M),M
  228 FORMAT(3X,I3,1X,6F10.3,1X,F10.4,33X,I3)
      GOTO 250
  229 WRITE(6,230) M,(CS(I,M),I=1,6),EQS(M),EQPS(M),DEQE(M),HDL,M
  230 FORMAT(3X,I3,1X,6F10.3,1X,F10.4,2F10.6,F10.4,3X,I3)
      IF(DEQE(M).GT.-.1E-5) GOTO 250
      NEQ = 1
      M1 = M
      DEQN = DEQE(M)
  250 DEQE(M) = 0.
      IF(NYLIM.GT.NEL/10) GOTO 300
      IF(NEQ.EQ.1) GOTO 800
      IF(NEQ.EQ.3) GOTO 1000
C
C     VERIFY IF STEADY STATE HAS BEEN ACHIEVED
C
      IF(DDR.LT.0.0005) GOTO 300
      IF(DR.GE.PRESC) GOTO 300
      IF(PREV.GE.APL) STOP
      NM = NM + 1
      TIME = TIME + DTIME
      N3 = NND - NIF
      COMPAR = 1.
      IF(NYL.LT.NEL/IPN) GOTO 60
      IPN = IPN/2 + 1
      STP = STP/2.
      DINCR = DINCR/2.
      GOTO 60
  300 DR = 0.
      DO 320 N = 1, NND
      ICP(N) = 1
      W(N) = 0.
      DO 320 I = 1, 3
  320 DLD(I,N) = DU(I,N) = XLD(I,N) = U(I,N) = 0.
      DO 340 M = 1, NEL
      YELD1(M) = YIELD
      HD(M) = G3
  340 DEQE(M) = EQS(M) = EQPS(M) = 0.          (MODULE 9)
      NM = 1
      GOTO 56
```

```
C
C      PLASTIC STRAIN INCREMENT
C
  800 WRITE(6,805) M1,DEPN
  805 FORMAT(1H1////30X,11H AT ELEMENT,I5 //
     1       30X,43H THE PLASTIC STRAIN INCREMENT CHANGES SIGN //
     2       30X,14H ITS VALUE IS ,F10.5 //
     3       30X,27H THE PROBLEM IS TERMINATED )
 1000 STOP
      END
```

(MODULE 9)

Functions

a) EQST

```
      FUNCTION EQST(CS)
C
C     EULERIAN EQUIVALENT STRESS FOR ONE ELEMENT
C
      DIMENSION  CS(6)
      EQST = SQRT(((CS(1)-CS(2))*(CS(1)-CS(2)) +
     1    (CS(2)-CS(3))*(CS(2)-CS(3)) + (CS(3)-CS(1))*(CS(3)-CS(1)))/2.
     2 + 3.*(CS(4)*CS(4) + CS(5)*CS(5) + CS(6)*CS(6)))
      RETURN
      END
```

b) KNV

```
      FUNCTION KNV(I,J)
C
C     CONVERTS INDICES OF THIRD ORDER TENSORS INTO INDICES OF
C                              SIXTH ORDER VECTORS
C
      K = (I + J)/2 + 3*IABS(I - J)
      KNV = MIN0(K,6)
      RETURN
      END
```

c) KVN

```
      FUNCTION KVN(I,J)
C
C     CONVERTS INDICES OF THIRD ORDER TENSORS INTO INDICES OF
C                              NINTH ORDER VECTORS
C
      K = I - J
      KVN = (I + J)/2 + 3*IABS(K)
      IF(K.EQ.1)  KVN = KVN + 2
      IF(K.EQ.2)  KVN = KVN + 1
      RETURN
      END
```

d) RATST

```
      FUNCTION RATST(EQE,PEQS,PCS,DCS)
C
C     COMPUTES CORRECTING FACTORS FOR STRESS INCREMENTS
C
      DIMENSION  PCS(6) , DCS(6)
C
      PCH = (PCS(1) + PCS(2) + PCS(3))/3.
      DCH = (DCS(1) + DCS(2) + DCS(3))/3.
      A = B = 0.
      DO 2 I = 1, 3
      A = A + 3.*((PCS(I) - PCH)*(DCS(I) - DCH) + 2.*PCS(I+3)*DCS(I+3))
    2 B = B + 3.*((DCS(I) - DCH)*(DCS(I) - DCH) + 2.*DCS(I+3)*DCS(I+3))
      B = AMAX1(B,0.0001)
      RATST = (SQRT(A*A + 2.*B*(EQE*EQE - PEQS*PEQS)) - A)/B
      RETURN
      END
```

Subroutines

a) COEFF

```
      SUBROUTINE COEFF(ND,A,V6)
C
C     GEOMETRICAL CALCULATIONS ON THE ELEMENTS (ELEMENT BY ELEMENT)
C              SHAPE FUNCTION DERIVATIVES AND ELEMENTAL VOLUMES
C     MEAN COORDINATES OF ELEMENTAL EXTERIOR FACES
C
      DIMENSION  X(3,96), A(4,3), B(4), ND(4)
      COMMON     /CRD/ X
C
C     GENERATE INTERNAL ORDERING  OF ELEMENTAL NODES
C
      DO 20 N = 1, 4
      J = N + 1
      K = N + 2
      L = N + 3
      IF(J.GT.4) J = J - 4
      IF(K.GT.4) K = K - 4
      IF(L.GT.4) L = L - 4
      I = ND(N)
      J = ND(J)
      K = ND(K)
      L = ND(L)
C
C     INTERIM VALUES FOR SHAPE FUNCTION DERIVATIVES
C
   10 DO 18 N1 = 1, 3
      GOTO (12,14,16),N1
   12 A(N,1) = X(2,K)*X(3,L) - X(2,L)*X(3,K) - X(2,J)*X(3,L) +
     1        X(2,L)*X(3,J) + X(2,J)*X(3,K) - X(2,K)*X(3,J)
      GOTO 18
   14 A(N,2) = X(3,K)*X(1,L) - X(3,L)*X(1,K) - X(3,J)*X(1,L) +
     1        X(3,L)*X(1,J) + X(3,J)*X(1,K) - X(3,K)*X(1,J)
      GOTO 18
   16 A(N,3) = X(1,K)*X(2,L) - X(1,L)*X(2,K) - X(1,J)*X(2,L) +
     1        X(1,L)*X(2,J) + X(1,J)*X(2,K) - X(1,K)*X(2,J)
```

a) COEFF

```
   18 IF(MOD(N,2).NE.0) A(N,N1) = - A(N,N1)
      B  (N) = X(1,J)*(X(2,K)*X(3,L) - X(2,L)*X(3,K)) +
     1         X(1,K)*(X(2,L)*X(3,J) - X(2,J)*X(3,L)) +
     2         X(1,L)*(X(2,J)*X(3,K) - X(2,K)*X(3,J))
   20 IF(MOD(N,2).NE.1) B(N) = - B(N)
C
C     VOLUME OF MTH ELEMENT, TIMES A FACTOR OF 6.
C
      V6 = B(1) + B(2) + B(3) + B(4)
      IF(V6.GT.1.E-35) GOTO 28
      N1 = ND(3)
      ND(3) = ND(2)
      ND(2) = N1
      V6 = - V6
      DO 26 N = 1, 3
      PROV =  - A(3,N)
      A(1,N) = - A(1,N)
      A(4,N) = - A(4,N)
      A(3,N) = - A(2,N)
   26 A(2,N) = PROV
C
C     CORRECTION  OF THE SHAPE FUNCTION DERIVATIVE VALUES
C
   28 DO 30 N = 1, 4
      DO 30 N1= 1, 3
   30 A(N,N1) = A(N,N1)/V6
C
   50 RETURN
      END
```

b) DERIV

```
      SUBROUTINE DERIV(ND,A)
C
C     LAGRANGIAN DISPLACEMENT DERIVATIVE AND TRANSFORMATION JACOBEAN
C     EULERIAN DERIVATIVES FOR THE INITIAL COORDINATES (ELEMENTAL)
C
      DIMENSION  A(4,3), ND(4), DERU(3,3), DXNT(3,3), DXST(3,3), U(3,96)
      COMMON     /DSP/ U,DERU          /EDI/ DXNT,DXST,XJC
      DO 6 M = 1, 3
      DO 6 N = 1, 3
      DERU(M,N) = 0.
      DO 6 I = 1, 4
      J = ND(I)
    6 DERU(M,N) = DERU(M,N) + A(I,N)*U(M,J)
C
C     JACOBEAN OF THE COORDINATE TRANSFORMATION
C
      XJC = 1. + DERU(1,1)*(DERU(2,2)*DERU(3,3) - DERU(2,3)*DERU(3,2)) +
     1           DERU(1,2)*(DERU(2,3)*DERU(3,1) - DERU(2,1)*DERU(3,3)) +
     2           DERU(1,3)*(DERU(2,1)*DERU(3,2) - DERU(2,2)*DERU(3,1)) +
     3           DERU(1,1)*DERU(2,2) - DERU(1,2)*DERU(2,1) + DERU(1,1) +
     4           DERU(2,2)*DERU(3,3) - DERU(2,3)*DERU(3,2) + DERU(2,2) +
     5           DERU(3,3)*DERU(1,1) - DERU(3,1)*DERU(1,3) + DERU(3,3)
C
```

b) DERIV

```
      ADD = (1. + DERU(1,1) + DERU(2,2) + DERU(3,3))/XJC
      DO 10 M = 1, 3
      M1 = MOD(M ,3) + 1
      M2 = MOD(M1,3) + 1
      DO  8 N = 1, 3
      DXST(M,N) = DERU(M,N)
      N1 = MOD(N ,3) + 1
      N2 = MOD(N1,3) + 1
    8 DXNT(M,N) = (DERU(N1,M1)*DERU(N2,M2) - DERU(N1,M2)*DERU(N2,M1) -
     1              DERU(M,N))/XJC
      DXST(M,M) = DXST(M,M) + 1.
   10 DXNT(M,M) = DXNT(M,M) + ADD
      RETURN
      END
```

c) DERI2

```
      SUBROUTINE DERI2(ND,A,DEDU)
C
C     LAGRANGEAN DERIVATIVES OF DISPLACEMENT INCREMENTS
C
      DIMENSION  A(4,3), ND(4), DEDU(3,3), DU(3,96)
      COMMON     /GSS/ DU
      DO 2 M = 1, 3
      DO 2 N = 1, 3
      DEDU(M,N) = 0.
      DO 2 I = 1, 4
      J = ND(I)
    2 DEDU(M,N) = DEDU(M,N) + A(I,N)*DU(M,J)
      RETURN
      END
```

d) EPMM

```
      SUBROUTINE EPMM(CS,R,M)
C
C     ELASTIC-PLASTIC ( EULERIAN ) MATERIAL MATRIX  D
C     ELASTIC-PLASTIC (LAGRANGEAN) MATERIAL MATRICES  DT, DEP
C
      DIMENSION  CS(6) , CD(6), D(6,6), DE(6,6), DEP(6,6), DXNT(3,3),
     1           DT(6,6,215), DXST(3,3)
      COMMON     /EDI/ DXNT,DXST,XJC          /EMM/ DE,DT
C
C     EQS   IS THE CONVENTIONAL EQUIVALENT STRESS
C
      CH = (CS(1) + CS(2) + CS(3))/3.
      DO  1 I = 1, 3
      CD(I) = CS(I) - CH
    1 CD(I+3) = CS(I+3)
      DO 8 I = 1, 6
      DO 8 J = 1, 6
      DEP(I,J) = 0.
    8 D  (I,J) = DE(I,J) - CD(I)*CD(J)*R
      DO 40  I = 1, 3
      DO 40 J = I, 3
      IJ = KNV(I,J)
      DO 40 M1 = 1, 3
      FAA = XJC*DXNT(I,M1)
```

d) EPMM

```
      DO 40 N1 = 1, 3
      MN = KNV(M1,N1)
      FAB = FAA*DXNT(J,N1)
      DO 40  K = 1, 3
      DO 40 M2 = 1, 3
      FAC = FAB*DXNT(K,M2)
      DO 40  L = K, 3
      KL = KNV(K,L)
      DO 40 N2 = 1, 3
      NM1 = KNV(M2,N2)
      DEP(IJ,KL) = DEP(IJ,KL) + FAC*DXNT(L,N2)*D(MN,NM1)
   40 CONTINUE
      DO 50 I = 1, 6
      DO 50 J = 1, 6
   50 DT(I,J,M) = DEP(I,J)
   55 RETURN
      END
```

e) FIRST

```
      SUBROUTINE FIRST(CS,B,ME)
C
C     ELEMENTARY STIFFNESS MATRIX FOR FIRST LOAD INCREMENT
C
      DIMENSION  A(4,3), DE(6,6), CS(6), XK(12,12),
     1           B(3,3), D (6,6), DT(6,6,215)
      COMMON     /EMM/ DE,DT    /STF/ XK,A,V6
C
      DO 6 I = 1, 6
      DO 6 J = 1, 6
    6 D(I,J) = DT(I,J,ME)
C
      DO 40 I = 1, 12
      L = 1 + (I - 1)/3
   12 K = MOD(I,3)
      IF(K.EQ.0) K = 3
      FLG = 0.
      FLAG = 0.
      DO 40 J = I, 12
      XK(I,J) = XK(J,I) = 0.
      IF(I.NE.J) FLG = 1.
      M = 1 + (J - 1)/3
   15 N = MOD(J,3)
      IF(N.EQ.0) N = 3
      IF(K.EQ.N)   FLAG = 1.
C
C     USUAL (SMALL DISPLACEMENT) STIFFNESS TERM
C        AND INITIAL STRESS STIFFNESS TERM
C
      DO 40 I1 = 1, 3
      FACTL = V6*A(L,I1)/6.
      KI = KNV(K,I1)
      DO 40 J1 = 1, 3
      FACTA = FACTL*A(M,J1)
      NJ = KNV(N,J1)
      IJ = KNV(I1,J1)
      ADD = FACTA*(D(KI,NJ) + FLAG*CS(IJ))
      XK(I,J) = XK(I,J) + ADD
      XK(J,I) = XK(J,I) + ADD*FLG
```

e) FIRST

```
C
C       INITIAL DISPLACEMENT STIFFNESS TERM
C
        DO 40 M1 = 1, 3
        JM = KNV(J1,M1)
        IM = KNV(I1,M1)
        ADD = FACTA*(D(KI,JM)*B(N,M1) + D(IM,NJ)*B(K,M1))
        XK(I,J) = XK(I,J) + ADD
        XK(J,I) = XK(J,I) + ADD*FLG
   40 CONTINUE
C
        RETURN
        END
```

f) GAUSS

```
      SUBROUTINE GAUSS (NCC,NCY,OVS,TOL,NIF,NOD,NM,NMG,N1,
     1                                  RMIN,RPM,RAT,     IW)
C
C     PERFORM SUCCESSIVE OVER-RELAXATION ITERATIONS ON THE STIFFNESS
C          MATRIX FOR THE ENTIRE SYSTEM
C
      DIMENSION  OLD(3,96), XKT(9,19,96), DDU(3), NAP(96), RN (96),
     1           DU (3,96), NANP (19,96), R  (3), ICP(96), X(3,96),
     2           Q  (3,96), XLD   (3,96), F  (9), CFA(96), U(3,96),
     3           DMU(3,96), CFB(96), NBC(96)
      COMMON     CFA,CFB,XKT,NANP,NAP,ICP,OLD,XLD,NBC,RN,DMU,
     1           ND(4,215),XDUM(26,215)
     2           /CRD/ X         /GSS/ DU              /DSP/ U,DUM(3,3)
      NND = NOD
      CALL SECOND(XT1)
C
C     MODIFY SELF-FLEXIBILITY MATRICES FOR RESTRAINED BOUNDARY NODES
C
      IF(NMG.NE.0) GOTO 18
      SUMLD = 0.
   16 DO 17 N = 1, NND
      IF(ICP(N).NE.0) GOTO 17
      BETA = X(2,N)/X(1,N)
      IF(RPM.LT.1.E-50) BETA = 0.
      CFB(N+3) = SQRT(1. - BETA*X(1,N)/RN(N)*BETA*X(1,N)/RN(N))
      RADFL = (XKT(1,1,N) + BETA*(XKT(4,1,N) + XKT(6,1,N)) +
     1         BETA*BETA*XKT(2,1,N))*CFB(N+3)*CFB(N+3)
      CFA(N) = 1./RADFL
      SUMLD = SUMLD + CFA(N)
      DMU(2,N+3) = 0.
      CFA(N+3) = BETA
   17 CONTINUE
   18 CONTINUE
      IF(NCC.GT.NCY) GOTO 20
      IF(IW.EQ.0) GOTO 20
      WRITE(6,19)
   19 FORMAT(1H1/////15X,39H PROGRESS OF THE GAUSS-SEIDEL ITERATION ,
     1                   20H TOWARDS CONVERGENCE /
     2                15X,39H ----------------------------------- ,
     3                   20H-------------------- ///
     4  5X, 5HCYCLE,1X,14HCURRENT  DIFF.,
     5  2X,47HOVER-REL. FCT.  OPT. OVER-REL.  SPECTRAL RADIUS /)
```

(MODULE 1)

```
      OVR = PSDO = 1.
      DIF = 1.
      OVO = OVS
      POVO = OVO - (2. - OVO)/4.
      NBAD = 0
   20 NC   = 0
   25 SO = SDO = 0.
      SUM = 0.
      CTL = TOL
      DO 34 N = 1, NND
      IF(ICP(N).NE.0.OR.CFC.LT.1.E-4) GOTO 24
      DMU(1,N+3) = AMAX1(0., - DLD(1,N))
      DO 23 I = 1, 3
   23 DLD(I,N) = DLD(I,N) + DMU(I,N)*(DMU(1,N+3) - DMU(2,N+3))
   24 NIA = NAP(N)
      DO 30 I = 1, 3
      Q(I,N) = 0.
      DO 28 IA = 2, NIA
      NP = NAMP(IA,N)
      DO 28 J = 1, 3
      IJ = KVN(I,J)
   28 Q(I,N) = Q(1,N) + XKT(IJ,IA,N)*DU(J,NP)
   30 R(I) = DLD(I,N) - Q(I,N)
      IF(ABS(RN(N)-RMIN).LT.0.01) GOTO 33
      IF(NPC(N).EQ.0) GOTO 26
      IF(RPM.GT.1.E-50) GOTO 27
      IF(N.GT.NIF)      GOTO 27
   26 CONTINUE
      R(2) = - (XKT(6,1,N)*R(1) + XKT(5,1,N)*R(3))/XKT(2,1,N)
      DLD(2,N) = R(2) + Q(2,N)
      IF(ABS(X(3,N)).GT.0.001) GOTO 29
      DEN = XKT(2,1,N)*XKT(3,1,N) - XKT(5,1,N)*XKT(7,1,N)
      R(2) = (XKT(9,1,N)*XKT(5,1,N) - XKT(6,1,N)*XKT(3,1,N))*R(1)/DEN
      R(3) = (XKT(7,1,N)*XKT(6,1,N) - XKT(2,1,N)*XKT(9,1,N))*R(1)/DEN
      DLD(2,N) = R(2) + Q(2,N)
      DLD(3,N) = R(3) + Q(3,N)
      GOTO 29
   27 IF(ABS(X(3,N)).GT.0.001) GOTO 29
      R(3) = - (XKT(9,1,N)*R(1) + XKT(7,1,N)*R(2))/XKT(3,1,N)
      DLD(3,N) = R(3) + Q(3,N)
      GOTO 29
   33 DLD(1,N) = Q(1,N)
      DLD(2,N) = Q(2,N)
      DLD(3,N) = Q(3,N)
      R(1) = R(2) = R(3) = 0.                          (MODULE 2)
   29 DO 31 I = 1, 3
      DDU(I) = - DU(I,N)
      DO 31 J = 1, 3
      IJ = KVN(I,J)
   31 DDU(I) = DDU(I) +  XKT(IJ,1,N)*R(J)
      IF(RPM.LT.1.E-50.AND.N.LE.NIF) DDU(2) = 0.
      IF(ABS(RN(N)-RMIN).LT.0.01) DDU(1) = DDU(2) = DDU(3) = 0.
      IF(NPC(N).EQ.0) DDU(2) = 0.
      IF(ABS(X(3,N)).LT.0.001)        DDU(3) = 0.
      IF(ICP(N).NE.0) GOTO 32
      DDR = CFB(N) = (CFA(N+3)*DDU(2) + DDU(1))*CFB(N+3)*OVR
      SUM = SUM + DDR*CFA(N)
      DMU(2,N+3) = DMU(1,N+3)
```

f) GAUSS

```
   32 DO 34 I = 1, 3
      DU(I,N) = DU(I,N) + OVR*DDU(I)
      SD  = SD  + ABS(DU(I,N))
      SDD = SDD + ABS(DDU(I))
   34 CONTINUE
C
CC    REDISTRIBUTE APPLIED LOADS
C
      FACT = 1.
      DDRM = SUM/SUMLD
      DO 40 N = 1, NND
      IF(ICP(N).NE.0) GOTO 40
      DO 36 I = 1, 9
   36 F(I) = XKT(I,1,N)
      BETA = CFA(N+3)
      PROP = (DDRM - CFB(N))*CFB(N+3)
      DU(1,N) = DU(1,N) + PROP
      DU(2,N) = DU(2,N) + PROP*BETA
      IF(N.NE.N1.OR.NMG.NE.0) GOTO 37
      FACT = DU(1,N1)/RAT
      IF(FACT.GE.2.    ) FACT = 0.5*FACT
      IF(FACT.LT.0.667) FACT = 2.0*FACT
   37 IF(ABS(X(3,N)).LT.0.01) GOTO 38
      FCT = PROP/(F(1)*F(2) - F(4)*F(6))
      DU(3,N) = DU(3,N) +(F(9)*F(2) - F(7)*F(6) +
     1                  BETA*(F(7)*F(1) - F(9)*F(4)))*FCT
      DLD(1,N) = DLD(1,N) + (F(2) - BETA*F(4))*FCT/OVR
      DLD(2,N) = DLD(2,N) - (F(6) - BETA*F(1))*FCT/OVR
      DLD(1,N) = AMIN1(DLD(1,N), -FACT*XLD(1,N))
      GOTO 40
   38 FCT = PROP/OVR/(F(1)*(F(2)*F(3) - F(5)*F(7)) + F(4)*(F(5)*F(9) -
     1    F(6)*F(3)) + F(8)*(F(6)*F(7) - F(2)*F(9)))
      DLD(1,N) = DLD(1,N) + ( F(2)*F(3) - F(5)*F(7)  -
     1                  BETA*(F(4)*F(3) - F(8)*F(7)))*FCT
      DLD(2,N) = DLD(2,N) - ( F(6)*F(3) - F(5)*F(9)  -
     1                  BETA*(F(1)*F(3) - F(8)*F(9)))*FCT
      DLD(3,N) = DLD(3,N) + ( F(6)*F(7) - F(2)*F(9)  -
     1                  BETA*(F(1)*F(3) - F(4)*F(9)))*FCT
      DLD(1,N) = AMIN1(DLD(1,N), -FACT*XLD(1,N))
   40 CONTINUE
C
CC    TEST FOR CONVERGENCE AND REESTIMATION OF OPTIMUM OVER-
C          RELAXATION FACTOR
C
      IF(SD.LT.1.E-35) SD = 1.E-35
      RELDIF = SDD/SD
      NC = NC + 1
      SPRAD = SDD/PSDD
      PSDD = SDD
      IF(NC.EQ.2) OVR = ROVO
      IF(SPRAD.GE.0.96) CTL = 2.*TOL
      IF(SPRAD.GE.0.99) CTL = 5.*TOL
      NBAD = NBAD + 1
      IF(SPRAD.LT.0.995) NBAD = 0
      IF(NBAD.GE.NCY/6) GOTO 58
      IF(NCC.GT.NCY.OR.MOD(NC,NCC).NE.0) GOTO 50
```

(MODULE 2)

(MODULE 3)

(MODULE 4)

```
      IF(IW.EQ.0) GOTO 48
      WRITE(6,49) NC,RELDIF,OVR,OVO,SPRAD
   49 FORMAT(5X,I5,4(1X,F14.5,1X))
   48 IF(SPRAD.GT.1.) GOTO 51
      DDIF = RELDIF - DIF
      DIF = RELDIF
      IF(DDIF.GE.0.) GOTO 51
      DOV = ABS(OVO - POVO)
      POVO = OVO
      OVO = 2./(1.+SQRT(1.-(SPRAD+OVR-1.)*(SPRAD+OVR-1.)/SPRAD/OVR/OVR))
      OVO = AMIN1(OVO,POVO + 0.75*DOV)
      OVR  = OVO - (2. - OVO)/4.
      OVR = AMIN1(OVR,0.8375 + 0.8125*SPRAD)
      OVR = AMAX1(1.01,OVR)
      GOTO 50
   51 OVR = (OVR + 1.)/2.
   50 IF(RELDIF.GT.CTL) GOTO 60
      IF(IW.EQ.0) GOTO 76
      WRITE(6,55) NC
   55 FORMAT(    /////28H THE ITERATION HAS CONVERGED ,
     1        6H AFTER,I5,8H CYCLES.)
      GOTO 70
   58 WRITE(6,59)
   59 FORMAT(//21H THE PROCESS DIVERGES  //
     1          21H EXECUTION TERMINATED )
      STOP
   60 IF(NC.LT.NCY) GOTO 25
      IF(IW.EQ.0) GOTO 76
      WRITE(6,65) NC,RELDIF,CTL
   65 FORMAT(    /////28H THE ITERATION HAS COMPLETED,I5,12H CYCLES, THE/
     1        53H MAXIMUM NUMBER OF CYCLES WITHOUT CONVERGING, BUT HAS /
     2        34H ACHIEVED A RELATIVE DIFFERENCE OF,E13.5, /
     3        33H AGAINST A SPECIFIED TOLERANCE OF,E13.5,1H./
     4        43H THE UNCONVERGED RESULTS ARE WRITTEN BELOW.)
C
C     OUTPUT THE CALCULATED RESULTS
C
   70 WRITE(6,75)
   75 FORMAT(/////
     1        35X,24H DISPLACEMENT INCREMENTS,30X,16H LOAD INCREMENTS /
     2        35X,24H ------------------------,30X,16H ---------------- ///
     3        15X,5H NODE,10X,3H DU,12X,3H DV,12X,3H DW,16X,4H DLU,
     5        11X,4H DLV,11X,4H DLW,6X,8H CONTACT //)
   76 R(1) = R(2) = R(3) = 0.
      RATIO = 1./FACT
      DO 80 N = 1, NND
      DO 78 I = 1, 3
      DLD(I,N) = RATIO*DLD(I,N)
      DU (I,N) = RATIO*DU (I,N)
   78 R(I) = R(I) + DLD(I,N)
      IF(IW.EQ.0) GOTO 90
   80 WRITE(6,85) N,(DU(I,N),I=1,3),(DLD(I,N),I=1,3),ICP(N)
   85 FORMAT(12X,I6,2(5X,3E15.5),I6)
      WRITE(6,88) R
   88 FORMAT(/73X,3E15.5/)
   90 CONTINUE
      WRITE(6,92) NM,RATIO
   92 FORMAT(//5X,I3,38HTH LOAD INCREMENT - SCALING-UP FACTOR ,F10.5/)
```

(MODULE 4)

(MODULE 5)

f) GAUSS

(MODULE 5)

```
      CALL SECOND(XT2)
      DXT = XT2 - XT1
      WRITE(6,200) DXT
  200 FORMAT(5X,15H TIME IN GAUSS ,F10.3,2X,7HSECONDS)
      RETURN
      END
```

g) STIFF

```
      SUBROUTINE STIFF(XKS,B,ME)
C
C     ELEMENTARY STIFFNESS  MATRIX  XK
C
      DIMENSION  A(4,3), D (6,6), XK(12,12), XKS(6),
     1           B(3,3), DE(6,6), DT(6,6,215)
      COMMON     /EMM/ DE,DT    /STF/ XK,A,V6
C
C     STIFFNESS MATRIX IS ASSEMBLED TERM BY TERM
C
      DO 10 I = 1, 6
      DO 10 J = 1, 6
   10 D(I,J) = DT(I,J,ME)
      DO 40 I = 1, 12
      L = 1 + (I - 1)/3
   12 K = MOD(I,3)
      IF(K.EQ.0) K = 3
      FLG = 0.
      DO 40 J = I, 12
      IF(I.NE.J) FLG = 1.
      XK(I,J) = XK(J,I) = 0.
C
      M = 1 + (J - 1)/3
   15 N = MOD(J,3)
      IF(N.EQ.0) N = 3
      IFLG = 1
      IF(K.NE.N) IFLG = 2
      DO 40 I1 = 1, 3
      FACTL = V6*A(L,I1)/6.
      IK = KNV(K,I1)
      DO 40 J1 = 1, 3
      JI = KNV(I1,J1)
      JN = KNV(N,J1)
      FACTA = FACTL*A(M,J1)
C
C     ADD USUAL (SMALL DISPLACEMENT) STIFFNESS TERM
C
      XK(I,J) = XK(I,J) + FACTA*D(IK,JN)
      XK(J,I) = XK(J,I) + FACTA*D(JN,IK)*FLG
C
C
C     ADD INITIAL STRESS STIFFNESS TERM
C
      GOTO(20,30),IFLG
   20 ADD = FACTA*XKS(JI)
      XK(I,J) = XK(I,J) + ADD
      XK(J,I) = XK(J,I) + ADD*FLG
```

g) STIFF

```
C
C       AND NOW ADD INTTIAL DISPLACEMENT STIFFNESS TERM
C
   30 DO 40 M1 = 1, 3
      JM = KNV(J1,M1)
      IM = KNV(I1,M1)
      AD1 = FACTA*(D(IK,JM)*B(N,M1) + D(IM,JN)*B(K,M1))
      DO 40 N1 = 1, 3
      JJ = KNV(J1,N1)
      ADD = AD1 + FACTA*D(IM,JJ)*B(K,M1)*B(N,N1)
      XK(I,J) = XK(I,J) + ADD
      XK(J,I) = XK(J,I) + ADD*FLG
   40 CONTINUE
C
      RETURN
      END
```

h) TSTIFF

```
      SUBROUTINE TSTIFF(NEL,NOD,HD)
C
C     TOTAL STIFFNESS MATRIX  XKT  FOR THE WHOLE SYSTEM
C
      DIMENSION  DMU(3,96), ICP(96), XKT(9,19,96), ND(4,215), DERU(3,3),
     1           DLD(3,96), NAP(96), NANP (19,96), HD  (215), AL(4,3),
     2           U  (3,96), NBC(96), A  (4,3,215), EQS (215), F   (9),
     3           X  (3,96), RN (96), CS   (6,215), V6  (215), PROV(9),
     4           XLD(3,96), XKL (6), XKS  (6,215), XK(12,12), LN  (4)
      COMMON     DUMM(2,96),XKT,NANP,NAP,ICP,DLD,XLD,NBC,RN,DMU,
     1           ND,XKS,CS,EQS,A,V6
     2           /CRD/ X     /DSP/ U,DERU
     1           /STF/ XK,AL,V6L
C
C       PREPARE TO SUM STIFFNESS COEFFICIENTS
C
        NND = NOD
        DO 6 N = 1, NND
        DO 5 IQ = 1, 19
        NANP(IQ,N) = 0
        DO 5 J = 1, 9
     5  XKT(J,IQ,N) = 0.
        NANP(1,N) = N
        NAP(N) = 1
     6  CONTINUE
C
C       FORM ELEMENTAL STIFFNESS MATRICES
C       ASSEMBLE TOTAL STIFFNESS MATRIX
C
        CALL SECOND(XT9)
     4  DO 32 M = 1, NEL
        DO 1 I = 1, 12
        DO 1 J = 1, 12
     1  XK(I,J) = 0.
        V6L = V6(M)
        HDL  = HD(M)
        DO 8 I = 1, 6
        XKL(I) = XKS(I,M)
```

```
      IF(I.GT.4) GOTO 8
      LN(I) = ND(I,M)
      DO 7 J = 1, 3
    7 AL(I,J) = A(I,J,M)
    8 CONTINUE
      CALL DERIV(LN,AL)
      IF(HDL.LT.1000.) GOTO 10
      CALL FIRST(XKL,DERU,M)
      GOTO 15
   10 CALL STIFF(XKL,DERU,M)
   15 DO 28 L1 = 1, 4
      N = LN(L1)
      DO 27 L2 = 1, 4
      IQ = 0
   16 IQ = IQ + 1
      IF(IQ.LE.19) GOTO 20
      WRITE(6,18) N
   18 FORMAT(1H1///// 5H NODE,I5,15H HAS MORE THAN  /
     1                27H  EIGHTEEN ADJACENT NODES  //
     2                26H THE PROBLEM IS ABANDONED )
      STOP
   20 IF(NANP(IQ,N).EQ.LN(L2)) GOTO 25
      IF(NANP(IQ,N).NE.0)      GOTO 16
      NANP(IQ,N) = LN(L2)
      NAP(N) = IQ
   25 DO 26 I = 1, 3
      L3 = 3*L1 + I - 3
      DO 26 J = 1, 3
      L4 = 3*L2 + J - 3
      IJ = KVN(I,J)
   26 XKT(IJ,IQ,N) = XKT(IJ,IQ,N) + XK(L3,L4)
   27 CONTINUE
   28 CONTINUE
   32 CONTINUE
      CALL SECOND(XT10)
      DXT9 = XT10- XT9
      WRITE(6,500) DXT9
  500 FORMAT(2X,35H OVERALL SCANNING OF ELEMENTS TAKES,F10.3,2X,
     1       8H SECONDS )
C
C     BY INVERSION OF THE MAIN DIAGONAL STIFFNESS SUBMATRIX, FIND THE
C     FLEXIBILITY SUBMATRIX AT EACH NODE, DISPLACED BY FORCES AT ITSELF
C
      DO 70 N = 1, NND
      DO 33 I = 1, 9
   33 PROV(I) = XKT(I,1,N)
      DLT = PROV(1)*(PROV(2)*PROV(3) - PROV(5)*PROV(7)) +
     1      PROV(6)*(PROV(7)*PROV(8) - PROV(3)*PROV(4)) +
     2      PROV(9)*(PROV(4)*PROV(5) - PROV(8)*PROV(2))
         F(1) = PROV(2)*PROV(3) - PROV(5)*PROV(7)
         F(2) = PROV(1)*PROV(3) - PROV(8)*PROV(9)
         F(3) = PROV(1)*PROV(2) - PROV(4)*PROV(6)
         F(4) = PROV(8)*PROV(7) - PROV(4)*PROV(3)
         F(5) = PROV(8)*PROV(6) - PROV(1)*PROV(5)
         F(6) = PROV(5)*PROV(9) - PROV(6)*PROV(3)
         F(7) = PROV(4)*PROV(9) - PROV(1)*PROV(7)
         F(8) = PROV(4)*PROV(5) - PROV(8)*PROV(2)
         F(9) = PROV(6)*PROV(7) - PROV(2)*PROV(9)
```

h) TSTIFF

```
      IF(ABS(DLT).LT.1.E-60) DLT = SIGN(1.E-60,DLT)
C
      DO 60 I = 1, 9
   60 XKT(I,1,N) = F(I)/DLT
   70 CONTINUE
      CALL SECOND(XT11)
      DXT10 = XT11 - XT10
      WRITE(6,600) DXT10
  600 FORMAT(2X,35H OVERALL SCANNING OF  MODES   TAKES,F10.3,2X,
     1       8H SECONDS )
  100 RETURN
      END
```

APPENDIX 3

EPFELDA

LISTING OF VARIABLES

CONVENTION	
ia - Integer array variable	ra - Real array variable
is - Integer single variable	rs - Real single variable
par - Function or subroutine parameters	

MAIN PROGRAM

A	ra	/ /	Cofactors of volume determinants for all elements
AL	ra		Cofactors of volume determinant for one element
APL	rs		Trial value of total external initial load
BULK	rs		Bulk modulus of specimen material
CAN	rs		Angular coordinate of a node, used solely to compute the nodal Cartesian coordinates
CFC	rs		Coulomb friction factor
CF1,CF2	rs		Parameters of the prescribed stress-strain curve
CH	rs		Hydrostatic stress for an element
COMPAR	rs		Comparison parameter, initialized as zero, but changed to unity whenever the application of the initial stress procedure is required
CS	ra	/ /	Cauchy stresses for all elements
CSE	ra		Working vector used to store the elemental components of either the Truesdell or the Cauchy (true) stress increments (in Module 5); an interim stress

MAIN PROGRAM (Contd.)

			vector, correct stress increments and residual stresses (successively in Module 7)
CSI	rs		Central angle of basic block
CSIM	rs		Total central angle covered by the mesh
C1,C2	rs		Auxiliary parameters in the generation of new load increments, in the radial upsetting problem
D	ra	EMM	Lagrangean elastic-plastic material (constitutive) matrices for all elements in the mesh
DC	ra		Director cosines of the external applied nodal forces
DCE	ra		Incremental Almansi strain vectors for an element
DCS	ra		Interim stress increments (Modules 5 and 7) and corrected Truesdell stress increments (Module 7), for all elements in the finite element mesh
DCSH	rs		Hydrostatic component of corrected stress increments
DDR	rs		Incremental radial penetration achieved in one load increment
DE	ra	EMM	Elastic (Eulerian) constitutive matrix
DEDU	ra		The elemental increments $\Delta u_{i,j}$
DEN	rs		Denominator in the generation of C1 and C2
DENOM	rs		Denominator in the computation of the equivalent plastic strain increment
DEQE	ra		Total plastic strain increments, for all elements in the finite element mesh, corresponding to a load increment (after the last initial stress corrective cycle)
DEQIN	rs		Plastic strain increment for an element, during one cycle in the initial stress method
DEQN	rs		Local variable, stores an eventual negative component of the array DEQE for print-out and execution termination
DERU	ra	DSP	The elemental derivatives $u_{i,j}$ for one element
DGS	ra		Green strain increments for all elements
DINCR	rs		Parameter used to progressively increase the magnitude of the successive load increments or eventually to "moderate" them, in case of risk of plastic instability
DKS	ra		Kirchhoff stress increments for all elements
DLD	ra	/ /	Active or reactive load increments for all nodes in the finite element mesh
DMU	ra	/ /	Nodal friction functions (The factors multiplying |P| in Eqns. (4-3a,b,c))

MAIN PROGRAM (Contd.)

DR	rs		Total radial penetration of roller
DTIME	rs		Time increment between successive load increments
DU	ra	GSS	Displacement increments for all nodes in the mesh
DXNT	ra	EDI	The derivatives $X_{i/j}$ for one element in the mesh
DXST	ra	EDI	The derivatives $x_{j,i}$ for one element in the mesh
E	rs		Young's modulus of specimen material
EQE	rs		Interim value of the equivalent stress for an element at several stages of Module 7
EQPS	ra		Total plastic strains for all elements in mesh
EQS	ra	/ /	Equivalent stress for all elements in the mesh
F	rs		The distance f in Eqn. (4-9a) and Fig. 4-6
FACT FACTA FACTB FACT1 FACT2	rs		Working variables representing intermediate factors in several expressions
G	rs		Shear modulus of specimen material
G1,G2	rs		Working variables, depending on G and XNU, used when assembling matrices DE and D
G3	rs		Slope of of the stress-strain curve in a triaxial elastic situation
HD	ra		Instantaneous slope of the stress-strain curve for all elements (elastic or plastic)
HDIF	rs		The interim slope $\hat{H}'$, from Eqn. (3-23)
HDL	rs		Local variable storing the elemental value of HD
HDLC	rs		Corrected (final) slope of the stress-strain curve, in an initial stress corrective cycle
I,J,K,L	is		Running indices in several DO-loops
ICP	ia	/ /	Parameter defining if a node is in contact with the roller (ICP = 0) or not (ICP = 1)
IJ,IK, JK,KL, LK,M1	is		Derived indices, generally used when calling the function KNV
IPN	is		A denominator, depending on the number of unstable elements (NYL), used in the redefinition of the parameters STP and DINCR, to minimize the risk of plastic instability problems
IW	is		Parameter defining the amount of data to be written out. If IW = 1, all data are produced, and if IW = 0, only a limited part is written out
LN	ia		Local variable, listing the elemental node numbers, for one element

MAIN PROGRAM (Contd.)

L1,L2	is		Index of particular components of the array LN ; also derived indices
M	is		Running index, generally used when scanning elements
N	is		Running index, generally used when scanning nodes
NANP	ia	/ /	Indices of each particular node in the finite element mesh, and of the nodes connected to it
NAP	ia	/ /	Number of nodes connected to every particular node in the mesh, plus one for the node itself
NB	is		Running index, scanning the basic blocks
NBC	ia	/ /	Parameter defining the node boundary condition: NBC = 2 External cylindrical mantle NBC = 1 Side face NBC = 0 Mesh boundaries with the rest of specimen NBC = -1 Interior nodes The mid-plane condition is checked directly from the X_3 - coordinate
NBL	is		Number of basic blocks in the finite element mesh
NCC,NCY	is		Parameters of over-relaxation (See GAUSS)
ND	ia	/ /	Indices of the elemental nodes, for all elements
NE	is		Running index used in extending the previous indices from the first to the subsequent basic blocks
NEB	is		Number of elements in the basic block
NEL	is		Total number of elements in the whole mesh
NEQ	is		Parameter used to divert and stop execution if negative plastic strain increments are encountered; usually set to zero, it is set to unity if this condition occurs
NF	is		Running index used to scan nodes when computing nodal coordinates, and in other applications
NI	is		Running index, scans mid-plane nodes in the external cylindrical mantle
NIF	is		Number of nodes in the interfaces between adjacent nodes
NLL	is		Index defining the number of basic blocks preceding the nodes initially loaded
NM	is		Index defining the number of load increments
NMD	is		Number of mid-plane nodes in the external cylindrical mantle
NMG	is		Index defining the number of order of the corrective initial stress cycles
NMGL	is		Input parameter defining the maximum number of corrective initial stress cycles
NMGO	is		The same limiting parameter, but set to a local variable and eventually reduced in magnitude

MAIN PROGRAM (Contd.)

NMP	ia		Indices of the mid-plane nodes lying in the external cylindrical mantle
NN	is		Index scanning nodes in the block interfaces
NND	is		Total number of nodes in the whole mesh
NS	is		Index counting the number of load increments applied over one basic block
NSUB	is		Maximum number of load increments applied over a basic block
NYL	is		Number of plastically unstable elements (that is, for which HD is less than EQS)
NYLIM	is		Number of elements surpassing the maximum prescribed plastic strain (0.3)
N1	is		Index of first loaded mid-plane node
N3,N4	is		Index of loaded nodes situated in the cylindrical mantle and on the last loaded radial plane
OVS	rs		Input parameter, initial over-relaxation factor (to be transferred to GAUSS)
PCS	ra		Local vector, stores previous values of the elemental stresses
PDR	rs		Previous value of DR
PEQS	rs		Previous value of EQS for an element
PHD	rs		Previous value of HD for an element
PHLC	rs		Previous value of HDLC
PI	rs		The number $\pi = 3.14159$
PRESC	rs		Maximum prescribed value of radial penetration, used in a termination criterion (Input parameter)
PREV	rs		Previous value of APL
R	rs		A factor in the plastic component of the elastic-plastic constitutive matrix
RANG	rs		Rotation angle (in multiples of CSI)
RAT	rs		Multiplying factor used (in GAUSS) to round off the produced value of radial penetration
RATEQ	rs		The parameter ζ of Eqn. (3-28), for one element
RD	ra		Parameter defining if there is the need to estimate residual forces corresponding to the residual stresses over an element (RD = 1.) or not (RD = 0.)
RDS	rs		Distance from a node to the axis of the forming roller, used to define contact
REL	rs		Working variable, expresses a ratio of slopes
RI	rs		Instantaneous radial coordinate of a node
RMIN	rs		Radius of the internal cylindrical mantle of the mesh

MAIN PROGRAM (Contd.)

RN	ra	/ /	Radial coordinates (original) of all nodes
RO	rs		Radius of undeformed specimen, mm
RPM	rs		Angular velocity of specimen, in rpm
RR	rs		Radius of forming roller, mm
SN	rs		As variable NS, but converted to real form
STEP	rs		Input parameter, defining the basic increment in applied force in the successive load increments
STI	rs		Maximum instantaneous semithickness of deformed mesh
STP	rs		Minimum value of radial displacement produced in a load increment
SUB	rs		As NSUB, but converted to real form
TEMP	rs		Forming temperature, in ^{o}C
TFC	rs		Input parameter used to define the third (axial) coordinate of a node
TH	rs		Original (undeformed) thickness of specimen, mm
TIME	rs		Time elapsed since the beginning of deformation
TOL	rs		Parameter of the over-relaxation problem (See GAUSS)
U	ra	DSP	Total displacements, for all nodes in the mesh
V6	ra	/ /	Volumes of all elements in the mesh (times six)
W	ra		Absolute value of force acting over a node
WP	rs		Interim value of W., for one node, in the "initial load" correction
X	ra	CRD	Original (undeformed) Cartesian coordinates for all nodes, mm
XD	ra	/ /	Dummy array residing in the unlabelled common block
XE1,XE2	rs		Instantaneous first two coordinates of a node
XI1,XI2	rs		Instantaneous first two coordinates of node N1
XJC	rs	EDI	Jacobean of the original/instantaneous coordinate transformation
XKS	ra	/ /	Kirchhoff stresses for all elements in the mesh
XKSE	ra		Local vector storing Kirchhoff stresses, or their increments, for one element of the mesh
XL	ra		Interim components of XLD, for one node, in the "initial load" correction
XLD	ra		Total (active or reactive) nodal loads
XNU	rs		Poisson's ratio of specimen material
YCOMP	rs		New value of the yield stress for an element, following a load increment
YELD1	ra		Yield stresses for all elements, at the start of a load increment

MAIN PROGRAM (Contd.)

YFUN	rs		Parameter of the prescribed stress-strain curve
YIELD	rs		Yield stress of undeformed material, at the temperature TEMP , in MN/m^2

Function EQST

CS	ra	par	Stress vector for one element
EQST	rs		Resulting equivalent stress (Output)

Functions KNV and KVN

I,J	is	par	Input indices
K	is		Intermediate derived index
KNV or KVN	is		Output indices

Function RATST

A	rs		Equivalent to $-\Gamma$, in Eqn. (3-28)
B	rs		The denominator in the same equation
DCH	rs		Hydrostatic component of incremental stresses
DCS	ra	par	Incremental stresses for one element
EQE	rs	par	Present equivalent stress for the element (k , in Eqn. (3-28)
I	is		Running index
PCH	rs		Hydrostatic component of total stresses
PCS	ra	par	Total stresses for one element
PEQS	rs	par	Previous equivalent stress for the element ($\bar{\bar{s}}$, in Eqn. (3-28)
RATST	rs		The parameter of Eqn. (3-28) (Output)

Subroutine COEFF

A	ra	par	Elemental components of the array A described in EPFELDA (Thus corresponding to a set AL)
B	ra		Vector storing the cofactors of the fourth column of the volume determinant
J,K,L,N	is		Indices replacing the components of ND in the four possible cyclic permutations
ND	ia	par	Indices of the elemental nodes
N1	is		Running or substitutional index

Subroutine COEFF (Contd.)

V6	rs	par	Elemental volume (times six)
X	ra	CRD	As in the Main Program

Subroutine DERIV

A	ra	par	As in COEFF
ADD	rs		Working variable, additive term to DXNT
DERU	ra	DSP	As in the Main Program
DXNT, DXST	ra	EDI	As in the Main Program
I,J	is		Indices (internal and global) of the elemental nodes
M,N	is		Running indices
M1,M2, N1,N2	is		Derived indices
ND	ia	par	As in COEFF
U	ra	DSP	As in the Main Program
XJC	rs	EDI	As in the Main Program

Subroutine DERI2

A	ra	par	As in COEFF
DEDU	ra	par	As in the Main Program
DU	ra	GSS	As in the Main Program
I,J	is		Indices (internal and global) of the elemental nodes
M,N	is		Running indices
ND	ia	par	As in COEFF

Subroutine EPMM

CD	ra		Deviatoric stresses for one element
CH	rs		Hydrostatic stress for one element
CS	ra	par	As in EQST
D	ra		Elastic-plastic (Eulerian) constitutive matrix for one element, from Eqn. (2-24)
DE	ra	EMM	As in the Main Program
DEP	ra		Elastic-plastic (Lagrangean) constitutive matrix for one element, from Eqn. (2-32)

Subroutine EPMM (Contd.)

DT	ra	EMM	Equivalent to the array D in the Main Program
DXNT, DXST	ra	EDI	As in the Main Program (DXST dummy in this subroutine)
FAA, FAB, FAC	rs		Working variables (Intermediate factors at several stages in the subroutine)
I, J, K, L M1, M2, N1, N2	is		Running indices
M	is	par	Index of the element under consideration
IJ, KL, MN, NM1	is		Indices derived via function KNV
R	rs	par	As in the Main Program
XJC	rs	EDI	As in the Main Program

Subroutine FIRST

A	ra	STF	As in COEFF
ADD	rs		Working variables representing terms to be added to XK
B	ra	par	As DERU in the Main Program
CS	ra	par	As in EQST
D	ra		As DEP in EPMM
DE, DT	ra	EMM	As DE and D in the Main Program
FACTA, FACTL	rs		Working variables, intermediate factors
FLAG	rs		Discriminator for initial stress stiffness term (Real Kronecker delta)
FLG	rs		Discriminator to avoid computing the elements in the main diagonal of XK twice (Also a Kronecker delta)
I, J, K, L I1, J1, M1	is		Running indices
IJ, IM, JM, K, KI L, M, N, NJ	is		Derived indices
ME	is	par	Index of the element under consideration
V6	rs	STF	As in COEFF
XK	ra	STF	The elemental stiffness matrix

Subroutine GAUSS

BETA	rs		Angular parameter in the load redistribution
CFA,CFB	ra	/ /	Working arrays storing factors involved in the load redistribution
CTL	rs		A local variable replacing TOL , and eventually reducing its value
DDIF	rs		Change in the parameter RELDIF between successive corrections of the over-relaxation factor
DDR	rs		Residual of the radial displacement, for a node in the contact zone
DDRM	rs		Weighted average of these residuals
DDU	ra		Displacement residuals for a node
DIF	rs		The previous value of RELDIF
DLD	ra	/ /	As in the Main Program
DOV	rs		Change in the over-relaxation after a reestimation
DU	ra	GSS	As in the Main Program
DUM	ra	DSP	Dummy array in this subroutine
DXT	rs		Time consummed by the subroutine, CDC 6600 seconds
F	ra		Local array storing the nodal self-flexibilities
FACT	rs		Working variable, equals the inverse of RATIO
FCT	rs		Working variable, an intermediate factor in some calculations
I,J	is		Running indices in several DO - loops
IA	is		Running index scanning the interconnection of nodes
ICP	ia	/ /	As in the Main Program
IJ	is		Derived index, from the application of function KVN
IW	is	par	As in the Main Program
N	is		Running index scanning all nodes
NANP, NAP,NBC	ia	/ /	As in the Main Program
NBAD	is		Parameter counting the number of consecutive cycles presenting a spectral radius greater than 0.995
NC	is		Index counting the number of cycles in the successive over-relaxation procedure
NCC	is	par	Number of cycles after which a new estimate of the optimum over-relaxation factor is made, and an output is produced, on the progress of the iteration
NCY	is	par	Parameter prescribing the maximum number of over-relaxation cycles

Subroutine GAUSS (Contd.)

ND	ia	/ /	As in the Main Program
NIA	is		Local variable, stores the NAP content for a particular node
NIF,NM, NMG,N1	is	par	As in the Main Program
NND	is		As in the Main Program
NOD	is		As NND
NP	is		Index of a node which is connected to another (reference) node
OVO	rs		Current estimate of the optimum over-relaxation factor
OVR	rs		Current estimate of the over-relaxation factor
OVS	rs	par	As in the Main Program
POVO	rs		Previous estimate of OVO
PROP	rs		Working variable used in connection with DDRM
PSDD	rs		Previous value of the norm SDD
Q	ra		Internal force increments, for all nodes
R	ra		Equivalent force increments, for one node
RADFL	rs		Radial-radial self-flexibility component of an externally loaded node
RAT	rs	par	As in the Main Program
RATIO	rs		Multiplication factor to correct displacement and force increments
RELDIF	rs		Convergence criterion parameter in the successive over-relaxation procedure
RMIN	rs	par	
RN	ra	/ /	As in the Main Program
RPM	rs	par	
SD	rs		Sum of the absolute values of the computed displacements at the end of a cycle
SDD	rs		Norm, or sum of the absolute values of the residuals of displacements, at the end of a cycle
SPRAD	rs		Spectral radius
SUM, SUMLD	rs		Numerator and denominator, respectively, in the expression of DDRM
TOL	rs	par	Convergence tolerance prescribed in the successive over-relaxation procedure
U	ra	DSP	As in the Main Program
X	ra	CRD	
XDUM	ra	/ /	Real dummy array residing in the unlabelled common block
XKT	ra	/ /	Total stiffness matrix for all nodes

Subroutine GAUSS (Contd.)

XLD	ra	/ /	As in the Main Program
XT1,XT2	rs		Execution time at the beginning and end of the subroutine, in CDC 6600 seconds, respectively

Subroutine STIFF

A	ra	STF	As in COEFF
ADD,AD1	rs		Working variables, added to XK
B	ra	par	As DERU in the Main Program
DE DT	ra	EMM	As DE and D in the Main Program
FACTA, FACTL	rs		Working variables, intermediate factors at several stages of execution
FLG	rs		As in FIRST
IFLG	is		As FLAG in FIRST, but in integer form
I,I1, J,J1, K,L, M1,N1	is		Running indices in several DO - loops
IK,IM, JI,JJ, JM,JN	is		Indices derived via function KNV
K,L,M,N	is		Indices derived from the pair (I,J)
ME	is	par	As in FIRST
V6	rs	STF	As in COEFF
XK	ra	STF	As in FIRST
XKS	ra	par	Kirchhoff stress components for one element

Subroutine TSTIFF

A	ra	/ /	As in the Main Program
AL	ra	STF	As A in COEFF
CS	ra	/ /	
DERU	ra	DSP	As in the Main Program
DLD,DMU	ra	/ /	
DLT	rs		Determinant of the self-stiffnesses, for a node
DUMM	ra	/ /	Dummy array residing in the unlabelled common
DXT9, DXT10	rs		Time required by the subroutine to scan elements (and assemble the stiffness matrix), and to scan nodes (and invert the self-stiffnesses) respectively
EQS	ra	/ /	As in the Main Program

Subroutine TSTIFF (Contd.)

F	ra		As in GAUSS
HD HDL	ra rs	par	As in the Main Program
I,J	is		Running indices in several DO - loops
ICP	ia	/ /	As in the Main Program
IJ	is		Derived index (via function KVN)
IQ	is		As in the Main Program
LN	ia		As in the Main Program
L1,L2	is		Running indices scanning the elemental nodes
L3,L4	is		Derived indices, in the two-dimensional representation of the stiffness matrix
M	is		Running index scanning the elements in the mesh
N	is		Running index scanning the nodes in the mesh
NANP NAP NBC ND	ia	/ /	As in the Main Program
NEL	is	par	As in the Main Program
NND	is		As in the Main Program
NOD	is		As NND
PROV	ra		Interim array storing nodal self-stiffnesses, prior to inversion
RN	ra	/ /	
U	ra	DSP	As in the Main Program
V6	ra	/ /	
V6L	rs		Local variable, the volume of one element (times 6)
X	ra	CRD	As in the Main Program
XK	ra	STF	As in FIRST
XKL	ra		Local vector storing the elemental Kirchhoff stress components
XKS	ra	/ /	As in the Main Program
XKT	ra	/ /	As in GAUSS
XLD	ra	/ /	As in the Main Program
XT9, XT10 XT11	rs		Execution times at the beginning of TSTIFF, after the assembly of XKT and at the end of TSTIFF, respectively

APPENDIX 4

TEMPERATURE DISTRIBUTION IN THE RADIAL UPSETTING OF A FLAT DISC

PROCEEDINGS OF THE

SECOND NORTH AMERICAN METALWORKING

RESEARCH CONFERENCE

Univ. of Wisconsin

Madison

pgs. 60 - 72

May 1974

TEMPERATURE DISTRIBUTION IN THE RADIAL UPSETTING OF A FLAT DISC

ARNO BLASS, Professor
University of Santa Catarina, Florianopolis, Brazil - at present with the Department of Mechanical Engineering, Imperial College of Science and Technology, London, U.K.

DR. B. LENGYEL, Senior Lecturer
Department of Mechanical Engineering, Imperial College of Science and Technology, London, U.K.

ABSTRACT

A clamped disc is heated locally along part of its circumference while rotated around its axis in such a manner, that the hot portion subsequently contacts a roller which forces the material radially inwards raising the thickness of the disc locally. In order to determine the required initial temperatures applied by the heat source, in this case an induction coil, the temperature distribution in the deforming region is calculated as a function of the contact time between disc and roller and in terms of the initial temperatures of the disc, clamps and roller respectively. Heat transfer in the disc and between clamps and disc on the one hand and roller and disc on the other, are considered. The computed temperatures are then used in selecting the relevant stress/strain data for the material elements when theoretical values of stresses, strains and forming loads are determined.

INTRODUCTION

In metalworking normally large lumps of material are formed, requiring the application of vast forces, enormous equipment and large initial capital outlay. If the deformation could be confined to smaller volumes of material at a time, that is if processes could be developed to work the material in stages, in a step-wise manner, initial equipment cost could be greatly reduced (particularly important in low-volume production) and new ways of producing particular shapes developed.

One such stage-by-stage method is the edge upsetting of a flat disc by rolling which could become particularly important in the forming of thick flanges on engineering components made of thinner materials.

In the experimental apparatus a slowly rotating disc (1) representing the flange is heated locally by a stationary induction coil (2) and subsequently the material is radially formed by a roller (3) to raise the cross-sectional area of the disc locally. As the disc rotates the deformation is extended to its full circumference. Subsequently the roller is moved by a small amount radially towards the centre of the disc and the process is repeated. In this manner thick flanges could be built up on a thin-walled

component pre-formed, for example, by sheet drawing. Separate shaping tools (4,5) can be added to allow material flow only in the desired direction, resulting in a very versatile process.

A knowledge of the temperature distribution in the forming region is important for the theoretical analysis of the process, since different temperatures bring about different material properties, altering the energy requirements of the process. It is necessary to know the stress/strain relations which must be assigned to particular material elements when strains, stresses and forming loads are determined theoretically. Furthermore, conclusions relating to the properties of the product can be drawn only if the temperature distribution is known.

Temperature computations in various metalworking processes have been carried out by several workers [1,2,3], a field of research activity adequately covered by a number of surveys [4,5]. In the following a method of determining the temperature distribution in a disc in the deformation zone during edge rolling will be outlined and its application will be illustrated on an example.

MATHEMATICAL FORMULATION

Fig 2 illustrates the simplified model used in the derivations. The region of the specimen disc, in which the temperature distribution is computed, is bounded by straight lines $\overline{S_0S_0'}$ and $\overline{S_1S_1'}$ and by circular arcs S_0S_1 at the specimen-roller interface and $S_0'S_1'$ at the specimen-clamp interface. Adjoining the circular area S_0S_1 is the zone of plastic deformation, not shown in this illustration.

The material enters this region along $\overline{S_0S_0'}$ at time $t = 0$ and leaves it along $\overline{S_1S_1'}$ at time t_1. An intermediate position is reached at $\overline{SS'}$ at time t. As the radial penetration of the roller Δ is very small, it is assumed that $\overline{S_0S_0'} = \overline{SS'} = \overline{S_1S_1'} = R$. The error in this assumption is less than 2 mm over $R = 60$ mm, about 3%.

The initial temperature distribution along $\overline{S_0S_0'}$ has been found by experiments and is shown in the inset in Fig 2. This temperature distribution is one of the boundary conditions, expressed by equation (7). The temperature at the clamp T_c is a function of the initial temperature of the disc. T_s has been determined by experiments and can be expressed as $T_c\,^{o}C = 250 + 0.18\ T_s\,^{o}C$.

On passing through this zone the temperature of the disc material changes due to heat conduction within the disc and due to heat losses to the roller and to the clamps. The temperature changes in the roller are taken into account when calculating the temperature distribution in the disc, but the temperature of the clamps is assumed to remain constant at its initial value. This assumption is justified by the large mass of the clamps, shaft, etc., relative to that of the disc. Convection losses have at first been considered but found small, so in the following they are neglected, consequently the thickness of the specimen-disc has no effect on the calculations.

The instantaneous geometric coordinates of an element of material are determined by distance r from the disc-roller interface, at angle β from $\overline{S_0S_0'}$, Fig 2. In the following, indices r, s and c refer to the roller, specimen-disc and clamps respectively. (Notation is given at the end of the paper.)

The temporal coordinate is defined by

$$t = \frac{\beta}{\beta_r} \cdot t_1 \quad , \tag{1}$$

where

$$t_1 = \frac{30\beta_s}{\pi\omega} \quad \text{sec}, \tag{2}$$

β_s and β_r being the enclosed angles, given, due to their small values, by

$$\beta_r = \cos^{-1}\left(1 - \frac{\Delta}{R_r}\right) \tag{3}$$

and

$$\beta_s = \frac{R_r}{R_s} \cdot \beta_r \cdot \tag{4}$$

Let the temperature of a point in the instantaneous situation be $T(r,t)$. The governing differential equation is then [6,7,8,9]

$$\frac{\partial T}{\partial t} = c\,\frac{\partial^2 T}{\partial r^2} \quad , \tag{5}$$

c being the diffusivity of the material in question, either the roller's or the specimen's, as appropriate. The boundary conditions are

$$\left.\begin{aligned} \frac{\partial T}{\partial r}(-R_r,t) &= 0, \\ K_r\,\frac{\partial T}{\partial r}(0^-,t) &= K_s\,\frac{\partial T}{\partial r}(0^+,t), \\ T(R,t) &= T_c \end{aligned}\right\} \tag{6}$$

The initial condition should express the temperature distribution along $\overline{S_0S_1'}$ when the material enters the forming region. A distribution compatible with the experimental observations is

$$T(r,0) = \left\{\begin{array}{ll} T_r & r < 0 \\ T_s & 0 < r \le R/2 \\ T_c\left[\dfrac{T_s}{T_c}\right]^{2(1-r/R)} & R/2 < r \le R \end{array}\right\} \tag{7}$$

The coordinate r is taken from the roller/disc interface. At $r = 0$ a weighted mean of T_r and T_s applies, the weights being the conductivities of the materials in contact.

Introducing non-dimensional quantities

$$\rho = \frac{r}{R}, \quad \tau = \frac{t}{t_1} \quad \text{and} \quad \theta = \frac{T(r,t) - T_c}{T_s - T_c} \tag{8}$$

Differential equation (5) then becomes

$$\frac{\partial\theta}{\partial\tau} = \frac{t_1 c}{R^2} \cdot \frac{\partial^2\theta}{\partial\rho^2}, \tag{9}$$

and boundary conditions (6)

$$\begin{aligned} &\frac{\partial\theta}{\partial\rho}(-\rho_r,\tau) = 0, \\ &K_r \frac{\partial\theta}{\partial\rho}(0^-,\tau) = K_s \frac{\partial\theta}{\partial\rho}(0^+,\tau), \\ &\theta(1,\tau) = 0. \end{aligned} \tag{10}$$

Initial condition (7) becomes

$$\theta(\rho,0) = \begin{cases} \theta_r & \rho < 0 \\ 1 & 0 < \rho \leq 1/2 \\ \dfrac{T_c}{T_s - T_c}\left[\left[\dfrac{T_s}{T_c}\right]^{2(1-\rho)} - 1\right] & 1/2 < \rho \leq 1. \end{cases} \tag{11}$$

An analytical solution by separation of variables, as described, in Ref. 8, Vol.2, p.589, may be tried. The solution obtained would be expressed as

$$\theta(\rho,\tau) = \sum_{m=1} e^{-\lambda_m^2\tau} A_m \frac{K_s}{K_r}\sqrt{\frac{c_r}{c_s}} \cot\left[\frac{\lambda_m R}{\sqrt{t_1 c_s}}\right]\left[\cot\left[\frac{\lambda_m R\rho_r}{\sqrt{t_1 c_r}}\right]\cos\left[\frac{\lambda_m R\rho}{\sqrt{t_1 c_r}}\right] - \sin\left[\frac{\lambda_m R\rho}{\sqrt{t_1 c_r}}\right]\right] \quad (\rho \leq 0)$$

or

$$\theta(\rho,\tau) = \sum_{m=1} e^{-\lambda_m^2\tau} A_m \left[\cos\left[\frac{\lambda_m R\rho}{\sqrt{t_1 c_s}}\right] - \cot\left[\frac{\lambda_m R}{\sqrt{t_1 c_s}}\right]\sin\left[\frac{\lambda_m R\rho}{\sqrt{t_1 c_s}}\right]\right] \quad (\rho \geq 0) \tag{12}$$

with the eigenvalues λ_m given by the indicial equation

$$\frac{K_s}{K_r}\sqrt{\frac{c_r}{c_s}} \cot\left[\frac{\lambda_m R}{\sqrt{t_1 c_s}}\right] \cot\left[\frac{\lambda_m R\rho_r}{\sqrt{t_1 c_r}}\right] = 1 \tag{13}$$

and the coefficients A_m judiciously chosen to satisfy the initial condition.

First the eigenvalues would have to be obtained from the indicial equation by numerical methods and the coefficients would be computed afterwards by successive trials, up to an order leading to a reasonably good description of the initial condition [9]. The cumbersomeness of such a procedure is evident. The selection of the coefficients A_m could be improved by imposing that the initial conditions should be exactly satisfied in at least a specified number of points in the integration interval. For this purpose, one of the weighted residual methods could be used [10].

In the following a simpler numerical procedure will be applied for the direct integration of the differential equation. An implicit method is preferable [11], in order to allow a stable solution for larger time increments, thus reducing the computing time. Crank-Nicholson's method is used in what follows.

Assume the integration interval $[-\rho_r,1]$ is divided into N-1 subintervals of length $\Delta\rho$, and that the N_0-th node coincides with $\rho = 0$. Assume also a time increment $\Delta\tau$. Let $\theta_{i,j}$ denote the temperature at the i-th geometrical node and at the j-th temporal node; $j = 1$ denotes the initial condition. The differential equation can then be rewritten in difference form by means of Crank-Nicholson's formula [11]

$$\frac{\theta_{i,j+1}-\theta_{i,j}}{\Delta\tau} = \frac{tc}{2R^2\Delta\rho^2}\left[\theta_{i+1,j+1}-2\theta_{i,j+1}+\theta_{i-1,j+1}+\theta_{i+1,j}-2\theta_{i,j}+\theta_{i-1,j}\right] \tag{14}$$

By denoting

$$\alpha = \frac{2R^2\Delta\rho^2}{\Delta\tau t_1 c} \tag{15}$$

and

$$S_i = \theta_{i+1,j} + (\alpha - 2)\,\theta_{i,j} + \theta_{i-1,j} \tag{16}$$

equation (14) becomes

$$-\theta_{i-1,j+1} + (\alpha + 2)\,\theta_{i,j+1} - \theta_{i+1,j+1} = S_i\,. \tag{17}$$

The values of α from equation (15) are different for roller and specimen. The right-hand side term in equation (17) expresses a function of the known temperatures at three adjacent nodes at time τ while the left-hand side gives the temperatures at the same nodes, but at time $\tau + \Delta\tau$. The equation will not apply either to the extreme nodes or to the interfacial nodes. For these, the boundary conditions can be rewritten as

$$\left.\begin{aligned} &\theta_{1,j+1} - \theta_{2,j+1} = 0 \\ &-\frac{K_r}{K_s}\cdot\theta_{N_0-1,j+1} + \left(1+\frac{K_r}{K_s}\right)\theta_{N_0,j+1} - \theta_{N_0+1,j+1} = 0 \\ &\theta_{N,j+1} = 0\,. \end{aligned}\right\} \tag{18}$$

All these equations can be expressed in matrix form, giving

$$\begin{bmatrix} 1 & -1 & 0 & 0 & 0 & 0 & 0 & 0 & 0 & 0 & 0 \\ -1 & \alpha_r+2 & -1 & 0 & 0 & 0 & 0 & 0 & 0 & 0 & 0 \\ 0 & -1 & \alpha_r+2 & -1 & 0 & 0 & 0 & 0 & 0 & 0 & 0 \\ \multicolumn{11}{c}{\text{---------------------------------------}} \\ 0 & 0 & 0 & -1 & \alpha_r+2 & -1 & 0 & 0 & 0 & 0 & 0 \\ 0 & 0 & 0 & 0 & -\psi & 1+\psi & -1 & 0 & 0 & 0 & 0 \\ 0 & 0 & 0 & 0 & 0 & -1 & \alpha_s+2 & -1 & 0 & 0 & 0 \\ \multicolumn{11}{c}{\text{---------------------------------------}} \\ 0 & 0 & 0 & 0 & 0 & 0 & 0 & -1 & \alpha_s+2 & -1 & 0 \\ 0 & 0 & 0 & 0 & 0 & 0 & 0 & 0 & -1 & \alpha_s+2 & -1 \\ 0 & 0 & 0 & 0 & 0 & 0 & 0 & 0 & 0 & 0 & 1 \end{bmatrix} \begin{Bmatrix} \theta_1 \\ \theta_2 \\ \theta_3 \\ \text{-----} \\ \theta_{N_0-1} \\ \theta_N \\ \theta_{N_0+1} \\ \text{-----} \\ \theta_{N-2} \\ \theta_{N-1} \\ \theta_N \end{Bmatrix} = \begin{Bmatrix} 0 \\ S_2 \\ S_3 \\ \text{-----} \\ S_{N_0-1} \\ 0 \\ S_{N_0+1} \\ \text{-----} \\ S_{N-2} \\ S_{N-1} \\ 0 \end{Bmatrix} \qquad (19)$$

where

$$\psi = K_r/K_s \ .$$

The system matrix is banded, with semi-bandwidth 2, so the system can be solved by Gaussian elimination.

RESULTS AND CONCLUSIONS

A computer program was written as shown on page to compute temperatures for a commercial purity aluminium disc with steel rollers and clamps of the following dimensions.

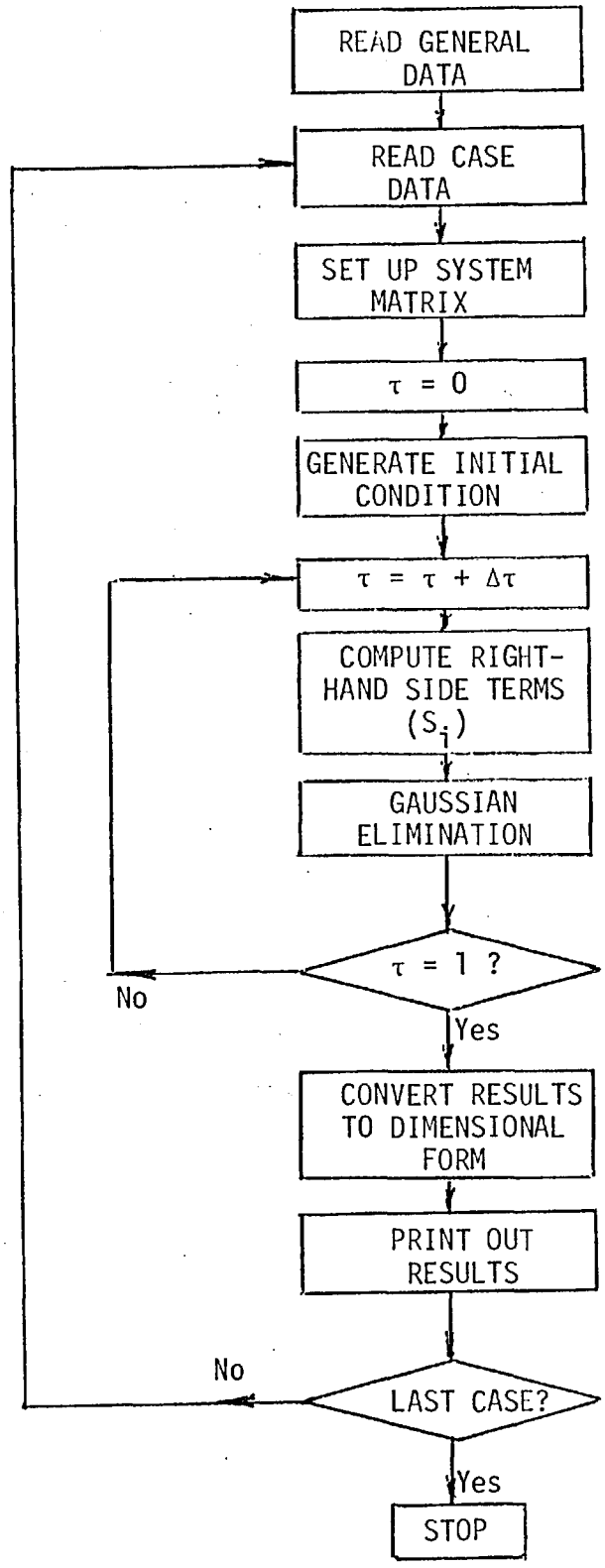
Radius of specimen-disc	R_S	= 150 mm
Radius of supporting clamp	R_C	= 90 mm
Depth of section	R	= 60 mm
Radius of forming roller	R_r	= 50 mm
Angular velocity of rotation	ω	= 2π rad/min

Initial disc temperatures T_S = 450°C to 550°C have been considered. It was assumed that the roller is pre-heated, the temperatures ranging from 100°C to 200°C.

One value of the geometrical increment $\Delta\rho$ = 0.05 and two values of the time increment $\Delta\tau$ = 0.01 and 0.005 have been used, both time increments giving the same results.

The shaded areas correspond to the various roller temperatures within the considered range. Figs. 3,4 give the temperature of the disc in terms of relative travel, i.e. the distance travelled by the particular point from entry at $\overline{S_0S_0'}$ relative to the total travel to $\overline{S_1S_1'}$, for entry temperatures T_S = 450°C (Fig 3a and b) and 500°C (Fig 4a and b), in both cases for roller temperatures T_r = 100°C (A) and 200°C (B), at the roller/disc interface and at 6, 12, 18, 24 and 30 mm from it. The temperature of a particular element of material drops appreciably by the time it leaves the deformation zone; this decrease is

300


READ GENERAL DATA
READ CASE DATA
SET UP SYSTEM MATRIX
τ = 0
GENERATE INITIAL CONDITION
τ = τ + Δτ
COMPUTE RIGHT-HAND SIDE TERMS (S_i)
GAUSSIAN ELIMINATION
τ = 1 ?
No
Yes
CONVERT RESULTS TO DIMENSIONAL FORM
PRINT OUT RESULTS
No
LAST CASE?
Yes
STOP

more pronounced for those elements which are close to the roller/disc interface, where most of the plastic deformation takes place. There are even lower temperatures further away from the roller partly because of the lower initial specimen temperature, partly due to heat losses to the clamps, but temperatures in this region are less important because plastic deformation should not extend that far due to the very nature of the process.

Varying roller temperatures have a significant effect close to the roller, noticeable up to a distance of 18 mm away from the roller/specimen interface. Low roller temperatures have an important effect at the interface when, immediately on entry, the specimen temperature drops from 450°C to 417°C and 422°C, if the initial roller temperatures are 200°C and 100°C respectively (Fig 3b).

Specimen temperatures have been recorded, with an infra-red radiometer, in the exit region, i.e. at time $t = t_1$, $\tau = 1$, at a distance of 6 mm away from the roller/specimen interface. The experimental values agree well with the computed results. The latter are plotted in Fig 5 for an element 6 mm away from the roller and for that in contact with the roller, for roller temperatures T_r = 100°C (A) and 200°C (B). It is clear that, for example, if the specimen temperature everywhere must exceed 400°C, the initial temperature must be about 500°C.

From this the significance of these computations in the present case is quite clear. On the one hand entry temperatures can be determined and suitably adjusted only when the temperature distribution is known, which ensure that temperatures in the whole deformation region exceed the minimum required for the process and are below a safe maximum for the particular material.

The results also indicate that temperatures in the deformation zone vary within wide limits and, consequently, the yield stress of the deforming material assumes significantly different values from point to point. For example, the yield stress of commercial purity aluminium at 400°C is over double of that at 500°C, at low strain rates of interest in the present work [12]. This implies the difficulty in obtaining a theoretical solution in the closed form for calculating loads, stresses, etc. in this problem with any accuracy, when an average yield stress of the material must be used. Alternatively, if a numerical method is adopted the yield stress for each element of material can be suitably selected according to the temperature of the particular element. If the calculations are then based on these actual yield stress values for each element, the inherent accuracy of the solution must improve appreciably.

This indicates not only the desirability of finding a suitable numerical solution for the computation of loads in this type of problem, but also that even those theoretical methods which are able to take account of the stress/strain behaviour of each material element in some cases might represent little improvement unless accompanied by an assessment of the temperature distribution and its effect on the yield stress of the deforming material. The present example is certainly one such case.

ACKNOWLEDGMENTS

The authors thank Professor J.M. Alexander for permission to use facilities in the Metalworking Laboratory, Department of Mechanical Engineering, Imperial College, and Mr. P.G. Ashford and others for help with the experimental apparatus.

NOTATION

A_m	coefficients of the series
c, c_r, c_s	thermal diffusivities of the materials
c	as index refers to the clamps
i	as index denotes the generic geometrical node in the numerical solution
j	as index denotes the generic temporal node in the numerical solution
K_r, K_s	thermal conductivities of roller and specimen, respectively
N	index of last geometrical node
N_0	index of geometrical node coinciding with the roller-specimen interface
r	radial distance of material element from the roller-specimen interface as index denotes the roller
R	unclamped radial dimension of specimen
R_c, R_r, R_s	radii of clamp, roller and specimen respectively
s	as index denotes the specimen
S, S_0, S_1	in Fig 2 denote the instantaneous, initial and final position of the material
S_i	abbreviated expression for the right-hand side terms of the Crank-Nicholson equations
t, t_1	time variable and time taken by the material to cross the forming region
T, T_c, T_r, T_s	generic temperature and its initial values in the clamps, roller and specimen respectively
α, α_r, α_s	auxiliary function used in the Crank-Nicholson equations, and its values for roller and specimen, respectively
β, β_r, β_s	angle defining the instantaneous position of the material and contact angles
Δ	radial penetration of roller
$\Delta\rho$, $\Delta\tau$	increments of non-dimensional variables
ψ	ratio of thermal conductivities
λ_m	eigenvalues in analytical solution
ρ	non-dimensional geometric variable
θ	non-dimensional temperature
τ	non-dimensional temporal variable
ω	angular velocity of specimen

REFERENCES

1. H. Preisendanz, P. Schüler and K. Koschnitzke, "Berechung der zeitabhängigen Oberflächentemperatur heisser Blöcke während der Kontaktdauer von Block und Walze". Eisenhüttenwesen, 38 (12), 905-913 (1967).

2. R.M. Guha and B. Lengyel, "Temperature Distribution in Hydrostatic Extrusion-Drawing". Annals CIRP, 21/1 (1972).

3. M. Mohitpour and B. Lengyel, "Temperature Rise in the High Speed Compression of Right Cylindrical Billets". Proceedings of the Second North American Metalworking Research Conference, University of Wisconsin, 1974.

4. M. Mohitpour, Ph.D. Thesis, University of London, 1972.

5. R.M. Guha, M.Sc. Thesis, University of London, 1972.

6. G.F.C. Rogers and Y.R. Mayhew, "Engineering Thermodynamics, Work and Heat Transfer". Longmans, London, 1967.

7. H.S. Carslaw and J.C. Jaeger, "Conduction of Heat in Solids". Oxford Univ. Press, London, 1947.

8. P. Frank and R. v. Mises, "Die Differential- und Integralgleichungen der Mechanik und der Physik". Mary S. Rosenberg, New York, 1943.

9. Gröber, Erk and Grigull, "Die Grundgesetze der Wärmeübertragung". Springer, Berlin, 1961.

10. B.A. Finlayson and L.E. Scriven, "The Method of Weighted Residuals - a Review". Appl. Mech. Revs., 19 (9), 735-748 (1966).

11. G.D. Smith, "Numerical Solution of Partial Differential Equations". Oxford Univ. Press, London, 1969.

12. H. Suzuki, S. Hashzume, Y. Yabuki, Y. Ichihara, S. Nakajima and K. Kenmochi, "Studies on the flow stress of metals and alloys". Report of the Institute of Industrial Science, The University of Tokyo, 18, No.3, 1968.

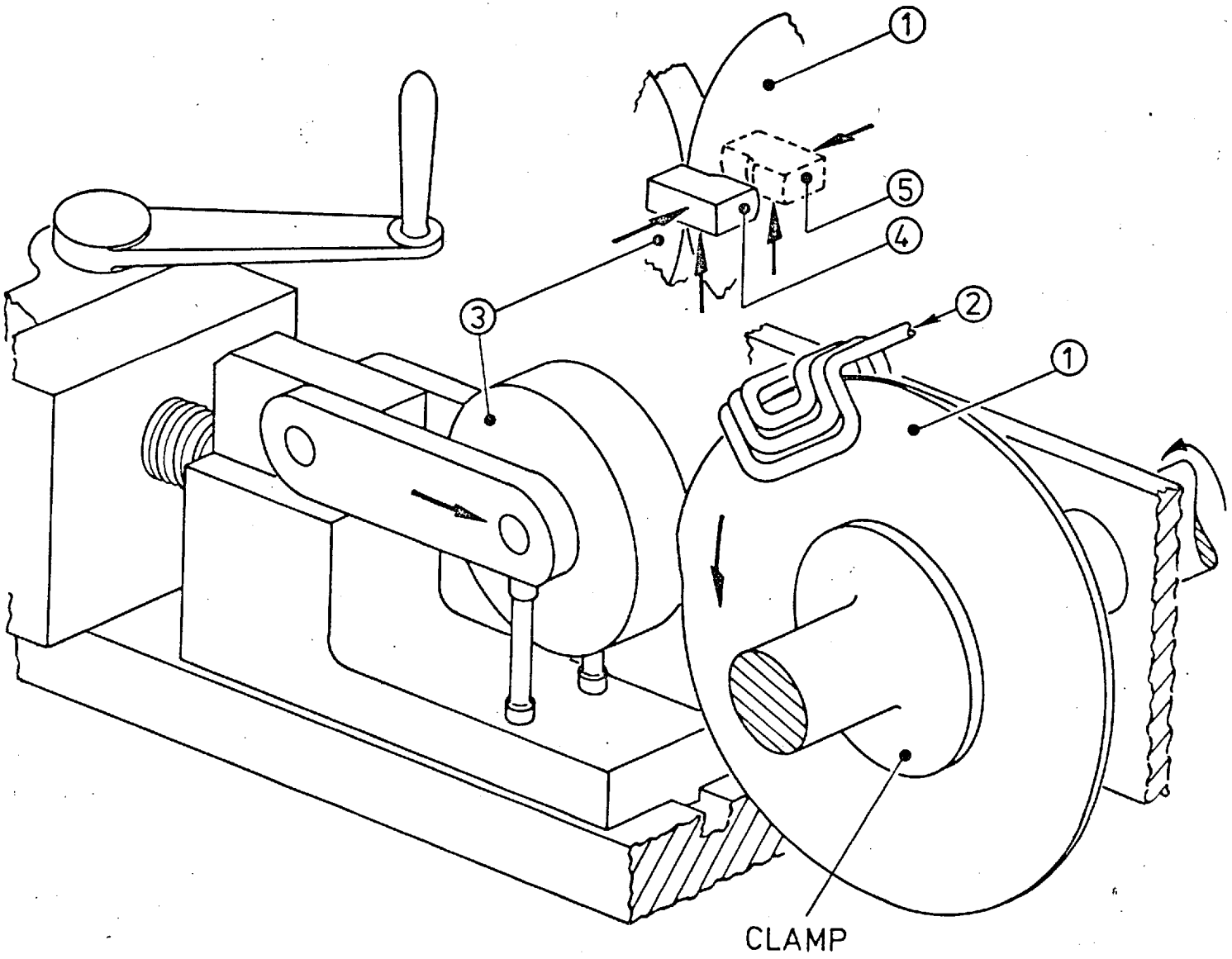


Fig.1. EXPERIMENTAL ARRANGEMENT.

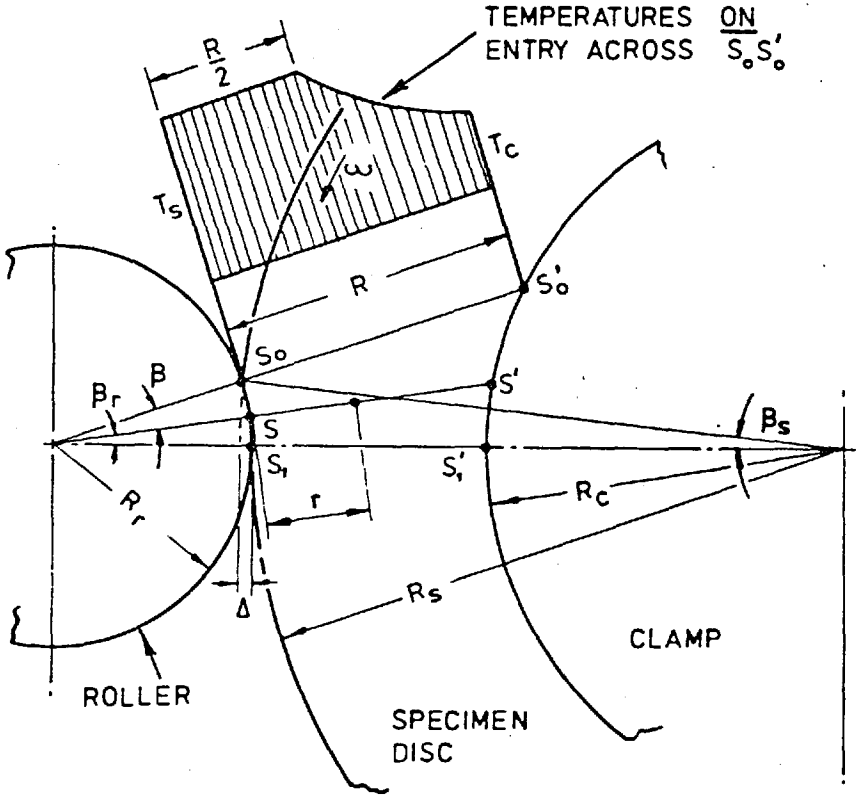


Fig 2. SIMPLIFIED MODEL.

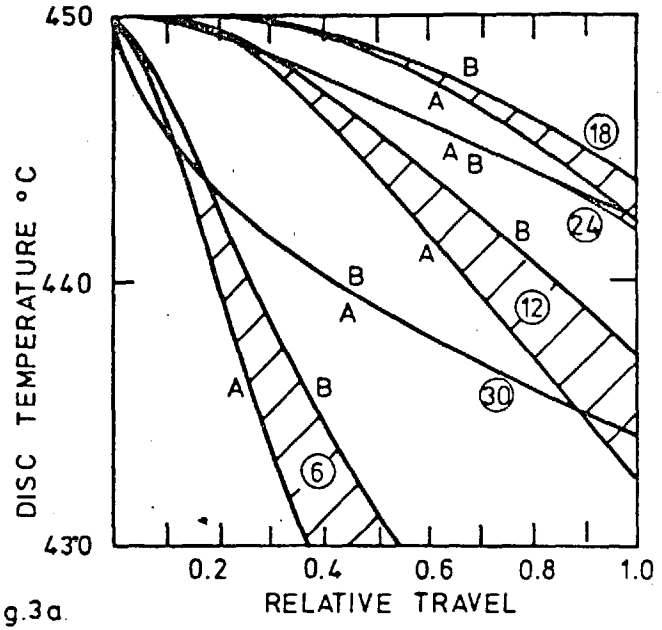


Fig.3a.

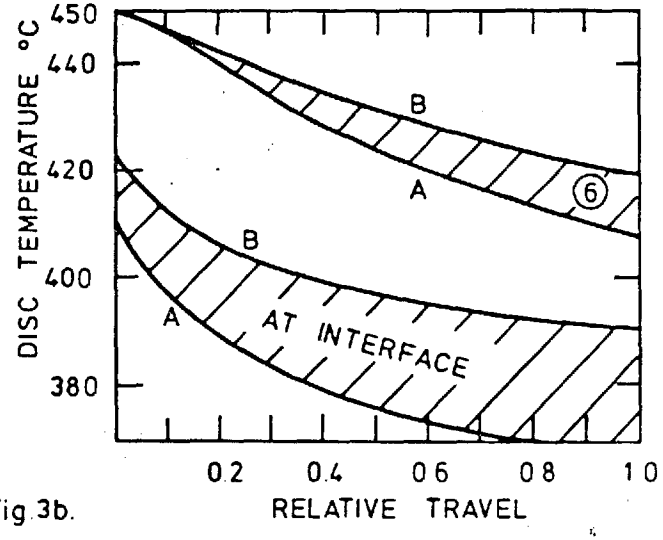


Fig.3b.

Fig.3.a,b. DISC TEMPERATURE vs. RELATIVE TRAVEL
INITIAL TEMPERATURE T_s = 450 °C
⑥ indicates distance from roller, mm

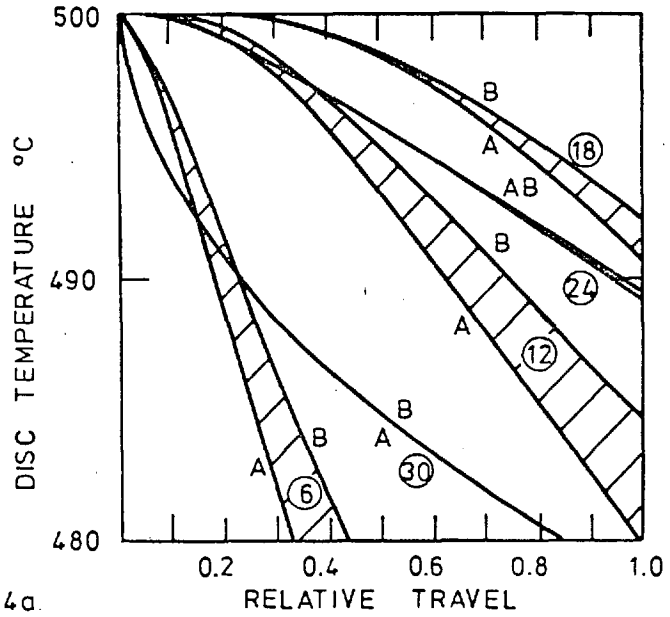


Fig 4a

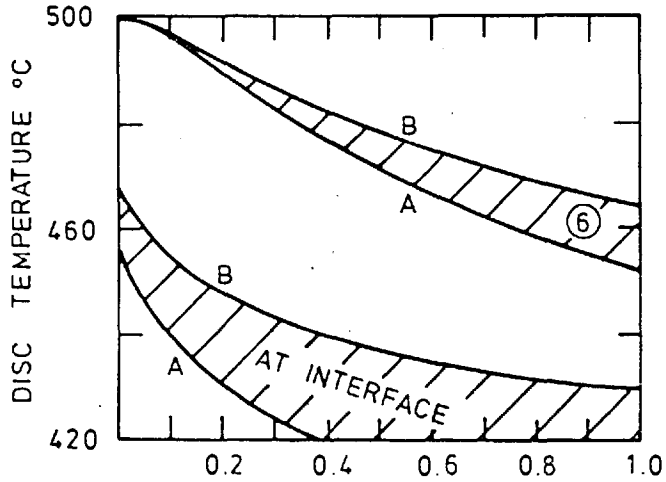


Fig.4 b

Fig.4.a,b DISC TEMPERATURE vs RELATIVE TRAVEL. INITIAL TEMPERATURE $T_S = 500\,°C$

⑥ indicates distance from roller, mm

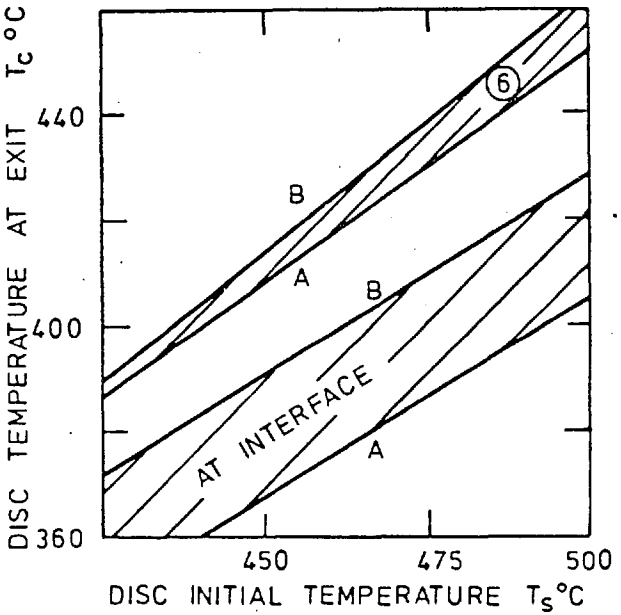


Fig.5 CORRELATION BETWEEN EXIT AND ENTRY TEMPERATURES

⑥ indicates distance from roller, mm

APPENDIX 5

RADIAL UPSETTING OF FLANGES

To be presented at the

FOURTH NORTH AMERICAN METALWORKING

RESEARCH CONFERENCE

to be held in

Columbus (Ohio)

in May, 1976

and to be published

in the

PROCEEDINGS

of that

Conference

RADIAL UPSETTING OF FLANGES

by

B. LENGYEL, Senior Lecturer, Department of Mechanical Engineering, Imperial College of Science and Technology, London, U.K.
A. BLASS, Professor, University of Santa Catarina, Florianopolis, Brazil,
at present with
Department of Mechanical Engineering, Imperial College of Science and Technology, London, U.K.

ABSTRACT. Radial upsetting has been developed to form thick flanges on thin-walled metal components. The experimental equipment is described and an upper bound solution presented to predict forming loads. The computed results show reasonable agreement with experiments.

NOTATION.

A_c	Contact area between specimen and roller
F, G, H	Trial functions, dependent on r and θ
H (Fig.4)	Depth of forming zone
J*	Total power of deformation
m	Constant friction factor
p	Average pressure in the contact zone
p_{rel}	Relative pressure in the contact zone
P	Total forming force
r, R	Radial coordinates in forming zone and contact area
R_n	Radial coordinate of the neutral position
R_o	Radius of undeformed specimen
R_p	Radius of elastic-plastic boundary
R_r	Radius of the forming roller
t	Time of travel for a section from the initial to the instantaneous position
T, T_o	Thickness of specimen (instantaneous, initial)
$\dot{U}_r$, $\dot{U}_\theta$, $\dot{U}_z$	Velocity components in the coordinate directions
$\dot{U}_R$	Tangential velocity of the roller
$\dot{U}_t$	Tangential velocity of the specimen in contact area
$\dot{W}_{d_r}$, $\dot{W}_{d_z}$	Dissipation power terms due to the radial and axial velocity discontinuities at the entrance to the forming zone
$\dot{W}_f$	Friction power
$\dot{W}_i$	Internal power of deformation
z	Axial coordinate
α, β	Nondimensional parameters
Δ	Radial penetration of roller
Δv	Velocity discontinuity
$\dot{\epsilon}_{rr}$, ...	Strain-rate components
ϵ_{zz}	Axial strain component
σ_o	Flow stress of specimen material
τ	Shear stress
θ, θ_1	Specimen contact angles
ψ, ψ_1	Roller contact angles
ω, ω_r	Angular velocities of specimen and roller

INTRODUCTION. A progressive method of metalworking is the radial upsetting, or edge-rolling of a flat disc, where the deformation is confined to small volumes of material at a time.(1) Thick flanges can be produced in this way on engineering components made of thinner materials. In the experimental apparatus (Fig.1) the specimen is a slowly rotating disc (1) which is heated locally by a stationary induction coil (2); subsequently, the material is radially formed by a roller (3), to raise the cross-sectional area of the disc locally. As the disc rotates, the deformation is extended to its full circumference, then the roller is moved by a small amount radially towards the centre of the disc, and the process is repeated. In this manner thick flanges could be built up on a thin-walled component preformed, for example, by sheet drawing. Separate shaping tools (4, 5) can be added to allow material to flow only in the desired direction. Components (6) and (7) are strain gauged to measure the horizontal (radial) and vertical (tangential) components of force. The geometry of the forming zone is complicated and the boundary conditions

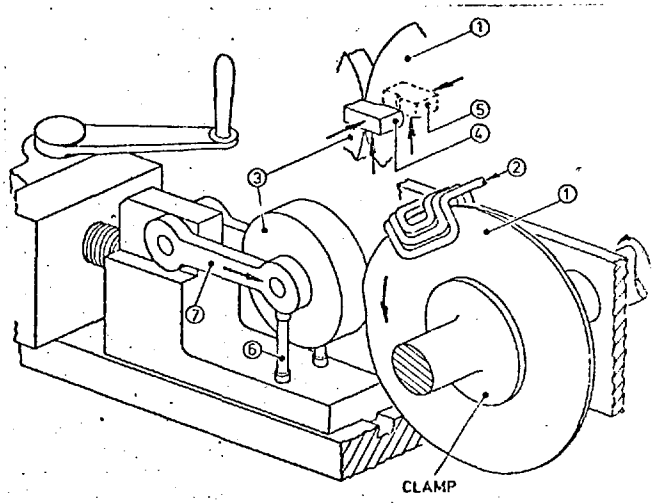


Fig.1 EXPERIMENTAL EQUIPMENT

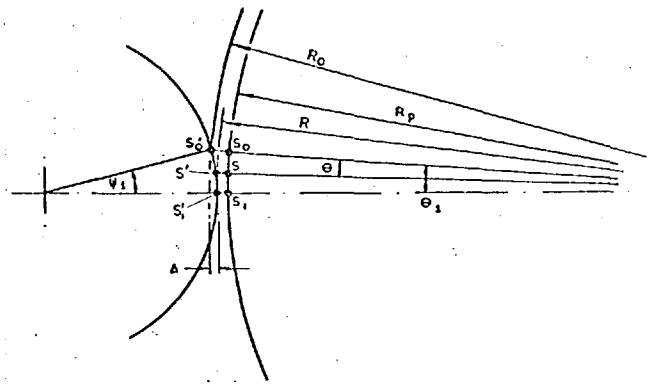


Fig.2 SIMPLIFIED MODEL

lead to an elaborate formulation. In the following an upper bound solution will be presented assuming a rigid-plastic material.

THEORY. Figure 2 illustrates the simplified model used in the derivations. The deformation zone is bounded by straight lines $\overline{S_oS_o'}$ and $\overline{S_1S_1'}$, by circular arcs $\overline{S_o'S_1'}$ at the specimen-roller interface, and S_oS_1 at the rigid-plastic boundary, assumed to be cylindrical, of radius R_p. The material enters this region along $\overline{S_oS_o'}$ at time $t = 0$, and leaves it along $\overline{S_1S_1'}$ at time $t = t_1$, after a radial penetration Δ. An intermediate position is represented by $\overline{SS'}$, being reached at time t.

The angles of the full arc of contact are ψ_1 and θ_1 from the centre of the roller and specimen respectively. Two equations can be established for these con-

tact angles:

$$R_r\cos\psi_1 + R_o\cos\theta_1 = R_r + R_o - \Delta$$

$$R_r\sin\psi_1 - R_o\sin\theta_1 = 0.$$

Since angle θ_1 is small, and neglecting higher order terms, θ_1 is obtained as

$$\theta_1 = \sqrt{\frac{\Delta}{R_o}\frac{2R_r - \Delta}{R_o + R_r - \Delta}\left[1 - \frac{4\Delta}{R_o}\left(\frac{2R_r - \Delta}{R_o + R_r - \Delta}\right)\right]} \qquad (1)$$

Details of all derivations are given elsewhere.(2)

The instantaneous contact radius R can be expressed as a linear function of the instantaneous angle θ

$$R = R_o - \Delta\,\frac{\theta}{\theta_1} \qquad (2)$$

The velocity components outside the forming region are

$$\dot{U}_r = \dot{U}_z = 0, \qquad \dot{U}_\theta = \omega r$$

so all strain-rate components are zero.

Along the boundaries continuity conditions are expressed by

$$\dot{U}_r(R_p,\theta,z) = 0, \quad \dot{U}_\theta(r,0,z) = \dot{U}_\theta(r,\theta_1,z) = \omega r,$$

$$\dot{U}_z(r,\theta,0) = 0 \qquad (3a,b,c)$$

The last equation expresses that deformation is symmetrical with respect to the axial coordinate.

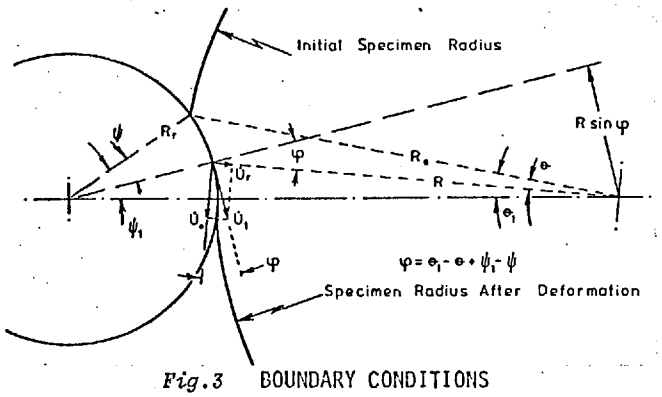


Fig.3 BOUNDARY CONDITIONS

Since there is no interpenetration between specimen and roller and no voids are formed at the interface, the specimen velocity must be tangential to the roller (Fig. 3) consequently

$$\dot{U}_t\Big|_{r=R} = \sqrt{\dot{U}_r^2 + \dot{U}_\theta^2}\Big|_{r=R} \quad \text{and}$$

$$\dot{U}_r\Big|_{r=R} = -\,\dot{U}_\theta\Big|_{r=R}\tan(\theta_1 - \theta + \psi_1 - \psi),$$

The relationship between the contact angles can be expressed as

$$\psi_1 - \psi = \frac{R}{R_r}(\theta_1 - \theta) \sim \frac{R_o}{R_r}(\theta_1 - \theta)$$

since the roller penetration is small relative to the radius of the specimen.

By introducing the dimensionless parameter $\alpha = 1 + R_{o/R_r}$, at the interface

$$\dot{U}_r\Big|_{r=R} = -\alpha(\theta_1-\theta)\left[1 + \frac{\alpha^2}{3}(\theta_1-\theta)^2\right]\dot{U}_\theta\Big|_{r=R} \qquad (4)$$

with the tangent expression replaced by the first two terms of its series expansion.

To Eqns. (3,4) the incompressibility condition must be added, so that

$$\dot{\varepsilon}_{rr} + \dot{\varepsilon}_{\theta\theta} + \dot{\varepsilon}_{zz} = 0$$

Initially in the deformation zone the velocity components are expressed by the yet unknown functions

$$\dot{U}_r = F(r,\theta), \quad \dot{U}_\theta = \omega r + G(r,\theta), \quad \dot{U}_z = zH(r,\theta).$$

The conditions represented by Eqns. (3a,b,c) can be rewritten as

$$F(R_p,0) = 0, \quad G(r,0) = G(r,\theta_1) = 0 \qquad (5a,b)$$

Condition (3c) is automatically satisfied by the assumed functions.

The strain-rate components then become

$$\dot{\varepsilon}_{rr} = \frac{\partial\dot{U}_r}{\partial r} = \frac{\partial F}{\partial r}, \quad \dot{\varepsilon}_{\theta\theta} = \frac{1}{r}\left[\frac{\partial\dot{U}_\theta}{\partial\theta} + \dot{U}_r\right] = \frac{1}{r}\left(F + \frac{\partial G}{\partial\theta}\right)$$

$$\dot{\varepsilon}_{zz} = \frac{\partial\dot{U}_z}{\partial z} = H$$

$$\dot{\varepsilon}_{r\theta} = \frac{1}{2}\left[\frac{\partial\dot{U}_\theta}{\partial r} + \frac{1}{r}\frac{\partial\dot{U}_r}{\partial\theta} - \frac{\dot{U}_\theta}{r}\right] = \frac{1}{2}\left[\frac{\partial G}{\partial r} + \frac{1}{r}\frac{\partial F}{\partial\theta} - \frac{G}{r}\right]$$

$$\dot{\varepsilon}_{\theta z} = \frac{1}{2}\left[\frac{1}{r}\frac{\partial\dot{U}_z}{\partial\theta} + \frac{\partial\dot{U}_\theta}{\partial z}\right] = \frac{z}{2r}\frac{\partial H}{\partial\theta}$$

$$\dot{\varepsilon}_{zr} = \frac{1}{2}\left[\frac{\partial\dot{U}_r}{\partial z} + \frac{\partial\dot{U}_z}{\partial r}\right] = \frac{z}{2}\frac{\partial H}{\partial r},$$

and the incompressibility condition rewrites to

$$H = -\frac{\partial F}{\partial r} - \frac{1}{r}\left[F + \frac{\partial G}{\partial\theta}\right]. \qquad (6)$$

Experiments indicate that planes initially radial remain approximately radial in the deformation zone so the trial function G can be set identically zero, when Eqn. (4) rewrites to

$$F(R,\theta) = -\omega R\alpha(\theta_1-\theta)\left[1 + \frac{\alpha^2}{3}(\theta_1-\theta)^2\right].$$

This equation fully defines function F in the deformation zone while, according to Eqn. (5a), it vanishes at radius R_p. Assuming a quadratic expression for F such that the related function H (Eqn.(6)) produces a velocity component $\dot{U}_z$ which represents no velocity discontinuity at R_p

$$F(r,\theta) = -\omega\alpha\left[1 + \frac{\alpha^2}{3}(\theta_1-\theta)^2\right](\theta_1-\theta)\frac{R}{(R-R_p)^2}(r-R_p)^2,$$

which satisfies all prescribed boundary conditions, and for which Eqn. (6) produces

$$H(r,\theta) = \omega\alpha\left[1 + \frac{\alpha^2}{3}(\theta_1-\theta)^2\right](\theta_1-\theta)\frac{R}{(R-R_p)^2}\,\frac{(r-R_p)(3r-R_p)}{r}.$$

The velocity components then become

$$\dot{U}_r = -\omega\alpha\left[1 + \frac{\alpha^2}{3}(\theta_1-\theta)^2\right](\theta_1-\theta)\frac{R}{(R-R_p)}(r-R_p)^2, \qquad (7a)$$

$$\dot{U}_\theta = \omega r \qquad (7b)$$

$$\dot{U}_z = \omega\alpha\left[1 + \frac{\alpha^2}{3}(\theta_1-\theta)^2\right](\theta_1-\theta)\frac{R}{(R-R_p)^2}\,\frac{(r-R_p)(3r-R_p)}{r}\,z \qquad (7c)$$

The strain-rate components become

$$\dot{\varepsilon}_{rr} = -2\omega\alpha\left[1 + \frac{\alpha^2}{3}(\theta_1-\theta)^2\right](\theta_1-\theta)\frac{R}{(R-R_p)^2}(r-R_p)$$

$$\dot{\varepsilon}_{\theta\theta} = -\omega\alpha\left[1 + \frac{\alpha^2}{3}(\theta_1-\theta)^2\right](\theta_1-\theta)\frac{R}{(R-R_p)^2}\,\frac{(r-R_p)^2}{r}$$

$$\dot{\varepsilon}_{zz} = \omega\alpha\left[1+\frac{\alpha^2}{3}(\theta_1-\theta)^2\right](\theta_1-\theta)\frac{R}{(R-R_p)^2}\frac{(r-R_p)(3r-R_p)}{r}$$

$$\dot{\varepsilon}_{r\theta} = \frac{1}{2}\omega\alpha\left\{\left[1+\alpha^2(\theta_1-\theta)^2\right](\theta_1-\theta)\frac{R}{(R-R_p)^2} - \left[1+\frac{\alpha^2}{3}(\theta_1-\theta)^2\right](\theta_1-\theta)\frac{\Delta(R+R_p)}{(R-R_p)^3}\right\}\frac{(r-R_p)^2}{r}$$

$$\dot{\varepsilon}_{\theta z} = -\frac{1}{2}\omega\alpha\left\{\left[1+\alpha^2(\theta_1-\theta)^2\right]\frac{R}{(R-R_p)^2} - \left[1+\frac{\alpha^2}{3}(\theta_1-\theta)^2\right](\theta_1-\theta)\frac{\Delta(R+R_p)}{(R-R_p)^3}\right\}\frac{(r-R_p)(3r-R_p)z}{r^2}$$

$$\dot{\varepsilon}_{zr} = \frac{1}{2}\omega\alpha\left[1+\frac{\alpha^2}{3}(\theta_1-\theta)^2\right](\theta_1-\theta)\frac{R}{(R-R_p)^2}\frac{(r-R_p)(3r-R_p)z}{r^2}.$$

The time required for the section $\overline{SS'}$ (Fig.2) of the specimen to travel angle θ is $t = \theta/\omega$ so the axial strain

$$\varepsilon_{zz} = \int_0^t \dot{\varepsilon}_{zz}\,dt = \frac{1}{\omega}\int_0^t \dot{\varepsilon}_{zz}\,d\theta$$ can be expressed as

$$\varepsilon_{zz} = \frac{\alpha R_o\theta}{2(R_o-R_p)^2}\frac{(r-R_p)(3r-R_p)}{r}\left\{2\theta_1-\theta+\right.$$

$$\frac{1}{3}\frac{\Delta}{R_o}\frac{R_o+R_p}{R_o-R_p}\frac{\theta}{\theta_1}(3\theta_1-2\theta) + \frac{1}{6}\frac{\Delta^2}{R_o}\frac{(R_o-2R_p)}{(R_o-R_p)^2}\frac{\theta^2}{\theta_1^2}(4\theta_1-3\theta) +$$

$$\frac{\alpha^2}{6}\left[4\theta_1^3-6\theta_1^2\theta+4\theta_1\theta^2-\theta^3+\frac{1}{15}\frac{\Delta}{R_o}\frac{R_o+R_p}{R_o-R_p}\frac{\theta}{\theta_1}(30\theta_1^3-60\theta_1^2\theta+45\theta_1\theta^2-\right.$$

$$\left.\left.12\theta^3) + \frac{1}{15}\frac{\Delta^2}{R_o}\frac{(R_o-2R_p)}{(R_o-R_p)^2}\frac{\theta^2}{\theta_1^2}(20\theta_1^3-45\theta_1^2\theta+36\theta_1\theta^2-10\theta^3)\right]\right\}.$$

All derivations can be simplified because Δ is very small relative to the specimen radius and because the higher order powers of θ can be neglected since θ_1 is only 0.085 radians at most in the present case. The expression above can be shown to be matched quite satisfactorily by the much simpler relation

$$\varepsilon_{zz} = \frac{\beta}{R_o-R_p}\theta(2\theta_1-\theta)\frac{(r-R_p)(3r-R_p)}{r} \qquad (8)$$

with the dimensionless parameter β defined as

$$\beta = \frac{\alpha}{2}\frac{R_o}{R_o-R_p}\left[1+\frac{1}{3}\frac{\Delta}{R_o}\frac{R+R}{R_o-R_p}\left[1+\frac{\alpha^2\theta_1^2}{6}\right]\right].$$

α and β depend only on the fixed parameters; therefore, they are constants in a particular case.

The instantaneous local thickness of the specimen in the deformation zone can thus be obtained from

$$T(r,\theta) = T_o(1+\varepsilon_{zz}) \qquad (9)$$

Assuming that the yield criterion of von Mises holds, the internal power of deformation can be expressed as

$$\dot{W}_i = \frac{2\sigma_o}{\sqrt{3}}\int_0^{\theta_1}\int_{R_p}^{R}\int_{-T/2}^{T/2}\sqrt{\frac{1}{2}\left[\dot{\varepsilon}_{rr}^2+\dot{\varepsilon}_{\theta\theta}^2+\dot{\varepsilon}_{zz}^2+2(\dot{\varepsilon}_{r\theta}^2+\dot{\varepsilon}_{\theta z}^2+\dot{\varepsilon}_{zr}^2)\right]}\times r\,dr\,d\theta\,dz.$$

Introducing the expressions previously obtained for the strain-rate components, after a few simple operations this equation rewrites to

$$\dot{W}_i = \frac{2\sigma_o}{\sqrt{3}}\int_0^{\theta_1}\int_{R_p}^{R}\int_{-T/2}^{T/2}\left[1+\frac{\alpha^2}{3}(\theta_1-\theta)^2\right]\frac{r-R_p}{(R-R_p)^2}\omega\alpha$$

$$\sqrt{(\theta_1-\theta)^2R^2\left[7r^2-4rR_p+R_p^2+\frac{z^2}{4r^2}(3r-R_p)^2\right]+\left(\frac{R}{2}\frac{\left[1+\alpha^2(\theta_1-\theta)^2\right]}{\left[1+\frac{\alpha^2}{3}(\theta_1-\theta)^2\right]}-\frac{\Delta}{2}(\theta_1-\theta)\frac{R+R_p}{R-R_p}\right)^2\left[(r-R_p)^2+\right.}$$

$$\left.\left.\frac{z^2}{r^2}(3r-R_p)^2\right]}\,dr\,d\theta\,dz.$$

The second term inside the square root can be shown to be negligible relative to the first one except near the exit where the first term tends to vanish, while the second term attains comparatively small values. The terms involving the ratio z^2/r^2 are clearly negligible. With these considerations the internal power of deformation can be approximated by

$$\dot{W}_i = \frac{2\sigma_o}{\sqrt{3}}\omega\alpha\int_0^{\theta_1}\int_{R_p}^{R}\int_{-T/2}^{T/2}(\theta_1-\theta)\left[1+\frac{\alpha^2}{3}(\theta_1-\theta)^2\right]\frac{R(r-R_p)}{(R-R_p)^2}$$

$$\sqrt{7r^2-4rR_p+R_p^2}\,dr\,d\theta\,dz.$$

On integration the square root term would give cumbersome transcendental functions in r which, after substituting the integration limits, produce complicated functions which must then be integrated with respect to θ. Considering that R_p is not exceeded by R by more than 7.5%, a simpler alternative is to replace the radicandum by an upper bound $(3r-R_p)^2$ thus, in part, compensating for the terms previously abandoned. Integration now becomes much simpler. Integrating first with respect to z, the local thickness given by Eqn. (9) is introduced. In the subsequent integration, with respect to r, a logarithmic term appears, which is best replaced by its truncated series expansion

$$\ln\frac{R}{R_p} = \frac{R-R_p}{R_p} - \frac{1}{2}\left[\frac{R-R_p}{R_p}\right]^2.$$

Such a term appears also in subsequent integrations, and the same procedure will be applied in every case. This leads to

$$\dot{W}_i = \frac{2\sigma_o}{\sqrt{3}}\omega\alpha T_o\int_0^{\theta_1}(\theta_1-\theta)\left[1+\frac{\alpha^2}{3}(\theta_1-\theta)^2\right]R^2$$

$$\left[1+\frac{\theta}{4(R_o-R_p)}(2\theta_1-\theta)\frac{R-R_p}{R}(9R-5R_p)\right]d\theta$$

Neglecting the higher order terms in Δ and θ_1

$$\dot{W}_i = \frac{\sigma_o}{\sqrt{3}}\omega\alpha T_o R_o^2\theta_1^2\left\{1+\frac{\alpha^2\theta_1^2}{6}-\frac{2\Delta}{3R_o}+\frac{\beta}{8}\frac{R_o\theta_1^2}{R_o-R_p}\left[9-14\frac{R_p}{R_o}+5\frac{R_p^2}{R_o^2}-\frac{7}{15}\left(27-23\frac{R_p}{R_o}+5\frac{R_p^2}{R_o^2}\right)\frac{\Delta}{R_o}\right]\right\}. \qquad (10)$$

At the boundary on entry the velocity discontinuities in $\dot{U}_r$ and $\dot{U}_z$ produce a shear stress $\tau = \sigma_o/\sqrt{3}$.

The energy dissipated at this velocity discontinuity can be written as

$$\dot{W}_d = \int_{R_p}^{R_o} \int_{-T/2}^{T/2} \tau |\Delta v| \, dr \, dz ,$$

where $|\Delta v|$ is the velocity discontinuity, Eqns. (7a,c). On integration the power terms due to redundant deformation become

$$\dot{W}_{d_r} = \frac{1}{3} \frac{\sigma_o}{\sqrt{3}} \omega \alpha T_o R_o (R_o - R_p) \theta_1 \left(1 + \frac{\alpha^2}{3} \theta_1^2\right) \qquad (11)$$

$$\dot{W}_{d_z} = \frac{1}{4} \frac{\sigma_o}{\sqrt{3}} \omega \alpha T_o^2 R_o \theta_1 \left(1 + \frac{\alpha^2}{3} \theta_1^2\right) \qquad (12)$$

It is clear from Eqns. (7a,b,c) that velocity discontinuities are present only on entry to the deformation zone, $\theta = 0$. Both $\dot{U}_r$ and $\dot{U}_z$ vanish on approaching the exit where $\theta = \theta_1$ or at the plastic-rigid radius $r = R_p$.

The velocity discontinuity at the roller/specimen interface is, as the material slides over the roller surface in the axial direction,

$$|\Delta v| = \dot{U}_z \Big|_{r=R} .$$

The interfacial shear stress for constant friction is given by $\tau = m\sigma_o/\sqrt{3}$. Integrating and after retaining only the significant terms, the frictional power becomes

$$\dot{W}_f = \int_0^{\theta_1} \int_{-T/2}^{T/2} \tau |\Delta v| R \, d\theta \, dz = \frac{m}{8} \frac{\sigma_o}{\sqrt{3}} \omega \alpha T_o^2 R_o \frac{3R_o - R_p}{R_o - R_p} \theta_1^2$$
$$\left[1 + \frac{\alpha^2 \theta_1^2}{6} - \frac{9R_o^2 - 8R_o R_p + R_p^2}{3(R_o - R_p)(3R_o - R_p)} \frac{\Delta}{R_o} + \right.$$
$$\left. \beta \frac{3R_o - R_o}{R_o} \theta_1^2 \left(1 - \frac{4}{5} \frac{\Delta}{3R_o - R_p}\right)\right] \qquad (13)$$

Similar to the rolling process, on each side of a neutral position in the r,θ plane relative slip can be envisaged between specimen and roller. The dissipation term due to this effect has been calculated on the assumption that the neutral position is half-way between the entry and exit sections. It has been found that this term increases the required power by less than 1% for sticking friction and a roller penetration of 2 mm.(2) Consequently it has been neglected.

According to the upper-bound theorem(3,4),

$$J^* = \dot{W}_i + \dot{W}_{d_r} + \dot{W}_{d_z} + \dot{W}_f ,$$

where J^* is the external power required to rotate the specimen. The force acting over an element of the contact area $pRd\theta dz$ requires an elemental torque

$$pRd\theta dz \, R\sin(\theta_1 - \theta + \psi_1 - \psi) = pR^2 \sin\alpha(\theta_1 - \theta) d\theta \, dz$$

(Fig.3), thus the required external power becomes

$$J^* = \int_0^{\theta_1} \int_{-T/2}^{T/2} p\omega R^2 \sin\alpha(\theta_1 - \theta) \, d\theta \, dz .$$

Expanding the trigonometric factor in series, integrating and neglecting the higher order terms

$$J^* = \frac{1}{2} p\omega\alpha T_o R_o^2 \theta_1^2 \left\{1 - \frac{2\Delta}{3R_o} - \frac{\alpha^2\theta_1^2}{12} + \right.$$
$$\left. \frac{\beta\theta_1^2}{2} \frac{(3R_o - R_p)}{R_o} \left[1 - \frac{7}{15} \frac{(9R_o^2 - 3R_o R_p + R_p^2)\Delta}{R_o(R_o - R_p)(3R_o - R_p)} + \right.\right.$$
$$\left.\left. \frac{4}{15} \frac{(9R_o - 4R_p)\Delta^2}{R_o(R_o - R_p)(3R_o - R_p)}\right]\right\} . \qquad (14)$$

By using Eqns. (10) to (14) the average relative pressure can be obtained

$$p_{rel} = \frac{p}{\sigma_o/\sqrt{3}}$$

The forming force is given by

$$P = pA_c = \frac{\sigma_o}{\sqrt{3}} p_{rel} A_c ,$$

with the contact area expressed as

$$A_c = \int_0^{\theta_1} \int_{-T/2}^{T/2} R \, d\theta \, dz = T_o R_o \theta_1 \left\{1 - \frac{\Delta}{2R_o} + \right.$$
$$\left. \frac{2\beta}{3} \frac{3R_o - R_p}{R_o} \theta_1^2 \left[1 - \frac{5}{4} \frac{3R_o - 2R_p}{3R_o - R_p} \frac{\Delta}{R_o - R_p}\right]\right\} .$$

COMPUTED AND EXPERIMENTAL RESULTS. Experiments have been carried out with specimens of commercial purity aluminium, under the following conditions:

Radius of forming roller	R_r = 50 mm
Initial radius of specimen-disc	R_o = 150 mm
Initial thickness of specimen-disc	T_o = 6.35 mm
Angular velocity of specimen	ω = $\pi/30$ rad/s
Average flow stress of specimen material at a low strain-rate and at the working temperature of 400°C(5)	σ_o = 25 MN/m²
Maximum radial penetration of the roller	Δ = 2 mm

In the experimental equipment the specimen is rotated by an induction motor through a speed reducer to obtain the desired low velocities. The tangential and normal components of the load are recorded, via an ultraviolet light recorder, by strain gauges attached to members (6) and (7) (Fig.1). Heating is by an induction coil from a generator of 28 kW capacity with a range of operating frequencies from 2 to 5 kHz. The shape of the induction coil and its cooling are critical. Temperatures are recorded by an infra-red radiometer, calibrated for the conditions of the experiments.(2)

The position of the rigid-plastic boundary was obtained experimentally. In Fig.4 the typical cross-section

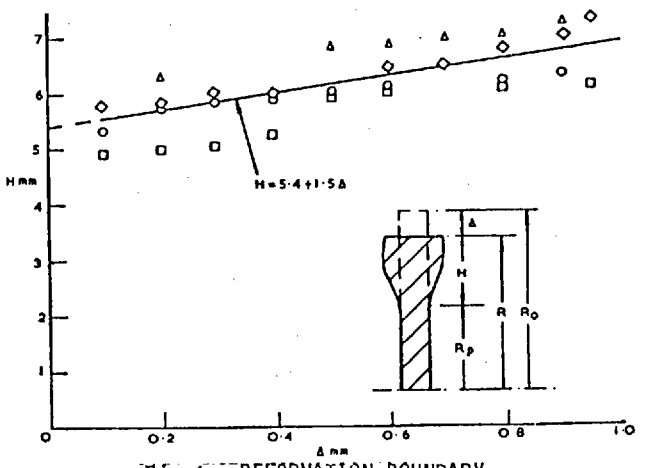


Fig.4 DEFORMATION BOUNDARY

of the deformed zone is shown. In practice it is difficult to define exactly where the deformed zone ends, so the measured height of the deformed bulge H and the limiting plastic radius R_p show some scatter. The experimental points can be approximated by

$$R_p = 0.964\, R_o - 2.5\Delta \ .$$

A computer program has been written to calculate contact angles and areas, relative pressure, power terms and the forming force for particular values of penetration.

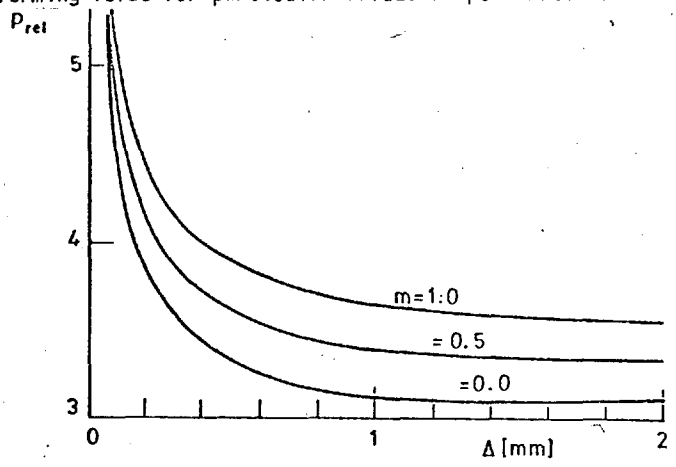


Fig.5 RELATIVE PRESSURE VERSUS DEPTH OF PENETRATION

Figure 5 shows the relative pressure to be extremely high for very small values of pentration, dropping sharply up to penetrations of the order of 0.5 mm, and more slowly afterwards. Sticking friction could account for a large proportion of the relative pressure in the large deformation range, but its effect becomes less noticeable for smaller penetrations.

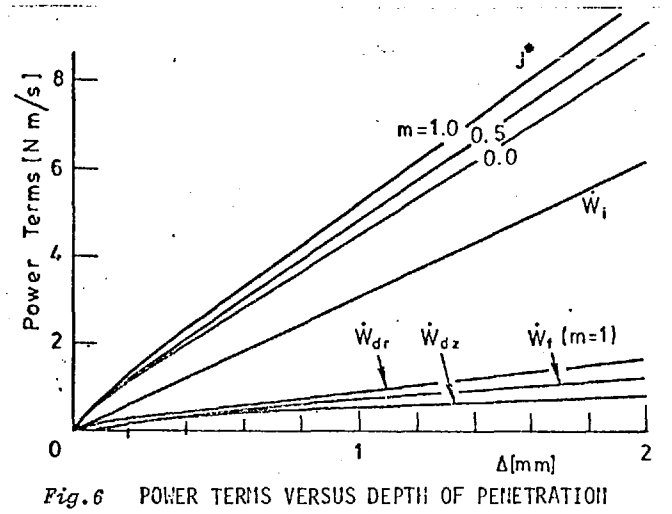


Fig.6 POWER TERMS VERSUS DEPTH OF PENETRATION

In Fig.6 the power terms are plotted, all of them quasi-linear with respect to penetration. For $\Delta < 0.1$mm $\dot{W}_{dr}$ and $\dot{W}_{dz}$ become relatively dominant as Δ tends to zero. The forming force in terms of the depth of penetration and friction is plotted in Fig.7. This is again quasi-linear except for small values of Δ. For comparison, some of the experimental results are also shown, obtained for penetrations in multiples of 0.1 mm, up to 1.8 mm. At smaller Δ the range refers to not less than five readings per penetration while a smaller number of readings was used for $\Delta > 1$ mm. The upper bound character of the theoretical solution is clear.

CONCLUSIONS. An upper bound solution has been developed to predict forming loads in radial upsetting without lateral restraints which agrees reasonably well with experiments. To compute theoretical loads the deformation boundary must first be determined experimentally, which is difficult to do accurately at very small values of penetration. While this is unlikely to be critical in practical cases, it would clearly be desirable to develop a theoretical approach to predict the plastic boundary

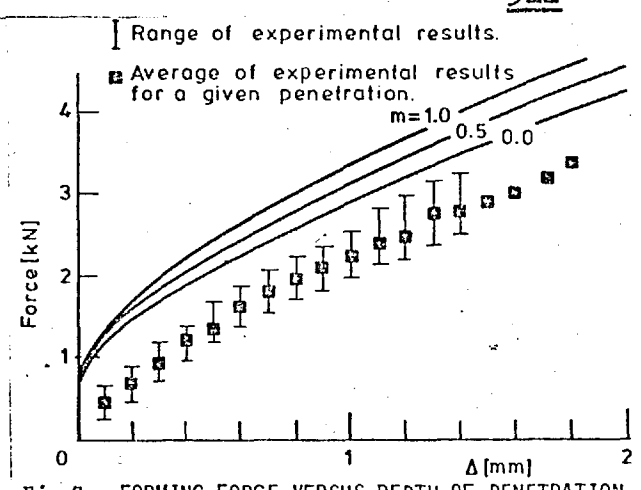


Fig.7 FORMING FORCE VERSUS DEPTH OF PENETRATION

together with strains and stresses in the deformation zone from which forming loads could be directly calculated.

ACKNOWLEDGEMENTS. The authors thank Professor J.M. Alexander for use of experimental facilities in the Metalworking Laboratory of the Department of Mechanical Engineering, Imperial College of Science and Technology, and the laboratory staff for assistance with experiments.

REFERENCES.

(1) "Temperature Distribution in the Radial Upsetting of a Flat Disc", A. Blass and B. Lengyel, Proc. of the Second North-American Metalworking Research Conference, Univ. of Wisconsin, Madison, May 1974, pp.60-69.

(2) "A Finite Element Approach to Metalworking", A. Blass, Ph.D. Thesis, London University, 1976.

(3) "Metal Forming: Processes and Analysis", B. Avitzur, McGraw-Hill, New York, 1968.

(4) "Mechanics of Plastic Deformation in Metal Processing", E.G. Thomsen, C.T. Yang and S. Kobayashi, Macmillan, New York, 1965.

(5) "On Relating the Flow-Stress of Aluminium to Strain, Strain-rate and Temperature", J.E. Hockett, Trans. Met. Soc. AIME 239, 969-976 (1967).

A. BLASS

A FINITE ELEMENT APPROACH IN METALWORKING AND ITS APPLICATION TO THE RADIAL UPSETTING PROCESS

Ph.D. Thesis 1976

ERRATA

Page	Line	Where printed	Should read
21	- 1	is a limiting	(remove)
36	- 12	2-10	2-11
41	- 6	c = 3	$c = 1/3$
44	12	based	is based
125	9	4 x 4	4 x 3
133	- 9	=	$\neq$
139	- 5	besic	basic
142	17	45.0 MN	100 KN
162	- 11	colateral	incidental
185	4	the the	the
195	1	mm,	mm;
198	- 6	discrepate	differ
209	- 8	patological	unacceptable
210	11	patological	unacceptable
243	- 12	$A = \begin{vmatrix} D1 & A1 \\ D2 & A2 \end{vmatrix}$	$A = \begin{vmatrix} D1 & A1 \\ A2 & D2 \end{vmatrix}$
309	- 4 (Col.2)	R - Rp	$(R - Rp)^2$
310	10 (Col.1)	$\int_o^t \varepsilon_{zz}\, d\theta$	$\int_o^\theta \varepsilon_{zz}\, d\theta$
310	- 10 (Col.1)	R + R	Ro + Rp
311	- 21 (Col.1)	3Ro - Ro	3Ro - Rp